Investigating the neuroprotective and anti-epileptogenic mechanisms of inducible nitric oxide synthase and Src family kinase/Fyn inhibitors in experimental models of temporal lobe epilepsy

by

Shaunik Sharma

A dissertation submitted to the graduate faculty

in partial fulfillment of the requirements for the degree of

DOCTOR OF PHILOSOPHY

Major: Biomedical Sciences (Cell Biology)

Program of Study Committee:
Thimmasettappa Thippeswamy, Major Professor
Mary W Greenlee
Chandrashekhar Charavaryamath
Wilson K Rumbeiha
Anumantha G Kanthasamy

The student author, whose presentation of the scholarship herein was approved by the program of study committee, is solely responsible for the content of this dissertation. The Graduate College will ensure this dissertation is globally accessible and will not permit alterations after a degree is conferred.

Iowa State University

Ames, Iowa

2019

TABLE OF CONTENTS

ABSTRACT

Epilepsy is a neurological disorder characterized by spontaneous recurrent seizures (SRS) that affects over 65 million people worldwide, making it one of the most common neurological disorder globally. Etiology for epilepsy is unknown, however, gene mutation and exposure to neurotoxins or head trauma can cause seizures predisposing brain to epilepsy. In an acquired experimental models of temporal lobe epilepsy (TLE), epileptogenesis occurs soon after the induction of status epilepticus. We show herein, through the characterization of a mouse kainate model, the classical features of epileptogenesis such as development of SRS and epileptiform spiking patterns to understand neuronal hyper-excitability, and immunohistochemistry (IHC) on brain sections to investigate the mechanisms of neuroinflammation caused by reactive gliosis, synaptic reorganization, and neurodegeneration. These parameters served as a readout for interventional studies in the rat KA model of TLE.

An inducible nitric oxide synthase (iNOS) and Src family kinase (SFK) mutually regulate each other's expression and promote neuroinflammation and neurodegeneration. Therefore, we tested the disease modifying properties of 1400W, an iNOS inhibitor, and Saracatinib (SAR), SFK inhibitor, in our rat model. The results conclusively demonstrated that both 1400W and SAR significantly reduced spike frequency and SRS in 4-6 month of continuous EEG studies when compared to the vehicle-treated group. IHC on brain sections and Western blot results revealed reduced gliosis, serum albumin and neurodegeneration and enhanced Kir4.1 channel levels after 1400W treatment. In addition, SAR decreased translocation of Fyn and PKCδ into the nucleus with diminished expression of TNFα, IL-1β and iNOS mRNA; serum IL-6, IL-12, TNFα, IL-1β levels; and nitro-oxidative stress

markers 4-HNE, gp91^{phox}, 3-NT and iNOS in the hippocampus suggesting the role of Fyn as an upstream mediator of neuroinflammation in epileptogenesis. IHC results further revealed a significant reduction in Fyn and PKCδ immunopositive reactive glia and neurons and neurodegeneration in the brain after SAR treatment. In the vehicle treated group, Fyn and PKCδ levels were persistently upregulated during post-SE suggesting that Fyn-PKCδ drives neuroinflammation during epileptogenesis. Collectively, these findings reveal that iNOS and SFK/Fyn are principal mediators of neuroinflammation during epileptogenesis, and are potential therapeutic targets to prevent/treat epilepsy.

CHAPTER I

GENERAL INTRODUCTION

Thesis Layout and Organization

The alternative format was chosen for this thesis which include manuscripts that have either been published, or are being prepared for submission. This thesis contains general introduction, four research items and conclusion that briefly summarizes the overall research goals, findings, discussion and future directions for each project. Chapter 1 provides an overview on epilepsy and its epidemiology, etiology and pathophysiology focusing mainly on the role of neuronal and glial source of inflammation and the inflammatory mediators involved. This chapter also introduces to antiepileptic and antiepileptogenic agents and different animal models of epilepsy. Background and literature review I and II introduces to the general role of nitric oxide and nitric oxide synthase and Fyn kinase and their signaling during normal physiological and pathological conditions. The structure, function and pharmacological properties of therapeutic intervention compounds are also illustrated briefly under this section. Chapter II describes the effectiveness of repeated low dose method in inducing immediate epileptogenesis. The finding was based on behavioral convulsive seizures and electrographic non-convulsive seizures, as evident from the long-term (18 weeks) continuous video-EEG recordings. Chapter III demonstrates the impact of immediate epileptogenesis on C57BL/6J mouse, the strain that is resistant to kainate-induced neurotoxicity. It also describes the impact of mild and severe SE, and spontaneous convulsive/non-convulsive seizures on the structure and function of the hippocampus, entorhinal cortex, and amygdala at various time-points. Chapter IV and V describes the disease modifying properties of intervention compounds/pharmacological inhibitors and gene manipulation (from $Fyn^{-/-}$ and $Fyn^{+/+}$ mice

studies) in modifying epileptogenesis in mice and rat models of temporal lobe epilepsy. The references from each chapter are listed at the end of the chapter.

All the experimental data and results described by the author in this thesis were performed during the course of his Ph.D. study at Iowa State University, Department of Biomedical Scienes, under the guidance of Dr. Thimmasettappa Thippeswamy.

Introduction to Epilepsy

Epilepsy is the fourth most common neurological disorder in humans and animals worldwide (Beghi, 2016; Bernstein et al., 2010; De Risio et al., 2015; Kirkley et al., 2014; Pakozdy et al., 2014; Vos et al., 2015). It is a chronic and debilitating disorder that affects both men and women of all ages (Vos et al., 2015). The lifetime prevalence of active epilepsy worldwide is ~2% (>65 million people). According to a report from the Centers for Disease Control and Prevention, it is estimated that ~10% of Americans experience a seizure during their lifetime and that ~3% of them develop epilepsy by the time they are 80 years of age. In the United States alone, about 150,000 new cases of epilepsy are reported annually (Austin et al., 2012; Hesdorffer et al., 2011; Hesdorffer & Begley, 2013; Koh et al., 2014). Epilepsy affects nearly 3.2 million Americans, and its management, including caregiver expenses, costs an estimated $15.5 billion annually (Bernstein et al., 2010). Apart from the direct impact of epilepsy on the economy, the epilepsy disorder spectrum has a huge secondary impact on physical, psychological, and social issues (Austin et al., 2012; Krumholz et al., 2015). Although more than 30 antiseizure or antiepileptic drugs (ASDs/AEDs) are available to treat epilepsy, > 50% of people with epilepsy (PWE) experiencing their first seizure do not become seizure-free with the first ASD/AED therapy. Moreover, about 17% of PWE require

combination therapy (Krumholz et al., 2015; Kwan & Brodie, 2000). Whether the first seizure is appropriately treated or not, or the second seizure is treated, current AEDs do not reduce/prevent the long-term probability of seizure freedom and comorbidity. Furthermore, about one-third of PWE are refractory to the current AEDs (Kwan et al., 2011; Musicco et al., 1997). Although AEDs control seizures in the other two-thirds of PWE, they do not cure or modify the disease process in temporal lobe epilepsy (TLE) (Kwan et al., 2011). TLE is the most common type among all epilepsies with cognitive dysfunction as a prevailing comorbidity (Pearson et al., 2015; Rzezak et al., 2016; Thompson et al., 2016). The majority of AEDs (including 47 failed drugs in human trials) that are not very effective, or do not cure the disease, are ion channel–targeted drugs (Temkin et al., 2001; Sharma et al., 2017; Varvel et al., 2015). This suggests the need for the development of drugs that target alternative pathways to cure/modify the disease. To achieve this, a better understanding of the mechanisms of epileptogenesis in animal models is required.

Status Epilepticus

Status epilepticus (SE) is a life-threatning condition which is defined as the continuous seizurogenic activity when the inhibitory mechanisms fail to terminate seizures and/or initiation of the mechanisms that cause prolonged seizures leading to the long-term consequences (Sharma et al., 2017; Trinka et al., 2015). These adverse events can cause long-term structural, molecular and functional changes in the brain leading to the spontaneous recurrent seizures (SRS) as shown in figure 1.

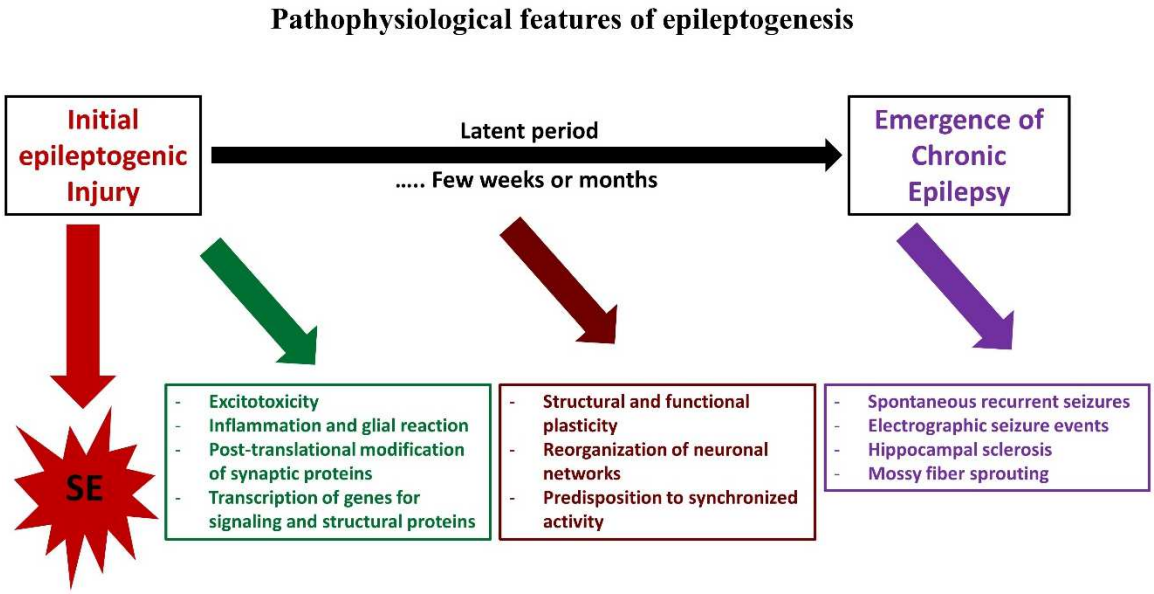

Figure 1. The pathophysiological basis of epileptogenesis. Following SE, long-term adverse events take place in the brain (also known as a period of epileptogenesis) that lasts from weeks to months leading to the development of epilepsy characterized by spontaneous recurrent seizures. Neuronal injury and neuroinflammation plays an important role in the overall pathogenesis of epilepsy.

Several studies have documented the impact of the severity of initial SE on epileptogenesis and epilepsy in the long term (Loscher, 2002; Mikati, 2004; Pitkanen et al., 2002; Sharma et al., 2018b; White et al., 2010). Studies have shown that the severity of SE determines epileptogeneis. Convulsive status epilepticus (CSE) that is experimentally induced in rodents by neurotoxins such as kainate (KA) or pilocarpine or diisopropylfluorophosphate, an organophosphate, causes irreversible brain damage if not adequately treated immediately (Brandt et al., 2016; Furtado et al., 2012; Iyer et al., 2015; Puttachary et al., 2016a; Sharma et al., 2017). The duration and severity of SE determines the outcome of epileptogenesis. Traditionally, it has been accepted that the duration of convulsive seizures during SE is sufficient to cause long-term brain injury/damage to enable the brain to generate spontaneous seizures—that is, “an enduring epilepticus” (Gastaut, 1983). The initial duration of SE for humans was 60 min, which was then reduced to 30 min. This duration is now widely accepted

for studies that investigate the long-term consequences of SE—that is, epileptogenesis and epilepsy (Dodson et al., 1993). Seizures normally self-terminate by activating the inhibitory mechanism; however, if this mechanism fails it can lead to prolonged seizures (i.e., SE), which may then require administration of intervention drugs to terminate SE (Manno, 2011). In chemoconvulsant animal models, it has been known that a minimum of 10 min of convulsive SE is sufficient to cause brain injury and to induce TLE (Nairismagi et al., 2004; Puttachary et al., 2015b).

The majority of chemoconvulsant-induced SE in rats and mice will develop progressive epilepsy, which is generally characterized by reactive gliosis, neurodegeneration, spontaneous recurrent seizures, and cognitive deficits (Buckmaster, 2004; Rattka et al., 2013; Robel et al., 2015; Sharma et al., 2018a; Sutula, 2004; White et al., 2010; Williams et al. 2009). SE induction by chemoconvulsants in mice and rats revealed a huge variation in latency to convulsive SE onset, duration of CS, and mortality. A refined method of inducing SE with repeated low dose (RLD) of kainate, 5 mg/kg, administered at 30 min intervals via the intraperitoneal route, has shown to reduce inconsistency in SE severity across different strains (Glien et al., 2001; Hellier et al., 1998; Rao et al., 2006). Moreover, the RLD method of kainate administration revealed that the surgical procedure for intracranial electrode implantation reduces the threshold for CS onset. About 40% less kainate was required to induce convulsive SE in the telemetry animals when compared to the non-telemetry animals (Puttachary et al., 2015b and 2016a; Sharma et al., 2018b). The SE induction by either SHD or RLD of kainate (i.p.) will lead to the development of epilepsy in the majority of animals. However, the frequency of spontaneous convulsive (tonic–clonic) seizures significantly varies between models. For example, the RLD method in both rats and mice induced epilepsy and the

C57BL/6J mice had almost the same numbers of spontaneous CS as the rats during the first 4 weeks, but the frequency of seizures reduced after 4–6 weeks in the mice (Puttachary et al., 2015b). Interestingly, in a 4-month continuous video-EEG study from the C57BL/6J mouse kainate model, irrespective of initial severity of SE (severe or mild SE), high numbers of electrographic non-convulsive seizures (NCS) were detected on EEG, which persisted during entire length of the study (Puttachary et al. 2015b). However, the frequency of spontaneous convulsive seizures (CS), a readout for the classification of the severity of disease, was related to the initial severity of SE in both rats and mice (Bortel et al., 2010; Klitgaard et al., 2002; Puttachary et al., 2015b and 2016b). Therefore, it is imperative to review and refine the methods of induction and quantification of severity of SE (the type and duration of seizures) to understand its impact on the disease progression and, importantly, to determine disease modifying effects of drugs in experimental models of TLE.

The hallmarks of epileptogenesis

Epileptogenesis is the process that follows immediately after status epilepticus characterized by a series of molecular and cellular changes in the brain (Chang and Lowenstein, 2003; Walker et al., 2002; Williams et al., 2009) that continues to occur even after the development of epilepsy (Loscher, 2015; Pitkanen et al., 2015). Many studies have provided the evidence that the frequency of SRS continues to increase after the first unprovoked seizure suggesting that epileptogenesis can be a long and perpetual process (Dudek and Staley, 2011 and 2012). The fundamental understanding of epileptogenesis comes from *in vivo* and *in vitro* models of acquired epilepsies, primarily focused on focal stroke, post-traumatic and organotypic hippocampal slice culture models exposed to convulsant conditions,

however, the translational significance of these models is difficult to discern (Heinemann and Staley, 2014; Pitkanen et al., 2015).

Traditionally, epileptogenesis was limited to the 'latent period', the duration between the brain insult and the onset of spontaneous recurrent seizures. As per the new guidelines of ILAE, epileptogenesis extends from the time of first brain insult, such as SE, with a consequence of structural (cellular and molecular) and functional changes in the brain, leading to a decreased seizure threshold for onset of spontaneous recurrent seizures, which continue to progress thereafter (Hellier at al., 1998; Kadam et al., 2010; Pitkanen & Engel, 2014; Pitkanen et al., 2015; Williams et al., 2009). The process of epileptogenesis follows immediately after SE, and the brain changes continue to progress beyond the first couple of spontaneous seizures. Several studies have shown that epileptogenesis could start as soon as the SE begins (Bumanglag & Sloviter, 2008; Loscher & Brandt, 2010; Sloviter, 2008). The hyperexcitability of neurons, manifested by epileptiform spiking, occurring during SE triggers a series of overlapping molecular and cellular changes in the brain (Aronica et al., 2017; Barker-Haliski et al., 2017; Klee et al., 2017). In the rat and mouse kainate models, though the behavioral seizures stop after diazepam treatment, the electrographic seizures continue to persist for several hours (Puttachary et al., 2016a). This could be due to the residual effects of kainate in the brain. Therefore, the initial epileptiform activity during the post-SE period could be due to the direct effects of kainate receptors' activation. The hyperexcited neurons modify the internal and external milieu as a result of altered membrane potential for exchange of ions, which ultimately sensitizes the glial cells (Vezzani et al., 2007 and 2011). The intrinsic changes that occur in neurons during SE, and thereafter, determine the fate of the neurons and the brain as a whole (Varvel et al., 2015). The altered neurons' intrinsic properties and their subsequent

communication with glial cells can trigger either a compensatory survival mechanism or neurodegeneration. In a recent *in vivo* 2-photon live imaging study, it was shown that the microglia, the resident macrophages of the brain, become activated as early as 30 min following an insult to the brain. The microglia migrate to the synaptic terminals and engage in dendritic pruning to limit the damage (Parkhurst et al., 2013; Szalay et al., 2016). In addition, microglia initially tend to support neuronal survival by producing trophic agents (Vezzani et al., 2011). The astrocytes, being close to the synaptic terminals and the blood vessels, tend to support neurons by uptaking the extra synaptic glutamate and potassium, and by transporting glucose from blood vessels to the neurons (David et al., 2009; Murphy et al., 2017; Puttachary et al., 2016a; Vezzani et al., 2011). It is also suggested that astrocytes, in concurrence with endothelial cells and pericytes, regulate blood-brain barrier (BBB) function, which is compromised during SE (Puttachary et al., 2016a). If these compensatory mechanisms fail, miscommunication between neurons and glia can turn the normal brain into an epileptic brain. Therefore, identification of inflammatory molecules that play a critical role in such miscommunication could be a potential therapeutic target for epileptogenesis (Thippeswamy et al., 2006).

Role of inflammation in epilepsy

An injury to the brain can elicit production of inflammatory mediators in the blood and tissues that can activate innate and adaptive immune system. The stimulation of innate immune system is generally due to the glial and neuronal activation after the injury or SE (Banks et al., 2010; Vezzani et al., 2011). The consequences of SE are reactive gliosis, excessive production of reactive oxygen/nitrogen species and proinflammatory cytokines and chemokines, increased

epileptiform spiking, neurodegeneration, excessive neurogenesis (with aberrant migration of neuroblasts and inappropriate integration), and spontaneous CS with or without mossy fiber sprouting (Bertram, 2013; Buckmaster, 2010; Goldberg & Coulter, 2013; Ryan et al., 2014; Sharma et al., 2017; Vezzani et al., 2011). These are some of the well known hallmark features of epileptogenesis that play an important role in regulating neuroinflammation as shown in figure 2.

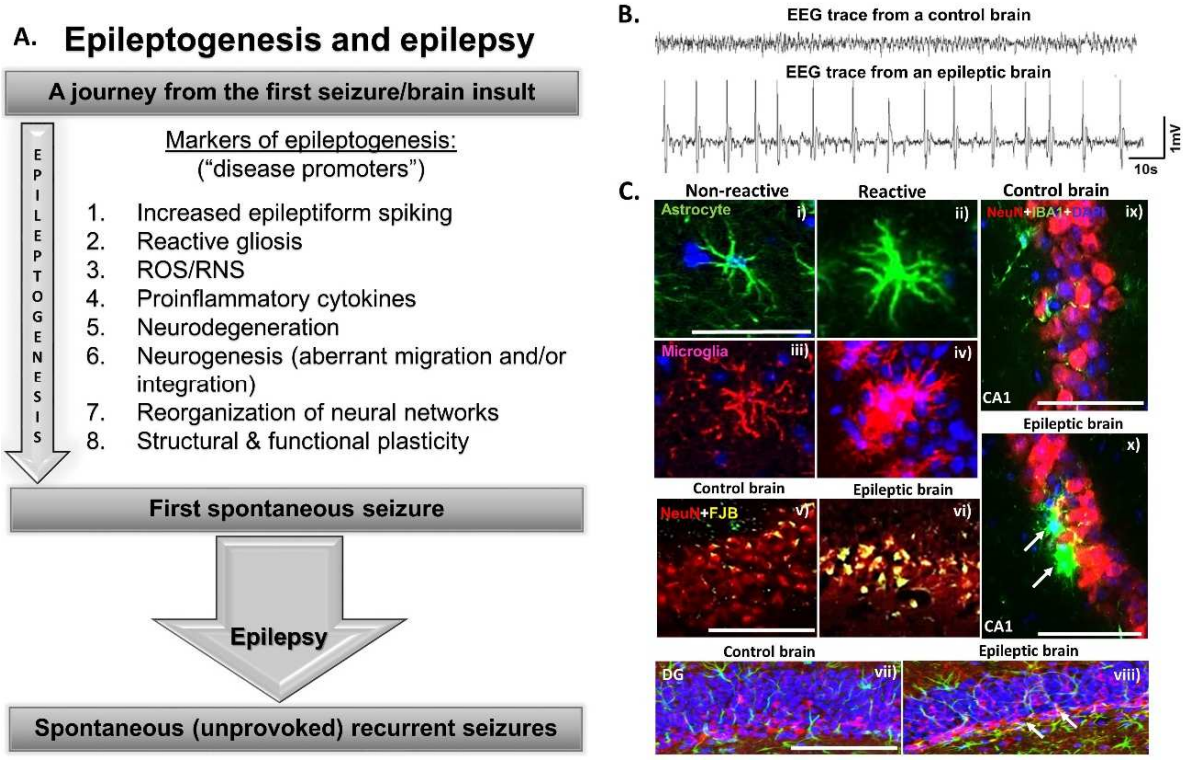

Figure 2. (a) Common features of epileptogenesis that occur soon after SE. (b) An example of epileptiform spikes on EEG from an epileptic brain is compared with a normal brain. (c) IHC images from the hippocampus (i–vi and ix–x) and the dentate gyrus (vii, viii). The astrocytes [green in (i) and (ii)] and microglia [red in (iii) and (iv), and green in (ix) and (x)] become reactive (ii, iv, x) in an epileptic brain. Reactive gliosis causes production of proinflammatory cytokines, chemokines, and reactive oxygen/nitrogen species to induce neurodegeneration [FJB1 NeuN (vi)]. Red-labeled cells are $NeuN^{+}$ in panels v, vi, ix, and x. Yellow in (v) and (vi) represents FJB1 cells. Epileptic brain showed increased production of neuroblasts (pink-labeled cells) in the subgranular zone of the dentate gyrus (white arrows in viii) in contrast to the control brain (vii). Further details on these parameters and the quantified data can be found in Puttachary, Sharma, Thippeswamy, et al., 2016, and Puttachary, Sharma, Verma, et al., 2016. Scale bar, all 100 mm. Adopted and modified from Sharma et al., 2018 (288).

1. Inflammatory mediators: An overview of their role in epileptogenesis

Inflammation in the central nervous system (CNS) can cause BBB damage by inducing inflammation through immune cell activation in the brain, serum albumin extravasation and infiltration of leukocytes from the blood (Banks et al., 2000; Puttachary et al., 2016a). The conditions like stroke, traumatic brain injury, cerebral infections, hypoxic ischemia etc. compromises BBB integrity and are also known to induce epileptogenesis by driving systemic inflammation through cytokine involvement (Vezzani et al., 2011; Wheless et al., 2007). For instance, the activation of tumor necrosis factor alpha (TNFα) in the immune cells by lipopolysaccharide (LPS) caused barrier dysfunction by disrupting tight junctions and modified the transendothelial transport system effecting the normal physiology of the cerebrovasculature (Kuperberg and Wadgaonkar, 2017). In other models, administration of kainate in rats caused severe SE which led to the loss of BBB integrity as shown by serum albumin extravasation, and its increased uptake by astrocytes and neurons in the brain (Puttachary et al., 2016a). These events activate astrocytes and immune cells such a microglia that release enormous amounts of proinflammatory cytokines such as interleukin (IL) IL-1β, IL-2, IL-6, IL-12, TNFα etc. causing neuronal excitotoxicity by increasing calcium influx through N-methyl-D-aspartate (NMDA) receptor activation (Rana and Musto, 2018; Wilson et al., 2002). The activation of NMDA receptors, caused by excessive glutamate accumulation, and increased calcium influx stimulates phospholipase A2 production from the intracellular stores releasing arachidonic acid that gets converted into prostaglandins in the presence of cyclooxygenases. The released prostaglandins, after binding to its receptors (EP1 and EP2), increases intracellular calcium production and mediates cAMP activation leading to excessive neuronal hyperexcitability resulting in chronic epileptic conditions (Lalitha et al., 2018).

The activation of glial cells and hyperexcitation of neurons cause enhanced production of interleukins, interferons, growth factors, chemokines, TNFα, cyclooxygenases, nitric oxide, prostaglandins, adhesion molecules and HMGB1 complement activation (Rana and Musto, 2018; Vezzani et al., 2011 and 2013). The release of such molecules cause further loss of BBB integrity generating seizures of high severity (Rana and Musto, 2018; Sanchez-Munoz et al., 2008; Vezzani et al., 2011; Yarlagadda et al., 2009;). Moreover, the release of aforementioned factors also cause the activation of transcriptional and non transcriptional events in glia and neurons modulating ion channels' release of excitatory and inhibitory neurotransmitters such as glutamate and GABA hence worsening neuroinflammation (Rana and Musto, 2018; Vezzani et al., 2013). The clinical studies from the patients suffering from focal cortical dysplasia, Hashimoto's encephalopathy, Rasmussen encephalitis, systemic lupus erythematosus, Crohn's and other autoimmine diseases have also shown the stimulation of immune regulation in these patients suggesting an important role of immune system activation in different forms of epilepsies (Bien et al., 2007; Dalmau et al., 2008; Rasmussen et al., 1958).

2. Seizure: A consequence or cause of inflammation?

The reports from multiple animal and human studies have shown that the inflammation can be a cause as well as a consequence of epilepsy (Choi et al., 2009; Vezzani et al., 2011 and 2013). Numerous studies on experimental models of TLE have demonstrated that chronic seizures during SE causes increased production of proinflammatory cytokines and later, generation of SRS leading to altered neuronal hyperexcitability and the maintenance of seizure-induced neuropathology (Balosso et al., 2005; Samland et al., 2003). The cytokines such as chemokines, a chemoattractant molecules, guide the migration of leukocytes from the

blood to the site of injury in the brain across the cerebrovasculature (Wilson et al., 2010). Under normal conditions, these molecules regulate physiological functions such as microglial motility, membrane ruffling, axonal guidance, maintenance of synaptic plasticity, angiogenesis and neurogenesis (Semple et al., 2010). But under pathological conditions, when they are highly upregulated, cause infectious, inflammatory and neurodegenerative diseases (Murdoch and Finn, 2000). The clinical studies on the refractory epileptic patients have shown that the excessive production of chemokines cause damage to the cerebrovasculature allowing leukocyte migration and infiltration into the brain parenchyma compromising BBB integrity (Fabene et al., 2008; Librizzi et al., 2010; Ravizza et al., 2008**)**. IHC and other studies on the rodent models of epileptogenesis have demonstrated the upregulation of inflammatory mediators, reactive gliosis, markers of oxidative and nitrosative stress and neurodegeneration in the hippocampus and other regions of the brain in various cell populations (Puttachary, 2015a and 2016a and 2016b). The findings from these studies have shown that the immune cells such as microglia becomes activated as early as 4h post-SE with the upregulation of molecules like Fyn and PKCδ in the brain and proinflammatory cytokines in the serum in infected animals (Sharma et al., 2018a). Some of these early events are followed by an upregulation of arachidonic acid, COX-2, inducible nitric oxide synthase, prostaglandins, series of complement cascade proteins and oxidative stress markers such as 4-HNE, $gp91^{phox}$ and 3-NT in glial cells and neurons (Aronica et al., 2007; Rozovsky et al., 1994).

Oxidative stress and mitochondrial dysfunction have long been recognized as key mechanisms involved in several neurological disorders. An emerging evidence confirms that oxidative stress manifests as a consequence of the first seizure insult, which turns out later to become a major cause of epileptogenesis (Liang and Patel, 2006). During brain injury, a

significant increase in neuronal glucose uptake and metabolism takes place (de Graaf et al., 2004; Liang and Patel, 2006) followed by an increase in the cerebral blood flow to cope up with the glucose hypermetabolism that results in lactate accumulation, therefore overwhelming the normal glycolysis and tricarboxylic acid cycle. The recurrent seizures results in overproduction of mitochondrial superoxide radicals in rodent models (Puttachary et al., 2015a) that gets converted to hydroxyl radical via Fenton and Haber-Weiss reaction. The hydroxyl radical in the presence of Cu^{2+} and Fe^{2+} ions readily oxidizes proteins, lipids, and DNA resulting in altered protein function, membrane permeability, and gene expression, respectively. These events increase neuronal excitability and decrease seizure threshold. Several lines of evidence showing the link between oxidative stress and the mitochondrial dysfunction, due to seizures, have been observed in human patients and rodent models of TLE. For example, changes in the mitochondrial membrane potential and increased nicotinamide adenine dinucleotide phosphate (NADPH) levels, (Kann et al., 2005), inactivation of mitochondrial aconitase levels after SE, reduction of mitochondrial N-acetyl aspartate (a metabolite synthesized from aspartate and acetylcoenzyme) (Helms et al., 2006), dysfunctional electron transport chain complexes (1, 3, and 4) (Chuang et al., 2004), rise in mitochondrial H_2O_2 production, lipid peroxidation (increased malondialdehyde and thiobarbituric acid) and mitochondrial DNA damage following a seizure (Cini and Moretti, 1995; Dexter et al., 1989; Pizzol et al., 2000). The above data from animal and human models suggest that the process of epileptogenesis, after SE, is a continuous process of inflammation development and progression that gets worse over time, as evident from the human and animal chronic epilepsy studies supporting the notion that inflammation can be the cause of seizures (Vezzani et al., 2011).

Another question that also arises is whether seizure is the cause of inflammation or not is a chicken-egg-chicken situation. Several lines of evidence confirms that brain inflammation promotes neuronal excitability (Vezzani et al., 2011). Studies from the experimental models have shown the activation of proinflammatory mediators such as TNFα and IL-1β and the role of complementary proteins in seizure generation and exacerbation (Xiong et al., 2003). Other lines of evidence includes occurrence of seizures during fever, also known as febrile seizures. Elevated inflammation in the neurons of the hypothalamus modulate systemic inflammatory response by recruiting inflammatory mediators such as cytokines and prostaglandins from the system (Berg et al., 1998; Zetterstrom et al., 1998). This further regulates and increases the production of proinflammatory cytokines, TNFα and IL-1β, within the brain during fever and reduces the threshold for seizures by generating more of such cytokines (Gatti et al., 2002). Furthermore, the activation of TLR4 receptors, after LPS or HMGB1 binding, have also been shown to cause seizures following inflammation. TLR4 activates MYD88-TRAF6 complex and phosphorylates MAP kinase resulting in NFkB translocation to the nucleus stimulating transcription of proinflammatory genes causing hyperexcitation and inflammation (Lalitha et al., 2018). An increased transcription of these inflammatory mediators activate their receptors on the glial cells leading to a vicious cycle of seizures and inflammation (Lalitha et al., 2018; Vezzani et al., 2011).

3. Oxidative stress and temporal lobe epilepsy

An insult to the brain (such as the first seizure) causes excitotoxicity, neuroinflammation and production of reactive oxygen/nitrogen species (ROS/RNS). ROS and RNS produced during status epilepticus negatively overwhelms the mitochondrial natural

antioxidant defense mechanism. This leads to mitochondrial dysfunction and damage to the mitochondrial DNA. This in turn affects synthesis of various enzyme complexes involved in electron transport chain. The resultant effects that occur during epileptogenesis include lipid peroxidation, reactive gliosis, hippocampal neurodegeneration, reorganization of neural networks and hypersynchronicity. These factors predispose the brain to spontaneous recurrent seizures, which ultimately establishes into temporal lobe epilepsy (Puttachary et al., 2015a).

3.1 Free radicals of oxygen and nitrogen species

Under normal physiological conditions, ROS and/or RNS levels are fairly well controlled to perform important functions such as autophagy, chemical signaling, cell division, and mitogen activated protein kinase signaling and apoptosis (Mao and Franke, 2013). Due to a highly reactive nature of these molecules, the ROS and/or RNS are tightly regulated. The mitochondrial dysfunction due to excessive generation of ROS and RNS is a continuous process during epileptogenesis which is normally associated with neurodegeneration (Patel, 2004).

The free radicals contain one or more unpaired electrons in their outermost shell which confers them for being chemically reactive. They are generated either by a loss or a gain of an electron during homolytic cleavage (Cardenas-Rodrigues at al., 2013; Lobo et al., 2010). The resultant effect of this cleavage is the formation of free radicals which may or may not carry an electric charge. Due to the presence of an excess electron or a lack of electron in their outermost orbits, these radicals behave as a strong oxidizing or reducing agents. Free radicals are highly unstable reactive species which can initiate a chain reaction by pulling electrons from the nearby molecular fragments to form stable bonds. As a result of this, the

morphological and functional changes take place in proteins and lipids that can impact cellular and mitochondrial DNA. This results in cross-linking of base pairs causing gene mutations and generation of free radicals. The free radicals of oxygen and nitrogen species include hydroxyl radical ($OH^{\cdot}$), superoxide anion (O_2^-), hydrogen peroxide (H_2O_2), alkoxy radical (RO), peroxy radical (ROO), hypochlorite (ClO^-), nitric oxide radical ($NO^{\cdot}$), peroxynitrite radical ($ONOO^-$), nitroxyl anion HNO, nitrosonium cation (NO^+), higher oxides of nitrogen (N_2O_3, NO2·), and S-nitrosothiols (RSNO) (Cheeseman, 1993; Puttachary et al., 2015a). The production of these radicals within the cell in excessive amounts lead to oxidative stress.

3.2 Free radical production and oxidative stress

An oxidative stress generally refers to a biochemical state where ROS or RNS production is upregulated resulting in damage to the cell membrane, proteins, enzymes, and DNA components within the nucleus and the mitochondria (Cardenas-Rodriguez, 2013). Majority of RNS are generated from the interactions between nitric oxide (NO) and molecular oxygen. NO is a second messenger/signaling molecule, which can also act as a free radical due to the presence of an unpaired electron in its outermost orbit (6 valence electrons from oxygen and 5 from nitrogen) (Puttachary et al., 2015a). NO is produced from the substrate L-arginine, with the help of a co-factor NADPH and molecular oxygen, and enzyme nitric oxide synthase (NOS). There are three major isoforms of NOS: (a) neuronal NOS (nNOS) produced by neurons, (b) endothelial NOS (eNOS) expressed mainly in endothelial cells, and (c) inducible NOS (iNOS) expressed in immune cells, astrocytes and also in neurons. The roles performed by NO varies based on its synthesis from NOS and the tissue it is synthesized in (Alderton et al., 2001; Knowles and Moncada, 1994). The physiological concentrations of NO produced by

nNOS regulate calcium dependent protein modification (S-nitrosylation), energy metabolism (through cytochrome C oxidase), synaptic plasticity, and neuroprotection. The NO produced by eNOS plays an important role in calcium dependent cyclic guanosine monophosphate (cGMP) mediated vasodilation and helps in maintaining a vascular tone of the cerebral blood vessels. The NO by iNOS is important for immune response or killing pathogens by generating free radicals (Cosgrave et al., 2010; Thippeswamy et al., 2005 and 2006). However, excessive amount of NO produced by iNOS-mediated mechanism is harmful to the host cells.

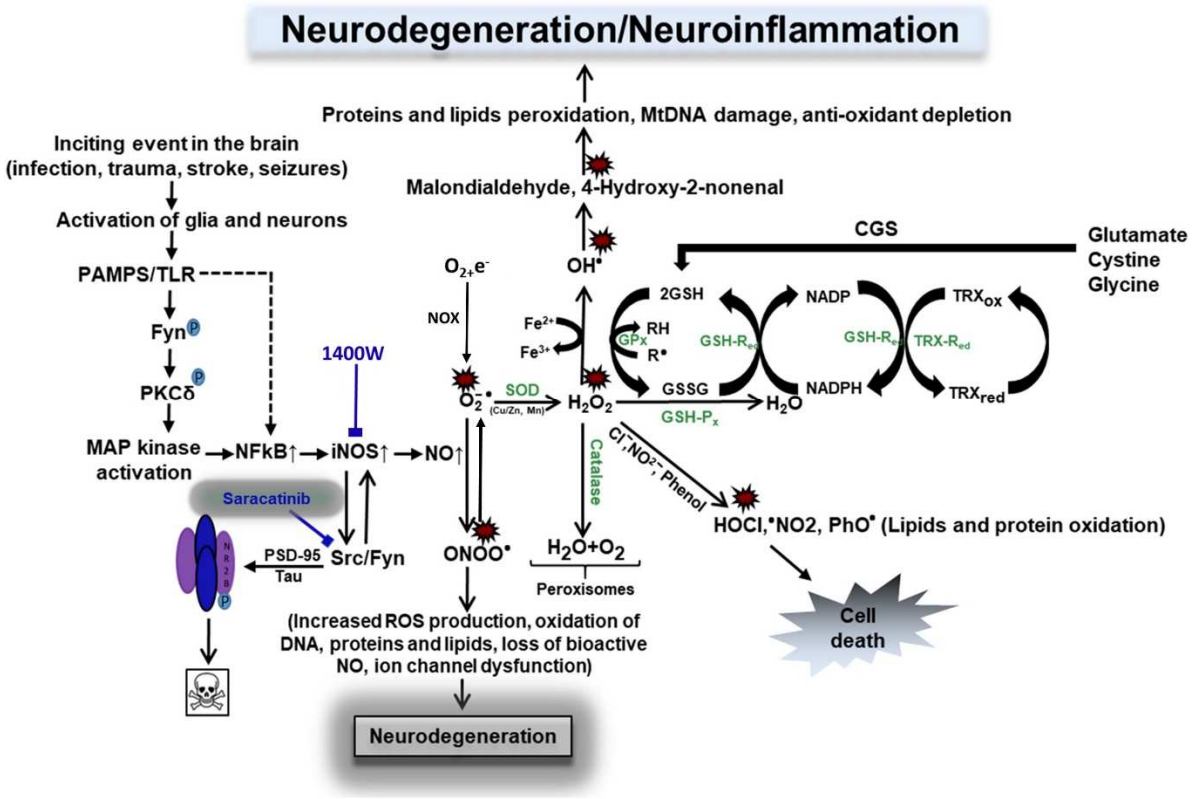

Figure 3. Biochemical reactions of ROS/RNS production and their mitigation by endogenous antioxidants. Components in blue represent nonenzymatic antioxidants; green represents oxidative and antioxidant enzymes; and small red explosion sign represents generation of free radicals. NOX is the key enzymatic source of ROS. It reduces oxygen to superoxide anion and hydrogen peroxide. O_2· forms H_2O_2 which is the most reactive radical among its group that is produced via Fenton reaction. OH· leads to lipid peroxidation by producing harmful metabolites such as MDA and 4-HNE leading to mitochondrial dysfunction and cell death. It also produces HOCl· and PhO· which are extremely toxic oxidants that disrupt tight junctions and increase paracellular permeability. H_2O_2 is eliminated by CAT, in peroxisomes, and GPx (location varies). At rapid rates, superoxide anions compete with NO which

results in the formation of highly reactive molecule called peroxynitrite ($ONOO^{\cdot}$), in cytoplasm, leading to increased ROS production, oxidation of DNA, RNA, and proteins, ion channel dysfunction, and loss of bioactive $NO^{\cdot}$. Peroxynitrite inactivates Mn-SOD, thereby increasing the flux of superoxide anions available to react with NO. SOD catalyzes the reduction of superoxide anions into H_2O_2, in mitochondria in the presence of enzymes GPx and CAT; H_2O_2 gets converted into water and oxygen. Antioxidant enzymes such as GPx oxidize GSH to GSSG and GSHred recycles GSH back from GSSG. NADPH gets reduced to NADP by GSHred. GSH/GSSG is a commonly used biomarker of oxidative stress in biological systems. However, GPx also catalyzes H_2O_2 into H_2O by using reduced TRXred. Antioxidant defense against toxic oxygen intermediates comprises an intricate network which is heavily influenced by nutrition (vitamins A, E, and C and fatty acids). CGS plays an important role in glutathione metabolism and acts as an antioxidant in glial cells such as astrocytes. Extracellular oxidized cysteine is reduced to cysteine by thioredoxin reductase or glutathione that helps to maintain the steady state balance between antioxidants and ROS. ROS, reactive oxygen species; NADPH, nicotinamide adenine dinucleotide phosphate; NOX, NADPH oxidase; SOD, superoxide dismutase (Cu/Zn—copper/zinc, Mn—manganese); CAT, catalase; $O_2^{-}\cdot$, superoxide anion; H_2O_2, hydrogen peroxide; NO, nitric oxide; ONOO−, peroxynitrite; HOCl, hypochlorous acid; $PhO^{\cdot}$, phenoxy radical; $OH^{\cdot}$, hydroxyl radical; GSH, glutathione; GSSG, oxidized glutathione; TRXox/red, thioredoxin reduced and oxidized; TRXred, thioredoxin reductase; GSHred, glutathione reductase; GPx, glutathione peroxidase; CGS, cystine/glutamate antiporter system. Adopted and modified from Puttachary et al., 2015 (251).

Generation of free radicals under normal and pathological conditions within a cell is shown in Figure 2. In the cytoplasmic membrane, NADPH oxidase reduces molecular oxygen into superoxide anion (O_2^{-}). These superoxides can also be generated by the action of molecular oxygen on xanthine oxidase during the production of uric acid. These superoxides are converted into H_2O_2 in the presence of superoxide dismutase (SOD). H_2O_2 is a lipophilic molecule, which crosses lipid membranes into peroxisomes where it is finally eliminated by catalase (CAT) releasing H_2O and O_2 (Bae et al., 2011; Puttachary et al., 2015a). However, if the antioxidant action of SOD or CAT is impaired, the reaction of superoxide with H_2O_2 yields toxic OH radical in the presence of Fe^{2+} (called Fenton and Haber-Weiss reaction). These OH radicals can also be generated by the action of superoxides on hypochlorite (ClO^{-}) (Bradman et al., 2011; Puttachary et al., 2015a). The hypochlorite (ClO^{-}) is formed by the action of chloride (Cl^{-}) on H_2O_2, a reaction catalyzed by peroxidases. The OH radical is a harmful free

radical of oxygen which has a short half-life but remains highly reactive. Further, the hydroxyl radical can also react with NO to form peroxynitrate ($ONOO^-$), a powerful oxidizing agent that causes lipid peroxidation, tyrosine nitration, and cytotoxicity (Halliwell et al., 1999). Other molecules such as NADPH oxidase and cyclooxygenase-2 (COX-2) also plays an important role in the production of free radicals and oxidative stress. At basal levels, NADPH oxidase plays a role in learning and memory consolidation (Aguiar et al., 2012; Infanger et al., 2006). However, under pathological conditions such as TLE, NADPH oxidase overproduces superoxide ions to initiate neuroinflammation and neurodegeneration (Gao et al., 2003; Sorce et al., 2012).

In addition to NADPH oxidase, the COX-2 also upregulates ROS by producing prostaglandins (specifically, F2 and H) (Madrigal et al., 2006**;** Puttachary et al., 2015a). It has been shown that prostaglandins stimulate astrocytes to produce proinflammatory cytokines initiating signaling mechanisms leading to neuronal death (Bezzi et al., 1998; Puttachary et al., 2015a). COX-2 is also responsible for generating number of inflammatory responses in the immue cells such as neutrophils (Ricciotti and Fitzgerald, 2011; Puttachary et al., 2015a). Clinical and animal studies have shown that COX-2 inhibition prevents lipid peroxidation by downregulating prostaglandin synthesis, and therefore can be a potential therapeutic target in the treatment of epilepsy (Madrigal et al., 2006; Serrano et al., 2011).

Antiepileptic and entiepileptogenic agents, and animal models of epilepsy

The vast majority of currently available anticonvulsant drugs have been, presumably, thoroughly screened using a battery of preclinical high-throughput tests. The most common methods used are acute seiure mouse/rat models such as maximal electroshock seizures (MES)

and pentylenetetrazole (PTZ) and electrophysiology of brain slices, and in recent years, the zebra fish model has been proposed (Baraban, 2013; Loscher, 2010; Rowley & White, 2010; White, 2002). The test drug of interest is administered either before inducing seizures or coadministered with chemoconvulsants to understand the therapeutic effect of the drug in controlling seizures. Indeed, this approach is useful for screening test compounds intended for the discovery of anticonvulsive drugs, but the outcome does not reveal whether the chosen compound would be useful as a potential antiepileptogenic and/or antiepileptic agent. Therefore it is important to screen any potential antiepileptic or antiepileptogenic test drug in relevant and highly reproducible preclinical/animal models of epilepsy to further advance it as a therapeutic agent.

The rat kainate chronic model of TLE is the most appropriate model for testing disease-modifying agents post-SE. Unlike certain mouse models, the rat kainate model has several advantages for studying epileptogenesis. The early epileptogenic hallmarks (the "disease promoters"), such as reactive gliosis, proinflammatory cytokine production, and neurodegeneration, are consistent, and spontaneous CSs are progressive in nature in the rat model, in contrast to the mouse model, especially with respect to frequency of CSs (Bertram et al., 1990; Jorgensen et al., 1993; Puttachary et al., 2016a; Rao et al., 2006; Vezzani et al., 2011; Williams et al., 2007 and 2009). Moreover, rats are easier to perform complicated procedures such as surgeries for electrode implantation, serial blood draws and also gives large sample volumes. The physiology of rat is closer to the humans (with 90% genome similarity) which helps to understand the complex physiological interactions in humans more accurately (Ellenbroek and Youn, 2016; Lannaccone and Jacob, 2009). Most of the genes responsible for human diseases are also present in the rats making them the most suitable model to study

neurodegenerative disorders. Moreover, rats have metabolic and physiological similarities, superior behavior modeling (rich behavior profile) and also technical advantages over mice making them a perfect model for mimicking human diseases. Rats are also more reliable in terms of drug efficacy and safety studies, that's why rats are preferred over mice for drug testing due to numerous pre-clinical and translational failures in mice. This might be due to the difference of response in their nervous and endocrine systems. For example, neurotransmitter receptor for serotonin (5-HT6) mRNA are higher in rats compared to mice. It is involved in reward, cognition, motor functioning and emotional regulation and also plays an important role in neuropsychiatric disorders. Pharmacological agonists/antagonists of 5-HT6 may not work well in mice but may work well in rats making them more suitable model for neurodegenerative disorder research (Ellenbroek and Youn, 2016).

It is also important to note that in some mouse models, even though the initial SE is severe and prolonged, the development of epilepsy may be compromised and may not manifest the classical features of epileptogenesis, such as progressive increase in the frequency of spontaneous CSs. For example, the SE induced by repeated low doses of kainate (i.p.) in a C57BL/6J mouse model produced severe SE, and continuous video electroencephalography (EEG) confirmed that they developed epilepsy in less than 5 days (Puttachary et al., 2015b; Sharma et al., 2017). A similar rapid epileptogenesis has been reported in the mouse pilocarpine model (Mazzuferi et al., 2012). The spontaneous CSs persist for about 4 to 6 weeks, but they become infrequent thereafter. However, electrographic nonconvulsive seizures (NCSs) persist for a longer period, up to 4 months post-SE (Puttachary et al., 2015b). Intrahippocampal kainate administration in the mouse model also produced similar results with respect to infrequent CS, but frequent electrographic NCS (Klee et al., 2017) and widespread

granule cell dispersion have been reported (Hester & Danzer, 2014; Murphy & Danzer, 2011; Suzuki et al., 2005). This could be due to the direct impact of intrahippocampal injection of kainate. It is also important to note that the kainate-induced SE via the intraperitoneal route in transgenic mice, bred on C57 genetic background (e.g., eGFP expressing mice), caused inconsistent epileptogenesis resulting in ~5 spontaneous CSs in the first month, and the CSs were completely absent in subsequent months (Sharma et al., 2017). However, as in the C57BL/6J mice, large numbers of electrographic NCSs persisted in transgenic mice in a 4-month continuous video EEG study. Therefore, mouse kainate (i.p.) models are not suitable for chronic studies if the experimental objective is to determine the effects of a disease modifier on the frequency of CSs. However, they can be useful to assess the impact of drugs on epileptiform spikes and/or electrographic NCSs in the absence of a CS paradigm. Therefore, in such scenarios, one could consider NCS and spike trains as variables, instead of CS, to compare between control and drug-treated groups. To mimic human TLE for translational purposes, a rat kainate model is more suitable in terms of the progressive nature of the disease because the frequency of spontaneous CSs increases consistently over time in rats in contrast to mouse kainate models (Sharma et al., 2017).

In a recent review article by Loscher et al., the impact of inter- and intrastrain differences in rats and mice for epilepsy research has been thoroughly discussed (Loscher et al., 2017). According to this review, the following variables should be controlled to achieve reproducibility and rigor, and to minimize experimental bias in epilepsy research. These are environmental (housing, enrichment, food, water, and litter size); experimental (seizure frequency and duration, and seizure threshold); biological (age and sex); and genetic (genetic background and gene manipulation). He also highlighted the relevance of strain-specific

differences in mice and rats and their implications in determining the choice of experimental models of seizure/epilepsy. The vast variation in seizure susceptibility in animal models is due to the diversity of their outbred genetic backgrounds. However, the C57BL/6J inbred mice response to chemoconvulsants such as kainate also varies between batches of mice and the source (Chaix et al., 2007; Bryant et al., 2008; Loscher et al., 2017; Sharma et al., 2018b).

In rats, the route of kainate administration, use of anesthesia while administering the kainate, and the strain used in the experiments also impact SE and epileptogenesis (Golden et al., 1995; Sharma et al., 2008). With respect to sensitivity and variability of response to a single dose of kainate by subcutaneous route, the Fischer-344 (F-344) rats are reported as a reliable strain (Golden et al., 1995; Sharma et al., 2008). In the adult male F-344 rats study, a single dose of kainate at 9 mg/kg (s.c.) induced SE in 93%, of which 95% survived and 80% developed epilepsy (Sharma et al., 2008). In another long-term study in F-344 rats, the kainate (3 mg/kg) was administered repeatedly at 1-hr intervals for 4 hr to induce SE (Rao et al., 2006). In this F-344 rat model, the duration and severity of seizures increased from the third to fourth month, and the average number of seizures was 2.57 to 2.63 per hour. Therefore, F-344 rats may be appropriate to model the extreme severe spectrum of the disease.

The diazepam is commonly used to terminate behavioral seizures. It is well documented that diazepam indeed controls behavioral seizures, but it has little or no impact on electrographic events if the SE is severe (Apland et al., 2014; Goodkin et al., 2008; Qashu et al., 2009). However, diazepam does suppress epileptiform activity in animals with mild SE. Diazepam has been known to reduce neurodegeneration after prolonged SE, but not in the hippocampus during epileptogenesis (Apland et al., 2014; Qashu et al., 2009). However, diazepam administration minimizes mortality to some extent and controls variability in the

duration of behavioral SE between animals (Puttachary et al., 2014, 2015b and 2016a).

The animal models have greatly improved our understanding of epilepsy which has proven to be very helpful in screening the novel candidate compounds for the treatment of epileptogenesis and epilepsy. However, there is still a growing concern about the efficacy of the new AEDs which hasn't improved in the recent years, especially in the case of refractory epilepsy (Loscher, 2010). It is important to note that some of these drugs that have been tested works well in the humans, against nonconvulsive seizures, but doesn't work well with animal models of PTZ, and other similar models. So it is important to understand the mechanism of AEDs action and right models should be chosen in order to predict right efficacy of AEDs against different kinds of seizure/epilepsies (Loscher, 2010).

Role of glial cells and neurons in CNS

The most important cells in the central nervous system are microglia, macroglia and neurons. The macroglia, of neuroecodermal origin, includes astrocytes, radial glia, ependymal cells and oligodendrocytes in the CNS and schwann cells, satellite cells and enteric glial cells in the peripheral nervous system (PNS) (Allen and Barres, 2009; Bezzi and Volterra, 2001; Walz, 1989). Neurons are the most important cells of the brain that functions by releasing signaling molecules called neurotransmitters, which requires calcium release during the action potential. The most basic functions of neurons include acquiring information through neurotransmitters, integrating the received information and communicating it between the cells/target cells such as other neurons, glial cells, muscle or gland cells etc (Allen and Barres, 2009; Bezzi and Volterra, 2001). The glial cells help to deliver all the necessary ingredients required for the proper functioning of the neurons and also provide protection. They maintain

normal and balanced homeostasis within the CNS by clearing out the pathogens and dead neurons from the system (Bezzi and Volterra, 2001). Glial cells such as astrocytes play an important role in maintaining the integrity of BBB by providing nutritional support, such as glucose and amino acids, to neurons from the blood vessels and surrounding tissues (Prat et al., 2001). Neuroglia, also called an information system of CNS, provide structural and metabolic support (Allen and Barres, 2009; Bezzi and Volterra, 2001; Walz, 1989), protection and nutrition to the neurons (Allen and Barres, 2009). They also help to keep ion balance in the extracellular space in control and play an important role in the maintenance of synaptic plasticity (Bezzi and Volterra, 2001; Walz, 1989). Glial cells cannot propagate action potential on their own, they release gliotransmitters which have receptors either on the other glial cells or on neurons to regulate neuronal function with the help of calcium release. Although neurons are the main cells in the brain that have the capability to control all the necessary functions of other organ systems in the body, they still need to communicate and interact with glial cells for this purpose. The glial cells in turn helps protect neurons by providing the structural, metabolic, functional and pathogenic support (Fields and Stevens-Graham, 2002). In the peripheral nervous system, glial cells are responsible for myelination, repair, regeneration and survival of peripheral axons by secreting growth promoting factors such as neurotrophins, transforming growth factor beta 1 and glial cell-line derived neurotrophic factor (Madduri and Gander, 2010; Pfrieger, 2009; Toy and Namgung, 2013; Zuchero and Barres, 2015). During pathological conditions, neuron-glia miscommunication occurs that causes modulation in the functional activity of glial cells generating release of proinflammatory molecules resulting in neuroinflammation and/or neurodegeneration. Therefore, it is extremely important to have

thorough understanding of neuronal-glia communication in order to fully understand their role during pathological conditions.

1. Role of microglia in pathophysiological conditions

Microglia are the resident immune cells, derived from the mesenchymal origin, that plays a crucial role in immune surveillance of the CNS. First discovered by Rio Hortega between 1919 and 1921, the macrophage like phagocytic properties revolutionized their role in CNS research. Their origin in CNS has been a topic of debate for a while and so far, only two theories have been proposed linked to their origin. First theory proclaims that they are derived from primitive and infiltrating myeloid cells during the first week of embryonic development in the yolk sac and according to the second theory, they populate the brain from the circulating monocytes during the postnatal period (Andjelkovic et al., 1998; Lisboa et al., 2016). Microglia have various subpopulation forms in the CNS based on their morphology and activation. These subtypes include M0, M2a, M2b, M2c, M2d and M1 (Franco and Fernancez-Suarez, 2015). M2 microglia, also known as ramified microglia, have anti-inflammatory properties, play a significant role in the maintenance of CNS homeostasis and plasticity, synaptic pruning, clearing of dying cells, removal of pathogens through phagocytosis, neural development, attenuation of inflammatory response, regulating neurotransmitter release, neurogenesis, release of neurotrophic factors, tissue/synaptic remodeling, healing and repair. On the other hand, M1 microglia, activated state amoeboid or rod-shaped, generally play a role in the regulation of inflammation by secreting proinflammatory cytokines and chemokines, BBB permeabilization, oxidative damage, neuronal death and recruitment, differentiation and activation of Th1 and Th17 cells (Dheen et al., 2007; Streit et al., 2004; Streit et al., 2014).

An inflammation activates body's innate immune system that fights infection by recruiting immune cells at the site of infection. Microglia are continuously scanning and surveilling our CNS microenvironment for the presence of any foreign pathogens and are the first cells to get activated in response to any kind of neuronal injury or infection (Nimmerjahn et al., 2005). Under some circumstances such as infection, these immune cells get overactivated and cause neurological problems associated with Alzheimer's, Huntington's, Parkinson's disease, Multiple Sclerosis and Epilepsy. During these conditions, microglia regulate enormous leukocyte infiltration in the CNS (Almolda et al., 2015), release excessive proinflammatory cytokines such as TNFα, IL-1β, IL-2, IL-6, IL-12 and chemokines CCL2, CCL20, monocyte chemoattractant protein-1 (MCP-1) and eotaxin, increase release of iNOS to generate NO causing protein nitrosylation, stimulates production and release of reactive oxygen and nitrogen species (Franco and Fernandez-Suarez, 2015), activates complementary system and stimulates COX-2 to produce prostaglandins. Microglia also causes increased levels of RANTES, which is responsible for T cell migration during infection (Chhor et al., 2013). In C57BL/6J mice Theiler's virus model of encephalitis, Kaufer et al. (2018) recently demonstrated that induction of seizures caused increased expression of chemokine receptors, CCR2, in monocytes and CX3CR1 in microglia. This caused enhanced myeloid cell accumulation in the hippocampus of the wild type animals which resulted in neurodegeneration while in $CCR2^{-/-}$ knockouts, neurodegeneration was reduced but this did not prevent occurrence of spontaneous recurrent seizures after the viral infection (Kaufer et al., 2018). The transcription of proinflammatory genes occur rapidly in the microglia following aforementioned events. All these functional changes in microglia, during inflammation, cause abnormal neuronal signaling which results in hyperexcitation and therefore neurodegeneration.

Numerous reports have discussed the activation of survival mechanisms that occurs concomitantly with neurodegenerative mechanisms (Buckmaster and Dudek, 1997; Vezzani et al., 2011). These mechanisms however depends upon several factors such as severity of the insult, time of glial activation, region of the brain involved, time and duration of insult and recruitment and activation of intercellular signaling molecules (Foresti et al, 2011). This regulated activation of microglia secretes certain growth factors such as brain- and glial cell derived neurotrophic factors and anti-inflammatory cytokines (IL-10 and IL-4) to attenuate infection, facilitate neuronal survival and maintain cellular homeostasis (Glezer et al., 2007; Napoli and Neumann, 2010).

2. Role of astrocytes in pathophysiological conditions

Astrocytes, first identified by Virchow in 1846 as a glue filling the interstitial fluid (Cui et al., 2012), are star-shaped cells in the CNS that play a significant role in the maintenance of the ionic balance, integration of the BBB, regulation of synaptogenesis and neurogenesis, immune modulation, provision of metabolic support to neurons/energy metabolsim, regulation of glutamate and potassium levels in the cell and in extracellular space, maintenance of gap junctions and production of anti-oxidants such as glutathione by regulating glutathione-cysteine antiporter system (Coulter and Steinhauser, 2015). Astrocytes are the most abundant type of glia cells in the brain and their concentration varies from species to species. They play a significant role in regulating neuronal functions. For example, they help to meet metabolic demands of the neurons by supplying nutrients from the blood vessels with the help of astrocytic end feets (Cui et al., 2012). Moreover, they also make ‘tripartite synapses’ with the pre- and post-synaptic neurons to regulate integration of synaptic function by means of

neurotransmitters and gliotransmitter release at these synapses, through calcium dependent mechanisms, controling electrophysiological excitability of the nerve cells (Cui et al., 2012). Most of this activity is controlled by astrocyte mediated glutamate release in the hippocampus, thalamus and olfactory bulb which governs synaptic plasticity in neurons by activating ionotropic (such as NMDA) and metabotropic glutamate receptors releasing calcium (Bezzi et al. 1998). Numerous studies employing molecular genetic approaches targeting calcium, using glutamate antagonists and IP_3R2 knockout transgenic mice, have highlighted the importance of calcium-mediated glutamate gliotransmission in astrocytes regulating neuronal functions. Apart from glutamate, other astrocytic neuroactive molecules known to regulate neuronal functions are $_D$-serine, GABA and adenosine triphosphate. $_D$-serine impacts synaptic activity through the induction of LTD and LTP in the prefrontal cortex (Fossat et al., 2011; Panatier et al., 2006). Astrocytic GABA synthesizing enzymes such as GAD67 and GABA-T has been shown to play an important role during development (Lake, 1992; Ochi et al., 1993). Astrocytic GABA also mediates tonic inhibition through Best1 ion channels in cerebellum and CA1 of hippocampus (Lee et al., 2010; Yoon et al., 2011). Moreover, astrocytic GABA receptors inhibits proinflammatory molecules such as TNFα through calcium dependent manner and transport of GABA through GABA transporters in calcium-independent manner (Lee et al., 2010). Adenosine triphosphate (ATP) has been shown to regulate calcium release and glial-neuronal communication via the activation of purinergic receptors on neurons (Zhang et al., 2003). An active metabolite of ATP, adenosine, plays an anti-inflammatory role by activating A1 receptors and inhibiting glutamate release, as has been shown in various animal models. It also plays a significant role in sleep homeostasis, synaptic plasticity and memory formation (Hasko et al., 2008; Panatier et al., 2006).

Besides playing a crucial role in regulating neuronal functions under normal physiological conditions, astrocytes also play an important role during pathological conditions in the CNS. Like microglia, these cells change their morphology in response to a change in their microenvironment and becomes reactive during inflammation (Cui et al., 2012; Pekny and Pekna, 2016). The morphological and pathognomonic features of reactive astrocytes include hypertrophic cell body, increased cell density at the inflammation site, short and thick processes, release of proinflammatory factors, increased expression of GFAP and vimentin, reduced potassium buffering (downregulation of potassium channels), reduced glutamate uptake/change in glutamate homeostasis (impaired glutamate transporters), excitotoxicity, oxidative stress and glial scar formation (Eddleston and Mucke, 1993; Sofronview et al., 1999). Like microglia, reactive astrocytes are also known to play a neuroprotective role during neurodegenerative conditions depending on the region, time, duration and severity of the insult. For example, ablation of reactive astrocytes was shown to cause neurodegeneration and increased neuroinflammation in the brain of adult transgenic mice (Sofronview et al., 1999). Other studies have demonstrated its role in neural and oligodendrocitic repair and protection from inflammation in traumatic brain injury models in transgenic mice (Sofronview, 2010). To date, most of the studies on astrocytes in the animal models of inflammation have primarily confirmed their role in regulating inflammation rather than as neuroprotective agents (Allaman et al., 2011; Chung et al., 2010; Vezzani et al., 2011).

The contribution of reactive astrocytes to neurodegenerative diseases involves alterations in astrocytic functions which includes several molecules and signaling pathways. Some of them include changes in potassium buffering, glutamate uptake from the extracellular space, modulation of aquaporins and adenosine activity, disturbance in gap junctions,

dysfunctional glutamate-glutamine cycle and cystine-glutamate antiporter system and mutations in potassium channel genes (Coulter and Steinhauser, 2015; de Lanerolle et al., 2010; Eddleston and Mucke, 1993; Eng and Ghirnikar, 1994). Several studies have documented the role of reactive astrocytes in exacerbating BBB integrity in TLE models. The damage to BBB during SE causes leukocyte infiltration in the CNS and extravasation of serum albumin in astrocytes (Puttachary et al. 2016a). The serum albumin binds to TGFβ receptors to phosphorylate Alk5 mediated SMAD2/3 complex and p-38 MAPK which translocates to the nucleus to transcribe proinflammatory genes promoting TGFβ and IL-6 production (Milikovsky et al., 2017).

Extravasation of serum albumin can impair potassium buffering and glutamate reuptake in astrocytes by downregulating Kir4.1 potassium channels and glutamate transporters resulting in increased extracellular K^+ and glutamate concentration causing hyperexcitability (Steinhauser et al., 2016). Excessive glutamate in the extracellular space can cause dysfunctional cystine/glutamate antiporter system (CGS). CGS is an important anti-oxidant system in the astrocytes that plays a protective role during oxidative stress by importing oxidized cystine into the cell in exchange for glutamate. CGS regulates movement of both the amino acids in and out of the cell, depending on the cellular requirements. This system has been described in few experimental models such as in human fetal lung fibroblasts by Bannai and Kitamura and in rat hepatoma cell line by Makowske and Christensen (Bannai, 1986; Lewerenz et al., 2013). CGS plays an important role in the regulation of immune system, resistance against anti-cancer drugs, cancer prevention/protection against carcinogenesis, maintenance of cellular redox homeostasis and modulation of memory and behaviour. The intracellular concentration of cystine is generally lower, exists in a reduced form, in the cell

while that of glutamate is higher (Lewerenz et al., 2013). Cystine is an important substrate for the production of glutathione. Inside the cell, oxidized cystine is reduced to form glutathione with the help of enzyme thioredoxin reductase 1 (Lewerenz et al., 2013; Mandal et al., 2010). During pathological conditions, dysfunctional CGS can result in oxidative stress in the cell due to its inability to maintain balance between anti-oxidant (such as glutathione) and oxidants which are generated as a result of glutamate excitotoxicity. When the levels of ROS and calcium reaches maximum, Bid (member of Bcl-2 family) translocates to the mitochondria. This mitochondria-Bid complex activates apoptosis inducing factor (AIF) which translocates into the nucleus resulting in the production of caspases causing cell death (Landshamer et al., 2008; Lewerenz et al., 2013). During inhibition of CGS, the glutathione levels decline. After an optimum level of glutathione depletion has reached, ROS production starts increasing. They do not cause cell death immediately but instead facilitate the activation of several signalling pathways that ultimately culminates into cell death. Several studies have reported that neuroprotective compounds that generally do not show beneficial effects during the chronic stages of the disease, when administered at early time-points (when ROS concentration is gradually increasing post insult), can have favourable outcomes (Lewerenz et al., 2013; Maher and Schubert, 2000). Studies have shown that an increase in CGS in conditions like brain tumours and multiple sclerosis could primarily be due to an increased glutamate accumulation and release (Chung et al., 2005; Pampliega et al., 2011). This rise in extracellular glutamate was a result of excitatory amino acid transporters (EAATs) downregulation that balance CGS mediated glutamate release. Therefore, inhibition of CGS, specifically targeting glutamate, may play an important role for treating CNS disorders by balancing excessive glutamate release (from CGS) into the extracellular space and their uptake by EAATs. The drugs that

protect from glutamate excitotoxicity acts mainly through this mechanism of action and inhibit excitotoxic effects of CGS by increasing glutathione synthesis and modulating glutamate release (Lewerenz et al., 2013).

The gap junction coupling between neurons and astrocytes is a mode of intercellular communication where the exchange of small molecules such a nutrients, ions and amino acids take place between the cells (Steinhauser et al., 2016). Although the role of gap junction dysregulation in epilepsy is still controversial, some studies have demonstrated anti-epileptic role of these junctions during astrocytic coupling. According to the spatial buffering concept, astrocytes pass excessive K^+ ions between their networks reducing K^+ concentration in extracellular space. Furthermore, studies on $Cx30^{-/-}$ mice (a gap junction protein) and brain slice experiments on these mice showed increased neuronal depolarization and reduced seizure threshold with disturbances in potassium and glutamate clearance in astrocytes. This caused abnormal neuronal synchronization and increased epileptic activity suggesting anti-epileptic role of gap junctional proteins in some epilepsy models (Steinhauser et al., 2016; Wallraff et al., 2006**)**.

The role of other molecules such as aquaporins and gliotransmitters like calcium, glutamate and ATP have also been widely explored in the pathogenesis of epilepsy and in other neurodegenerative conditions. Mutations in aquaporin 4 disrupts regulation of fluid osmolarity and potassium homeostasis (Schwartzkroin et al., 1998); disruption of glutamate-glutamine cycle results in unstable glutamate and GABA levels that causes imbalance between excitation and inhibition (Otis and Jahr, 1998; Steinhauser et al., 2016); rise in intracellular calcium levels cause increased proinflammatory molecules such a cytokines and prostaglandins (Bezzi and Volterra, 2001); ATP metabolizes to form adenosine, which has anti-convulsive effects but

can also be proconvulsive, if it binds to purinergic receptors such as P2X as have been shown in various animal models (Dunwiddie and Masino, 2001; Schubert et al., 1986).

Background and Literature Review – I

Nitric Oxide: An overview

Nitric oxide (NO) is a gaseous signaling molecule which is formed by the action of L-arginine on heme-containing enzyme nitric oxide synthase, in the presence of NADPH and molecular oxygen, and release NADP and citrulline as by-products (Benarroch, 2011; Dawson and Dawson, 1996; Nelson et al., 2003; Rodeberg et al., 1995). It is a diatomic free radical small lipid soluble molecule which can diffuse easily between the cell membranes.

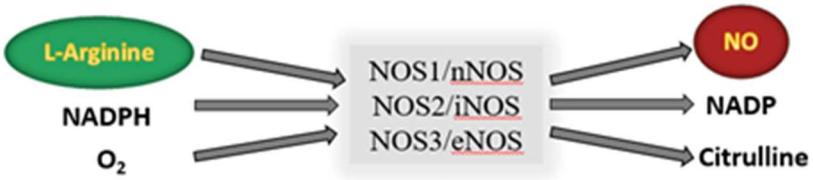

Figure 4. Formation of nitric oxide from the substrate L-arginine and nitric oxide synthase enzyme in the presence of cofactor NADPH and molecular oxygen.

Since it is not stored and easily degradable, NO reacts and is utilized quickly with a short half-life in the circulation. It plays an important role in the dilation of blood vessels, maintenance of synaptic plasticity, wound healing, regulation of blood flow, electrolyte homeostasis, vascular relaxation, synthesis of DNA repair enzymes, leukocyte adhesion, platelet aggregation, cognition and neural protection and neurotransmission (Rosselli et al., 1998; Tousoulis et al., 2012). Its cell-specific expression, type of NOS isoform activated, time, duration and severity of insult determines whether NO will regulate neuroprotective or neurotoxic effects (Benarroch, 2011). NO generally mediate most of its activities through

guanylyl cyclase activation. During normal conditions, soluble guanylyl cyclase displays anti-inflammatory effects by preventing gliosis (Brown, 2010). NO synthesizing enzyme, iNOS, plays a protective role in the regulation of blood pressure by inhibiting endothelin-1 (Lind et al., 2017). NO can also promote neuroprotection by stimulating CREB phosphorylation, activating antiapoptotic Akt pathway involved in neuromodulation and synaptic plasticity, inhibiting caspase-3 activation, heme oxygenase 1, histone deacetylase 2 and NFkB and regulating post-translational protein modification such as S-nitrosylation by modulating NMDA receptor induced calcium influx (Benarroch, 2011). Under pathophysiological conditions, excessive NO can cause DNA damage, affect protein synthesis, increase lipid peroxidation and nitrosylation of proteins and inactivate body's anti-oxidant system causing inhibiton of mitochondrial respiration resulting in oxidative stress (Puttachary et al., 2015a; Nelson et al., 2003). NO regulates its mechanism of action through intracellular guanylyl cyclase (GC) signaling (Nelson et al., 2003). The binding of NO to soluble GC catalyses the production of a second messenger, cyclic guanosine-3',5'-monophosphate cyclic (cGMP), which activates downstream effectors like protein kinases (protein kinase G), transcription factors (CREB) and cyclic nucleotide gated channels to arbitrate cellular effects and modulate gene expression through activation of MAP kinase and AP-1 (Lamas et al, 2007). For instance, in smooth muscle cells, NO regulated signaling causes inhibition of calcium channels which results in muscle relaxation and vessel dilation. Moreover, NO-GC-cGMP activation also plays an important role in treating erectile dyfunction problems, during peristalsis, neural blood vessels innervation, inhibition of platelet aggregation (Nelson et al., 2003), phosphorylation of various proteins, gating of cation channels, regulation of phosphodiesterases and activation of ADP-ribosylation factor responsible for neurotransmitter release (Dawson, 1992).

Nitric oxide synthases (NOSs)

NOS catalyzes the conversion of L-arginine into NO in the presence of molecular oxygen and NADPH to release NADP and citrulline (Benarroch, 2011; Dawson and Dawson, 1996; Rodeberg et al., 1995). NOS utilizes cofactors such as flavins like FMN and FAD and biopterin for its activation to produce NO and citrulline as byproducts (Andrew and Mayer, 1999; Dawson, 1992; Mayer and Andrew, 1998). It is generally present in two forms, constitutive and inducible. The constituve forms include nNOS and eNOS while inducible forms include iNOS. A fourth isoform has also been reported called mitochondrial nNOS (Bates et al., 1995), but it is not clear whether this isoform is an independent isoform or is a post-translational modification of nNOS. Although, all the three isoforms differ in their cellular specificity, activation and functions, the one thing that makes them identical is their carboxy reductase and amino oxygenase domain in their structure (Andrew and Mayer, 1999; Mayer and Andrew, 1998).

nNOS is abundantly concentrated around the post-synaptic membranes and in the cytoplasm of the neuronal cells (Brown, 2010**;** Cherian et al., 2006) of the central nervous system. It is mainly found in cerebral cortex, hippocampus, olfactory bulb, striatum, thalamus, hypothalamus, dorsal root ganglion and some blood vessels (Benarroch, 2011). In the brain, nNOS is generally activated by calcium-CamKII complex which involves the employment of NMDA receptors. This NMDA mediated calcium-CamKII regulated NO activation plays an important role in learning and memory via CREB activation in the hippocampus, (Andrew and Mayer, 1999; Mayer and Andrew, 1998) in the maintenance of synaptic plasticity (Kato et al., 2005), regulation of NMDA receptor function in the development of motor neuron dendrites, chemical transmission, cell protection and anti-apoptosis (Benarroch, 2011).

eNOS is found in the endothelium and is mainly involved in regulating blood flow in the cerebral vasculature and in the aggregation of platelets (Andrew and Mayer, 1999; Cherian et al., 2006; Moncada et al., 1991). It is abundantly found in vascular endothelium, pyramidal cells of hippocampus and granule cells of the dentate gyrus (Benarroch, 2011). Like nNOS, it is Ca^{2+} dependent which gets activated in response to a physical stimuli such as sheer stress (Andrew and Mayer, 1999; Mayer and Andrew, 1998; Moncada et al., 1991). The primary regulator of eNOS's expression is CREB which governs its activites like vasodilation and inhibition of platelet aggregation (Benarroch, 2011).

iNOS, an inducible form of NOS, is not constitutively expressed under normal conditions. It is mainly upregulated in the immune cells such as microglia and macrophage and also in astrocytes when exposed to endotoxins and proinflammatory cytokines like IL-1, TNFα and IFNγ. iNOS mechanism of action is governed under the control of expression regulators such as NFkB, interferon regulatory factor-1 and hypoxia-inducible factor 1 (Benarroch, 2011; Kato et al., 2005; Meyer & Andrew, 1998; Nomura and Kitamura, 1993) which regulate functions like cellular toxicity and apoptosis (Benarroch, 2011). Since iNOS is Ca^{2+} independent, it can therefore remain permanently activated and kill pathogens such as virus and bacteria even at smaller amounts. Nonetheless, iNOS can cause neuroinflammation and severe damage in the system, if overly expressed during this activation period (Xie and Nathan, 1994) as shown in various CNS and PNS models. However, there are some reports which have described the protective role of iNOS during pathological conditions. For example, experiments with infact rat models have shown that inhibiting iNOS caused increased cortical hypoperfusion and ischemic neuronal injury (Lind et al., 2017). Inhibiting iNOS has also been shown to cause increased atherosclerotic plaque formation (Brunner et al., 2015) while

decrease in atherosclerosis was linked to increased iNOS expression (Chan et al., 2016). Other reports on iNOS deficieny and $iNOS^{-/-}$ knockout models demonstrated high rates of mortality in mice with sepsis (Cobb et al., 1999), increased kidney problems exhibiting high rates of apoptotis in kidney tubules (Miyajima et al., 2001) and enhanced inflammation in the intestines of the $iNOS^{-/-}$ mice in comparison to wild types (McCafferty et al., 1997) suggesting important role of iNOS in both central and peripheral nervous system.

Nitric oxide during pathological conditions

NO can have both neuroprotective and neurotoxic effects on the brain depending on the concentration, type of NOS involved, region of the brain and the time of its release. An excessive NO production causes generation of inflammatory signals which results in excessive S-nitrosylation and/or nitrotyrosylation of proteins and formation of reactive species such as peroxynitites (Benarroch, 2011). Accumulation of these events, over time, can result in neurodegenerative conditions such as Alzheimer's diseas, Parkinson's, Huntington's and Epilepsy. During such conditions, NO forms a highly reactive molecule called peroxynitrite ($ONOO^-$) in the presence of superoxides released by mitochondria and xanthine oxidase. $ONOO^-$ also gets metabolizes into hydroxyl free radicals and nitrogen dioxide causing lipid peroxidation. The release of such oxidative stressors inhibit mitochondrial respiration, superoxide dismutase (SOD) and catalase disturbing the balance between oxidants and anti-oxidants. This alteres calcium homeostasis, modulates programmed cell death mechanisms and causes synaptic damage ensuing neurotoxicity and ultimately cell death (Dawson, 1992; Puttachary et al., 2015a; Yuste et al., 2015). Under physiological conditions, harmful peroxynitrites are reduced by SOD and anti-oxidant glutathione (GSH) that helps to keep cell

under stable homeostatic conditions. The shift of L-arginine/NO pathway towards the formation of free NO, that reacts with molecular oxygen and GSH to form S-nitrosoglutathione (GSNO), serves as a short term storage system for the release and transport of NO under physiological conditions (Andrew and Mayer, 1999; Gordge et al., 1996). The cleavage of GSNO releases free NO and oxidized glutathione (GSSG). Therefore, whether this cleavage and release of GSSG results in oxidative stress or is a defense mechanism against infection is yet not clear (Mayer and Andrew, 1998).

S-nitrosylation, a post-translational modification of proteins where NO reacts with oxygen to form nitrosonium ion and interacts with thiols to form S-nitrosothiol (Benarroch, 2011), can occur simultaneously to cause oxidative and nitrosative stress that can activate apoptotic factors in the mitochondria stimulating cell death and proinflammatory signaling pathways. This effects proteins like glyceraldehyde-3-phosphate dehydrogenase (GAPDH), Hsp90, parkin and complex I and IV that play a role in cellular metabolism, transcription, regular apoptosis, protein folding, mitophagy and cell survival (Benarroch, 2011). During these events, iNOS produces increased amounts of NO and concurrently triggers calcium dependent increase of nNOS resulting in calcium overload in the cell via NMDA receptor activation leading to excitotoxicity (Benarroch, 2011; Zhou and Zhu, 2009).

Several transcription factors, regulating the transcription of iNOS and inflammatory genes, are activated in the nucleus after NFkB translocation which binds to kB elements on iNOS promoter (Yuste et al., 2015). The NFkB mediated production of iNOS causes increased NO synthesis and ONOO- production in the glial cells followed by COX-2 production and prostaglandin synthesis. The binding of prostaglandins to prostanoid receptors, EP1 and EP2, on neurons activate these receptors stimulating intracellular calcium levels and activates

second messenger cAMP resulting in hyperexcitability, neuronal injury and inflammation (Lalitha, 2018). Increased intracellular calcium levels also increases enzymatic activity of phospholipaseA2 generating more prostaglandins through the action of COX-2 on arachidonic acid. TNFα and IL-1β are the key inflammatory cytokines in the brain. During inflammation, IL-1β is activated via NMDA receptor activity enhancing calcium release through Src family kinase activation (Viviani et al., 2003). Fyn, a member of Src family kinase, regulates iNOS expression via ERK phosphorylation as has been demonstrated in LPS-stimulated astrocytic cultures (Ko et al., 2018). The binding of IL-1β to IL-1β receptors activates MYD88-TRAF6 complex stimulating MAP kinase signaling pathway (Lalitha et al., 2018) resulting in NFkB nuclear translocation. In the nucleus, NFkB associates with p300 which is an acetyltransferase coactivator that causes acetylation of p65 subunit of NFkB at residue K310. This is important to achieve the transcriptional activity of NFkB for the transcription of inflammatory genes and iNOS (Ghasemi and Fatemi, 2014). iNOS can also activate COX-2 increasing the generation of ROS through NADPH oxidase dependent mechanism (Lind et al., 2017). Increased levels of NO also modulates glutamate and potassium buffering in the astrocytes by downregulating its channels and transporters through unknown mechanisms. As a consequence of this, potassium and glucose levels rise in the extracellular space causing hyperexcitability (Puttachary et al., 2016a).

Nitric oxide and epilepsy

The effects of NO are largely mediated either through the activation of soluble guanylyl cyclase and/or nitrosylation of cytosolic and membrane proteins. For example, S-nitrosylation modulates NMDA receptor activity (Lei et al., 1992; Manzoni et al., 1992) and limits excessive

Ca^{2+} influx to protect neurons. However, the role of NO as a protective or toxic molecule depends on the time and the source of NO production following an insult and, most importantly, the isoform of NO synthase (NOS) involved. The substrate for NO production is one of the essential amino acids, arginine, which is also a limiting factor for NO production/regulation. Three major isoforms of NOS catalyze the formation of NO. Based on the abundance of NOSs in various cell types, NOSs are classified as neuronal NOS (nNOS), inducible NOS (iNOS), and endothelial NOS (eNOS). Pharmacological inhibitors have been used to target these enzymes to regulate the levels of NO in various *in vitro* and *in vivo* models with conflicting outcomes (Thippeswamy et al., 2006). Several studies have also highlighted the controversial pathophysiological roles of NO in the peripheral and central nervous systems (Chung et al., 2005; Cosgrave et al., 2008; Moncada & Erusalimsky, 2002; Puttachary et al., 2016a; Thippeswamy et al., 2006). These conflicting outcomes could be due to inappropriate use of NOS inhibitors with respect to selectivity, dose and time of treatment (pre or post insult), solvents used as vehicle and the method of reconstitution, and route/method of administration (Kato et al., 2005; Kovacs et al., 2009). NO has been shown to have both anticonvulsive (Sardo & Ferraro, 2007) and proconvulsive actions (De Sarro & De Sarro, 1993), which seems to depend on the species and the types of chemoconvulsants employed in the study (Cosgrave et al., 2008). All three NOS isoforms are expressed during epilepsy, but at different stages of seizures or epileptogenesis. For example, eNOS is upregulated in a rodent model of SE within 3 to 24 hr of intracranial injection of kainate (Chuang et al., 2007), while nNOS and iNOS are upregulated in the mouse model of electrically induced SE (Catania et al., 2003). In the rat kainate model, nNOS and iNOS are upregulated in less than 3 days post SE and persist for a longer duration (Cosgrave et al., 2008; Vezzani et al., 2011).

nNOS in SE and epileptogenesis

It is challenging to develop a single drug to act on multiple targets without having any adverse effects. All drugs have off-targets to a variable proportion, which causes side effects accordingly. It is customary to weigh the benefits of a drug against side effects in a given situation. A drug that targets an event or molecules during SE may not be effective during the post-SE period if the target molecule of interest is not expressed in a significant amount during epileptogenesis. For example, the nNOS-mediated NO production was thought to play an important role during SE. The brain slice experiments have demonstrated the neuronal source of endogenous NO as a key promoter for initiating seizure-like events in the hippocampal formation and entorhinal cortex (Kovacs et al., 2009). Beamer et al. (2012) tested the hypothesis in the mouse kainate model with the nNOS-specific inhibitor L-NPA, which has 149- and 3158-fold greater selectivity over eNOS and iNOS, respectively (Beamer et al., 2012; Zhang et al., 1997). Initially they tested the anticonvulsive effect of nNOS inhibition in mice by treating with L-NPA (20 mg/kg, i.p.) 30 min prior to the induction of SE with kainate. Kainate is a glutamate analogue that causes seizures with a hippocampal focus and is widely used to develop models of TLE in rodents (Ben-Ari & Cossart, 2000). L-NPA pretreatment significantly reduced the severity and duration of CSs, gamma EEG power, and epileptiform spike rate during SE and also during the first 7 days post SE (Beamer et al., 2012). Moreover, the histology of brain sections revealed a significant reduction of c-Fos, a cellular marker of neuronal hyperexcitability, in dentate granule cells at 2 hr post SE (Beamer et al., 2012). These results suggest that nNOS also facilitates seizure generation during SE. Reactive gliosis, neurodegeneration, and neurogenesis are the most commonly recognized features of epileptogenesis (Parent & Lowenstein, 2002; Puttachary et al., 2016a; Vezzani et al., 2011).

To get a better understanding of these, IHC was performed on brain sections collected at 3 days post SE from the L-NPA experiments. A significant reduction in hippocampal microgliosis and astrogliosis was observed in the L-NPA–pretreated group compared with the vehicle control group, since the initial SE severity was compromised in the L-NPA–pretreated animals (Beamer et al., 2012). However, neurodegeneration and neurogenesis were not significantly changed at 3 days post SE. It was suggested that C57BL/6J mice are resistant to kainate-induced neurodegeneration (Schauwecker, 2012; Schauwecker & Steward, 1997). However, we have demonstrated neurodegeneration in C57BL/6J mice using Fluoro-Jade B and NeuN costaining in the hippocampal formation, entorhinal cortex, and amygdala at 7 days post SE (Puttachary et al., 2016b). Likewise, gliosis (both astrogliosis and microgliosis) reached its maximum at 7 days post SE, but decreased at later time points, in contrast to the rat kainate model of TLE (Puttachary et al., 2016a). These are important differences between the C57BL/6J mouse kainate model and the rat kainate model. In cross-bred mice and rats, we observed reactive gliosis and neurodegeneration as early as 24 hr post SE (personal observation, unpublished work), and in the rats they persisted throughout the period of epileptogenesis and also during the chronic phase (Puttachary et al., 2016a). Interestingly, neurogenesis persistently increased in C57BL/6J mice during epileptogenesis (at 7 days post SE), perhaps to compensate for the ongoing neurodegeneration (Puttachary et al., 2016b). It is also interesting to note that SE increases activity-dependent synaptogenesis in the outer and middle molecular layers of the dentate gyrus in the early stage of epileptogenesis, observed at 72 hr post SE in C57BL/6J mice, which was suppressed in the L-NPA–treated group (Beamer et al., 2012). The suppressed gliosis and neo-synaptogenesis at 3 days post SE in the LNPA–treated group were not due to the direct effects of nNOS inhibition but, instead, were due to

compromised initial severity of SE owing to the pretreatment approach. The results from pretreatment experiments of test drugs provide proof-of-concept for their antiseizure efficacy and confirm that the decreased severity of seizures during SE dampens the events of epileptogenesis. A similar conclusion can be drawn from gene knockout or transgenic mice experiments. Therefore, to confirm the antiepileptogenic or antiepileptic effects of a pharmacological agent or gene of interest from the translational aspect, intervention strategies during the post-SE period are appropriate for investigating disease-modifying agents in epilepsy.

Other inhibitors such as 7-nitroindazole (7-NI), a selective inhibitor if nNOS (Moore et al., 1993), has nociceptive actions and have been shown to be protective against neurodegenerative conditions such as Parkinson's disease (Schulz et al., 1995). However, some studies have argued on its nNOS selective role and have rather primarily focused on its non-NOS roles (Andrew and Mayer, 1999; Mayer and Andrew, 1998). Additional nNOS inhibitors include isothiourea derivaties such as AMITU and amidine derivative ARL 17477 (Shearer et al., 1997). Athough most of the compounds from these groups target nNOS activity, some reports have argued their stronger action towards NADPH-depenent O_2^- production than on nNOS directly. Moreover, in number of experiments on the cultured brain slices and in *in vivo* studies, these compounds have failed to show complete nNOS inhibition and inadequate pharmacokinetic profile (Andrew and Mayer, 1999). Therefore, there is an urgent need to explore strong, potent and isoform-selective NOS inhibitors, yet with low toxicity, as a promising agent for disease modification in epilepsy and for similar neurodegenerative conditions.

iNOS and NOS inhibitors in epileptogenesis

Some of the earlier NOS inhibitors that were discovered to study the role of NO in biological systems were N^G-methyl-L-arginine, N^G-nitro-L-arginine, L-Thiocitrulline etc. Although most of these compounds inhibited NOS with high affinity and potency, they did not reveal much information on the isoform selectivity of NOS. Moreover, these compounds were also not strong enough to prevent the generation of oxygen free radicals after their inhibiton (Andrew and Mayer, 1999). Therefore, the complex role of NOS in epilepsy and similar neurological conditions owes to cell-specific expression of its three different isoforms expressed at various stages of epileptogenesis. As mentioned earlier, the neuronal source of NO produced by nNOS-mediated mechanism promotes seizures. Both *in vitro* and *in vivo* studies have confirmed a proconvulsive role of NO in acute models (Beamer et al., 2012; Kovacs et al., 2009). IHC of the brain sections at 3 days post-SE in the rat kainate model of TLE showed a significant increase in nNOS levels in neurons and iNOS (iNOS/NOS2) in microglia (Cosgrave et al., 2008). Because we knew from our previous work that L-NPA pretreatment reduces SE severity and epileptiform spikes, we further tested whether post-treatment would have a similar beneficial effect or not. Surprisingly, we observed a marginal increase, rather than the anticipated significant decrease, in epileptiform spike rate and gliosis at 24 hr and 72 hr post SE between the vehicle and L-NPA–treated groups. This may suggest a beneficial role of nNOS during the early stages of epileptogenesis in contrast to its proconvulsive role during acute seizure onset (i.e., SE). It has been shown that a transient increase in nNOS, following insult to the brain, protects neurons by S-nitrosylation of the NR2B subunit of NMDAR to control excessive calcium influx (Campelo et al., 2012; Gidday et al., 1999). Because we did not observe expected modifications in early epileptogenesis by

inhibiting nNOS with L-NPA, we focused our investigation on the role of inducible nitric oxide synthse in epileptogenesis.

The increased levels of iNOS in the brain have not only been reported in various rodent models of TLE but also in other neurodegenerative disease models such as Parkinson's and Alzheimer's (Park et al., 2001; Puttachary et al., 2016a; Rehni et al., 2009). *In vitro* and *in vivo* studies have shown the upregulation of iNOS in glial cells after 4 h, reaching peak at 24 h, following LPS treatment. NO levels were significantly higher at 72 h after the initial insult (Nomura and Kitamure, 1993). Moreover, studies on mixed culture models demonstrated the role of iNOS in regulating neuronal cell death as early as 3 d post insult via calcium-CaMKII mediated mechanisms (Dawson and Dawson, 1996). In a recent study by Puttachary et al., (2016a) on the *in vivo* rat model of TLE, we demonstrated the neuropathological role of iNOS in regulating gliosis, neurodegeneration and in the maintenance of epileptiform activity and CS by using iNOS inhibitor, 1400W (Puttachary et al., 2016a). Similar studies have also demonstrated the role of iNOS in conditions like stroke and traumatic and ischaemic brain injury using pharmacological inhibitors of iNOS suggesting its potential role in neurodegenerative diseases (Armengou et al., 2003; Beamer, 2012; Jafarian-Tehrani et al., 2005).

1400W indeed significantly suppressed kainate-induced epileptiform spikes in the brain slices (Puttachary et al., 2016a). 1400W is a slow, tight binding, and highly selective pharmacological inhibitor of iNOS with a Kd value of 7 nM. It is > 5000-fold and > 200-fold selective for iNOS than eNOS and nNOS, respectively (Alderton at al., 2001; Garvey et al., 1997; Jafarian-Tehrani et al., 2005; Parmentier et al., 1999). It is biologically active *in vivo* and has no pulmonary or cardiovascular side effects, and the physiological activities mediated

by eNOS and nNOS are not compromised at the optimum dose of 20 mg/kg (Eissa and Huston, 2003; Garvey et al., 1997). 1400W is BBB permeable and has shown to suppress abnormal levels of NO metabolites in rodents (Crowell et al., 2003; Garvey et al., 1997; Parmentier et al., 1999). It is 100 times more potent than other iNOS inhibitors (ED50~ 0.3 mg) in reducing delayed vascular injury in the rat lipopolysaccharide model (Garvey et al., 1997). 1400W's mechanism of action involves targeting the binding site of L-arginine on NOS functional group. 1400W has amidine moiety which is a structural analogue of L-arginine's guanidine moiety. 1400W competes for L-arginine's binding site on iNOS's L-arginine's guanidine moiety on its functional group. The binding of 1400W on iNOS inhibits iNOS activation preventing NO synthesis (Garvey et al., 1997). iNOS-1400W binding is irreversible and can have a prolonged effect on its target (Alderton et al., 2001; Garvey et al., 1997). This may explain the reason why long-term neuroprotective effects of 1400W were observed in the rat kainate model even six months after the initial dosing of 1400W post-SE (Puttachary et al., 2016a).

Importantly, studies have shown that rats tolerated a dose of 120 mg/day for a 7-day period when 1400W was administered as intravenous infusion; however, it was lethal at 50 mg/ kg when given as a single intravenous bolus (Garvey et al., 1997). As discussed earlier, this is an important finding considering the reported controversial roles of NO in brain pathology (Chung et al., 2005; Dawson & Dawson, 1998; Dawson & Snyder, 1994; Moncada & Erusalimsky, 2002; Thippeswamy et al., 2006). The treatment with 1400W, at 20 mg/kg, effectively ameliorated brain pathology and suppressed seizures by > 90% in the rat kainate model of chronic epilepsy in a 6-month continuous video EEG study (Puttachary et al., 2016a). In traumatic brain injury (TBI) and stroke models, it reduced brain injury by decreasing

glutamate release (Jafarian-Tehrani et al., 2005; Parmentier et al., 1999; 2005). 1400W also protected BBB integrity, which is compromised soon after SE (Boje, 1996; Puttachary et al., 2016a). Serum albumin (SA) is considered as a biomarker for BBB leakage (Frigerio et al., 2012). Increased SA and glutamate levels induce reactive astrogliosis that cause hyperexcitability of neurons and, hence, seizures (Boje, 1996; Frigerio et al., 2012; Weissberg et al., 2015). Our previous studies from the rat and mouse epilepsy models have shown increased serum albumin and glial fibrillary acidic protein (GFAP) levels in the hippocampus at 7 days post SE, and 1400W treatment reduced their levels (Puttachary et al., 2016a). 1400W also reversed SE-induced suppression of Kir 4.1 and GLT1 levels, perhaps by reducing reactive gliosis, which could also be due to decreased levels of glutamate and SA (Puttachary et al., 2016a). Overall, these changes attenuated neuronal excitability, which was evident from a significant reduction in the epileptiform spike rate and seizures in the rat kainate model (Puttachary et al., 2016a). 1400W reduced neurodegeneration, as indicated by a reduction in the FJB positive neurons, both at 7 days and at 6 months post SE (Puttachary et al., 2016a). These findings provide evidence for the long-term neuroprotective role of 1400W and its disease-modifying properties in epilepsy.

1400W is commercially available as a pure (>99%) water-soluble compound. It has been tested in healthy human volunteers, patients with heart failure (Dover et al., 2006; Sharma et al., 2017), and liver cirrhosis (Ferguson et al., 2006). There were no adverse effects of 1400W in humans, and no toxicity has been reported. It effectively suppressed inflammatory mediators in human cartilage derived from osteoarthritic patients and in a rat neuropathic pain model (Jarvinen et al., 2008; Makuch et al., 2013). Other iNOS inhibitors such as L-NILTA (referred to as SC-51 in the literature), VAS203 (Sharma et al., 2017) and KD7040 are in

clinical trials for asthmatic humans (and healthy volunteers), TBI patients and neuropathic pain, respectively (Hansel et al., 2003). Collectively, these studies strongly support the therapeutic potential of iNOS inhibitors, and 1400W in particular, as a promising drug for disease modification not only in epilepsy but also for various other disorders.

Background and Literature Review – II

Fyn Kinase: Overview

Fyn kinase is a member of Src family kinase (SFK) which belongs to the non-receptor tyrosine kinase family of proteins. There are nine members in this group with similar structural features and amino acid sequence homology. The members in SrcA subfamily includes Fyn, Src, Yes and Fgr, SrcB subfamily includes Lck, Blk, Hck and Lyn and Frk forming its own subfamily (Thomas and Brugge, 1997). An alternate isoforms of Src (two neuron-specific isoform) and Fyn (T cell-specific isoform) have also been identified (Thomas and Brugge, 1997). Fyn kinase has 3 splice variant forms. Of these, two active forms are T and B. T is normally expressed in hematopoietic cells and B is ubiquitously expressed in the brain (Nygaard et al., 2014). These spliced isoforms differ in their amino acid sequence and functional properties (Lee et al., 2016). Src, Fyn and Yes are ubiquitously found in most of the tissues. Lyn, Fgr, Hck and Blk is mostly found in brain, B-cells and myeloid cells. Lck is expressed in T-cells and natural killer cells; Frk in the primary epithelial cells and Yrk is expressed only in the chickens (Thomas and Brugge, 1997). The Src family protein kinases have 3 Src homology (SH) domains (SH4, SH3 and SH2), one unique region, a catalytic or kinase domain and a regulatory tail. SH4 domain is responsible for regulating signals involved in lipid modification and palmitylation by cysteine (Resh, 1993), unique domain regulates

protein-protein interactions and SH3 and SH2 domains play an important role in regulating catalytic activities of SFKs. SH3 is a proline-rich domain which controls enzyme's catalytic and recruitment activities through strong inter- and intramolecular interactions between the enzyme and the target protein (Cohen et al., 1995). SH2, binds strongly to phosphotyrosine residues, also regulates the catalytic activities of the enzyme along with its localization properties (Cance et al., 1994). The catalytic or kinase domain is responsible for the majority of the enzyme's activities and gets phosphorylated/autophosphorylated at specific sites to get activated (Boggon and Eck, 2004). The difference in the activity/inactivity of SFK depends on the type of domain activated and/or phosphorylated (Boggon and Eck, 2004). For instance, SFKs are generally inactive when found in the closed loop form with C-terminal tyrosine residue phosphorylation at site 527 (Y527) during strong intramolecular interactions between SH2 and SH3 domains (Pawson 1997; Xu et al., 1997). The activation and inactivation of SFKs is controlled by several key signaling molecules and factors such as protein tyrosine phosphatases, C-terminal Src kinase (Csk) activity, Csk homologous kinase (Chk), displacement of intramolecular interactions and mutational activation, for example mutations or deletions of Y527, striatal enriched tyrosine phosphatase (STEP) and Shp2 (Frame, 2002; Thomas and Brugge, 1997). When tyrosine residue of kinase domain at site 416 (Y416) gets autophosphorylated, Y527 gets dephosphorylated, displaces from SH2 domain and becomes inactive, the enzyme forms an open loop structure. The changes in these events cause enzyme activation resulting in signaling of key events and majority of enzyme's kinase activity (Frame, 2002). For example, SFK member Src acts as a substrate for focal adhesion kinase, serves as a docking site for various proteins and phosphorylates adaptor molecules and other tyrosine kinases. Phosphorylation and activation of these molecules initiate pathways causing initiation

of translation and metabolism that regulates cellular activities such as motility, cell proliferation, survival, adhesion etc. through PI3/Akt, Ras-MAPK and STAT3 pathways. SFKs can also be activated by several receptors such a receptor tyrosine kinase (platelet-derived growth factor), integrin receptors by binding of ligands either to SH2 or SH3 domain of the enzyme and G-protein coupled receptors (β-adrenergic) (Martin, 2001). The activation through GPCR cascades (Gq) activate NMDA receptors through protein kinase C and cell adhesion kinase-β related mechanisms, whereas Gs-coupled cascade activates SFK by inhibiting RACK1 through PKA mediated mechanisms. Other receptors that increase SFK acitivities are EphB and cytokine receptors (Salter and Kalia, 2004). These receptor and non-receptor mediated events cause activation of downstream signaling pathways and proteins that play an important role in various CNS and non-CNS functions such as synaptic plasticity, synaptic density, myelination, cell migration, cell differentiation, platelet function, T-cell signaling, memory formation, cytoskeleton formation, apoptosis, long term potentiation, cell growth and gene transcription (Thomas and Brugge, 1997). The diverse role of these kinases is due to their ability to couple with different receptors and numerous cellular targets.

Role of Fyn kinase in glial cells and neurons

Fyn has been shown to be involved in the activation of several molecules and signaling pathways in various cells. For instance, in mast cells, Fyn interacts with FcεRI receptors causing PKCδ mediated degranulation, production of arachidonic acid and transcription and activation of proinflammatory cytokines through JNK and NFkB pathways (Furumoto et al., 2005). In adipocytes, it has has been shown to be involved in conditions like obesity and inflammation through GPRC5B association (Kim et al., 2012). In T cells, it plays a crucial role

in regulating T cell receptor signal transduction and proliferation and TCR mediated lymphocyte activation and secretion (Appleby et al., 1992; Cooke et al., 1991). Due to its tissue specificity and multidimensional role as both effector and regulator of various receptors/protein interactions, herein we will discuss its role in glial cells and neurons.

1. Role of Fyn kinase in microglia and astrocytes

The role of Fyn kinase in glial cells has not been widely explored. Under normal physiological conditions, glial cells are anti-inflammatory and play neuroprotective roles to support neurons and the surrounding cellular microenvironemnt (as discussed earlier). During pathological conditions, these cells secrete pro-inflammatory molecules such as cytokines and chemokines in response to inflammation. For instance, Panicker et al. (2015) recently demonstrated that Fyn kinase gets activated in microglia in response to inflammogens TNFα and LPS in the Prakinson's disease model. They further showed that Fyn activation phosphorylated PKCδ at Y311 resulting in MAP kinase activation and NFkB translocation into the nucleus (Panicker et al., 2015). NF-kB is responsible for regulating the transcription of more than 150 genes. NF-kB, after translocating into the nucleus, binds to the promoter region of the DNA thus transcribing inflammatory genes such as iNOS, IL-1β, IL-6, TNF-α etc. during inflammation (Lawrence, 2009; Liu et al., 2017). The nuclear translocation of Fyn negatively modulates the transcription of anti-oxidant genes. During stress, nuclear factor erythroid 2-related factor 2 (Nrf2) dissociates with KEAP1 complex and translocates into the nucleus to bind anti-oxidant response element activating an anti-oxidant defense system (Deshmukh et al., 2017; Kaspar and Jaiswal, 2011). Under extreme stressful conditions, Fyn also translocates to the nucleus either via GSK-3β activation or through direct translocation,

and phosphorylates Nrf2 at tyrosine 568. This exports Nrf2 from the nucleus into the cytoplasm where it undergoes proteosomal degradation. This causes dysregulation of anti-oxidant system therefore increasing inflammation (Kaspar and Jaiswal, 2011).

Recently, we demonstrated the role of Fyn as an upstream reglulator of neuroinflammation in a mice kainate model of TLE. Experiments with $Fyn^{+/+}$ (wild type) and $Fyn^{-/-}$ (knockouts) mice were performed to examine the expression of Fyn, PKCδ and other downstream regulators of inflammation in the hippocampus at different time points (4h, 24h and 7d) post-SE. Most of the oxidative stressors and proinflammatory markers were upregulated in the wild type mice and knocking out Fyn gene reversed their levels, reduced Fyn and PKCδ nuclear translocation and neurodegeneration (Sharma et al., 2018a). The inhibition of SFK, using pharmacological inhibitor Saracatinib, also alleviated Fyn and PKCδ nuclear translocation at early and late time-points as observed through nuclear fractionation studies. IHC results also revealed reduced levels of Fyn, PKCδ, 4-HNE and $gp91^{phox}$ in reactive microglia and neurodegeneration in CA3 and CA1 regions of hippocampus after saracatinib treatment suggesting the role of Fyn in epileptogenesis (chapter 5).

The role of Fyn in neurons and other cells have been widely explored but its role in glial cells such as astrocytes needs further investigation. In an experiment performed by Chun et al., (2004), Fyn mRNA expression was measured in neurons and astrocytes in different regions of the brain at various time-points using quantitative in situ hybridization in kainate induced seizures and enthorhinal cortex lesion models. They showed increased Fyn mRNA expression in reactive astrocytes which paralles with increased neurodegeneration in CA3 and CA1 region of the hippocampus. In DG, where the neurons were not damaged, lower levels of Fyn immunopositive reactive astrocytes were observed and higher Fyn expression in the

dentate granular neurons (Chun et al., 2004). Recently, in our rat model of TLE, we showed enhanced Fyn levels in reactive astrocytes in CA3 and CA1 region of hippocampus at 7 day and 4 month post-SE. Fyn immunopositive reactive astrocytes were also increased in DG, ENT and AMG at 4 month post-SE with higher number of FJB positive cells in these regions (chapter 5). Other studies, in concurrent to ours, have also shown early Fyn upregulation, and GFAP activation within 12 h of kainate administration. In these studies, Fyn was also observed in reactive glial cells at later time-points suggesting the role of Fyn in the subsequent stages of gliosis (Morgan et al., 1993; Sharma et al., 2018a). In Alzheimer's, an upregulation of spliced FynT isoform in reactive astrocytes, associated with neurofibriallry tangles and neuronal dysfunction, was observed in astrocytic cell cultures and mixed neuron-astrocyte culture models (Lee et al., 2016). The results from these and other studies provide stronger lines of evidence that upregulation of Fyn in reactive glial cells favor neuroinflammation and neurodegeneration.

2. Role of SFKs/Fyn kinase in Neurons

In neurons, Fyn plays an important role in modulating various ion channel activities of GABA and NMDA receptors. Reports have shown that Fyn has a modulatory effect on $GABA_A$ receptors, by acting on β2 and β3 subunits, and Fyn deletion alters GABA levels in the brain. The experiments on mice with genetic deletion of Fyn demonstrated that $GABA_A$ agonists had no effect on the behavioral and functional activities of these mice compared to the wild type (Boehm et al., 2004). Fyn also phoshphorylates γ2 subunit of $GABA_A$ receptor at sites Tyr 365/7 which plays a role in enhancing synaptic inhibition. Experiments have shown that knocking out Fyn gene reduced the intensity of γ2 phosphorylation, but did not completely

inhibit it, indicating the role of other SFKs such as Src in modulating $GABA_A$ activity (Jurd et al., 2010). The modulation of $GABA_A$ activity by Fyn not only plays a role in maintaining the inhibitory tone of these receptors but also in memory regulation. SFK, especially Fyn, phosphorylates Y365 and Y367 subunit of γ2 of $GABA_A$ receptors which dissociates AP2-clathrin complex with γ2 subunit. This complex promotes endocytosis of $GABA_A$ receptors and inhibits synaptic transmission. Dissociation of this complex with γ2 promotes downregulation of AP2 binding, inhibition of $GABA_A$ endocytosis and increases inhibitory synaptic transmission thus helping in the formation of spatial memory (Ohnishi et al., 2011).

Several SFKs, PKC and CaMKII are also known to phosphorylate NMDA receptors. Fyn phosphorylates NR2A and NR2B subunits of NMDA receptors, primarily NR2B at tyrosine residue site 1472 (Y1472) in forebrain synapses (Sala and Sheng, 1999). These events are associated with taste learning in insular cortex of the mice, long-term potentiation (LTP) induction in DG, CA1 of hippocampus and amygdala, regulation of endocytosis and fear-related learning in amygdala (Nakazawa et al., 2001; Ohnishi et al., 2011). SFK (Src and Fyn) mediated NMDAR NR2A activation on site Y1325 regulates depression-like behavior which involves DARP-32 site T34 phosphorylation by protein kinase A, after D1R stimulation. Moreover, SFK (Lyn) mediated phosphorylation of NR2B at site Y876 regulates AMPA receptor endocytosis via BRAG2-Arf6 mediated mechanism causing induction of long-term depression (LTD) (Ohnishi et al., 2011). Tyrosine phosphorylation of NMDA receptor is crucial for the maintenance of various cellular activities such as LTP and LTD for learning and memory, activation of cell signaling, regulation of developmental events, neurotransmitter release and modulation of ion channels (Kojima et al., 1998). The importance of Fyn in regulating multiple brain functions have consistently been demonstrated through numerous

gene knockout and knockdown studies. Mutations in Fyn gene in mice caused defective LTP and impaired spatial learning with defective hippocampal development (Grant et al., 1992). Other studies on hippocampal slices from Fyn-deficient mice showed less sensitivity towards ethanol mediated tyrosine phosphorylation of NMDA receptors which indicates that Fyn regulates biochemical, behavioral and physiological response to ethanol (Miyakawa et al., 1997). Similar experiments on Fyn deficient mice also demonstrated impaired myelination, lack of the presence of myelin-associated glycoproteins (Umemori et al., 1994), impairment of γ2 phosphorylation of $GABA_A$ and tyrosine phosphorylation of NR2B compared to wild types (Jurd et al., 2010; Sala and Sheng, 1999).

Apart from playing a key role in various CNS functions, the role of neuronal SFKs/Fyn has been widely explored during pathological conditions. Under these conditions, increased expression of SFK is generally associated with various neurodegenerative disorders, cancers and lymphomas (Sen and Johnson, 2011). The SFKs, especially Fyn and Src, forms a complex with PSD-95, a post-synaptic density protein and a member of MAGUK scaffolding protein, (Sala and Sheng, 1999) and phosphorylates NMDA receptors. Fyn is known to modulate about fifteen post synaptic density proteins (Chun et al., 2004). PSD-95 has three PDZ domains, one SH3 domain and a guanylate kinase domain (Murciano-Calles et al., 2014). PDZ2 domain interacts with NR2B subunit of NMDA receptors through C-terminal tail while PDZ3 binds to Fyn through its SH3 domain. Fyn phosphorylates Tau, and PSD-95 recruits Fyn-Tau complex to NMDA receptors and phosphorylates NR2B subunits at Y1472 thereby enhancing calcium influx, through NMDAR and L-type voltage-gated calcium channels (L-VGCC), into the cell. This causes enhanced glutamatergic currents leading to excessive SFK activation resulting in NMDA receptor trafficking at the post synaptic membrane causing excitotoxicity, spine

retraction and network dysfunction (Kalia and Salter, 2004; Nygaard et al., 2014). These events and Src/Fyn-PSD95-NR2A/2B complex activates proline-rich tyrosine kinase 2 either through PKC or calcium-calmodulin dependent mechanisms further enhancing Src/Fyn activity, NMDA receptor phosphorylation and/or L-VGCC causing calcium overload and subsequently cell death (Hou et al., 2002).

In Alzheimer's disease, amyloid β (Aβ) monomers forms Aβ oligomers. The molecular mechanism of how Fyn-Tau-Amyloid toxic triad is formed and regulated was briefly described by Haass et al., (2010). Fyn and Tau play an important role in maintaining the cytoskeletal structure of the cell. Fyn and Tau are normally localized in the dendrtites and axons of the cell. The Fyn-Tau-PSD-95 mediated NR2B phosphorylation of NMDA receptor results in excitotoxicity by stimulating toxic effects of Aβ oligomers (Haass and Mandelkow, 2010). These oligomers bind to membrane PrP^c proteins where it forms complex with mGluR5 and Fyn. This complex causes tau hyperphosphorylation, microtubule disintegration, tau aggregation and finally formation of neurofibrilliary tangles, a hallmark feature of Alzheimer's disease (Brody and Strittmatter, 2018). Tau cleavage and phosphorylation can also occur through Fyn-independent but NMDA and TNF receptor dependent mechanisms involving molecules like calpain, GSK-3β, caspase-3 and ASK1 (Avila et al., 2012; Larson et al., 2012).

Hou et al., (2003), through the rat model of transient brain ischemia, demonstrated that inhibition of PSD-95 suppressed tyrosine phosphorylation of NR2A subunit of NMDA receptor and Src and Fyn interaction with the receptor subunit in the hippocampus of the brain of postischemic Sprague dawley rats. The same group further showed that the inhibition of NMDA receptors by ketamine and L-VGCC by nifedipine inhibits similar events in those rats (Hou et al., 2003). Recently, in our rat kinate model of TLE, we detected high levels of Fyn

and PKCδ in the neurons of hippocampus, thalamus, ENT and amygdala in the vehicle-treated group at 7d, which persisted even after 4 months of post-SE. Post-treatment with SFK inhibitor, Saracatinib, reduced the levels of Fyn and PKCδ in these neurons at both the time-points (chapter 5). To date, not many studies were conducted describing the role of Fyn in the thalamus and ENT neurons, but some reports have briefly stated the role of these neurons in the development of thalamic networks and the regulation of behavior and formation of contextual memories in ENT (Yagi, 1994). Earlier experiments with transgenic mice expressing mutant and native Fyn showed that mutant Fyn mice were highly susceptible to seizures with higher mortality rates while animals with native Fyn, unlike mutant Fyn, displayed enhanced tyrosine phosphorylation of NR2B and Src kinase and increased amygdala kindling after the stimulus. Moreover, Cain et al. (1995) also demonstrated that Fyn is required for the induction of amygdalar kindling but not in the maintenance of kindling (Cain et al., 1995). Tyrosine phosphorylation of NR2A and NR2B is essential for the development of SE, therefore, in KA model of epilepsy on Long-Evans hooded rats, researchers have demonstrated that animals that develop SE exhibited higher rates of NR2A and NR2B tyrosine phosphorylation while those that did not develop SE exhibited diminished tyrosine phosphorylation (Moussa et al., 2001).

Since Fyn plays a significant role in regulating normal physiological functions in CNS, studies have shown that disruption or targeted deletion of Fyn is associated with the developmental and structural defects, especially in the hippocampus, affecting cognition due to the alterations in the factors controlling long-term potentiation and long-term depression (Kojima et al., 1998) therefore validating an important role of Fyn in the regulation of neurological functions both during normal and pathological conditions.

Src family kinase inhibitors

So far, over twenty SFK inhibitors have been identified. Of these, most widely explored ones are Dasatinib, PP2, PP1, SU6656, Quercetin, Bosutinib and Saracatinib. These inhibitors not only inhibit SFKs but also other molecules such as c-Abl, EGFR, EphB4, c-Raf, PDGFR, p38α and β, ALK, BRAF, S6, Sirtuin, PKC etc. Saracatinib, PP2, PP1 and SU6656 inhibits Fyn. Dasatinib, currently in phase 4 of clinical trials, has high inhibition potency towards Src, Abl and c-Kit with IC50 of 0.8 nM, 0.6 nM and 37 nM as has been shown in various cell-free assay experiments (O'Hare et al., 2005; Shah et al., 2006). Growth inhibition assays on BA/F3, T cell lines, HUVEC, DU145 and PC3 cell lines revealed its antiproliferative action against mouse BA/F3 cells expressing Bcr-Abl M351T and T315I mutants (Li et al., 2012) and anti-cytotoxic action against F486S, E255K, G250E, Q252H, Y253H and E359V mutants (Ren et al., 2013). Furthermore, Dasatinib was also shown to inhibit anti-CD3 and anti-CD28-induced T cell proliferation (Das et al., 2006), induce antiangiogenic activity in HUVEC co-cultured with vascular smooth muscle cells (Radi et al., 2012), inhibits human DU145 and PC3 cell adhesion and reduced pSrc-416 and phosphorylated FAK Y576/Y577 levels (Getlik et al., 2009).

PP1 and PP2 are potent and selective inhibitors of Lck and Fyn. They also inhibit EGFR, Kit, p97 and Syk (Hanke et al., 1996; Tatton et al., 2003). Functional, cytotoxic and proliferation assays of PP2 on human T cells, K562, KU812 and 8701-BC cells have revealed its inhibitory and antiproliferative activity against adhesion kinase and tyrosine phosphorylation of SFKs (Fedorov et al., 2007. Similar assays of PP1 on jurkat and mouse NIH/3T3 cells revealed its inhibition of MLR stimulated IL-2 production in jurkat cells (Arnold et al., 2000) and v-Src phosphorylation in mouse NIH/3T3 cells (Apsel et al., 2008).

SU6656 is a multi-targeted inhibitor of Src, Fyn, Lyn and Yes (Blake et al., 2000). Bosutinib is a dual inhibitor of Src/Abl and Quercetin is a multitargeted inhibitor of Sirtuins, PKC and PI3Kγ (Boschelli et al., 2001). Functional assays with SU6656 on Sf9 insect cells, functional and cytotoxicity assays with Quercetin on RBL-1, human HeLa cells, HT22, Bhuman BV2, jurkat T cells and other cell lines, and growth inhibition assays with Bosutinib on human and animal cell lines confirmed their anti-SFK, anti-oxidative and anti-cancer properties (Nguyen et al., 2014; Shi et al., 2014).

Although most of these SFK inhibitors moderately managed to inhibit the activity of a few SFKs at a given time, none of them were efficient enough to inhibit the activity of a wide range of enzymes with high potency. More importantly, off target effects of SFK inhibitors is another major problem, especially during the clinical trials. Therefore, there is an urgent need to identify novel candidate compounds for SFK inhibition with higher efficacy, potency and less off target side effects. Saracatinib is SFK inhibitor which inhibits most important and ubiquitous members of SFK such as Src, Lck, Fyn and Lyn with high potency and efficacy. It also inhibits c-Yes and EGFR (Chang et al., 2008; Green et al., 2009). Currently, it is in phase IIb of clinical trials against breast cancer (Sharma et al., 2018a) and has also been successfully tested against several forms of other cancers such as lung, bone, colorectal, skin and gastric (Dulsat et al., 2009). Its half-life in human plasma is 40 hours and no reports of toxicity have been reported in the patients at 2 and 5 mg/kg/day over the period of nine months in the human clinical trials (Nygaard et al., 2015). In other clinical studies, dose administered at 250 mg daily orally for 14 days with plasma peak concentration and terminal elimination half-life of 6 hours and 40 hours, was also rendered safe (Dulsat et al., 2009). Another phase I study conducted on healthy volunteers with different doses from 2.5 mg to 1000 mg revealed that

saracatinib was safer even at higher doses of 1000 mg, although not recommended in some cases. A very few of these patients, who were given 1000 mg, showed only mild adverse effects such as nausea, vomiting, headache, rashes and flu-like symptoms (Dulsat et al., 2009; Lockton et al., 2005). The safety profile of saracatinib was also tested in patients with different types of cancers with daily doses of 50 mg, 125 mg and 175 mg for 28 days. No side effects of saracatinib were reported in these patients (Dulsat et al., 2009) suggesting saracatinib is well tolerated and is safe even at higher doses.

Saracatinib (AZD0530) is an anilinoquinazoline compound which is now in phase III of clinical trials for Alzheimer's disease and cancer (Cummings et al., 2018). Saracatinib mode of action is primarily based on the ATP dependent mechanism. SFKs has an ATP binding moiety, where ATP molecule binds, that sits deep inside the hydrophobic and ribose pocket of the enzyme. ATP strongly binds to the enzyme with the help of two strong hydrogen bonds at Met341 and Tyr340. The most important and unique property of SFKs that makes them an excellent target for quinazoline compounds is 'gatekeeping'. SFKs have the 'gatekeeper' molecules that sits at the entrance of their pocket sites. This unique feature of the enzyme makes them even more selective for the compounds entering into their deep pockets. Due to the presence of C5 group position on the saracatinib, SFKs allow saracatinib to enter and bind to the enzyme's deep ribose pocket making strong dual hydrophobic interactions with ATP molecule and enzyme itself forming a powerful enzyme-inhibitor complex (Hannequin et al., 2006; Sharma et al, 2018a). The growth inhibition assays on various cancer cell lines and in Alzheimer's model have demonstrated saracatinib's strong inhibitory properties (Chang et al., 2008; Green et al., 2009). Recently we investigated inhibitory role of saracatinib in our rat kainate model of TLE. We observed that saracatinib treatment, after kainate administration,

reduced the number of spontaneous convulsive seizures and spike frequency in one month study (Sharma et al., 2018a). Further studies, from similar work, also revealed the short (7 day) and long-term (4 month) neuroprotective effects of saracatinib in a rat model of TLE. Its post-treatment not only reduced SRS and spike frequency during 4 month of post-SE, but also reduced reactive gliosis, oxidative stress, protein nitrosylation, neurodegeneration and Fyn and PKCδ immunoreactivity in microglia, astrocytes and neurons at both early and late time-points in DG, CA3, CA1, thalamus, ENT and amygdala (chapter 5). Furthermore, saracatinib also reduced Fyn and PKCδ nuclear translocation which prevented increased transcription of proinfammatory genes in the hippocampus (chapter 5).

Although being specific target for Src, Lck, Fyn and Lyn, saracatinib also targets c-YES, Abl and EGFR to a lesser extent. It also has an inhibitory action on other kinases such as platelet-derived growth factor receptor tyrosine kinase α and β (PDFGRα and β), cyclin-dependent kinase 2 (CDK2), Fms-like tyrosine kinase 1 and 4 (Flt-1 and 4), c-terminal Src kinase (Csk), fibrobast growth factor receptor tyrosine kinase (FGFR1) and aurora kinase-3 (AUR-3) (Green et al., 2009). Saracatinib treatment has also been show to cause cell cycle arrest and Akt blocade. It modulates the activity of Fgr, Blk, c-kit, ephrin receptor tyrosine kinase and kinase insert domain-containing receptor (KDR) (Green et al., 2009). The growth inhibition assays on various cell lines such as HT1080, DU145, PC3, PZ-HPV7, CTV-1 and BV-173 have demonstrated its strong inhibitory action against protein kinases, cancerous cell proliferation and invasion, EGF-induced cell scattering, tyrosine phosphorylation of Y419, paxillin phosphorylation, cell cycle arrest and cell migration (Chang et al., 2008; Green et al., 2009; Purnell et al., 2009).

References

1. Aguiar, C.C.T., Almeida, A.B., Araujo, P.V.P., et al. (2012). Oxidative stress and epilepsy: literature review. Oxidative Medicine and Cellular Longevity. Article ID 795259, 12 pages.

2. Alderton, W.K., Cooper, C.E., Knowles, R.G. (2001). Nitric oxide synthases: structure, function and inhibition. Biochemical Journal. 357(3):593–615.

3. Allen, N.J. and Barres, B.A. (2009). Glia- more than just brain glue. Nature. 457(7230):675-7.

4. Allaman, I., Belanger, M., Magistretti, P.J. (2011). Astrocyte-neuron metabolic relationships: for better and for worse. Trends Neurosci. 34:76–87.

5. Almoda, B., Gonzalez, B., Castellano, B. (2015). Are microglial cells the regulators of lymphocyte responses in the CNS? Front Cell Neurosci. 9:440.

6. Andjelkovic, A.V., Nikolic, B., and Pachter, J.S., Zecevic, N. (1998). Macrophages/microglial cells in human central system during development: an immunohistochemical study. Brain Rev. 814(1-2):13-25.

7. Andrew, P.J. and Mayer, B. (1999). Enzymatic function of nitric oxide synthases. Cardiovacs Res. 43(3):521-31.

8. Apland, J.P., Aroniadou-Anderjaska, V., Figueiredo, T.H., Rossetti, F., Miller, S.L., Braga, MF. (2014). The limitations of diazepam as a treatment for nerve agent-induced seizures and neuropathology in rats: comparison with UBP302. J Pharmacol Exp Ther. 351:359–72.

9. Appleby, M.W., Gross, J.A., Cooke, M.P., Levin, S.D., Qian, X., Perlmutter, R.M. (1992). Defective T cell receptor signaling in mice lacking the thymic isoform of p59fyn. Cell. 70, 751-763.

10. Apsel, B., Blair, J. A., Gonzalez, B., Nazif, T. M., Feldman, M. E., Aizenstein, B., Knight, Z. A. (2008). Targeted polypharmacology: Discovery of dual inhibitors of tyrosine and phosphoinositide kinases. Nature Chemical Biology. 4(11):691-699.

11. Andjelkovic, A., Nikolic, B., Pachter, J., & Zecevic, N. (1998). Macrophages/microglial cells in human central nervous system during development: An immunohistochemical study. Brain Research. 814(1-2):13-25.

12. Armengou, A., Hurtado, O., Leira, R., Obón, M., Pascual, C., Moro, M.A., et al. (2003). L-arginine levels in blood as a marker of nitric oxide-mediated brain damage in acute stroke: a clinical and experimental study. J. Cereb. Blood Flow Metab. 23: 978–984.

13. Aronica, E., Bauer, S., Bozzi, Y., Caleo, M., Dingledine, R., Gorter, J. A., et al. (2017). Neuroinflammatory targets and treatments for epilepsy validated in experimental models. Epilepsia. 3, 27–38.

14. Aronica, E., Boer, K., van Vliet, E.A., et al. (2007). Complement activation in experimental and human temporal lobe epilepsy. Neurobiol. Dis. 26, 497–511.

15. Arnold, L. D., Calderwood, D. J., Dixon, R. W., Johnston, D. N., Kamens, J. S., Munschauer, R., Ratnofsky, S. E. (2000). ChemInform Abstract: Pyrrolo[2,3-d]pyrimidines Containing an Extended 5-Substituent as Potent and Selective Inhibitors of lck I. ChemInform. 31(52).

16. Austin, J. K., Hesdorffer, D. C., Liverman, C. T., & Schultz, A. M. (2012). Testimonies submitted for the Institute of Medicine report: Epilepsy across the spectrum: Promoting health and understanding. Epilepsy & Behavior. 25, 634–661.

17. Avila, J., Leon-Espinosa, G., Garcia, E., Garcia-Escudero, V., Hernandez, F., Defelipe, J. (2012). Tau phosphorylation by GSK3 in different conditions. Int J Alzheimers Dis. 2012:578373.

18. Bae, Y.S., Oh, H., Rhee, S.G., Yoo, Y.D. (2011). Regulation of reactive oxygen species generation in cell signaling. Molecules and Cells. 32(6):491–509.

19. Banks W.A., Erickson M.A. (2010). The blood–brain barrier and immune function and dysfunction. Neurobiol. Dis. 37(1):26–32.

20. Banks, W.A., Farr, S.A., Morey, J.E. (2000). Permeabiity of the blood-brain barrier to albumin and insulin in the young and aged SAMP8 mouse. J Gerontol A Biol Sci Med Sci. 55(12):B601-6.

21. Bannaai, S. (1986). Exchange of cysteine and glutamate across plasma membrane of human fibroblasts. J Biol Chem. 261(5):2256-63.

22. Baraban, S. C. (2013). Forebrain electrophysiological recording in larval zebrafish. Journal of Visualized Experiments. (71), 50104.

23. Barker-Haliski, M. L., Loscher, W., White, H. S., Galanopoulou, A. S. (2017). Neuroinflammation in epileptogenesis: Insights and translational perspectives from new models of epilepsy. Epilepsia. 3, 39–47.

24. Beamer, E., Otahal, J., Sills, G. J., Thippeswamy, T. (2012). N (w) -propyl-L-arginine (L-NPA) reduces status epilepticus and early epileptogenic events in a mouse model of epilepsy: Behavioural, EEG and immunohistochemical analyses. European Journal Neuroscience. 36, 3194–3203.

25. Beghi, E. (2016). Addressing the burden of epilepsy: Many unmet needs. Pharmacological Research. 107, 79–84.

26. Berg, A.T., Darefsky, A.S., Holford, T.R., Shinnar, S. (1998). Seizures with fever after unprovoked seizures: an analysis in children followed from the time of a first febrile seizure. Epilepsia. 39:77–80.

27. Bernstein, A., Bilheimer, L. T., Makuc, D. M. (2010). Health, United States, 2010: With special feature on death and dying. Atlanta, GA: Centers for Disease Control and Prevention, National Center for Health Statistics. Report no. 2011-1232.

28. Bertram, E. H. (2013). Neuronal circuits in epilepsy: Do they matter? Experimental Neurology. 244, 67–74.

29. Bertram, E. H., Lotham, E. W., & Lenn, N. J. (1990). The hippocampus in experimental chronic epilepsy: A morphometric analysis. Annals of Neurology. 27, 43–48.

30. Bezzi, P., Carmignoto, G., Pasti, L., et al. (1998). Prostaglandins stimulate calcium-dependent glutamate release in astrocytes. Nature. 391(6664):281–285.

31. Bezzi, P. and Volterra, A. (2001). A neuron-glia signaling network in the active brain. Curr Opin Neurobiol. 11(3):387-94.

32. Bien C.G., et al. (2007). Limbic encephalitis as a precipitating event in adult-onset temporal lobe epilepsy. Neurology. 69:1236–1244.

33. Balosso, S., et al. (2005). Tumor necrosis factor-α inhibits seizures in mice via p75 receptors. Ann. Neurol. 57:804–812.

34. Benarroch, E.E. (2011). Nitric oxide: A pleiotropic signal in the nervous system. Neurology. 77: 1568–1576.

35. Bates, T.E., Loesch, A., Burnstock, G., Clark, J.B. (1995). Immunocytochemical evidence for a mitochondrially located nitric oxide synthase in brain and liver. Biochem. & Biophys. Res. Comm. 213(3):896 – 900.

36. Ben-Ari, Y., & Cossart, R. (2000). Kainate, a double agent that generates seizures: Two decades of progress. Trends in Neurosciences. 23, 580–587.

37. Blake, R.A., Broome, M.A., Liu, X., Wu, J., Gishizky, M., Sun, L., Courtneidge, S.A. (2000). SU6656, a selective src family kinase inhibitor, used to probe growth factor signaling. Mol Cell Biol. 20(23):9018-27.

38. Boehm, S.L., Peden, L., Harris, R.A., Blednov, Y.A. (2004). Deletion of the Fyn-kinase gene alters sensitivity to GABAergic drugs: dependence on β2/β3 $GABA_A$ receptor subunits. J. Pharmacol. Exp. Ther. 309, 1154–1159.

39. Boggon, T.J. and Eck, M.J. (2004). Structure and regulation of Src family kinases. Oncogene. 23, 7918-7927.

40. Boje, K. M. (1996). Inhibition of nitric oxide synthase attenuates blood-brain barrier disruption during experimental meningitis. Brain Research. 720, 75–83.

41. Bortel, A., Lévesque, M., Biagini, G., Gotman, J., Avoli, M. (2010). Convulsive status epilepticus duration as determinant for epileptogenesis and interictal discharge generation in the rat limbic system. Neurobiol Dis. 40:478–89.

42. Boschelli, D. H., Ye, F., Wang, Y. D., Dutia, M., Johnson, S. L., Wu, B., et al. (2001). Optimization of 4-Phenylamino-3-quinolinecarbonitriles as Potent Inhibitors of Src Kinase Activity. Journal of Medicinal Chemistry. 44(23):3965-3977.

43. Bradman, M.J.G., Morris, R., McArdle, A., Jackson, M.J., Thippeswamy, T. (2011). The effects of L-NAME on neuronal NOS and SOD1 expression in the DRG-spinal cord network of axotomised Thy 1.2 eGFP mice. Neuron Glia Biology. 7(2–4):129–141.

44. Brandt, C., Bankstahl, M., Tollner, K., Klee, R., Loscher, W. (2016). The pilocarpine model of temporal lobe epilepsy: Marked intrastrain differences in female Sprague–Dawley rats and the effect of estrous cycle. Epilepsy & Behavior. 61, 141–152.

45. Brody, A.H. and Strittmatter, S.M. (2018). Synaptotoxic Signaling by Amyloid Beta Oligomers in Alzheimer's Disease Through Prion Protein and mGluR5. Adv Pharmacol. 82:293-323.

46. Brown, G.C. (2010). Nitric oxide and neuronal death. Nitric Oxide. 23: 153–165.

47. Brunner, M., Gruber, M., Schmid, D., Baran, H., Moeslinger, T. (2015). Proliferation of macrophages due to the inhibition of inducible nitric oxide synthasis by oxidized low-density lipoproteins. EXCLI J. 14, 439–451.

48. Bryant, C.D., Zhang, N.N., Sokoloff, G., Fanselow, M.S., Ennes, H.S., Palmer, A.A., et al. (2008). Behavioral differences among C57BL/6 substrains: implications for transgenic and knockout studies. J Neurogenet. 22:315–31.

49. Buckmaster, P. S. (2004). Laboratory animal models of temporal lobe epilepsy. Comp Med. 54:473–85. 33.

50. Buckmaster, P. S. (2010). Mossy fiber sprouting in the dentate gyrus. Epilepsia. 51, 39–39.

51. Buckmaster, P.S., Dudek, F.E. (1997). Network properties of the dentate gyrus in epileptic rats with hilar neuron loss and granule cell axon reorganization. J. Neurophysiol. 77:2685–2696.

52. Bumanglag, A. V., Sloviter, R. S. (2008). Minimal latency to hippocampal epileptogenesis and clinical epilepsy after perforant pathway stimulation-induced status epilepticus in awake rats. Journal of Comparative Neurology. 510, 561–580.

53. Cain, D.P., Grant, S.G., Saucier, D., Hargreaves, E.L., Kandel, E.R. (1995). Fyn tyrosine kinase is required for normal amygdala kindling. Epilepsy Res. 22, 107–114.

54. Campelo, M. W., Oria, R. B., Lopes, L. G., Brito, G. A., Santos, A. A., Vasconcelos, R. C., et al. (2012). Preconditioning with a novel metallopharmaceutical NO donor in anesthetized rats subjected to brain ischemia/reperfusion. Neurochemical Research. 37, 749–758.

55. Cance, W.G., Craven, R.J., Bergman, M., Xu, L., Alitalo, K., Liu, E.T. (1994). Rak, a novel nuclear tyrosine kinase expressed in epithelial cells. Cell Growth Differ. 5(12):1347–55.

56. Cardenas-Rodrıguez, N., Coballase-Urrutia, E., Rivera-Espinosa, L., et al. (2013). Modulation of antioxidant enzymatic activities by certain antiepileptic drugs (valproic acid, oxcarbazepine, and topiramate): evidence in humans and experimental models. Oxidative Medicine and Cellular Longevity. 2013, Article ID 598493, 8 pages.

57. Catania, M. V., Giuffrida, R., Seminara, G., Barbagallo, G., Aronica, E., Gorter, J. A., et al. (2003). Upregulation of neuronal oxide synthase in in vitro stellate astrocytes and in vivo reactive astrocytes after electrically induced status epilepticus. Neurochemical Research. 28, 607–615.

58. Chaix, Y., Ferraro, T.N., Lapouble, E., Martin, B. (2007). Chemoconvulsant-induced seizure susceptibility: toward a common genetic basis? Epilepsia. 48:48–52.

59. Chan, K.C., Yu, M.H., Lin, M.C., Huang, C.N., Chung, D.J., Lee, Y.J., Wu, C.H., Wang, J. (2016). Pleiotropic effects of acarbose on atherosclerosis development in rabbits are mediated via upregulating AMPK signals. Sci. Rep. 6:38642.

60. Chang, B.S., and Lowenstein, D.H. (2003). Epilepsy. The New England Journal of Medicine. 349: 1257–1266.

61. Chang, Y., Bai, L., Liu, S., Yang, J. C., Kung, H., & Evans, C. P. (2008). Src family kinase oncogenic potential and pathways in prostate cancer as revealed by AZD0530. Oncogene. 27(49):6365-6375.

62. Cheeseman, K.H. (1993). Tissue injury by free radicals. Toxicology and Industrial Health. 9(1-2):39–51.

63. Cherian, L., Hlatky, R., Robertson, C.S. (2006). Nitric Oxide in Traumatic Brain Injury. Brain Pathology.14:195–201.

64. Choi J., Koh S. (2009) Role of brain inflammation in epileptogenesis. Yonsei Med J. 49(1):1.

65. Chhor, V., Le Charpentier, T., Lebon, S. et al. (2013). Characterization of phenotype markers and neuronotoxic potential of polarized primary microglia in vitro. Brain Behav Immun. 32, 70-85.

66. Cooke, M.P., Abraham, K.M., Forbush, K.A., and Perlmutter, R.M. (1991). Regulation of T cell receptor signaling by a src family protein-tyrosine kinase (p59fyn). Cell. 65, 281-291.

67. Chuang, Y.C., Chang, A.Y.W., Lin, J.W., Hsu, S.P., Chan, S.H.H. (2004). Mitochondrial dysfunction and ultrastructural damage in the hippocampus during kainic acid-induced status epilepticus in the rat. Epilepsia. 45(10):1202–1209.

68. Chuang, Y. C., Chen, S. D., Lin, T. K., Liou, C. W., Chang, W. N., Chan, S. H. H., & Chang, A. Y. W. (2007). Upregulation of nitric oxide synthase II contributes to apoptotic cell death in the hippocampal CA3 subfield via a cytochrome c/caspse-3 signaling cascade following induction of experimental temporal lobe status epilepticus in the rat. Neuropharmacology. 52, 1263–1273.

69. Chun, J.T., Crispino, M., Tocco, G. (2004). The dual response of protein kinase Fyn to neural trauma: early induction in neurons and delayed induction in reactive astrocytes. Exp Neurol. 185(1):109-19.

70. Chung, W. J. (2005). Inhibition of Cystine Uptake Disrupts the Growth of Primary Brain Tumors. Journal of Neuroscience. 25(31):7101-7110.

71. Chung, Y.C., Ko, H.W., Bok, E., Park, E.S., Huh, S.H., Nam, J.H., et al. (2010). The role of neuroinflammation on the pathogenesis of Parkinson's disease. BMB Rep. 43(4):225–232.

72. Cini, M., and Moretti, A. (1995). Studies on lipid peroxidation and protein oxidation in the aging brain. Neurobiology of Aging. 16(1):53–57.

73. Cobb, J.P.., Hotchkiss, R.S., Swanson, P.E., Chang, K., Qiu, Y., Laubach, V.E., Karl, I.E., Buchman, T.G. (1999). Inducible nitric oxide synthase (iNOS) gene deficiency increases themortality of sepsis in mice. Surgery. 126:438–442.

74. Cohen, G.B., Ren, R., Baltimore, D. (1995). Modular binding domains in signal transduction. Cell. 80:237–48.

75. Cosgrave, A. S., McKay, J. S., Bubb, V., Morris, R., Quinn, J. P., & Thippeswamy, T. (2008). Regulation of activity-dependent neuroprotective protein (ADNP) by the NO-cGMP pathway in the hippocampus during kainic acid-induced seizure. Neurobiology of Disease. 30, 281–292.

76. Cosgrave, A.S., McKay, J.S., Morris, R., Quinn, J.P., Thippeswamy, T. (2010). The effects of nitric oxide inhibition prior to kainic acid treatment on neuro- and gliogenesis in the rat dentate gyrus in vivo and in vitro. Histology and Histopathology. 25(7):841–856.

77. Coulter, D.A. and Steinhauser, C. (2015). Role of astrocyte in epilepsy. Cold Spring Harb Perspect Med. 5(3):a022434. Springer, Boston. ISBN 978-1-4614-4729-0, 1-587.

78. Crowell, J. A., Steele, V. E., Sigman, C. C., Fay, J. R. (2003). Is inducible nitric oxide synthase a target for chemoprevention? Molecular Cancer Therapeutics. 2, 815–823.

79. Cui, C., Grandison, C., Noronha, L. (2013). Neural-immune interactions in brain function and alcohol related disorders. Springer, 2013 edition. ISBN 978-1-4614-4729-0.

80. Cummings, J., Lee, G., Ritter, A., Zhong, K. (2018). Alzheimer's disease drug development pipeline: 2018. Alzheimers Dement. 4:195-214.

81. Dalmau J., Gleichman, A.J., Hugher, E.G., Rossi, J.E., Peng, X., et al. (2008). Anti-NMDA-receptor encephalitis: case series and analysis of the effects of antibodies. Lancet Neurol. 7(12):1091–1098.

82. Das, J., Chen, P., Norris, D., Padmanabha, R., Lin, J., Moquin, R. V., et al. (2006). 2-Aminothiazole as a Novel Kinase Inhibitor Template. Structure−Activity Relationship Studies toward the Discovery ofN-(2-Chloro-6-methylphenyl)-2-[[6-[4-(2-hydroxyethyl)-1- piperazinyl)]-2-methyl-4-pyrimidinyl]amino)]-1,3-thiazole-5-carboxamide (Dasatinib, BMS-354825) as a Potentpan-Src Kinase Inhibitor. Journal of Medicinal Chemistry. 49(23):6819-32.

83. David, Y., Cacheaux, L. P., Ivens, S., Lapilover, E., Heinemann, U., Kaufer, D., Friedman, A. (2009). Astrocytic dysfunction in epileptogenesis: Consequence of altered potassium and glutamate homeostasis? Journal of Neuroscience. 29, 10588–10599.

84. Dawson, T. M., Snyder, S. H. (1994). Gases as biological messengers: Nitric oxide and carbon monoxide in the brain. Journal of Neuroscience. 14, 5147–5159.

85. Dawson, V.L., Dawson, T.M. (1996). Nitric oxide neurotoxicity. Journal of Chemical Neuroanatomy. 10: 179–190.

86. Dawson, V. L., Dawson, T. M. (1998). Nitric oxide in neurodegeneration. Progress in Brain Research. 118, 215–229.

87. Dawson, T. M., Dawson, V. L., Snyder, S. H. (1992). A novel neuronal messenger molecule in brain: The free radical, nitric oxide. Annals of Neurology. 32(3):297-311.

88. de Graaf, R.A., Mason, G.F., Patel, A.B., Rothman, D.L., Behar, K.L. (2004). Regional glucose metabolism glutamatergic neurotransmission rat in vivo. Proceedings of the National Academy of Sciences of the United States of America. 101(34): 12700–12705.

89. de Lanerolle, N.C., Lee, T.S., Spencer, D.D. (2010). Astrocytes and epilepsy. Neurotherapeutics. 7(4):424–438.

90. De Risio, L. D., Bhatti, S., Munana, K., Penderis, J., Stein, V., Tipold, A., Berendt, A., et al. (2015). International veterinary epilepsy task force consensus proposal: Diagnostic approach to epilepsy in dogs. BMC Veterinary Research. 11, 148.

91. De Sarro, G. B., & De Sarro, A. (1993). Anticonvulsant properties of noncompetitive antagonists of the N-methyl-D-aspartate receptor in genetically epilepsy-prone rats: Comparison with CPPene. Neuropharmacology. 32, 51–58.

92. Deshukh, P., Unni, S., Krishnappa, G., Padmanabhan, B. (2017). The Keap-1-Nrf2 pathway: promising therapeutic target to counteract ROS-mediated damage in cancers and neurodegenerative diseases. Biophys Rev. 9(1):41-56.

93. Dexter, D.T., Carter, C.J., Wells, F.R., et al. (1989). Basal lipid peroxidation in substantia nigra is increased in Parkinson's disease. Journal of Neurochemistry. 52(2): 381–389.

94. Dheen, S.T., Kaur, C., Ling, E.A. (2007). Microglial activation and its implications in the brain diseases. Curr Med Chem. 14(11):1189-97.

95. Dodson, W. E., DeLorenzo, R. J., Pedley, T. A., Shinnar, S., Treiman, D. M., Wannamaker, B. B. (1993). Treatment of convulsive status epilepticus. Recommendations of the Epilepsy Foundation of Americas Working Group on Status Epilepticus. JAMA. 270, 854–859.

96. Dover, A. R., Chia, S., Ferguson, J. W., Cruden, N. L., Megson, I. L., Fox, K. A., Newby, D. E. (2006). Inducible nitric oxide synthase activity does not contribute to the maintenance of peripheral vascular tone in patients with heart failure. Clinical Science. 111, 275–280.

97. Dudek, F.E., Staley, K.J. (2011). The time course of acquired epilepsy: Implications for therapeutic intervention to suppress epileptogenesis. Neurosci Lett. 497, 240–246.

98. Dudek, F.E., Staley, K.J. (2012). The time course and circuit mechanisms of acquired epileptogenesis. In Jasper's basic mechanisms of the epilepsies (ed. Noebels JL, et al.). National Center for Biotechnology Information, Bethesda, MD.

99. Dulsat, C., Mealy, N., Castaner, R. (2009). Saracatinib. Drugs of the future. 34(2):106-114.

100. Dunwiddie, T.V., Masino, S.A. (2001). The role and regulation of adenosine in the central nervous system. Annu Rev Neurosci. 24:31–55.

101. Eddleston, L., Mucke, L. (1993). Molecular profile of reactive astrocytes–implications for their role in neurologic disease. Neuroscience. 54, 15-36.

102. Eissa, N. T., Huston, D. P. (2003). Therapeutic Targets in Airway Inflammation (1st edition), Lung Biology in Health and Disease. Retrieved from http://books.google.com.

103. Ellenbroek, B., Youn, J. (2016). Rodent models in neuroscience research: is it a rat race? Dis Model Mech. 9(10):1079-1087.

104. Eng, L.F., Ghirnikar, R.S. (1994). GFAP and astrogliosis. Brain Pathol. 4, 229-237.

105. Fabene, P.F., et al. (2008). A role for leukocyte-endothelial adhesion mechanisms in epilepsy. Nat. Med. 14:1377–1383.

106. Fedorov, O., Marsden, B., Pogacic, V., Rellos, P., Muller, S., Bullock, A. N., et al. (2007). A systematic interaction map of validated kinase inhibitors with Ser/Thr kinases. Proceedings of the National Academy of Sciences. 104(51):20523-20528.

107. Ferguson, J. W., Dover, A. R., Chia, S., Cruden, N. L., Hayes, P. C., & Newby, D. E. (2006). Inducible nitric oxide synthase activity contributes to the regulation of peripheral vascular tone in patients with cirrhosis and ascites. Gut. 55, 542–546.

108. Fields, R.D. and Stevens-Graham, B. (2002). New insights into neuron-glia communication. Science. 298(5593):556-62.

109. Foresti, M.L., Arisi, G.M & Shapiro, L.A. (2011). Role of glia in epilepsy-associated neuropathology, neuroinflammation and neurogenesis. Brain res Rev. 66(1):115–122.

110. Fossat, P., Turpin, F.R., Sacchi, S., Dulong, J., Shi, T., Rivet, J.M., et al. (2011). Glial $_{D}$-serine gates NMDA receptors at excitatory synapses in prefrontal cortex. Cereb Cortex. 22(3):595–606.

111. Frame, M. C. (2002). Src in cancer: Deregulation and consequences for cell behaviour. Biochimica Biophysica Acta (BBA) - Reviews on Cancer. 1602(2):14-130.

112. Frigerio, F., Frasca, A., Weissberg, I., Parrella, S., Friedman, A., Vezzani, A., Noe, F. M. (2012). Long-lasting pro-ictogenic effects induced in vivo by rat brain exposure to serum albumin in the absence of concomitant pathology. Epilepsia. 53, 1887–1897.

113. Franco, R., Fernandez-Suarez, D. (2015). Alternatively activated microglia and macrophages in the central nervous system. Prog Neurobiol. 131:65-86.

114. Furtado, M. D. A., Rossetti, F., Chanda, S., Yourick, D. (2012). Exposure to nerve agents: From status epilepticus to neuroinflammation, brain damage, neurogenesis and epilepsy. Neurotoxicology. 33, 1476–1490.

115. Furumoto, Y., Gomez, G., Gonzalez-Espinosa, C., Kovarova, M., Odom, S., Ryan, J.J., Rivera, J. (2005). The role of Src family kinases in mast cell effector function. Novartis Found Symp. 271, 39-47.

116. Gao, H.M., Liu, B., Zhang, W., Hong, J.S. (2003). Synergistic dopaminergic neurotoxicity of MPTP and inflammogen lipopolysaccharide: relevance to the etiology of Parkinson's disease. The FASEB Journal. 17(13):1957–1959.

117. Garvey, E. P., Oplinger, J. A., Furfine, E. S., Kiff, R. J., Laszlo, F., Whittle, B. J., & Knowles, R. G. (1997). 1400W is a slow, tight binding, and highly selective inhibitor of inducible nitric-oxide synthase in vitro and in vivo. Journal of Biological Chemistry, 272, 4959–4963.

118. Gastaut, H. (1983). Classification of status epilepticus. Advances in Neurology. 34, 15–35.

119. Gatti, S., Vezzani, A., Bartfai, T. (2002). In: Febrile Seizures. Baram TZ, Shinnar S, editors. Ch. 12. San Diego: Academic Press. 169–184.

120. Getlik, M., Grütter, C., Simard, J. R., Klüter, S., Rabiller, M., Rode, H. B., et al., (2009). Hybrid Compound Design To Overcome the Gatekeeper T338M Mutation in cSrc#. Journal of Medicinal Chemistry. 52(13):3915-3926.

121. Gidday, J. M., Shah, A. R., Maceren, R. G., Wang, Q., Pelligrino, D. A., Holtzman, D. M., Park, T. S. (1999). Nitric oxide mediates cerebral ischemia tolerance in neonatal rat model of hypoxic preconditioning. Journal of Cerebral Blood Flow and Metabolism. 19, 331–340.

122. Glezer, I., Simard, A.R., Rivest, S. (2007). Neuroprotective role of the innate immune system by microglia. Neuroscience. 147, 867-883.

123. Glien, M., Brandt, C., Potschka, H., Voigt, H., Ebert, U., Löscher, W. (2001). Repeated lowdose treatment of rats with pilocarpine: low mortality but high proportion of rats developing epilepsy. Epilepsy Res. 46:111–9.

124. Ghasemi, M., Fatemi, A. (2014). Pathologic role of glial nitric oxide in adult and pediatric neuroinflammatory diseases. Neurosci Biobehav Rev. 45:168-82.

125. Goldberg, E. M., Coulter, D. A. (2013). Mechanisms of epileptogenesis: A convergence on neural circuit dysfunction. Nature Reviews Neuroscience, 14, 337–349.

126. Golden, G.T., Smith, G.G., Ferraro, T.N., Reyes, P.F. (1995). Rat strain and age differences in kainic acid induced seizures. Epilepsy Res. 20:151–9.

127. Goodkin, H.P., Joshi, S., Mtchedlishvili, Z., Brar, J., Kapur, J. (2008). Subunit-specific trafficking of GABAA receptors during status epilepticus. J Neurosci. 28:2527–38.

128. Gordge, M.P., Hothersall, J.S., Neild, G.H., Dutra, A.A.N. (1996). Role of a copper(I)-dependent enzyme in the anti-platelet action of Snitrosoglutathione. Br J Pharmacol. 119:533–538.

129. Grant, S.G., O'Dell, T.J., Karl, K.A., Stein, P.L., Soriano, P., Kandel, E.R. (1992). Impaired long-term potentiation, spatial learning, and hippocampal development in Fyn mutant mice. Science. 258, 1903–1910.

130. Green, T. P., Fennell, M., Whittaker, R., Curwen, J., Jacobs, V., Allen, J., et al. (2009). Preclinical anticancer activity of the potent, oral Src inhibitor AZD0530. Molecular Oncology. 3(3):248-261.

131. Haass, C., Mandelkow, E. (2010). Fyn-Tau-Amyloid: A Toxic Triad. Cell. 142(3), 356-358.

132. Halliwell, B., Zhao, K., Whiteman, M. (1999). Nitric oxide and peroxynitrite. The ugly, the uglier and the not so good: a personal view of recent controversies. Free Radical Research. 31(6):651–669.

133. Hanke, J. H., Gardner, J. P., Dow, R. L., Changelian, P. S., Brissette, W. H., Weringer, E. J., Connelly, P. A. (1996). Discovery of a Novel, Potent, and Src Family-selective Tyrosine Kinase Inhibitor. Journal of Biological Chemistry. 271(2):695-701.

134. Hansel, T. T., Kharitonov, S. A., Donnelly, L. E., Erin, E. M., Currie, M. G., Moore, W. M., et al. (2003). A selective inhibitor of inducible nitric oxide synthase inhibits exhaled breath nitric oxide in healthy volunteers and asthmatics. FASEB Journal. 17, 1298–1300.

135. Hasko, G., Linden, J., Cronstein, B., Pacher, P. (2008). Adenosine receptors: therapeutic aspects for inflammatory and immune diseases. Nat Rev Drug Discov. 7(9):759-770.

136. Heinemann, U., Staley, K.J. (2014). What is the clinical relevance of in vitro epileptiform activity? Adv Exp Med Biol. 813, 25–41.

137. Hellier, J. L., Patrylo, P. R., Buckmaster, P. S., Dudek, F. E. (1998). Recurrent spontaneous motor seizures after repeated low-dose systemic treatment with kainate: Assessment of a rat model of temporal lobe epilepsy. Epilepsy Research. 31, 73–84.

138. Helms, G., Ciumas, C., Kyaga, S., I. Savic, I. (2006). Increased thalamus levels of glutamate and glutamine (Glx) in patients with idiopathic generalised epilepsy. Journal of Neurology, Neurosurgery and Psychiatry. 77(4):489–494.

139. Hennequin, L.F., Allen, J., Breed, J., Curwen, J., Fennell, M., et al., (2006). N-(5-chloro-1,3-benzodioxol-4-yl)-7-[2-(4-methypiperazin1-yl)ethoxy]-5-(tetrahydro-2H-pyran-4-yloxy)quinazolin-4-amine, a novel, highly selective, orally available, dual-specific c-Src/Abl kinase inhibitor. J. Med. Chem. 49, 6465–6488.

140. Hesdorffer, D. C., Begley, C. E. (2013). Surveillance of epilepsy and prevention of epilepsy and its sequelae: Lessons from the Institute of Medicine report. Current Opinion in Neurology. 26, 168–173.

141. Hesdorffer, D. C., Logroscino, G., Benn, E. K. T., Katri, N., Cascino, G., & Hauser, W. A. (2011). Estimating risk for developing epilepsy: A population-based study in Rochester, Minnesota. Neurology. 76, 23–27.

142. Hester, M. S., Danzer, S. C. (2014). Hippocampal granule cell pathology in epilepsy—a possible structural basis for epileptic co-morbidities? Epilepsy and Behavior. 38, 105–116.

143. Hou, X.Y., Zhang, G.Y., Yan, J.Z., Chen, M., Liu, Y. (2002). Activation of NMDA receptors and L-type voltage-gated calcium channels mediates enhanced formation of Fyn-PSD95-NR2A complex after transient brain ischemia. Brain Res. 955(1-2):123-32.

144. Infanger, D.W., Sharma, R.V., Davisson, R.L. (2006). NADPH oxidases of the brain: distribution, regulation, and function. Antioxidants and Redox Signaling. 8(9-10):1583–1596.

145. Iyer, R., Iken, B., Leon, A. (2015). Developments in alternative treatments for organophosphate poisoning. Toxicology Letters. 233, 200– 206.

146. Jafarian-Tehrani, M., Louin, G., Royo, N.C., and Besson, V.C. (2005). 1400W, a potent selective inducible NOS inhibitor, improves histopathological outcome following traumatic brain injury in rats. Nitric Oxide. 12: 61–69.

147. Jarvinen, K., Vuolteenaho, K., Nieminen, R., Moilanen, T., Knowles, R. G., & Moilanen, E. (2008). Selective iNOS inhibitor 1400W enhances anti-catabolic IL-10

and reduces destructive MMP-10 in OA cartilage. Survey of the effects of 1400W on inflammatory mediators produced by OA cartilage as detected by protein antibody array. Clinical and Experimental Rheumatology. 26, 275–282.

148. Jorgensen, M. B., Finsen, B. R., Jensen, M. B., Castellano, B., Diemer, N. H., Zimmer, J. (1993). Microglial and astroglial reactions to ischemic and kainic acid-induced lesions of the adult rat hippocampus. Experimental Neurology. 120, 70–88.

149. Jurd, R., Tretter, V., Walker, J., Brandon, N.J., Moss, S.J. (2010). Fyn kinase contributes to tyrosine phosphorylation of the GABAA receptor γ2 subunit. Mol. Cell. Neurosci. 44, 129–134.

150. Kadam, S. D., White, A. M., Staley, K. J., Dudek, F. E. (2010). Continuous electroencephalographic monitoring with radio-telemetry in a rat model of perinatal hypoxia-ischemia reveals progressive post-stroke epilepsy. Journal of Neuroscience. 30, 404–415.

151. Kann, O., Kovacs, R., Njunting, M., et al. (2005). Metabolic dysfunction during neuronal activation in the ex vivo hippocampus from chronic epileptic rats and humans. Brain. 128(10):2396–2407.

152. Kaspar, J.W., Jaiswal, A.K. (2011). Tyrosine phosphorylation controls nuclear export of Fyn, allowing Ntf2 activation of cytoprotective gene expression. FASEB J. 25(3):1076-87.

153. Kato, N., Sato, S., Yokoyama, H., Kayama, T., Yoshimura, T. (2005). Sequential changes of nitric oxide levels in the temporal lobes of kainic acid-treated mice following application of nitric oxide synthase inhibitors and phenobarbital. Epilepsy Research. 65: 81–91.

154. Kaufer, C., Chhatbar, C., Broer, S., et al. (2018). Chemokine receptors CCR2 and CX3CR1 regulate viral encephalitis-induced hippocampal damage but not seizures. Proc Natl Acad Sci USA. 115(38):E8929-E8938.

155. Kim, Y.J., Sano, T., Nabetani, T., Asano, Y., Hirabayashi, Y. (2012). GPRC5B activates obesity-associated inflammatory signaling in adipocytes. Sci Signal. 5(251):ra85.

156. Kirkley, K. S., Madl, J. E., Duncan, C., Gulland, F. M., & Tjalkens, R. B. (2014). Domoic acid-induced seizures in California sea lions (Zalophus californianus) are associated with neuroinflammatory brain injury. Aquatic Toxicology. 156, 259–268.

157. Klee, R., Brandt, C., Tollner, K., Loscher, W. (2017). Various modifica- € tions of the intrahippocampal kainate model of mesial temporal lobe epilepsy in rats fail to resolve the marked rat-to-mouse differences in type and frequency of spontaneous seizures in this model. Epilepsy Behavior. 68, 129–140.

158. Klitgaard, H., Matagne, A., Vanneste-Goemaere, J., Margineanu, D. G. (2002). Pilocarpineinduced epileptogenesis in the rat: impact of initial duration of status epilepticus on electrophysiological and neuropathological alterations. Epilepsy Res. 51(1–2):93–107.

159. Knowles, R.G., Moncada, S. (1994). Nitric oxide synthases in mammals. Biochemical Journal. 298(2):249–258.

160. Ko, H.M., Lee, S.H., Bang, M., Kim, K.C., Jeon, S.J., Park, Y.M., Han, S.H., Kim, H.Y., Lee, J., Shin, C.Y. (2018). Tyrosine kinase Fyn regulates iNOS expression in LPS-stimulated astrocytes via modulation of ERK phosphorylation. Biochem Biophys Res Commun. 495(1):1214-1220.

161. Koh, H. K., Kobau, R., Whittemore, V. H., Mann, M. Y., Johnson, J. G., Hutter, J. D., Jones, W. K. (2014). Toward an integrated public health approach for epilepsy in the 21st century. Preventing Chronic Disease. 11, E146.

162. Kojima, N., Ishibashi, H., Obata, K., Kandel, E.R. (1998). Higher seizure susceptibility and enhanced tyrosine phosphorylation of N-Methyl-D-Aspartate receptor subunit 2B in Fyn transgenic mice. Learn Mem. 5(6):429–445.

163. Kovacs, R., Rabanus, A., Otahal, J., Patzak, A., Kardos, J., Albus, K., et al. (2009). Endogenous nitric oxide is a key promoting factor for initiation of seizure-like events in hippocampal and entorhinal cortex slices. Journal of Neuroscience. 29, 8565–8577.

164. Krumholz, A., Wiebe, S., Gronseth, G. S., Gloss, D. S., Sanchez, A. M., Kabir, A. A., et al. (2015). Evidence-based guideline: Management of an unprovoked first seizure in adults: Report of the Guideline Development Subcommittee of the American Academy of Neurology and the American Epilepsy Society Author Response. Neurology. 84, 1705–1713.

165. Kuperberg, S. J., Wadgaonkar, R. (2017). Sepsis-Associated Encephalopathy: The Blood–Brain Barrier and the Sphingolipid Rheostat. Frontiers in Immunology. 8.

166. Kwan, P., Brodie, M. J. (2000). Epilepsy after the first drug fails: Substitution or add-on? Seizure. 9, 464–468.

167. Kwan, P., Schachter, S. C., Brodie, M. J. (2011). Drug-resistant epilepsy. New England Journal of Medicine. 365, 919–926.

168. Landshamer, S., Hoehn, M., Barth, N., Duvezin-Caubet, S., Schwake, G., Tobaben, S., Kazhdan, I., et al. (2008). Bid-induced release of AIF from mitochondria causes immediate neuronal cell death. Cell Death Differ. 15(10):1553-63.

169. Lawrence, T. (2009). The nuclear factor NFkB pathway in inflammation. Cold Spring Harb Perspect Biol. 1(6):a001651.

170. Librizzi, L., Ravizza, T., Vezzani, A., de Curtis, M. (2010). Expression of IL-1β induced by epileptiform activity in the isolated guinea pig brain *in vitro*. Presented at the 9th European Congress on Epileptology; Rhodes.

171. Lake, N. (1992). Taurine, GABA and GFAP immunoreactivity in the developing and adult-rat optic-nerve. Brain Res. 596(1–2):124–132.

172. Lalitha, S., Minz, R. W., Medhi, B. (2018). Understanding the controversial drug targets in epilepsy and pharmacoresistant epilepsy. Reviews in the Neurosciences. 29(3), 333-345.

173. Lamas, S., Lowenstein, C.J. Michael, T. (2007). Nitric oxide signalling comes of age: 20 years and thriving. Cardiovasc. Res. 75, 207 – 209.

174. Lannaccone, P.M. and Jacob, H.J. (2009). Rats! Dis Model Mech. 2(5-6):206-10.

175. Larson, M., Sherman, M.A., Amar, F., Nuvolone, M., Schneider, J.A., Bennett, D.A., Aguzzi, A., Lesne, S.E. (2012). The complex PrP(c)-Fyn couples human oligomeric Aβ with pathological tau changes in Alzheimer's disease. J Neurosci. 32(47):16857-71a.

176. Li, Y., Shen, M., Zhang, Z., Luo, J., Pan, X., Lu, X., Long, H., Wen, D., Zhang, F., Leng, F., Li, Y., Tu, Z., Ren, X., Ding, K. (2012). Design, synthesis, and biological evaluation of 3-(1H-1,2,3-triazol-1-yl)benzamide derivatives as Potent Pan Bcr-Abl inhibitors including the threonine(315)→isoleucine(315) mutant. J Med Chem. 55(22):10033-46.

177. Liang, L.P., Patel, M. (2006). Seizure-induced changes in mitochondrial redox status. Free Radical Biology and Medicine. 40(2):316–322.

178. Lee, C., Low, C.Y., Francis, P.T., Attems, J., Wong, P.T., Lai, M.K., Tan, M.G. (2016). An isoform-specific role of fynT tyrosine kinase in Alzheimer's disease. J Neurochem. 136(3):637-50.

179. Lee, S., Yoon, B.E., Berglund, K., Oh, S.J., Park, H., Shin, H.S., et al. (2010). Channel-mediated tonic GABA release from glia. Science. 330(6005):790–796.

180. Lei, S. Z., Pan, Z. H., Aggarwal, S. K., Chen, H. S., Hartman, J., Sucher, N. J., Lipton, S. A. (1992). Effect of nitric oxide production on the redox modulatory site of the NMDA receptor-channel complex. Neuron. 8, 1087–1099.

181. Lewerenz, J., Hewett, S. J., Huang, Y., Lambros, M., Gout, P. W., Kalivas, P. W., et al. (2013). The Cystine/Glutamate Antiporter System x_c^- in Health and Disease:

From Molecular Mechanisms to Novel Therapeutic Opportunities. Antioxidants & Redox Signaling. 18(5):522-555.

182. Lind, M., Hayes, A., Caprnda, M., Petrovic, D., Rodrigo, D., Kruzliak, P., Zulli, A. (2017). Inducible nitric oxide synthase: good or bad? Biomed Pharmacother. 93:370-375.

183. Lisboa, S.F., Gomes, F.V., Guimaraes, F.S., Campos, A.C. (2016). Microglial cells as a link between cannabinoids and the immune hypothesis of psychiatric disorders. Front Neurol. 7:5.

184. Liu, T., Zhang, L., Joo, D., Sun, S.C. (2017). NFkB signaling in inflammation. Signal Transduct Target Ther. 2,pii:17023.

185. Lobo, V., Patil, A., Phatak, A., Chandra, N. (2010). Free radicals, antioxidants and functional foods: impact on human health. Pharmacognosy Reviews. 4(8):118–126.

186. Lockton, J.A., Smethurst, D., Macpherson, M., Tootell, R., Marshall, A.L., Clack, G. (2005). Phase I ascending single and multiple dose studies to assess the safety, tolerability and pharmacokinetics of AZD0530, a highly selective, dual-specific Src-Abl inhibitor. Journal of Clinical Oncology. 23(16):3125.

187. Loscher W. (2002). Animal models of epilepsy for the development of antiepileptogenic and disease-modifying drugs. A comparison of the pharmacology of kindling and post-status epilepticus models of temporal lobe epilepsy. Epilepsy Res. 50:105–23.

188. Loscher, W., & Brandt, C. (2010). Prevention or modification of epileptogenesis after brain insults: Experimental approaches and translational research. Pharmacological Reviews. 62, 668–700.

189. Loscher, W., Ferland, R.J., Ferraro, T.N. (2017). The relevance of inter- and intrastrain differences in mice and rats and their implications for models of seizures and epilepsy. Epilepsy Behav. 73:214–35.

190. Loscher, W., Hirsch, L. J., & Schmidt, D. (2015). The enigma of the latent period in the development of symptomatic acquired epilepsy — Traditional view versus new concepts. Epilepsy & Behavior. 52, 78-92.

191. Madrigal, J.L.M., Garcıa-Bueno, B., Caso, J.R., Perez-Nievas, B.G., Leza, J.C. (2006). Stress-induced oxidative changes in brain. CNS and Neurological Disorders: Drug Targets. 5(5):561–568.

192. Madduri, S., Gander, B. (2010). Scwann cell delivery of neurotrophic factors for peripheral nerve regeneration. J Peripher Nerv Syst. 15(2):93-103.

193. Maher, P., Schubert, D. (2000). Signaling by reactive oxygen species in the nervous system. Cell Mol Life Sci. 57(8-9):1287-305.

194. Makuch, W., Mika, J., Rojewska, E., Zychowska, M., & Przewlocka, B. (2013). Effects of selective and non-selective inhibitors of nitric oxide synthase on morphine- and endomorphin-1-induced analgesia in acute and neuropathic pain in rats. Neuropharmacology. 75, 445– 457.

195. Mandal, P. K., Seiler, A., Perisic, T., Kolle, P., Canak, A. B., Förster, H., et al. (2010). System x_c^- and Thioredoxin Reductase 1 Cooperatively Rescue Glutathione Deficiency. Journal of Biological Chemistry. 285(29):22244-53.

196. Manno, E. M. (2011). Status epilepticus. Neurohospitalist. 1, 23–31.

197. Mao, L and Franke, J. (2013). Hormesis in aging and neurodegeneration—a prodigy awaiting dissection. International Journal of Molecular Sciences. 14(7):13109–13128.

198. Manzoni, O., Prezeau, L., Marin, P., Desagher, S., Bockaert, J., Fagni, L. (1992). Nitric oxide-induced blockade of NMDA receptors. Neuron. 8, 653–662.

199. Martin, G. S. (2001). The hunting of the Src. Nature Reviews Molecular Cell Biology. 2(6):467-475.

200. Mayer, B. and Andrew, P. (1998). Nitric oxide synthase: catalytic function and progress towards selective inhibition. Naunyn Schmeidebergs Arch Pharmacol. 358(1):127-33.

201. Mazzuferi, M., Kumar, G., & Kaminski, R. M. (2012). Rapid epileptogenesis in the mouse pilocarpine model: Video-EEG, pharmacokinetic and histopathological characterization. Experimental Neurology. 238, 156– 167.

202. McCafferty, D.M., Mudgett, J.S., Swain, M.G., Kubes, P. (1997). Inducible nitric oxide synthase plays a critical role in resolving intestinal inflammation. Gastroenterology. 112:1022–1027.

203. Mikati, M. (2004). Neuronal cell death in a rat model of mesial temporal lobe epilepsy is induced by the initial status epilepticus and not by later repeated spontaneous seizures. Epilepsia. 45:296–296.

204. Milikovsky, D. Z., Weissberg, I., Kamintsky, L., Lippmann, K., Schefenbauer, O., Frigerio, F., Rizzi, M., et al. (2017). Electrocorticographic Dynamics as a Novel Biomarker in Five Models of Epileptogenesis. The Journal of Neuroscience. 37(17):4450-4461.

205. Miyajima, A., Chen, J., Poppas, D.P., Vaughan, E.D. Jr., Felsen, D. (2001). Role of nitric oxide in renal tubular apoptosis of unilateral ureteral obstruction. Kidney Int. 59:1290–1303.

206. Miyakawa, T., Yagi, T., Kitazawa, H., Yasuda, M., Kawai, N., Tsuboi, K., Niki, H. (1997). Fyn-kinase as a determinant of ethanol sensitivity: relation to NMDA-receptor function. Science. 278(5338):698-701.

207. Moncada, S., & Erusalimsky, J. D. (2002). Does nitric oxide modulate mitochondrial energy generation and apoptosis? Nature Reviews Molecular Cell Biology. 3, 214–220.

208. Moncada, S., Palmer, R.M.J., Higgs, E.A. (1991). Nitric oxide–physiology, pathophysiology, and pharmacology. Pharmacol Rev. 43:109–142.

209. Moore, P.K., Babbedge, R.C., Wallace, P., Gaffen, Z.A., Hart, S.L. (1993). 7-NI, an inhibitor of nitric oxide synthase, exhibits anti-nociceptive activity in the mouse without increasing blood pressure. Br J Pharmacol. 108(2):296-7.

210. Morgan, T.E., Nichols, N.R., Pasinetti, G.M., Finch, C.E. (1993). TGF-beta 1 mRNA increases in macrophage/microglial cells of the hippocampus in response to deafferentation and kainic acid-induced neurodegeneration. Exp. Neurol. 120, 291–301.

211. Moussa, R.C., Ikeda-Douglas, C.J., Thakur, V., Milgram, N.W., Gurd, J.W. (2001). Seizure activity results in increased tyrosine phosphorylation of the N-methyl-D-aspartate receptor in the hippocampus. Brain Res. Mol. Brain Res. 95, 36–47.

212. Murciano-Calles, J., Corbi-Verge, C., Candel, A.M., Luque, I., Martinez, J.C. (2014). Post-translational modifications modulate ligand recognition by the third PDZ domain of the MAGUK protein PSD-95. PLoS One. 9(2):e90030.

213. Murdoch, C., Finn, A. (2000). Chemokine receptors and their role in inflammation and infectious diseases. Blood. 95(10):3032-43.

214. Murphy, B. L., Danzer, S. C. (2011). Somatic translocation: A novel mechanism of granule cell dendritic dysmorphogenesis and dispersion. Journal of Neuroscience. 31, 2959–2964.

215. Murphy, T. R., Binder, D. K., Fiacco, T. A. (2017). Turning down the volume: Astrocyte volume change in the generation and termination of epileptic seizures. Neurobiology of Disease. 104, 24–32.

216. Musicco, M., Beghi, E., Solari, A., Viani, F. (1997). Treatment of first tonic-clonic seizure does not improve the prognosis of epilepsy. Neurology. 49, 991–998.

217. Nairismagi, J., Grohn, O. H. J., Kettunen, M. I., Nissinen, J., Kauppinen, R. A., Pitkanen, A. (2004). Progression of brain damage after status epilepticus and its association with epileptogenesis: A quantitative MRI study in a rat model of temporal lobe epilepsy. Epilepsia. 45, 1024–1034.

218. Nomura, Y., and Kitamura, Y. (1993). Inducible nitric oxide synthase in glial cells. Neuroscience Research. 103–107.

219. Nakazawa, T., Komai, S., Tezuka, T., Hisatsune, C., Umemori, H., et al. (2001). Characterization of Fyn-mediated tyrosine phosphorylation sites on GluR epsilon 2 (NR2B) subunit of the N-Methyl-D-aspartate Receptor. J Biol Chem. 276, 693–699.

220. Napoli, I., Neumann, H. (2010). Protective effects of microglia in multiple sclerosis. Exp Neurol. 225, 24-28.

221. Nelson, E.J., Connolly, J., Connolly, J., McArthur, P., McArthur, P. (2003). Nitric oxide and S□nitrosylation: excitotoxic and cell signaling mechanism. Biology of the Cell. 95: 3–8.

222. Nguyen, T., Yang, T., Go, M. (2014). Functionalized acridin-9-yl phenylamines protected neuronal HT22 cells from glutamate-induced cell death by reducing intracellular levels of free radical species. Bioorganic & Medicinal Chemistry Letters. 24(7):1830-1838.

223. Nimmerjahn, A., Kirchhoff, F., and Helmchen, F. (2005). Resting microglial cells are highly dynamic surveillants of brain parenchyma in vivo. Science. 308, 1314-1318.

224. Nygaard, H.B., van Dyck, C.H., Strittmatter, S.M. (2014). Fyn kinase inhibition as a novel therapy for Alzheimer's disease. Alzheimers Res. Ther. 6(1):8.

225. Ochi, S., Lim, J.Y., Rand, M.N., During, M.J., Sakatani, K., Kocsis, J.D. (1993). Transient presence of GABA in astrocytes of the developing optic-nerve. Glia. 9(3):188–198.

226. Ohare, T., Walters, D. K., Stoffregen, E. P., Jia, T., Manley, P. W., Mestan, J., Druker, B. J. (2005). In vitroActivity of Bcr-Abl Inhibitors AMN107 and BMS-354825 against Clinically Relevant Imatinib-Resistant Abl Kinase Domain Mutants. Cancer Research. 65(11), 4500-4505.

227. Ohnishi, H., Murata, Y., Okazawa, H., Matozaki, T. (2011). Src family kinases: modulators of neurotransmitters receptor function and behavior. Trends Neurosci. 34(12):629-37.

228. Otis, T.S., Jahr, C.E. (1998). Anion currents and predicted glutamate flux through a neuronal glutamate transporter. J Neurosci. 18:7099–7110.

229. Pakozdy, A., Halasz, P., Klang, A. (2014). Epilepsy in cats: Theory and practice. Journal of Veterinary Internal Medicine. 28, 255–263.

230. Pampliega, O., Domercq, M., Soria, F. N., Villoslada, P., Rodríguez-Antiguedad, A., Matute, C. (2011). Increased expression of cystine/glutamate antiporter in multiple sclerosis. Journal of Neuroinflammation. 8(1):63.

231. Panatier, A., Theodosis, D.T., Mothet, J.P., Touquet, B., Pollegioni, L., Poulain, D.A., et al. (2006). Glia derived $_{D}$-serine controls NMDA receptor activity and synaptic memory. Cell. 125(4):775–784.

232. Panicker, N., Saminathan, H., Jin, H., Neal, M., Harischandra, D.S., Gordon, R., Kanthasamy, K., Lawana, V., Sarkar, S., Luo, J., et al. (2015). Fyn Kinase Regulates Microglial Neuroinflammatory Responses in Cell Culture and Animal Models of Parkinson's Disease. J Neurosci. 35(27):10058-10077.

233. Parent, J. M., Lowenstein, D. H. (2002). Seizure-induced neurogenesis: Are more new neurons good for an adult brain? Progress in Brain Research. 135, 121–131.

234. Park, K.K., Reuben, J.S., Soliman, K.F. (2001). The role of inducible-nitric oxide in cocaine-induced kindling. Exp Biol Med. (Maywood). 226, 185–190.

235. Parkhurst, C. N., Yang, G., Ninan, I., Savas, J. N., Yates, J. R., Lafaille, J. J., et al. (2013). Microglia promote learning-dependent synapse formation through BDNF. Cell. 155, 1596–1609.

236. Parmentier, S., Bohme, G. A., Lerouet, D., Damour, D., Stutzmann, J. M., Margaill, I., Plotkine, M. (1999). Selective inhibition of inducible nitric oxide synthase prevents ischaemic brain injury. British Journal of Pharmacology. 127, 546–552.

237. Patel, M. (2004). Mitochondrial dysfunction and oxidative stress: cause and consequence of epileptic seizures. Free Radical Biology and Medicine. 37(12):1951–1962.

238. Pawson, T. (1997). Protein tyrosine kinases: new impressions of Src and Hck. Nature. 385:582.

239. Pearson, J. N., Rowley, S., Liang, L.-P., White, A. M., Day, B. J., & Patel, M. (2015). Reactive oxygen species mediate cognitive deficits in experimental temporal lobe epilepsy. Neurobiology of Disease. 82, 289–297.

240. Pekny, M., Pekna, M. (2016). Reactive gliosis in the pathogenesis of CNS diseases. Biochemica Biophysica Acta. 1862(3):483-491.

241. Pfrieger, F.W. (2009). Role of glial cells in synapse development. Cell Mol Life Sci. 66(13):2037-2047.

242. Pitkanen, A., Engel, J., Jr. (2014). Past and present definitions of epileptogenesis and its biomarkers. Neurotherapeutics. 11, 231–241.

243. Pitkanen, A., Lukasiuk, K., Dudek, F. E., Staley, K. J. (2015). Epileptogenesis. Cold Spring Harbor Perspectives in Medicine. 18, 5(10).

244. Pitkänen, A., Nissinen, J., Nairismägi, J., Lukasiuk, K., Gröhn, O.H., Miettinen, R., Kauppinen, R. (2002). Progression of neuronal damage after status epilepticus and during spontaneous seizures in a rat model of temporal lobe epilepsy. Prog Brain Res. 135:67–83.

245. Pizzol, F., Klamt, F., Vianna, M.M.R., et al. (2000). Lipid peroxidation in hippocampus early and late after status epilepticus induced by pilocarpine or kainic acid in Wistar rats. Neuroscience Letters. 291(3):179–182.

246. Prat, A., Biernacki, K., Wosik, K., Antel, J.P. (2001). Glial cell influence on the human blood-brain barrier. Glia. 36(2):145-55.

247. Purnell, P. R., Mack, P. C., Tepper, C. G., Evans, C. P., Green, T. P., Gumerlock, P. H., Gautschi, O. (2009). The Src Inhibitor AZD0530 Blocks Invasion and May Act as a Radiosensitizer in Lung Cancer Cells. Journal of Thoracic Oncology. 4(4):448-454.

248. Puttachary, S., Sharma, S., Stark, S., Thippeswamy, T. (2015a). Seizure induced oxidative stress in temporal lobe epilepsy. BioMed Research International. 2015, 1–20.

249. Puttachary, S., Sharma, S., Thippeswamy, A., Thippeswamy, T. (2016b). Immediate epileptogenesis: Impact on brain in C57BL/6J mouse kainate model. Frontiers in Bioscience. 8, 390–411.

250. Puttachary, S., Sharma, S., Tse, K., Beamer, E., Sexton, A., Crutison, J., Thippeswamy, T. (2015b). Immediate epileptogenesis after kainateinduced status epilepticus in C57BL/6J mice: Evidence from long term continuous video-EEG telemetry. Plos One. 10, e0131705.

251. Puttachary, S., Sharma, S., Verma, S., Yang, Y., Putra, M., Thippeswamy, A., Luo, D., Thippeswamy, T. (2016a). 1400W, a highly selective inducible nitric oxide synthase inhibitor is a potential disease modifier in the rat kainate model of temporal lobe epilepsy. Neurobiology of Disease. 93, 184–200.

252. Qashu, F., Figueiredo, T.H., Aroniadou-Anderjaska, V., Apland, J.P., Braga, M.F.M. (2009). Diazepam administration after prolonged status epilepticus reduces neurodegeneration in the amygdala but not in the hippocampus during epileptogenesis. Amino Acids. 38:189–97.

253. Radi, M., Evensen, L., Dreassi, E., Zamperini, C., Caporicci, M., Falchi, F., et al. (2012). A combined targeted/phenotypic approach for the identification of new antiangiogenics agents active on a zebrafish model: From in silico screening to cyclodextrin formulation. Bioorganic & Medicinal Chemistry Letters. 22(17):5579-5583.

254. Rana, A., Musto, A. E. (2018). The role of inflammation in the development of epilepsy. Journal of Neuroinflammation. 15(1).

255. Rao, M. S., Hattiangady, B., Reddy, D. S., Shetty, A. K. (2006). Hippocampal neurodegeneration, spontaneous seizures, and mossy fiber sprouting in the F344 rat model of temporal lobe epilepsy. J Neurosci Res. 83:1088–105.

256. Rehni, A.K., Singh, T.G., Kalra, R., Singh, N. (2009). Pharmacological inhibition of inducible nitric oxide synthase attenuates the development of seizures in mice. Nitric Oxide. 21: 120–125.

257. Ren, X., Pan, X., Zhang, Z., Wang, D., Lu, X., Li, Y., et al. (2013). Identification of GZD824 as an Orally Bioavailable Inhibitor That Targets Phosphorylated and Nonphosphorylated Breakpoint Cluster Region–Abelson (Bcr-Abl) Kinase and Overcomes Clinically Acquired Mutation-Induced Resistance against Imatinib. Journal of Medicinal Chemistry. 56(3):879-894.

258. Resh, M.D. (1993). Interaction of tyrosine kinase oncoproteins with cellular membranes. Biochem. Biophys. Acta. 1155:307–22.

259. Rodeberg, D.A., Chaet, M.S., Bass, R.C., Arkovitz, M.S., Garcia, V.F. (1995). Nitric oxide: An overview. The American Journal of Surgery. 170: 292–303.

260. Rasmussen, T., Olsewski, J., Lloyd-Smith, D. (1958). Focal seizures due to chronic localized encephalitis. Neurology. 8:435–445.

261. Rattka, M., Brandt, C., Löscher, W. (2013). The intrahippocampal kainate model of temporal lobe epilepsy revisited: epileptogenesis, behavioral and cognitive alterations, pharmacological response, and hippoccampal damage in epileptic rats. Epilepsy Res. 103:135–52.

262. Ravizza, T., Gagliardi, B., Noe, F., Boer, K., Aronica, E., Vezani, A. (2008). Innate and adaptive immunity during epileptogenesis and spontaneous seizures: evidence from experimental models and human temporal lobe epilepsy. Neurobiol. Dis. 29:142–160.

263. Ricciotti, E., Fitzgerald, G.A. (2011). Prostaglandins and inflammation. Arteriosclerosis, Thrombosis, and Vascular Biology. 31(5):986–1000.

264. Robel, S., Buckingham, S. C., Boni, J. L., Campbell, S. L., Danbolt, N. C., Riedemann, T., et al. (2015). Reactive astrogliosis causes the development of spontaneous seizures. J Neurosci. 35, 3330–45.

265. Rosselli, M., Keller, P.J., Dubey, R.K. (1998). Role of nitric oxide in the biology, physiology and pathophysiology of reproduction. Hum Reprod Update. 4(1):3-24.

266. Rowley, N. M., White, H. S. (2010). Comparative anticonvulsant efficacy in the corneal kindled mouse model of partial epilepsy. Correlation with other seizure models. Epilepsy Research. 92, 163–169.

267. Rozovsky, I., Morgan, T.E., Willoughby, D.A., Dugichi-Djordjevich, M.M., Pasinetti, G.M., Johnson, S.A., Finch, C.E. (1994). Selective expression of clusterin (SGP-2) and complement C1qB and C4 during responses to neurotoxins *in vivo* and *in vitro*. Neuroscience. 62:741–758.

268. Ryan, K., Liang, L.-P., Rivard, C., Patel, M. (2014). Temporal and spatial increase of reactive nitrogen species in the kainate model of temporal lobe epilepsy. Neurobiology of Disease. 64, 8–15.

269. Rzezak, P., Lima, E. M., Pereira, F., Gargaro, A. C., Coimbra, E., Vincentiis, S., et al. (2016). Decision-making in patients with temporal lobe epilepsy: Delay gratification ability is not impaired in patients with hippocampal sclerosis. Epilepsy & Behavior. 60, 158–164.

270. Sala, C., Sheng, M. (1999). The Fyn art of N-methyl-D-aspartate receptor phosphorylation. Proc Natl Acad Sci. 96(2):335-337.

271. Salter, M.W., Kalia, L.V. (2004). Src kinases: a hub for NMDA receptor regulation. Nat. Rev. Neurosci. 5, 317–328.

272. Samland, H., Huitron-Resendiz, S., Masliah, E., Criado, J., Henriksen, S.J., Campbell, I.L. (2003). Profound increase in sensitivity to glutamatergic- but not cholinergic agonist-induced seizures in transgenic mice with astrocyte production of IL-6. J. Neurosci. Res. 73:176–187.

273. Sen, B., Johnson, F.M. (2011). Regulation of Src family kinases in human cancers. J Signal Transduct. 2011:865819.

274. Sanchez-Munoz F., Dominguez-Lopez A., Yamamoto-Furusho J.K. (2008). Role of cytokines in inflammatory bowel disease. World J Gastroenterol. 14(27):4280–4288.

275. Sardo, P., Ferraro, G. (2007). Modulatory effects of nitric oxide-active drugs on the anticonvulsant activity of lamotrigine in an experimental model of partial complex epilepsy in the rat. BMC Neuroscience. 8:47.

276. Schulz, J.B., Matthes, R.T., Muqit, M.M., Browne, S.E., Beal, M.F. (1995). Inhibition of neuronal oxide synthase by 7-NI protects against MPTP-induced neurotoxicity in mice. J Neurochem. 64(2):936-9.

277. Schauwecker, P. E. (2012). Strain differences in seizure-induced cell death following pilocarpine-induced status epilepticus. Neurobiology of Disease. 45, 297–304.

278. Schauwecker, P. E., Steward, O. (1997). Genetic determinants of susceptibility to excitotoxic cell death: Implications for gene targeting approaches. Proceedings of the National Academy of Sciences of the United States of America. 94, 4103–4108.

279. Schubert, P., Heinemann, U., Kolb, R. (1986). Differential effect of adenosine on pre-and postsynaptic calcium fuxes. Brain Res. 376:382–386.

280. Schwartzkroin, P.A., Baraban, S.C., Hochman, D.W. (1998). Osmolarity, ionic flux, and changes in brain excitability. Epilepsy Res. 32:275–285.

281. Semple, B.D., Kossmann, T., Morganti-Kossmann, M.C. (2010). Role of chemokines in CNS health and pathology: a focus on the CCL2/CCR2 and CXCL8/CXCR2 networks. J. Cereb. Blood Flow Metab. 30:459–473.

282. Serrano, G.E., Lelutiu, N., Rojas, A., et al. (2011). Ablation of cyclooxygenase-2 in forebrain neurons is neuroprotective and dampens brain inflammation after status epilepticus. Journal of Neuroscience. 31(42):14850–14860.

283. Shah, N. P. (2006). Dasatinib (BMS-354825) inhibits KITD816V, an imatinib-resistant activating mutation that triggers neoplastic growth in most patients with systemic mastocytosis. Blood. 108(1):286-291.

284. Sharma, S., Carlson, S., Puttachary, S., Sarkar, S., Showman, L., Putra, M., Kanthasamy, A.G., Thippeswamy, T. (2018a). Role of the Fyn-PKCδ signaling in SE-induced neuroinflammation and epileptogenesis in experimental models of temporal lobe epilepsy. Neurobiology of Disease. 110:102-121.

285. Sharma, S., Puttachary, S., Thippeswamy, T. (2017). Glial source of nitric oxide in epileptogenesis: a target for disease modification in epilepsy. J Neurosci Res.

286. Sharma, S., Puttachary, S., Thippeswamy, A., Kanthasamy, A.G., Thippeswamy, T. (2018b). Status Epilepticus: behavioral and electroencephalography seizure correlates in kainate experimental models. Front Neurol. 9:7.

287. Shearer, B.G., Lee, S.L., Oplinger, J.A., Frick, L.W., Garvey, E.P., Furfine, E.S. (1997). Substituted N-phenylisothioureas: potent inhibitors of human nitric oxide synthase with neuronal isoform selectivity. J Med Chem. 40:1901–1905.

288. Shi, Z., Li, N., Tang, Y., Shi, Q., Zhang, W., Zhang, P., et al. (2014). Synthesis, biological evaluation and SAR analysis of O -alkylated analogs of quercetin for anticancer. Bioorganic & Medicinal Chemistry Letters. 24(18):4424-4427.

289. Sloviter, R. S. (2008). Hippocampal epileptogenesis in animal models of mesial temporal lobe epilepsy with hippocampal sclerosis: The importance of the "latent period" and other concepts. Epilepsia. 49, 85–92.

290. Sofroniew, M.V., Bush, T.G., Blumauer, N., Lawrence, K., Mucke, L., Johnson, M.H. (1999). Genetically-targeted and conditionally-regulated ablation of astroglial cells in the central, enteric and peripheral nervous systems in adult transgenic mice. Brain Res. 835(1):91–95.

291. Sofroniew, M.V., Vinters, H.V. (2010). Astrocytes: biology and pathology. Acta Neuropathol. 119(1):7–35.

292. Sorce, S., Krause, K.H., Jaquet, V. (2012). Targeting NOX enzymes in the central nervous system: therapeutic opportunities. Cellular and Molecular Life Sciences. 69(14):2387–2407.

293. Steinhauser, C., Grunnet, M., Carmignoto, G. (2016). Crucial role of astrocytes in temporal lobe epilepsy. Neuroscience. 323:157-69.

294. Streit, W.J., Mrak, R.E., Griffin, W.S.T. (2004). Microglia and neuroinflammation: a pathological perspective. J Neuroinflammation. 1:14.

295. Streit, W.J., Xue, Q.S., Tischer, J., Bechmann, I. (2014). Miroglial pathology. Acta Neuropathol Commun. 2:142.

296. Sutula, T. P. (2004). Mechanisms of epilepsy progression: current theories and perspectives from neuroplasticity in adulthood and development. Epilepsy Res. 60:161–71.

297. Suzuki, F., Heinrich, C., Boehrer, A., Mitsuya, K., Kurokawa, K., Matsuda, M., & Depaulis, A. (2005). Glutamate receptor antagonists and benzodiazepine inhibit the progression of granule cell dispersion in a mouse model of mesial temporal lobe epilepsy. Epilepsia. 46, 193–202.

298. Szalay, G., Martinecz, B., Lenart, N., Kornyei, Z., Orsolits, B., Judak, L., et al. (2016). Microglia protect against brain injury and their selective elimination dysregulates neuronal network activity after stroke. Nature Communications. 7, 11499.

299. Tatton, L., Morley, G. M., Chopra, R., Khwaja, A. (2003). The Src-selective Kinase Inhibitor PP1 Also Inhibits Kit and Bcr-Abl Tyrosine Kinases. Journal of Biological Chemistry. 278(7):4847-4853.

300. Temkin, N. R. (2001). Antiepileptogenesis and seizure prevention trials with antiepileptic drugs: Meta-analysis of controlled trials. Epilepsia. 42, 515–524.

301. Thippeswamy, T., McKay, J. S., Quinn, J. P., Morris, R. (2006). Nitric oxide, a biological double-faced Janus—is this good or bad? Histology and Histopathology. 21, 445–458.

302. Thippeswamy, T., Howard, M.R., Cosgrave, A.S., Arora, D.K., McKay, J.S., Quinn, J.P. (2007). Nitric oxide-NGF mediated PPTA/SP, ADNP, and VIP expression in the peripheral nervous system. Journal of Molecular Neuroscience. 33(3):268–277.

303. Thippeswamy, T., McKay, J.S. (2005). Neuronal nitric oxide synthase and nerve growth factor expression in the enteric nervous system. Cellular and Molecular Biology. 51(3):293–298.

304. Thomas, S. M., Brugge, J. S. (1997). Cellular Functions Regulated By Src Family Kinases. Annual Review of Cell and Developmental Biology. 13(1):513-609.

305. Thompson, P. J., Conn, H., Baxendale, S. A., Donnachie, E., Mcgrath, K., Geraldi, C., Duncan, J. S. (2016). Optimizing memory function in temporal lobe epilepsy. Seizure. 38, 68–74.

306. Tousoulis, D., Kampoli, A.M., Tentolouris, C., Papageorgiou, N., Stefanadis, C. (2012). The role of nitric oxide on endothelial finction. Curr Vasc Pharmacol. 10(1):4-18.

307. Toy, D., Namgung, U. (2013). Role of glial cells in axonal regeneration. Exp Neurobiol. 22(2):68-76.

308. Trinka, E., Cock, H., Hesdorffer, D., Rossetti, A. O., Scheffer, I. E., Shinnar, Shorvon, S., Lowenstein, D. H. (2015). A definition and classification of status epilepticus—report of the ILAE Task Force on Classification of Status Epilepticus. Epilepsia. 56, 1515–1523.

309. Umemori, H., Sato, S., Yagi, T., Aizawa, S., Yamamoto, T. (1994). Initial events of myelination involve Fyn tyrosine kinase signaling. Nature. 367(6463):576-6.

310. Varvel, N. H., Jiang, J., Dingledine, R. (2015). Candidate drug targets for prevention or modification of epilepsy. Annual Review of Pharmacology and Toxicology. 55, 229–247.

311. Vezzani, A., Baram, T.Z. (2007). New roles for interleukin-1 beta in the mechanisms of epilepsy. Epilepsy Curr. 7, 45–50.

312. Vezzani, A., French, J., Bartfai, T., Baram, T.Z. (2011). The role of Inflammation in epilepsy. Nat Rev Neurol. 7(1):31-40.

313. Vezzani, A., Friedman, A., Dingledine, R.J. (2013). The role of inflammation in epileptogenesis. (2013). 69:16-24.

314. Viviani, B., Bartesaghi, S., Gardoni, F., Vezzani, A., Behrens, M. M., Bartfai, T., et al. (2003). Interleukin-1β Enhances NMDA Receptor-Mediated Intracellular Calcium Increase through Activation of the Src Family of Kinases. The Journal of Neuroscience. 23(25):8692-8700.

315. Vos, T., Barber, R. M., Bell, B., Bertozzi-Villa, A., Biryukov, S., Bolliger, I., Murray, C. J. (2015). Global, regional, and national incidence, prevalence, and years lived with disability for 301 acute and chronic diseases and injuries in 188 countries, 1990–2013: A systematic analysis for the Global Burden of Disease Study 2013. Lancet. 386, 743–800.

316. Walker, M.C., White, H.S., Sander, J.W.A.S. (2002). Disease modification in partial epilepsy. Brain. 125: 1937–1950.

317. Wallraff, A., Kohling, R., Heinemann, U., Theis, M., Willecke, K., Steinhauser, C. (2006). The impact of astrocytic gap junctional coupling on potassium buffering in the hippocampus. J Neurosci. 26:5438–5447.

318. Walz, W. (1989). Role of glial cells in the regulation of the brain ion microenvironment. 33(4):309-33.

319. Weissberg, I., Wood, L., Kamintsky, L., Vazquez, O., Milikovsky, D. Z., Alexander, A., et al. (2015). Albumin induces excitatory synaptogenesis through astrocytic TGF-b/ALK5 signaling in a model of acquired epilepsy following blood-brain barrier dysfunction. Neurobiology of Disease. 78, 115–125.

320. Wheless, J.W., Clarke, D.F., Arzimanoglou, A., Carpenter, D. (2007). Treatment of pediatric epilepsy: European expert opinion. Epileptic Disord. 9(4):353–412.

321. White, A., Williams, P. A., Hellier, J. L., Clark, S., Dudek, F. E., Staley, K. J. (2010). EEG spike activity precedes epilepsy after kainate-induced status epilepticus. Epilepsia. 51:371–83.

322. White, H. S. (2002). Animal models of epileptogenesis. Neurology. 59 (Suppl. 5): S7–S14.

323. Williams, P. A., Hellier, J. L., White, A. M., Staley, K. J., Dudek, F. E. (2007). Development of spontaneous seizures after experimental status epilepticus: Implications for understanding epileptogenesis. Epilepsia. 48, 157–163.

324. Williams, P. A., White, A. M., Clark, S., Ferraro, D. J., Swiercz, W., Staley, K. J., Dudek, F. E. (2009). Development of spontaneous recurrent seizures after kainate-induced status epilepticus. Journal of Neuroscience. 29, 2103–2112.

325. Wilson C., Finch C., Cohen H. (2002). Cytokines and cognition-the case for a head-to-toe inflammatory paradigm. J Am Geriatr Soc. 50(12):2041–2056.

326. Wilson, E.H., Weninger, W., Hunter, C.A. (2010). Trafficking of immune cells in the central nervous system. J. Clin. Invest. 120:1368–1379.

327. Xie, Q.W., Nathan, C. (1994). The high-output nitric oxide pathway: role and regulation. J Leukoc Biol. 56:576–582.

328. Xiong, Z.Q., Qian, W., Suzuki, K., McNamara, J.O. (2003). Formation of complement membrane attack complex in mammalian cerebral cortex evokes seizures and neurodegeneration. J. Neurosci. 23:955–960.

329. Xu, W., Harrison, S.C., Eck, M.J. (1997). Three dimensional structure of the tyrosine kinase c-Src. Nature. 385:595–602.

330. Yagi, T. (1994). Src Family Kinases Control Neural Development and Function. (gene targeting/tyrosine kinase/Fyn/behavior/learning/emotion). Development, Growth and Differentiation. 36(6):543-550.

331. Yarlagadda, A., Alfson, E., Clayton, A.H. (2009). The blood brain barrier and the role of cytokines in neuropsychiatry. Psychiatry (Edgmont). 6(11):18–22.

332. Yoon, B.E., Jo, S., Woo, J., Lee, J.H., Kim, T., Kim, D., et al. (2011). The amount of astrocytic GABA positively correlates with the degree of tonic inhibition in hippocampal CA1 and cerebellum. Mol Brain. 4(1):42.

333. Yuste, J.E., Tarragon, E., Campuzano, C.M., Ros-Bernal, F. (2015). Implications of glial nitric oxide in neurodegenerative diseases. 9:322.

334. Zetterstrom, M., Sundgren-Andersson, A.K., Ostlund, P., Bartfai, T. (1998). Delineation of the proinflammatory cytokine cascade in fever induction. Ann. N.Y. Acad. Sci. 856:48–52.

335. Zhang, H. Q., Fast, W., Marletta, M. A., Martasek, P., Silverman, R. B. (1997). Potent and selective inhibition of neuronal nitric oxide synthase by N omega-propyl-L-arginine. Journal of Medicinal Chemistry. 40, 3869–3870.

336. Zhang, J.M., Wang, H.K., Ye, C.Q., Ge, W., Chen, Y., Jiang, Z.L., et al. (2003). ATP released by astrocytes mediates glutamatergic activity-dependent heterosynaptic suppression. Neuron. 40(5):971–982.

337. Zhou, L., Zhu, D.Y. (2009). Neuronal nitric oxide synthase: Structure, subcellular localization, regulation, and clinical implications. Nitric Oxide. 20: 223– 230.

338. Zuchero, J.B., Barres, B.A. (2015). Glia in mammalian development and disease. Development. 142(22):3805-9.

CHAPTER II

IS C57BL/6J MOUSE KAINATE MODEL OF EPILEPTOGENESIS APPROPRIATE FOR TESTING DISEASE MODIFYING AGENTS? A LONG-TERM CONTINUOUS VIDEO-EEG STUDY

Modified from a paper published in *PLOS ONE*

Sreekanth Puttachary[1B], Shaunik Sharma[1,B], Karen Tse[2], Edward Beamer[2], Abby Sexton[1], Joseph Crutison[1], Thimmasettappa Thippeswamy[1C]

[1]Department of Biomedical Sciences, College of Veterinary Medicine, Iowa State University, Ames IA 50011-1250, United States of America.

[2]Institute of Aging and Chronic Disease, University of Liverpool, Liverpool, L69 3GA, United Kingdom.

[A]Reprinted with permission of *PLoS One*. 2015 Jul 10; 10(7):e0131705.

[B]Primary researchers and authors.

[C]Author for correspondence

Abstract

The C57BL/6J mouse as a model of seizure/epilepsy is challenging due to high mortality and huge variability in response to kainate. We have recently demonstrated that repeated administration of a low dose of kainate by intraperitoneal route can induce severe status epilepticus (SE) with 94% survival rate. In the present study, based on continuous video-EEG recording for 4-18 weeks from epidurally implanted electrodes on the cortex, we demonstrate that this method also induces immediate epileptogenesis (<1-5 days post-SE). This finding was based on identification of two types of spontaneous recurrent seizures; behavioral convulsive seizures (CS) and electrographic nonconvulsive seizures (NCS). The identification of the spontaneous CS, stage 3-5 types, was based on the behaviors (video) that were associated with the EEG characteristics (stage 3-5 epileptiform spikes), the power spectrum, and the activity counts. The electrographic NCS identification was based on the stage 1-2 epileptiform spike clusters on the EEG and their associated power spectrum. Severe SE induced immediate epileptogenesis in all the mice. The maximum numbers of spontaneous CS were observed during the first 4-6 weeks of the SE and they decreased thereafter. Mild SE also induced immediate epileptogenesis in some mice but the CS were less frequent. In both the severe and the mild SE groups, the spontaneous electrographic NCS persisted throughout the 18 week observation period, and therefore this could serve as a chronic model for complex seizures. However, unlike rat kainate models, the C57BL/6J mouse kainate model is a unique regressive CS model of epilepsy. Further studies are required to understand the mechanism of recovery from spontaneous CS in this model, which could reveal novel therapeutic targets for epilepsy.

Introduction

Temporal lobe epilepsy (TLE) is the most common form of human epilepsy [1]. To understand the pathogenesis of human TLE, rodent models of epilepsy have been developed and characterized. A variety of methods have been tried in rodent models to induce status epilepticus (SE) and epileptogenesis [2–4]. Hitherto, rat models (for example [5–8]) and some mouse models (for example [9, 10]) of TLE are well characterized and extensively studied. Several weeks after the induction of SE in these models, intermittent or continuous video-EEG recordings have provided convincing evidence for the onset of spontaneous recurrent seizures, SRS (for example [11–13]).

Kainate is one of the most common drug used to induce SE in rodents (reviewed by [14– 18]). Although several mouse models of epileptogenesis have been developed [19, 20], the C57BL/6J strain posed several challenges such as high mortality, inconsistent seizure response and resistance to kainate-induced neurotoxicity by the intraperitoneal (i.p.) route at a dose <30 mg/kg [21-24]. In the previous studies, a single dose of kainate by the i.p. route in these mice had failed to produce consistent severe SE without high mortality [25, 26]. Recently, we have addressed these issues in the C57BL/6J mice by administering kainate in repeated low doses (5 mg/kg i.p., at 30 min intervals), until they reach the stage-5 seizures [27].

In order to overcome the kainate-resistance to neurotoxicity in the C57BL/6J strain, by the i.p. or the subcutaneous (s.c.) route, kainate administration via the intra-hippocampal (for example [28, 29]), the intra-striatal [30] and the intra-amygdalar (for example [31]) routes were employed. It was known that severity of SE is the most important factor to induce epileptogenesis [32, 33]. Since the repeated low dose of kainate administration via the i.p. route

could induce severe SE in the C57BL/6J mice with least mortality [27], we hypothesized that this approach could also induce epileptogenesis. To test this hypothesis, we induced mild to severe SE with kainate by intraperitoneal route in the C57BL/6J mice using the same method as described in our recent publication [27]. In the present study, after the induction of SE, the mice were subjected to continuous video-EEG monitoring for 4–18 weeks. Like in other models of epilepsy (for example [32, 33]), the frequency of spontaneous convulsive seizures (CS) directly correlated with the severity of the SE in the C57BL/6J mice. In addition, we present unexpected and interesting findings from this study: i) immediate epileptogenesis occurred in both the severe and the mild SE groups ii) the frequency of spontaneous CS increased with the severity of the SE but they decreased after 4–6 weeks iii) irrespective of the severity of the SE, the spontaneous electrographic nonconvulsive seizures (NCS) persisted throughout the observation period. These findings are presented and discussed in this study.

Materials and Methods

Animal source and ethical approval

The experiments were performed using the C57BL/6J male mice of 6–7 weeks old. They were purchased from the Jackson Laboratory, ME, USA and maintained in the Laboratory of Animal Resources at Iowa State University (ISU). The mice were housed under controlled environmental conditions (19°C– 23°C, 12 hour light: 12 hour dark), with ad libitum access to food and water. All experiments were performed according to the approved protocol by the Institutional Animal Care and Use Committee, ISU, USA (protocol no. 10-12-7446-MR). All surgeries were performed under isoflurane anesthesia and all efforts were made to

minimize discomfort throughout the duration of the experimentation. All mice were euthanized with an overdose of pentobarbital sodium (100 mg/kg, i.p.) at the end of the experiments.

Terminologies. Duration of the entire SE, established SE, criteria for mild and severe SE classification, and the latent period.

Depending on the number of injections of kainate given, the overall duration of the entire SE varied from 3–6 hours. During this period of SE, all the mice had continuous epileptiform activity on EEG and the mice experienced continuous stage-1 and -2 (Racine scale 1 and 2) type behavioral seizures for greater than 10 minutes prior to the onset of stage 3 or 5 seizures (Racine scale 3 or 5). Once the mice reached stage 3 or 5 seizures, the behavioral and electrographic seizures fluctuated between stage 1 to stage-3 or -5 (Racine scale 3 or 5) for greater than 10 minutes. Overall, the SE in the present study met the criteria set by the International League Against Epilepsy [34, 35] i.e., SE was a continuous seizure activity that lasted for more than 10 minutes and also the different types of seizures (stage 1–5) were recurring at very short intervals (< 1 minute) during the established SE (Fig 1).

The “established SE” in the present study is the duration between the first onset of stage-3 or stage-5 seizure during the SE and the diazepam treatment, which is typically 2 hours (Fig 1, and also Illustrated by Tse et al., [27]).

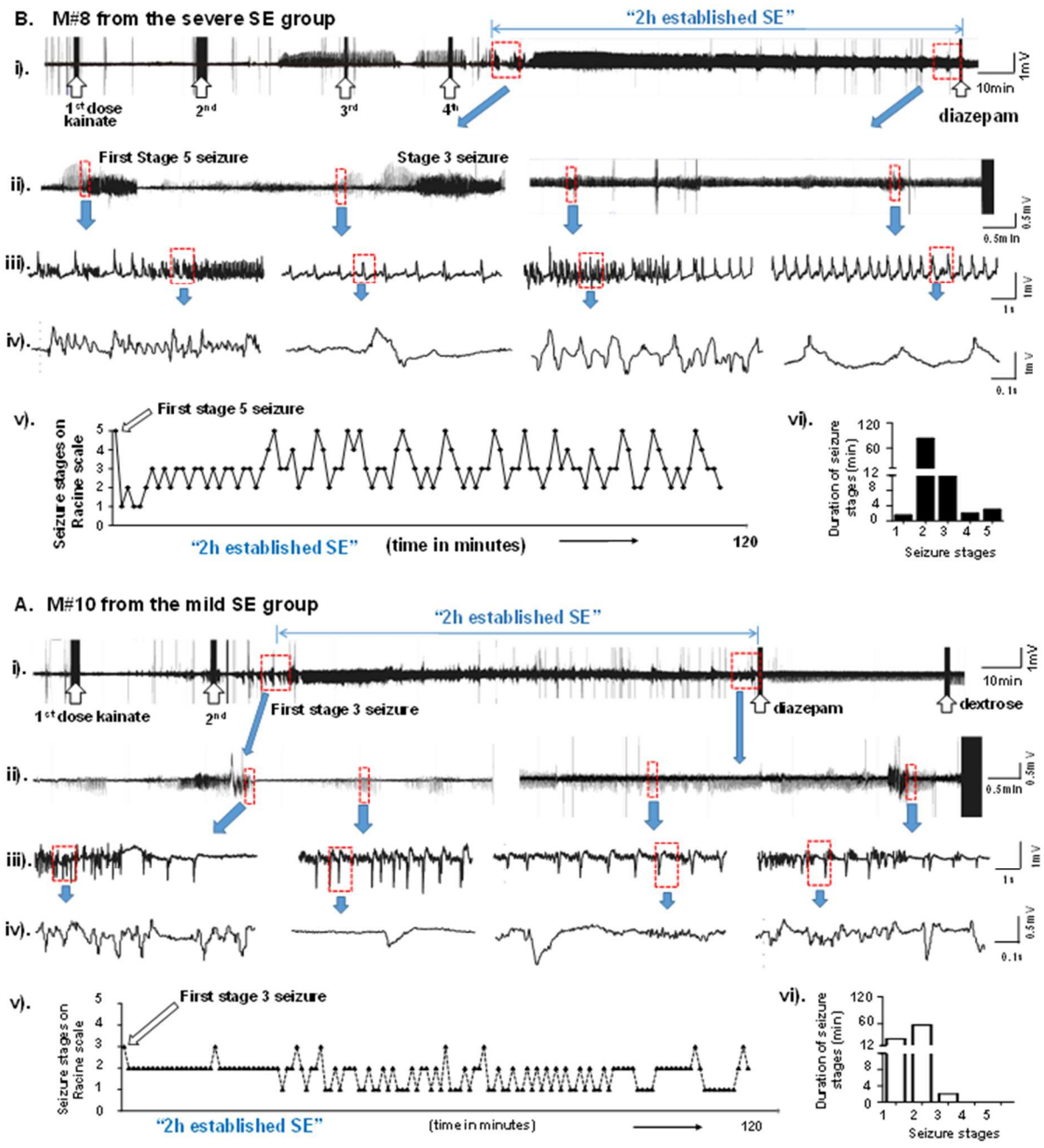

Fig 1. A (i to iv) and B (i to iv) are the representative EEG traces obtained during mild and severe SE, respectively, in this study. The behavioral scoring (Racine scale stages from 1 to 5) for these mice during the 2 hours established SE (v) and the duration of each stage was quantified (vi). The upward open arrows indicate the injections given [kainate (5 mg/kg)- first two arrows in A (i), and first four arrows in B (i); diazepam and dextrose at the other end of the trace]. The first episode of stage-3 seizure in the mild SE group (A, after the second dose of kainate) or the stage 5 in the severe SE group (B, after the fourth dose of kainate) is shown on the EEG traces (i and ii). The expanded EEG trace from the very end of the established SE, prior to the diazepam treatment, is shown in the panel (ii). A further expanded EEG traces are also shown in panels (iii) and (iv). The first stage 3 (in mild group) or the stage 5 (in the severe group) marked the beginning of the 2 hours established SE. During the 2 hour

period, the mouse [panel A, (v)] had stage 2 seizures continuously for first 30 minutes with a second episode of stage-3 seizure half-way through and changed to the stage-1 seizure. Beyond this point, the remaining 90 minutes, the mouse (panel A) had continuous seizures ranging from stage-1 to stage-3. The exact amount of time spent at each stage is given in the panel (vi), likewise for the mouse in the severe SE group (panel B). During the 2 hour period, the mouse (panel B) had a brief stage-1 seizures followed by continuous stage 2–5 seizures during the remaining period of 2 hours (v). The exact amount of time the mouse spent at each stage is given in the panel vi.

To classify mice under the "mild SE", the first stage-3 seizure and for the "severe SE", the first stage-5 seizure were considered as the starting points for the 2hour established SE. The end point for both groups was when the diazepam was administered. During the 2 hours established SE, in the mild group the seizures fluctuated between the stage-1 to stage-3, while in the severe group between stage-1 (most often stage-2) to stage-5. The other criterion considered was that the mice under "severe SE" group should have had experienced a minimum of continuous 10 minutes of stage 3–5 seizures in addition to continuous stage 1–2 seizures for a long period (often > 40 minutes). The "mild SE" group mice should have had experienced stage-3 seizures intermittently for less than 10 min but continuous stage-1 or -2 seizures often greater than 40 minutes (for example, Fig 1).

The latent period is the period between the diazepam treatment and the first occurrence of spontaneous behavioral CS ("motor seizure latent period") or the first onset of spontaneous electrographic NCS ("electrographic seizure latent period"). The period beyond the first spontaneous electrographic NCS was considered as the epileptic phase.

The "activity counts", in the present study, refers to the counts that were generated due to locomotor activity. These behaviors were detected by the radiotransmitter and relayed to the computer as "activity counts/minute". Higher the counts, greater the locomotor activity. The increased activity counts generated due to behavioral CS were associated with high amplitude and high frequency epileptiform spikes on the EEG and increased gamma power. The

distinguishing feature of activity counts associated with normal behavior was the lack of EEG power in the gamma band. The activity counts due to exploratory or grooming behavior lacked high frequency and high amplitude epileptiform spike clusters on EEG. Further details on artifact spikes and epileptiform spikes, and activity counts in C57BL/6J mouse using epidural electrode technique has been published recently [27].

Surgery, telemetry device implantation, SE induction with kainate and video-EEG monitoring

Twenty three mice were implanted with the telemetry device (Physiotel Multiplus ETA-F20, Data Science International, MN, USA), subcutaneously, 10 days prior to the induction of SE with kainate. The two electrodes were inserted into the burr holes bilaterally, 2.5 mm caudal to the bregma and 2.0 mm lateral to the midline, to record EEG from each hemisphere. The electrodes were positioned in contact with the dura mater over the surface of the cortex. The detailed surgical procedure for implanting the electrodes and the radiotransmitter has been described in our previous publications [27, 36].

The mouse cages were randomly allotted to the PhysioTel RPC receiver pads that transmit the data from the telemetry devices to Windows PC via the data exchange matrix. We used the Dataquest ART software to acquire real-time data at a sampling frequency of 1000 Hertz (Hz) and the NeuroScore software (DSI, MN, USA) to analyze the EEG recordings. The data acquired from the telemetry device included the EEG, the activity counts/minute and the mouse body temperature. The video-EEG recording was started soon after the surgery to acquire baseline EEG from each mouse that consisted of day and night cycles. The video was recorded at 25 frames/sec.

Nineteen out of 23 mice received kainate (Abcam, USA), which was prepared fresh in sterile distilled water at a concentration of 2 mg/ml. The remaining four mice received equal volumes of sterile distilled water, instead of kainate. These mice served as control. A repeated low dose of kainate at 5 mg/kg per injection was given i.p. at 30 minutes intervals. This method was useful to titrate the mice to achieve either mild or severe SE. The stages in the SE were identified and recorded according to the modified Racine scale (stage-1 to -5) [27]. Nine mice were titrated to achieve severe SE with a duration of >10 minutes of continuous stage 3–5 seizures during the 2 hours established SE. The 2 hour duration of the established SE started from the first onset of the stage-5 seizure to the time point when the mice were administered with diazepam (10 mg/kg, i.p.). The remaining 10 mice were titrated to achieve mild SE for a duration of <10 minutes of intermittent stage-3 seizures during the 2 hours established SE. In both mild and severe groups, all mice experienced continuous stage1-2 seizures for greater than 10 minutes. During the induction of SE, the behavior of the mice was video-EEG recorded and, simultaneously, two personnel directly scored the behavioral seizures based on the modified Racine scale [37], in 5 minutes epochs [27, 36]. The behavioral seizures during the SE were also further scored from the "standalone videos" by two other personnel who were blind to the experiments. The average score was used to calculate cumulative seizure severity score (CSSS) for the behavioral seizures.

The behavioral SE was terminated with diazepam, and immediately all the mice received dextrose normal saline (1 ml, s.c). From our experience, we knew that the mice with severe SE will lose their bodyweight (about 5%) in the first 2-3d of post-SE. To overcome this, dextrose normal saline injection were continued once a day and soft food pellets were provided

until the mice regained their body weight (usually by third day). After the diazepam administration, the video-EEG recording was continued for 4–18 weeks.

The four (out of 23) mice that received sterile distilled water instead of kainate were also treated with diazepam and dextrose normal saline. Four injections of distilled water were given at 30 min intervals to match with the vast majority of the mice that received kainate in multiple injections. The diazepam was given 2 hours after the last dose of distilled water. These mice were also video-EEG monitored continuously for 4 weeks to investigate whether the surgeryinduced trauma, and the implanted electrodes, also induce epileptogenesis or spontaneous spike-wave discharges or epileptiform spiking as reported for the rat models [38–40].

CSSS index calculation to determine severity of the SE- based on the behavioral and the EEG characteristics during the SE

Four research assistants, who were unaware of the treatment groups, analyzed the video-EEG for severity of the SE and determined behavioral and electrographic CSSS indices. The details of the behavioral seizures at different stages, on Racine scale, during the SE in the C57BL/6J, induced by kainate, have been published [27, 36]. The duration between the first onset of the stage-5 seizure (severe SE group) or the stage-3 seizure (mild SE group) and the diazepam treatment was 2 hours. It is important to note that during the 2 hours of established SE, the seizures recurred continuously between stage-1 and stage-3 or -5. Behavioral CSSS (in minutes) for each mouse was calculated based on the exact amount of time the mouse spent at each stage of a convulsive seizure between stage-3 and stage-5 (total of all three stages from 3 to 5 in minutes for the severe group, stage-3 only in the mild group) during the 2 hour period.

It is also important to note that the duration of continuous stage-1 and -2 seizures, which was often greater than 40 min in both severe and mild groups, was not considered to calculate CSSS index. The electrographic CSSS was calculated for both the groups based on the exact duration of stage ≥3 epileptiform spikes on the EEG (total of all three stages from 3 to 5 in minutes for the severe group, stage-3 only in the mild group). The EEG characteristics were always correlated with the behavioral seizures (but certain behaviors during an episode were not always associated with the epileptiform spiking during the SE), spectral density characteristics and the activity counts [27]. To determine the SE as mild or severe, both the behavioral and the electrographic CSSS indices were considered.

Identification and quantification of spontaneous CS based on the realtime integrated video-EEG-power band characteristics and the activity counts

We have previously described the procedure for EEG quantification during kainate-induced SE in the C57BL/6J mice [27]. In our previous short term study, a minimum of 24 hours baseline EEG was recorded from each mouse before administering the kainate. In the present long term study, we considered 10 days of continuous baseline recording which included day and night cycle, sleep and awake state, and resting and exploratory activities. The video-EEG recording was continued during and after the kainate treatment for up to 4–18 weeks. All the post-kainate responses were normalized against the baseline from the same mouse [8, 9, 27, 36]. The EEG raw signal in 10 seconds epochs, after manually excluding the artifacts, was subjected to Fast Fourier Transformation (FFT) to derive power bands (power spectral density). The EEG signal component containing various frequencies were split into individual power bands corresponding to the delta (δ, 0.5–4 Hz), the theta (θ, 4–8 Hz), the alpha (α, 8–12 Hz), the sigma (S, 12–16 Hz), the beta (β, 16–24 Hz) and the gamma (γ, 24–80

Hz) [27, 36]. The power in different spectra changed depending on the stage of a seizure within an episode and the power in some bands increased as a seizure progressed from stage-1 to -5. The baseline power for all the spectral bands were <5 mV^2. To differentiate the epileptiform spikes from the normal baseline spikes or from the spikes due to electrical or mechanical artefacts, we considered individual spike characteristics such as amplitude, duration, frequency, inter-spike intervals and the activity counts (per minute) during this period. The spike amplitude threshold for the baseline was 100μV. The epileptiform spikes were detected using the NeuroScore software by setting the following parameters; amplitude threshold between 150 and 1500μV with the individual spike duration 15 and 500ms, inter-spike interval 80 and 5000ms, and the spike train join interval was 100 and 5000ms within an episode (Table 1).

Table 1. The epileptiform spike characteristics for the spontaneous behavioral CS and the electrographic NCS and during the post-SE period in the C57BL/6J mice.

Seizure stages	Length of episode (sec)	Spike Amplitude (μV)	Inter-spike interval (ms)	Spike frequency/ min(within an episode)
Stage-1 inter-ictal spikes	300–1500	200–300	1000–4000	15–60
Stage-2 inter-ictal spikes	300–1500	400–1500	2000–5000	12–30
Stage-1 episode	10–15	200–300	200–500	120–300
Stage-2 episode	20–40	400–1500	800–1200	48–72
Stage-3 episode	20–50	500–1500	100–300	180–600
Stage-4 episode	30–60	500–1500	100–300	180–600
Stage-5 episode	40–120	500–3000	80–300	180–720

The spikes/min column represents a minimum and a maximum number of spikes/min in an episode. The detailed explanation for the epileptiform spikes on the EEG that were associated with the behavior during the SE, and artifacts, are given elsewhere [27].

After detecting seizure episodes using the NeuroScore software, the EEG recordings were manually verified and all the recurrent spontaneous CS types were checked against the real-time videos, the spectral bands and the activity counts. The artifacts such as exploratory behavior and electrical interference were detected based on the individual spike characteristics, the power spectrum, and the activity counts [27].

Identification and quantification of spontaneous electrographic NCS based on the EEG and the power band characteristics

The spontaneous electrographic NCS episodes included the stage-1 and -2 type epileptiform spike clusters along with their respective pre-, post- and inter-ictal spikes. The stage-1 electrographic NCS episode included the stage-1 epileptiform spikes along with its associated stage-1 pre- and post-ictal spikes. Similarly, the stage-2 electrographic NCS episode included the stage-2 epileptiform spikes with its associated stage-2 pre- and post-ictal spikes. The duration of some of the spontaneous electrographic NCS episodes, usually the stage-2 type, were as long as 30 minutes with an inter-spike interval of 2-5s (frequency 0.2–0.4 Hz, Table 1), but we set a minimum of 12 seconds duration with a frequency ≥0.8 Hz to consider it as an electrographic NCS episode.

The numbers of spontaneous CS (stage -3,-4 and -5) and the spontaneous electrographic NCS episodes (stage-1 and -2) were plotted as group data for the duration of first 4 weeks, 5–8 weeks, 9–12 weeks and 13–18 weeks for both the severe and the mild SE groups. The spontaneous convulsive seizures occurred during the first four weeks after the SE, in both the severe and the mild SE groups, are also presented at 24 hour epochs to demonstrate mouse-to-mouse variability. The Mann-Whitney test was used to compare between the behavioral and the electrographic convulsive seizure severity score, and to compare between the total numbers of spontaneous seizures at different time points. The Kruskal-Wallis test was used to compare the seizures within the groups across different time points.

Results

The CSSS index to determine severity of the SE

As previously noted, there was no correlation between the CSSS index and the amount of kainate administered to achieve the SE [27]. All the mice in this study had continuous behavioral and electrographic stage 1–2 seizures for a minimum of 10 minutes prior to the onset of first stage-3 or -5 seizures and during the 2 hours established SE. After the onset of stage-3 or -5 behavioral seizures, the vast majority of the mice had continuous seizures that fluctuated between the stage-1 and the stage-3 in the mild group and between the stage-1 or 2 and the stage-5 in the severe group (for example, Fig 1). The severe SE group mice always had the stage-5 behavioral seizures that were characterized by generalized tonic clonic convulsions with lateral recumbence or jumping and/or wild running followed by generalized convulsions. The mild SE group mice always had the stage-3 behavioral seizures consisting of rearing with facial automatisms and forelimb clonus but never experienced generalized convulsions i.e. the stage-5 seizure. The video demonstrating the stage-3 to -5 in the C57BL/6J mouse has been published by our group [27]. In the vast majority of the mice, in both groups, the stage-1 and -2 seizures persisted continuously for >40 minutes (for example, Fig 1). The representative EEG trace and behavioral seizures score, during the 2 hour established SE, from the mouse that had severe or mild SE is demonstrated in Fig 1.

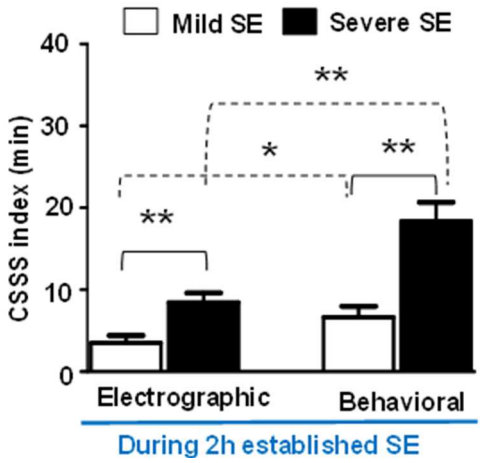

Fig 2. Behavioral and electrographic CSSS indices comparison between the severe and the mild SE groups during the 2 hours established SE. The CSSS indices for both behavioral and electrographic seizures were significantly higher in the severe SE group, when compared to the mild SE group (**p = 0.0047, electrographic CSSS; **p = 0.0011, behavioral CSSS; n = 9, Mann-Whitney test). There was almost 50% difference between the electrographic and the behavioral CSSS indices in both groups (*p = 0.037 for the mild group, **p = 0.0023 for the severe group, Mann-Whitney test).

The severe SE group mice that experienced stage-3 to -5 behavioral seizures had an average of 20 behavioral CSSS index and 10 electrographic CSSS index, while the mild SE group mice had only the stage-3 behavioral seizures intermittently for a period <10 minutes, and their CSSS indices were well below the severe SE group (Fig 2). The CSSS indices for both the behavioral stage ≥3 seizures and their associated EEG seizures were significantly higher in the severe SE group when compared to the mild SE group (p = 0.0047 for the electrographic CSSS and p = 0.0011 for the behavioral CSSS, the Mann-Whitney test; n = 9 each). Interestingly, there was about 50% difference between the behavioral and the electrographic CSSS values in both groups (Fig 2).

Both severe and mild SE induce immediate epileptogenesis

In this study, the period between the diazepam treatment and the first onset of spontaneous behavioral CS was considered as the “motor seizure latent period” while, the first

onset of electrographic NCS was considered as the "electrographic seizure latent period" [8]. Interestingly, as in the rat kainate models of epileptogenesis/epilepsy described in the literature [8, 12, 17, 41], there was no well-defined prolonged 'motor seizure latent period' for the C57BL6/J mice, in both groups, in this study. The first electrographic NCS was observed at 138 ± 66 minutes in the mild group and at 78± 60 minutes in the severe group after the diazepam treatment. There was no significant difference between the groups. The motor seizure latent periods for the mild and severe groups were 7±3.8 (n = 8, one being an outlier, 33 days) and 1.8±0.47 days (n = 9, mean ±SEM), respectively, and there was also no significant difference between the groups. Out of 9 epileptic mice under the severe SE group, one mouse had no motor seizure latent period, 4 mice had 1d, and 2 mice each had 2 and 4 days (Fig 3).

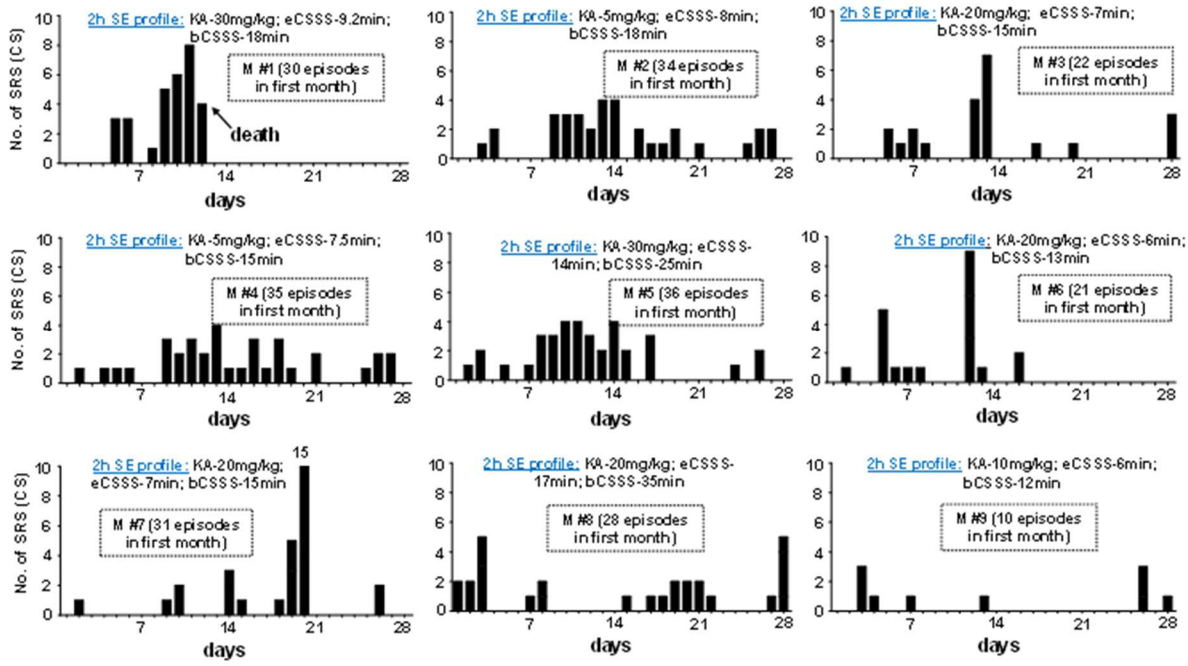

Fig 3. The frequency of spontaneous behavioral CS occurrence during the first 4 weeks of post-SE in the severe SE group. The 2 hour established SE profile, and the total numbers of spontaneous CS episodes/day during the first 4 weeks of post-SE are given for each mouse. All mice in the severe group had continuous stage-1 or 2 seizures for >40 min during the 2 hours established SE. There is no correlation between the amount of kainate received and the motor seizure latent period, and the numbers of spontaneous CS episodes. eCSSS = electrographic CSSS index (in min); bCSSS = behavioral CSSS index (in min)

In the mild SE group, out of 10 mice one mouse showed neither a behavioral CS nor an electrographic NCS throughout the 18 weeks period. Another mouse (Fig 4, M#15) in this group had only the electrographic NCS throughout the 18 weeks but no behavioral CS were observed. The motor seizure latent period in the mild SE group varied from 1 to 10 days (Fig 4) with an exception of 33 days in one mouse (M#16). In both mild and severe SE groups, spontaneous electrographic NCS always occurred prior to the behavioral CS.

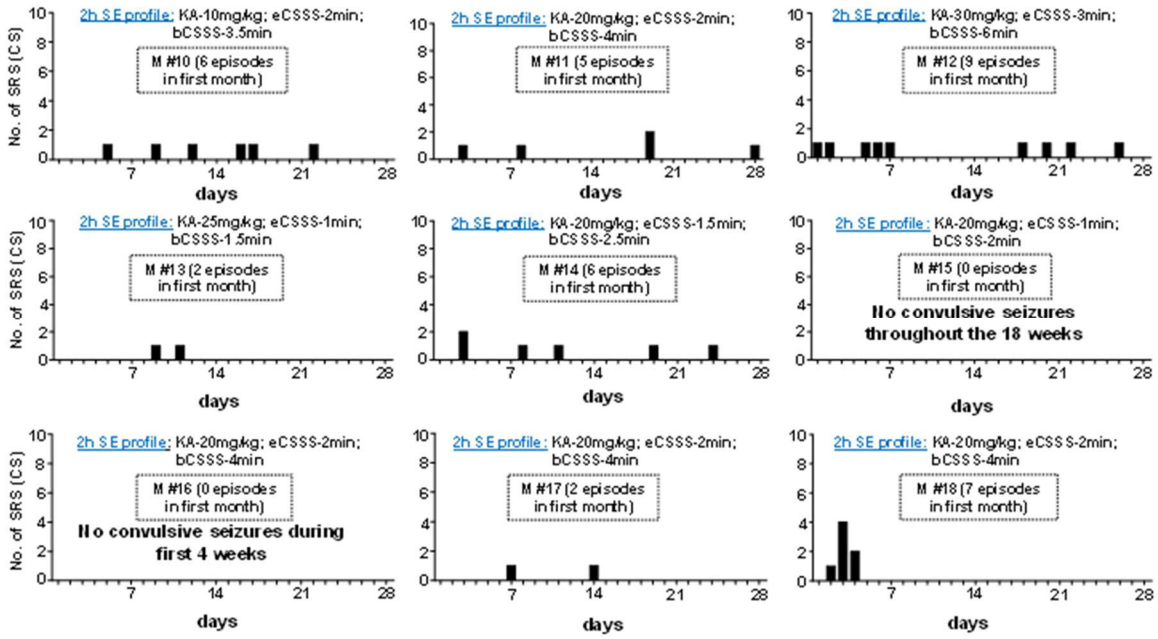

Fig 4. The frequency of spontaneous behavioral CS occurrence during the first 4 weeks of post-SE in the mild SE group. The 2 hour established SE profile, and the total numbers of spontaneous behavioral CS are given for each mouse. All mice in the mild group also had continuous stage-1 or 2 seizures for > 40 min during the 2 hours established SE (an example is shown in Fig 1). As in the severe SE group, there was no correlation between the amount of kainate given and the motor seizure latent period, and the number of CS episodes. Two mice did not become epileptic during first 4 weeks. eCSSS = electrographic CSSS index (in min); bCSSS = behavioral CSSS index (in min).

All the spontaneous behavioral CS, evident from the real-time videos, were always associated with the EEG and the power spectral characteristics, and the activity counts (Fig 5B–5F). The mice that became epileptic had the stage-3 to -5 types of spontaneous behavioral CS (Fig 5B–

5F) and/or the stage-1 to -2 types of spontaneous electrographic NCS (Fig 5A). In all the 5 types of spontaneous behavioral CS episodes, identified in this study, there was an increase in the gamma, theta and delta powers. These were due to the stage-3 spikes and/or the stage-5 spikes that were associated with wild running or jumping behavior. These behaviors were

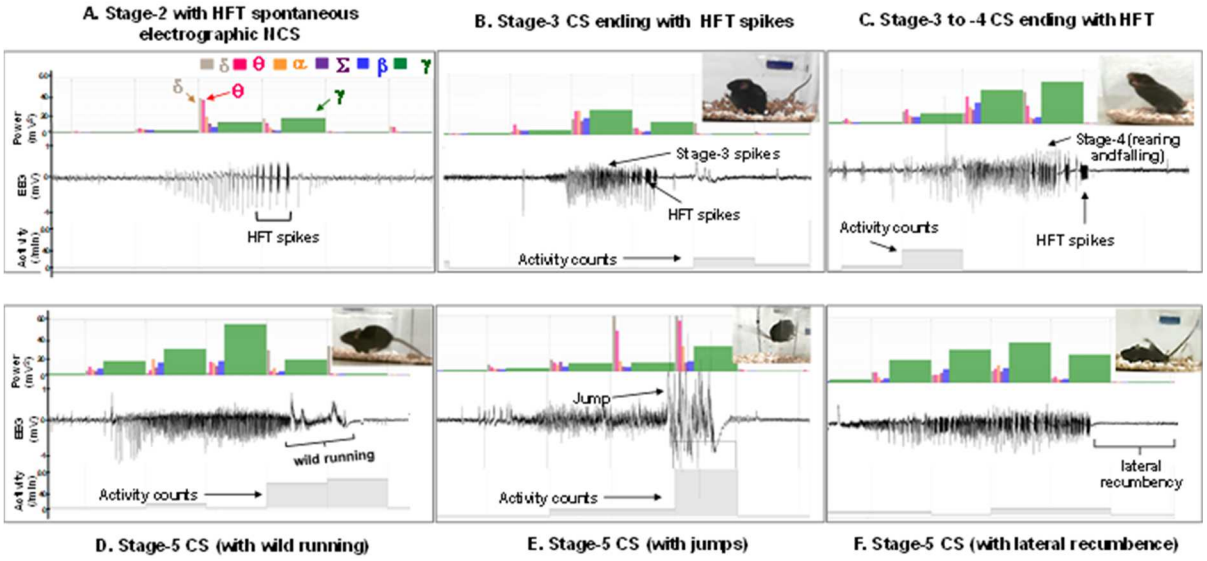

Fig 5. Types of spontaneous electrographic NCS (A) and behavioral CS episodes (B-F) observed during the first 4 weeks. (A) The stage-2 type of spontaneous electrographic NCS ending with the HFT spikes had no behavioral correlates. Five types of spontaneous behavioral CS were identified. (B) the stage-3 type ending with the HFT spikes (C) the stage-3 to -4 type episode ending with the HFT spikes, (D-F) the stage-5 episodes preceded by the stage-3 and -4 type spikes with wild running (D) or without wild running and/or ending with lateral recumbence/rigidity (F), which is characterized by low amplitude spikes on the EEG compared to the baseline. (E) The stage-5 episode was preceded by the stage-3 and -4 types followed by several jumps and may end with lateral recumbence/rigidity. In all the spontaneous CS types, the stage-3 component increases the gamma power while, the increase in the activity counts corresponds to the movements due to seizures during this period. The gamma power decreases in the stage-5 except during jumping and wild running, which also coincides with the increased activity counts.

detected by the radiotransmitter and displayed on the screen as the "activity counts/minute" that is shown at the bottom of each episode (Fig 5). These were also correlated with the behavioral CS, as evident from the video, and increased the gamma power on the EEG. All of these parameters were used to confirm spontaneous behavioral CS episodes. However, the

stage-4 behavioral CS (repeated rearing and falling) sometimes lacked activity counts when there was a limited movement (Fig 5C). The gamma power decreased during the stage-5 spikes when it was associated with the lateral recumbence or rigidity/restricted movement that coincided with the decreased activity counts (for example in Fig 5F). This pattern was also observed during the post-ictal depression (Fig 5B–5F). We could clearly distinguish the increased activity counts and the gamma power due to movement artifacts from the real seizure activity [27].

The spontaneous behavioral CS episodes decreased after the 4 weeks of SE but the spontaneous electrographic NCS continued to exist during the 18 weeks observation period

We quantified the spontaneous behavioral CS (stage 3–5) and the spontaneous electrographic NCS (stage 1–2) from both the severe and the mild SE groups. An example of an EEG trace from a mouse at 7d post-SE (Fig 6A) illustrates the stage 3–5 type spontaneous seizures that occurred in less than 3 minutes after the stage 1–2 electrographic NCS. This was the EEG pattern seen in all the epileptic mice in both groups during the first week. After the first week, the types of behavioral CS shown in the Fig 5 were most commonly observed in both groups. The EEG characteristics (Fig 6B) during the spontaneous behavioral CS were similar to the pattern observed during the SE. The spontaneous recurrent electrographic NCS were identified based on the stage-1 and stage-2 epileptiform spike characteristics on the EEG (Fig 6B) and increased power in the theta and delta bands, which were also similar to the EEG features identified during the SE in the present study and in earlier studies from C57BL/6J mouse kainate model [27, 36]. The spontaneous electrographic NCS, presented as stage-2 clusters, contained “high frequency trigger” (HFT) spikes during the first 4 weeks (an example

is shown in Fig 5A). However, the HFT spikes were rarely found in stage-2 clusters during the 5–18 weeks post-SE (for example Fig 6C, the EEG trace from 32 day post-SE is shown). A random analyses of three weeks video-EEG recordings revealed that about 80% of the

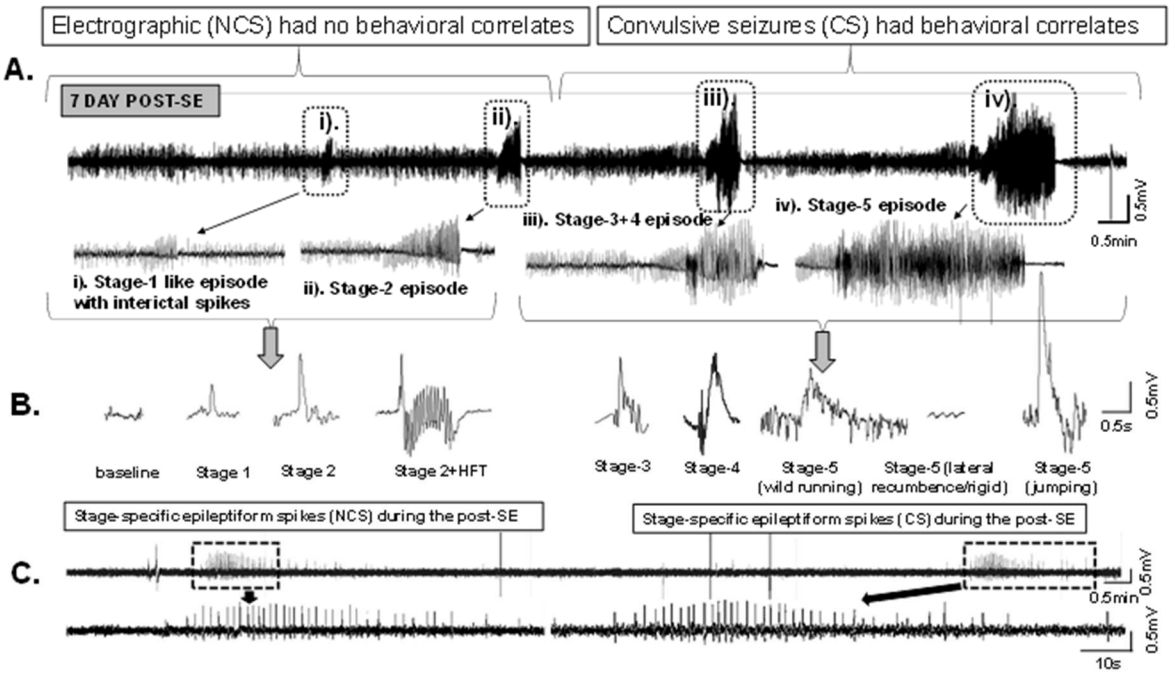

Fig 6. The EEG features of the spontaneous electrographic NCS and behavioral CS. A. A 20min EEG trace from the mouse at 7d post-SE. A pattern of the stage-1 and the stage-2 type NCS episodes (with no behavioral correlates unlike during the SE) preceded the stage 3–5 behavioral CS episodes. After 4 weeks, the stage 3–5 episodes were reduced, however the stage-1 and -2 continued to persist. B. The spike characteristics during the post-SE period. The HFT spikes reduced after the 4 weeks in all types of seizures in both the mild and severe SE groups. An example of an electrographic NCS on its own (without progressing to stage 3–5 seizure) is also shown in the panel C- a 20min trace showing spontaneous electrographic NCS of stage 2 type spiking at 32 day post-SE (from the severe SE group). Such electrographic NCS episodes persisted throughout the 18 weeks in the severe and the mild groups.

electrographic NCS were associated with behavioral phenotypes (observed from high resolution "standalone videos" rather than from the videos that were integrated with the EEG files). The remaining 20% of NCS episodes were the stage-2 with HFT spikes which lacked behavioral correlates. The HFT pattern observed in the C57BL/6J mouse has been described elsewhere [27].

During the first 4 week period, all the mice in the severe SE group were epileptic and had 27 ±3 episodes of spontaneous behavioral CS (stage ≥3). In the mild SE group, except three mice the rest had 4±1 behavioral CS during this period (Fig 7; p = 0.0004, severe SE versus mild SE group, Mann-Whitney test). After 4 weeks, the number of spontaneous behavioral CS significantly decreased in the severe group (Fig 7; p = 0.0026, 0–4 week versus the rest of the time intervals for up to 18 weeks; Kruskal-Wallis test). And there were no

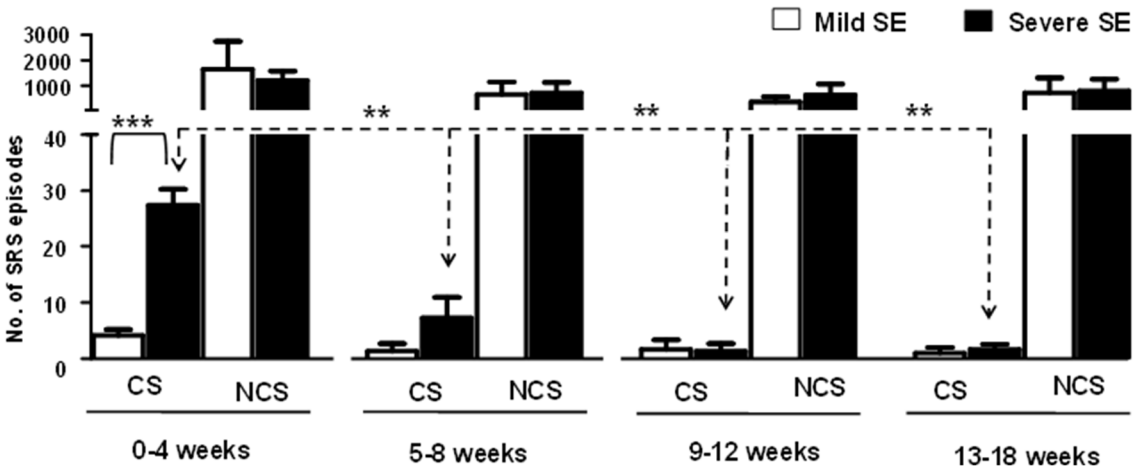

Fig 7. Comparison of the spontaneous behavioral CS and the spontaneous electrographic NCS occurrence in the severe and mild SE groups from 0–18 weeks. There was a significant increase in the number of behavioral CS episodes during the first 4 weeks in the severe SE group when compared to the mild SE group (***p = 0.0004, Mann-Whitney test, n = 9 each). The spontaneous CS in the severe group significantly reduced during 5–8 weeks or 9–12 weeks or 13–18 weeks when compared to 0–4 weeks (p = 0.0026, Kruskal-Wallis test). However, there was no significant difference in the spontaneous behavioral CS in the mild group across different time points. Further, spontaneous electrographic NCS episodes did not significantly change between the two groups at any time point and continued to exist throughout the 18 weeks period.

significant differences in the numbers of spontaneous behavioral CS between the severe and the mild groups during the 5–18 weeks period (Fig 7). Interestingly, there were also no significant differences in the numbers of the spontaneous electrographic NCS episodes between the severe and the mild groups throughout the 18 week period, including the first four weeks of post-SE (Fig 7). During the 18 week post-SE period, the mice in both the severe and

the mild SE groups had ~20 spontaneous electrographic NCS type episodes per day/night cycle. None of the four control mice that were monitored continuously for 4 weeks or the baseline EEG recordings from the 19 mice for 10 days (before the induction of SE) from the experimental groups had any epileptiform spikes either in isolation or in clusters. None of the mice from the control or the severe SE or the mild SE group had infection at the site of the electrodes or at the site of the radiotransmitter. There was no evidence of damage to the brain by the implanted electrodes. The mice body temperature, detected by the radiotransmitters in real-time, was also constant throughout the course of the experiment.

Discussion

The results of this study demonstrate that both severe and mild SE in C57BL/6J mice induce epileptogenesis soon after the SE. Severe SE increases the numbers of spontaneous behavioral CS during the first 4 weeks but they decrease thereafter. Mild SE also induces epileptogenesis but the numbers of spontaneous CS in the first 4 weeks were fewer than those found in the severe group. In both the severe and the mild SE groups, the spontaneous electrographic NCS continue to exist during the 18 weeks observation period. In both groups, all the spontaneous behavioral CS (stage 3–5) were associated with: characteristic EEG patterns (high frequency and high amplitude epileptiform spike clusters), the increased gamma, theta and delta powers in the power spectrum, and the increased activity counts. Considering the large numbers of spontaneous electrographic NCS occurred during the 18 weeks continuous study, a random observation of three weeks recordings revealed that about 80% of the electrographic NCS were associated with behavioral phenotypes in both groups. The remaining NCS episodes contained the stage-2 HFT pattern (for example, Fig 5A) which lacked behavioral correlates. The spontaneous electrographic NCS (EEG) patterns quantified

were similar to the EEG patterns observed during the SE in the present study, and also to our previous studies from C57BL/6J mouse model [27, 36]. The NCS were also characterized by the increase in power in delta and theta bands.

Severity of the SE, determined by the EEG and the behavioral characteristics, and its impact on latent periods, epileptogenesis and chronic epileptic period

The results from this study were based on continuous video-EEG recording from epidurally implanted electrodes on the surface of the cortex 10 days prior to the induction of SE. To our knowledge, there is little or no evidence of continuous (24/7) integrated video-EEG recording from C57BL/6J mice for a longer duration. Early epileptogenesis, less than a week after the SE, is also reported in the rat pilocarpine model [33, 42, 43, 44]. A similar observation was also made from the rat electroconvulsant model [7] and the pilocarpine mouse model of epilepsy [19]. These findings, except the study from Jung et al [44], were also based on continuous video-EEG monitoring, challenge the notion of "prolonged motor seizure latent period" after the induction of SE in rodent models.

In this study, there were no significant differences in the latency to the first onset of spontaneous electrographic NCS and behavioral CS between the mild and SE groups. And the NCS always occurred prior to the CS in both groups, which is in agreement with the other models of TLE [33, 43]. The effects of duration and severity of SE on latent period, epileptogenesis and chronic epileptic phase has been adequately addressed in rodent models of epilepsy [19, 32, 33, 43, 45]. It has been proposed that the duration of the latent period, whether for NCS or CS, depends on the duration of behavioral SE and the method of termination of SE in rodent models [43, 45]. In a pilocarpine rat model in which the behavioral seizures were

terminated by diazepam and ketamine, no significant differences were found in latency to the onset of spontaneous NCS or CS between the rats that had 30 minutes or 120 minutes SE [33]. In another pilocarpine rat model study in which SE was terminated by administering high dose of diazepam (20 mg/kg), it has been reported that the longer duration of SE progressively delays spontaneous seizure onset [45]. However, in the pilocarpine mouse (the NMRI strain) [19] and the rat model used by Klitgaard et al [32] and Bortel et al [33], about 30 minutes of SE was sufficient to induce epileptogenesis. It must be emphasized that in the present study all the mice had established SE for 2 hours that included seizures of various stages ranging from stage 1 to stage 3 or 5 (for example, Fig 1). It is important to note that in the present study we have considered the exact duration of the behavioral CS stage ≥3 and their associated EEG seizure duration to calculate the severity index (CSSS indices) for each mouse. The behavioral CSSS index was 50% higher than the electrographic CSSS index for the SE in both groups suggesting that the behavioral CS, during the SE, originated from the brain are due to a widespread effects of kainate. Since only two epidural electrodes were used in this study, it would require a multi electrode system to record electrical activity from different parts of the brain to understand exaggerated locomotor behaviors caused by kainate during SE.

Interestingly, the behavioral SE was not terminated in some rat kainate models of TLE [3, 7, 17]. And in one such study, the first spontaneous electrographic NCS was recorded in less than 24 hours in 5 out of 9 rats [9]. In the present study, electrographic NCS occurred in both mild and severe groups in less than 2 hours after terminating the behavioral SE with diazepam. A recent study reveals that the domoic acid, an analogue of kainate, has a beta half-life of about 5 hours in rodents [46], which may suggest that very early NCS could be due to the residual effects of kainate in this study. However, the occurrence of first spontaneous CS

in this study were unlikely due to the residual effects of kainate since they occurred during 24–36 hours after the last dose of kainate, the earliest time point observed in 2 out of 18 mice. The spontaneous CS observed in this study were also not due to surgery-induced trauma to the brain (the electrodes were placed epidurally on the surface of the cortex and the brains were always checked for electrodes-induced trauma after euthanasia) or infection or due to increased body temperature. In a rat kainate model of TLE, it has been reported that both hippocampal leads and the dural EEG lead show qualitatively similar activation throughout the recording period for all kainate-treated rats in that study [8]. This supports that the EEG signals originated from epidurally placed electrodes on the surface of the cortex in our experiments represents overall brain electrical activity during the SE and post-SE periods. Our previous studies from the C57BL/6J mouse kainate model using a similar technique, epidural electrodes on the surface of the cortex, demonstrated a correlation between the EEG changes and the changes occurring in the hippocampus bilaterally, for example increased Fos activation and reactive gliosis, and their modulation by an intervention drug during and after the SE [36].

The frequency of spontaneous behavioral CS was higher in the severe group than the mild group (both groups had received a similar range doses of kainate), implying that the severity of the SE influences the frequency of spontaneous CS. A similar findings were reported from the rat pilocarpine model by Bortel et al [33]. In contrast, the pilocarpine rat model study from Klitgaard et al [32], based on intermittent EEG recording, reported that the prolonged behavioral SE decreases the seizure frequency.

The route of administration of kainate to induce epileptogenesis: intraperitoneal versus other routes

Inducing severe SE using kainate via the intraperitoneal route in C57BL/6J mice had been a challenge due to high mortality and inconsistency in their seizure response to a single dose of kainate [25, 26]. We have recently addressed these important issues by repeated administration of a low dose of kainate via the i.p. route [27]. The previous studies from systemic administration of kainate via the i.p. or the s.c. route in the C57BL/6J mouse have demonstrated resistance to kainate-induced neurotoxicity at a dose less than 30 mg/kg [25, 26, 47–50]. In order to overcome the resistance and to induce severe SE, in view of achieving epileptogenesis in C57BL/6J mice, focal injections of kainate by the intra-hippocampal [10, 28, 51–54] or the intra-amygdalar [55] route has been successfully attempted. A similar method of unilateral intra-hippocampal kainate injection in the guinea pig induced focal epilepsy [56–57]. The focal injection methods also induced early epileptogenesis by 3–5 days post-SE in mice [51–53, 55, 58], and 2–3 weeks to several months in the other studies [10, 28, 51–53, 55, 58]. Two studies [10, 55] have recorded EEG, but not video, continuously for 2–4 weeks, while the other studies recorded both video and EEG, but only intermittently [28, 51–53, 55, 58]. The choice of timings for intermittent recordings in these studies were based on the reported "motor seizure latent period of 2–3 weeks for the Swiss mice" [for example, 59]. The intranasal route for kainate administration has also been tried in the C57BL/6J mice to overcome the kainate resistance with limited success [60]. The focal injections of kainate although produce severe SE and spontaneous recurrent seizures, these techniques are labor intensive, technically demanding and expensive. Moreover, the focal administration of kainate is done under general anesthesia, which could add further variables to the experiments during the SE, and also the

technique could damage the brain [61–63]. The i.p. route for administering kainate to induce SE is convenient and cost effective for non-telemetric studies. The systemic injection of kainate causes widespread neuronal loss in different parts of the brain in rats and in some mouse strains [64– 67]. Since C57BL/6J mice are resistant to the direct effects of kainate—induced neurotoxicity, a further investigation is required to understand whether the severity of the SE, induced by kainate, cause a widespread neuronal loss, in these models, as reported for the rat kainate models (for example [3, 68]).

Spontaneous behavioral CS decline after 4 weeks of the SE and the electrographic NCS continue to persist beyond 4 weeks

The most interesting and surprising result from this study is that the spontaneous behavioral CS decrease after 4 weeks of the SE. Unlike the rat models of kainate-induced acquired epilepsy and post-stroke epilepsy models [12, 69, 70] or rat pilocarpine models [32, 33] which are progressive, the C57BL/6J mouse kainate model is a regressive type. However, the spontaneous electrographic NCS continued to exist throughout the 18 weeks and their numbers did not change over time in both the severe and the mild SE groups, which suggest that these could serve as a chronic model for complex seizures. There were no differences in the numbers of electrographic NCS between the mild and severe SE groups at any time points in the 18 weeks continuous study (Fig 7). In contrast, in the rat pilocarpine model the NCS were 20% higher in severe SE compared to the mild SE rats in the 17-day continuous video-EEG study [33]. However, the frequency of convulsive seizures was higher in the severe SE rats in pilocarpine model, and they were progressive in both mild and severe SE groups [33]. In the present study, the behavioral CS frequency was also higher in the severe SE group when

compared with the mild SE group but they decreased after 4 weeks in both groups (Fig 7). The reasons for the decrease/ complete absence of spontaneous behavioral CS, in some mice, require further investigation. Identification of compensatory mechanism/s of recovery from behavioral epileptic phase could reveal a potential therapeutic targets for epilepsy. Our ongoing intensive video-EEG analysis from 4 weeks onwards in these mice revealed an important pattern in their EEG traces. The stage-2 type electrographic NCS during the late post-SE period (>4 weeks) more often lacked the HFT spikes, which were usually present during the first 4 weeks (for example, Fig 5A). We have recently described the importance of the HFT spikes in transition from stage-2 to stage-3, i.e., from nonconvulsive to convulsive seizure during the SE [27]. Perhaps, the absence or low numbers of HFT spikes on the EEG in some NCS clusters during the 5–18 weeks period could be one of the several reasons for decreased spontaneous behavioral CS during this period. The spontaneous electrographic NCS containing stage-2 spikes and the duration of such episodes observed in this study were similar to the EEG pattern described for the rat kainate model [71]. Also this pattern had the features of cortical EEG reported from the guinea pig kainate model [56], mouse kainate model [54], mouse model for absence seizures [72] and to some extent the EEG patterns corresponding to grade 2/3 seizures observed in the rat TBI model [73]. However, future studies of direct recording from the hippocampus, the entorhinal cortex and the amygdala are required to confirm the source of electrographic NCS and behavioral CS as demonstrated in other TLE models [10, 13, 31, 33, 56, 57].

In conclusion, the C57BL/6J mouse kainate model of epilepsy described in this study is useful to screen drugs for a short term course for behavioral CS. This model is also useful as a chronic complex seizure model to test long term effects of drugs on spontaneous

electrographic NCS. Because of immediate epileptogenesis in the C57BL/6J mouse model, it provides an early window of opportunity for intervention and reduces the duration of experiments. In contrast to rat models, the mouse model also reduces the amount of drugs. Since some of the transgenic mice are also bred on C57BL/6J genetic background, this model is useful as a critical wild-type control for transgenic mice studies in epilepsy research.

References

1. Scharfman HE. The neurobiology of epilepsy. Curr Neurol Neurosci Rep. 2007; 7(4):348–54. Epub 2007/07/10. PMID: 17618543.

2. Reddy DS, Kuruba R. Experimental Models of Status Epilepticus and Neuronal Injury for Evaluation of Therapeutic Interventions International Journal of Molecular Sciences. 2013; 14(9):18284–318. doi: 10. 3390/ijms140918284.

3. Rao MS, Hattiangady B, Reddy DS, Shetty AK. Hippocampal neurodegeneration, spontaneous seizures, and mossy fiber sprouting in the F344 rat model of temporal lobe epilepsy. J Neurosci Res. 2006; 83(6):1088–105. Epub 2006/02/24. doi: 10.1002/jnr.20802 PMID: 16493685.

4. Buckmaster PS. Laboratory animal models of temporal lobe epilepsy. Comp Med. 2004; 54(5):473–85. Epub 2004/12/04. PMID: 15575361.

5. Galanopoulou AS, Kokaia M, Loeb JA, Nehlig A, Pitkanen A, Rogawski MA, et al. Epilepsy therapy development: technical and methodologic issues in studies with animal models. Epilepsia. 2013; 54 Suppl 4:13–23. Epub 2013/08/09. doi: 10.1111/epi.12295 PMID: 23909850.

6. Raol YH, Brooks-Kayal AR. Experimental models of seizures and epilepsies. Prog Mol Biol Transl Sci. 2012; 105:57–82. Epub 2011/12/06. doi: B978-0-12-394596-9.00003–2 [pii] doi: 10.1016/B978-0-12- 394596-9.00003-2 PMID: 22137429.

7. Bumanglag AV, Sloviter RS. Minimal latency to hippocampal epileptogenesis and clinical epilepsy after perforant pathway stimulation-induced status epilepticus in awake rats. J Comp Neurol. 2008; 510 (6):561–80. Epub 2008/08/13. doi: 10.1002/cne.21801 PMID: 18697194.

8. Williams PA, White AM, Clark S, Ferraro DJ, Swiercz W, Staley KJ, et al. Development of spontaneous recurrent seizures after kainate-induced status

epilepticus. J Neurosci. 2009; 29(7):2103–12. Epub 2009/02/21. doi: 29/7/2103 [pii] doi: 10.1523/JNEUROSCI.0980-08.2009 PMID: 19228963.

9. Arabadzisz D, Antal K, Parpan F, Emri Z, Fritschy JM. Epileptogenesis and chronic seizures in a mouse model of temporal lobe epilepsy are associated with distinct EEG patterns and selective neurochemical alterations in the contralateral hippocampus. Exp Neurol. 2005; 194(1):76–90. Epub 2005/05/ 19. doi: S0014-4886(05)00048-8 [pii] doi: 10.1016/j.expneurol.2005.01.029 PMID: 15899245.

10. Le Duigou C, Bouilleret V, Miles R. Epileptiform activities in slices of hippocampus from mice after intrahippocampal injection of kainic acid. J Physiol. 2008; 586(Pt 20):4891–904. Epub 2008/08/30. doi: jphysiol.2008.156281 [pii] doi: 10.1113/jphysiol.2008.156281 PMID: 18755752.

11. Bastlund JF, Jennum P, Mohapel P, Vogel V, Watson WP. Measurement of cortical and hippocampal epileptiform activity in freely moving rats by means of implantable radiotelemetry. J Neurosci Methods. 2004; 138(1–2):65–72. Epub 2004/08/25. doi: 10.1016/j.jneumeth.2004.03.004 S016502700400113X [pii]. PMID: 15325113.

12. Hellier JL, Patrylo PR, Buckmaster PS, Dudek FE. Recurrent spontaneous motor seizures after repeated low-dose systemic treatment with kainate: assessment of a rat model of temporal lobe epilepsy. Epilepsy Res. 1998; 31(1):73–84. Epub 1998/08/08. doi: S0920-1211(98)00017-5 [pii]. PMID: 9696302.

13. Raedt R, Van Dycke A, Van Melkebeke D, De Smedt T, Claeys P, Wyckhuys T, et al. Seizures in the intrahippocampal kainic acid epilepsy model: characterization using long-term video-EEG monitoring in the rat. Acta Neurol Scand. 2009; 119(5):293–303. Epub 2009/04/24. PMID: 19388152.

14. Ben-Ari Y. Kainate and Temporal Lobe Epilepsies: 3 decades of progress. 2012. Epub 2012/07/13. doi: NBK98166 [bookaccession]. 22787646.

15. Rattka M, Brandt C, Loscher W. The intrahippocampal kainate model of temporal lobe epilepsy revisited: epileptogenesis, behavioral and cognitive alterations, pharmacological response, and hippoccampal damage in epileptic rats. Epilepsy Res. 2013; 103(2–3):135–52. Epub 2012/12/01. doi: S0920- 1211(12)00313-0 [pii] doi: 10.1016/j.eplepsyres.2012.09.015 PMID: 23196211.

16. Zheng XY, Zhang HL, Luo Q, Zhu J. Kainic acid-induced neurodegenerative model: potentials and limitations. J Biomed Biotechnol. 2011; 2011:457079. Epub 2010/12/04. doi: 10.1155/2011/457079 PMID: 21127706.

17. Williams PA, Hellier JL, White AM, Staley KJ, Dudek FE. Development of spontaneous seizures after experimental status epilepticus: implications for understanding epileptogenesis. Epilepsia. 2007; 48 Suppl 5:157–63. Epub 2007/10/04. doi: EPI1304 [pii] doi: 10.1111/j.1528-1167.2007.01304.x PMID: 17910596.

18. Levesque M, Avoli M. The kainic acid model of temporal lobe epilepsy. Neurosci Biobehav Rev. 2013; 37(10 Pt 2):2887–99. Epub 2013/11/05. doi: S0149-7634(13)00235-2 [pii] doi: 10.1016/j.neubiorev. 2013.10.011 PMID: 24184743.

19. Mazzuferi M, Kumar G, Rospo C, Kaminski RM. Rapid epileptogenesis in the mouse pilocarpine model: video-EEG, pharmacokinetic and histopathological characterization. Exp Neurol. 2012; 238 (2):156–67. Epub 2012/09/11. doi: S0014-4886(12)00331-7 [pii] doi: 10.1016/j.expneurol.2012.08.022 PMID: 22960187.

20. Bankstahl M, Muller CJ, Wilk E, Schughart K, Loscher W. Generation and characterization of pilocarpine-sensitive C57BL/6 mice as a model of temporal lobe epilepsy. Behav Brain Res. 2012; 230 (1):182–91. Epub 2012/02/22. doi: S0166-4328(12)00102-7 [pii] doi: 10.1016/j.bbr.2012.02.004 PMID: 22348894.

21. Benkovic SA, O'Callaghan JP, Miller DB. Sensitive indicators of injury reveal hippocampal damage in C57BL/6J mice treated with kainic acid in the absence of tonic-clonic seizures. Brain Res. 2004; 1024 (1–2):59–76. Epub 2004/09/29. [pii]. PMID: 15451367.

22. McCord MC, Lorenzana A, Bloom CS, Chancer ZO, Schauwecker PE. Effect of age on kainate-induced seizure severity and cell death. Neuroscience. 2008; 154(3):1143–53. Epub 2008/05/16. doi: S0306- 4522(08)00537-X [pii] doi: 10.1016/j.neuroscience.2008.03.082 PMID: 18479826.

23. Schauwecker PE. Genetic basis of kainate-induced excitotoxicity in mice: phenotypic modulation of seizure-induced cell death. Epilepsy Res. 2003; 55(3):201–10. Epub 2003/09/16. doi: S0920121103001153 [pii]. PMID: 12972174.

24. Yang J, Houk B, Shah J, Hauser KF, Luo Y, Smith G, et al. Genetic background regulates semaphorin gene expression and epileptogenesis in mouse brain after kainic acid status epilepticus. Neuroscience. 2005; 131(4):853–69. Epub 2005/03/08. doi: S0306-4522(04)00924-8 [pii] doi: 10.1016/j. neuroscience.2004.09.064 PMID: 15749340.

25. Benkovic SA, O'Callaghan JP, Miller DB. Regional neuropathology following kainic acid intoxication in adult and aged C57BL/6J mice. Brain Res. 2006; 1070(1):215–31. Epub 2006/01/13. doi: S0006-8993 (05)01601-X [pii] doi: 10.1016/j.brainres.2005.11.065 PMID: 16403473.

26. McLin JP, Steward O. Comparison of seizure phenotype and neurodegeneration induced by systemic kainic acid in inbred, outbred, and hybrid mouse strains. Eur J Neurosci. 2006; 24(8):2191–202. Epub 2006/11/01. doi: EJN5111 [pii] doi: 10.1111/j.1460-9568.2006.05111.x PMID: 17074044.

27. Tse K, Puttachary S, Beamer E, Sills GJ, Thippeswamy T. Advantages of repeated low dose against single high dose of kainate in C57BL/6J mouse model of status epilepticus: behavioral and electroencephalographic studies. PLoS One. 2014;

9(5):e96622. Epub 2014/05/08. doi: 10.1371/journal.pone. 0096622 PONE-D-13-53455 [pii]. PMID: 24802808.

28. Knuesel I, Riban V, Zuellig RA, Schaub MC, Grady RM, Sanes JR, et al. Increased vulnerability to kainate-induced seizures in utrophin-knockout mice. Eur J Neurosci. 2002; 15(9):1474–84. Epub 2002/05/ 25. doi: 1980 [pii]. PMID: 12028357.

29. Melo T, Bigini P, Sonnewald U, Balosso S, Cagnotto A, Barbera S, et al. Neuronal hyperexcitability and seizures are associated with changes in glial-neuronal interactions in the hippocampus of a mouse model of epilepsy with mental retardation. J Neurochem. 2010; 115(6):1445–54. Epub 2010/11/04. doi: 10.1111/j.1471-4159.2010.07048.x PMID: 21044073.

30. McLin JP, Thompson LM, Steward O. Differential susceptibility to striatal neurodegeneration induced by quinolinic acid and kainate in inbred, outbred and hybrid mouse strains. Eur J Neurosci. 2006; 24 (11):3134–40. Epub 2006/12/13. doi: EJN5198 [pii] doi: 10.1111/j.1460-9568.2006.05198.x PMID: 17156374.

31. Michalak Z, Sano T, Engel T, Miller-Delaney SF, Lerner-Natoli M, Henshall DC. Spatio-temporally restricted blood-brain barrier disruption after intra-amygdala kainic acid-induced status epilepticus in mice. Epilepsy Res. 2012; 103(2–3):167–79. Epub 2012/11/28. doi: S0920-1211(12)00315-4 [pii] doi: 10.1016/j.eplepsyres.2012.10.006 PMID: 23182415.

32. Klitgaard H, Matagne A, Vanneste-Goemaere J, Margineanu DG. Pilocarpine-induced epileptogenesis in the rat: impact of initial duration of status epilepticus on electrophysiological and neuropathological alterations. Epilepsy Res. 2002; 51(1–2):93–107. Epub 2002/09/28. doi: S0920121102000992 [pii]. PMID: 12350385.

33. Bortel A, Levesque M, Biagini G, Gotman J, Avoli M. Convulsive status epilepticus duration as determinant for epileptogenesis and interictal discharge generation in the rat limbic system. Neurobiol Dis. 2010; 40(2):478–89. Epub 2010/08/05. doi: S0969-9961(10)00240-8 [pii] doi: 10.1016/j.nbd.2010.07. 015 PMID: 20682341.

34. Lowenstein DH, Bleck T, Macdonald RL. It's time to revise the definition of status epilepticus. Epilepsia. 1999; 40(1):120–2. Epub 1999/01/30. PMID: 9924914.

35. Minicucci F, Muscas G, Perucca E, Capovilla G, Vigevano F, Tinuper P. Treatment of status epilepticus in adults: guidelines of the Italian League against Epilepsy. Epilepsia. 2006; 47 Suppl 5:9–15. Epub 2007/01/24. doi: EPI870 [pii] doi: 10.1111/j.1528-1167.2006.00870.x PMID: 17239099.

36. Beamer E, Otahal J, Sills GJ, Thippeswamy T. N (w)-propyl-L-arginine (L-NPA) reduces status epilepticus and early epileptogenic events in a mouse model of epilepsy: behavioural, EEG and immunohistochemical analyses. Eur J Neurosci. 2012; 36(9):3194–203. Epub 2012/09/05. doi: 10.1111/j.1460- 9568.2012.08234.x PMID: 22943535.

37. Racine RJ. Modification of seizure activity by electrical stimulation. II. Motor seizure. Electroencephalogr Clin Neurophysiol. 1972; 32(3):281–94. Epub 1972/03/01. PMID: 4110397.

38. Pearce PS, Friedman D, Lafrancois JJ, Iyengar SS, Fenton AA, Maclusky NJ, et al. Spike-wave discharges in adult Sprague-Dawley rats and their implications for animal models of temporal lobe epilepsy. Epilepsy Behav. 32:121–31. Epub 2014/02/19. doi: S1525-5050(14)00005-5 [pii] doi: 10.1016/j. yebeh.2014.01.004 PMID: 24534480.

39. Barth D, Dudek F, Rodgers K. Pattern recognition and quantification of spike and wave discharge in normal and brain injured Sprague Dawley rats. American Epilepsy Society Annual Meeting; Seattle, Washington2014.

40. Tang X, Yang L, Sanford LD. Sleep and EEG spectra in rats recorded via telemetry during surgical recovery. Sleep. 2007; 30(8):1057–61. Epub 2007/08/19. PMID: 17702276.

41. Sloviter RS. Hippocampal epileptogenesis in animal models of mesial temporal lobe epilepsy with hippocampal sclerosis: the importance of the "latent period" and other concepts. Epilepsia. 2008; 49 Suppl 9:85–92. Epub 2008/12/23. doi: EPI1931 [pii] doi: 10.1111/j.1528-1167.2008.01931.x PMID: 19087122.

42. Raol YH, Lund IV, Bandyopadhyay S, Zhang G, Roberts DS, Wolfe JH, et al. Enhancing GABA(A) receptor alpha 1 subunit levels in hippocampal dentate gyrus inhibits epilepsy development in an animal model of temporal lobe epilepsy. J Neurosci. 2006; 26(44):11342–6. Epub 2006/11/03. doi: 26/44/ 11342 [pii] doi: 10.1523/JNEUROSCI.3329-06.2006 PMID: 17079662.

43. Goffin K, Nissinen J, Van Laere K, Pitkanen A. Cyclicity of spontaneous recurrent seizures in pilocarpine model of temporal lobe epilepsy in rat. Exp Neurol. 2007; 205(2):501–5. Epub 2007/04/20. doi: S0014-4886(07)00104-5 [pii] doi: 10.1016/j.expneurol.2007.03.008 PMID: 17442304.

44. Jung S, Jones TD, Lugo JN Jr., Sheerin AH, Miller JW, D'Ambrosio R, et al. Progressive dendritic HCN channelopathy during epileptogenesis in the rat pilocarpine model of epilepsy. J Neurosci. 2007; 27 (47):13012–21. Epub 2007/11/23. doi: 27/47/13012 [pii] doi: 10.1523/JNEUROSCI.3605-07.2007 PMID: 18032674.

45. Biagini G, Baldelli E, Longo D, Pradelli L, Zini I, Rogawski MA, et al. Endogenous neurosteroids modulate epileptogenesis in a model of temporal lobe epilepsy. Exp Neurol. 2006; 201(2):519–24. Epub 2006/06/20. doi: S0014-4886(06)00271-8 [pii] doi: 10.1016/j.expneurol.2006.04.029 PMID: 16780839.

46. Maucher Fuquay J, Muha N, Wang Z, Ramsdell JS. Toxicokinetics of domoic acid in the fetal rat. Toxicology. 2012; 294(1):36–41. Epub 2012/02/07. doi: S0300-483X(12)00022-4 [pii] doi: 10.1016/j.tox. 2012.01.012 PMID: 22306965.

47. Schauwecker PE. Modulation of cell death by mouse genotype: differential vulnerability to excitatory amino acid-induced lesions. Exp Neurol. 2002; 178(2):219–35. Epub 2002/12/31. doi: S0014488602980386 [pii]. PMID: 12504881.

48. Schauwecker PE. The relevance of individual genetic background and its role in animal models of epilepsy. Epilepsy Res. 2011; 97(1–2):1–11. Epub 2011/10/18. doi: S0920-1211(11)00269-5 [pii] doi: 10. 1016/j.eplepsyres.2011.09.005 PMID: 22001434.

49. Schauwecker PE. Congenic strains provide evidence that a mapped locus on chromosome 15 influences excitotoxic cell death. Genes Brain Behav. 2010; 10(1):100–10. Epub 2010/09/03. doi: GBB644 [pii] doi: 10.1111/j.1601-183X.2010.00644.x PMID: 20807240.

50. McKhann GM 2nd, Wenzel HJ, Robbins CA, Sosunov AA, Schwartzkroin PA. Mouse strain differences in kainic acid sensitivity, seizure behavior, mortality, and hippocampal pathology. Neuroscience. 2003; 122(2):551–61. Epub 2003/11/15. doi: S0306452203005621 [pii]. PMID: 14614919.

51. Pernot F, Heinrich C, Barbier L, Peinnequin A, Carpentier P, Dhote F, et al. Inflammatory changes during epileptogenesis and spontaneous seizures in a mouse model of mesiotemporal lobe epilepsy. Epilepsia. 2011; 52(12):2315–25. Epub 2011/10/01. doi: 10.1111/j.1528-1167.2011.03273.x PMID: 21955106.

52. Huneau C, Benquet P, Dieuset G, Biraben A, Martin B, Wendling F. Shape features of epileptic spikes are a marker of epileptogenesis in mice. Epilepsia. 2013; 54(12):2219–27. Epub 2013/10/19. doi: 10. 1111/epi.12406 PMID: 24134559.

53. Huneau C, Demont-Guignard S, Benquet P, Martin B, Wendling F. Time-domain features of epileptic spikes as potential bio-markers of the epileptogenesis process. Conf Proc IEEE Eng Med Biol Soc. 2010; 2010:6007–10. Epub 2010/11/26. doi: 10.1109/IEMBS.2010.5627592 PMID: 21097111.

54. Bouilleret V, Ridoux V, Depaulis A, Marescaux C, Nehlig A, Le Gal La Salle G. Recurrent seizures and hippocampal sclerosis following intrahippocampal kainate injection in adult mice: electroencephalography, histopathology and synaptic reorganization similar to mesial temporal lobe epilepsy. Neuroscience. 1999; 89(3):717–29. Epub 1999/04/13. doi: S0306-4522(98)00401-1 [pii]. PMID: 10199607.

55. Mouri G, Jimenez-Mateos E, Engel T, Dunleavy M, Hatazaki S, Paucard A, et al. Unilateral hippocampal CA3-predominant damage and short latency epileptogenesis after intra-amygdala microinjection of kainic acid in mice. Brain Res. 2008; 1213:140–51. Epub 2008/05/06. doi: S0006-8993(08)00718-X [pii] doi: 10.1016/j.brainres.2008.03.061 PMID: 18455706.

56. Carriero G, Arcieri S, Cattalini A, Corsi L, Gnatkovsky V, de Curtis M. A guinea pig model of mesial temporal lobe epilepsy following nonconvulsive status epilepticus induced by unilateral intrahippocampal injection of kainic acid. Epilepsia. 2012; 53(11):1917–27. Epub 2012/09/25. doi: 10.1111/j.1528-1167. 2012.03669.x PMID: 22998690.

57. Arcieri S, Velotti R, Noe F, Carriero G, Cattalini A, Galbardi B, et al. Variable electrobehavioral patterns during focal nonconvulsive status epilepticus induced by unilateral intrahippocampal injection of kainic acid. Epilepsia. 2014; 55(12):1978–85. Epub 2014/11/08. doi: 10.1111/epi.12850 PMID: 25378199.

58. Heinrich C, Lahteinen S, Suzuki F, Anne-Marie L, Huber S, Haussler U, et al. Increase in BDNF-mediated TrkB signaling promotes epileptogenesis in a mouse model of mesial temporal lobe epilepsy. Neurobiol Dis. 2011; 42(1):35–47. Epub 2011/01/12. doi: S0969-9961(11)00002-7 [pii] doi: 10.1016/j.nbd. 2011.01.001 PMID: 21220014.

59. Riban V, Bouilleret V, Pham-Le BT, Fritschy JM, Marescaux C, Depaulis A. Evolution of hippocampal epileptic activity during the development of hippocampal sclerosis in a mouse model of temporal lobe epilepsy. Neuroscience. 2002; 112(1):101–11. Epub 2002/06/05. doi: S0306452202000647 [pii]. PMID: 12044475.

60. Chen Z, Ljunggren HG, Bogdanovic N, Nennesmo I, Winblad B, Zhu J. Excitotoxic neurodegeneration induced by intranasal administration of kainic acid in C57BL/6 mice. Brain Res. 2002; 931(2):135–45. Epub 2002/03/19. doi: S0006899302022680 [pii]. PMID: 11897099.

61. Hirshler YK, Polat U, Biegon A. Intracranial electrode implantation produces regional neuroinflammation and memory deficits in rats. Exp Neurol. 2009; 222(1):42–50. Epub 2009/12/23. doi: S0014-4886 (09)00484-1 [pii] doi: 10.1016/j.expneurol.2009.12.006 PMID: 20026042.

62. Pan JC, Pei YQ, An L, Lai L, D'Hooge R, De Deyn PP. Epileptiform activity and hippocampal damage produced by intrahippocampal injection of guanidinosuccinic acid in rat. Neurosci Lett. 1996; 209 (2):121–4. Epub 1996/05/10. doi: 030439409612615X [pii]. PMID: 8761997.

63. Kessler J, Markowitsch HJ. Different neuropathological effects of intrahippocampal injections of kainic acid and tetanus toxin. Experientia. 1983; 39(8):922–4. Epub 1983/08/15. PMID: 6873250.

64. Turski WA, Cavalheiro EA, Bortolotto ZA, Mello LM, Schwarz M, Turski L. Seizures produced by pilocarpine in mice: a behavioral, electroencephalographic and morphological analysis. Brain Res. 1984; 321(2):237–53. Epub 1984/11/12. doi: 0006-8993(84)90177-X [pii]. PMID: 6498517.

65. Ben-Ari Y, Cossart R. Kainate, a double agent that generates seizures: two decades of progress. Trends Neurosci. 2000; 23(11):580–7. Epub 2000/11/14. doi: S0166-2236(00)01659-3 [pii]. PMID: 11074268.

66. Morimoto K, Fahnestock M, Racine RJ. Kindling and status epilepticus models of epilepsy: rewiring the brain. Prog Neurobiol. 2004; 73(1):1–60. Epub 2004/06/15. doi: 10.1016/j.pneurobio.2004.03.009 S0301008204000449 [pii]. PMID: 15193778.

67. Curia G, Longo D, Biagini G, Jones RS, Avoli M. The pilocarpine model of temporal lobe epilepsy. J Neurosci Methods. 2008; 172(2):143–57. Epub 2008/06/14. doi: S0165-0270(08)00255-0 [pii] doi: 10. 1016/j.jneumeth.2008.04.019 PMID: 18550176.

68. Csernansky JG, Csernansky CA, Kogelman L, Montgomery EM, Bardgett ME. Progressive neurodegeneration after intracerebroventricular kainic acid administration in rats: implications for schizophrenia? Biol Psychiatry. 1998; 44(11):1143–50. Epub 1998/12/04. doi: S0006-3223(98)00019-5 [pii]. PMID: 9836017.

69. Dudek FE, Staley KJ. The time course of acquired epilepsy: implications for therapeutic intervention to suppress epileptogenesis. Neurosci Lett. 2011; 497(3):240–6. Epub 2011/04/05. doi: S0304-3940(11) 00385-5 [pii] doi: 10.1016/j.neulet.2011.03.071 PMID: 21458536.

70. Kadam SD, White AM, Staley KJ, Dudek FE. Continuous electroencephalographic monitoring with radio-telemetry in a rat model of perinatal hypoxia-ischemia reveals progressive post-stroke epilepsy. J Neurosci. 2010; 30(1):404–15. Epub 2010/01/08. doi: 30/1/404 [pii] doi: 10.1523/JNEUROSCI.4093- 09.2010 PMID: 20053921.

71. White A, Williams PA, Hellier JL, Clark S, Dudek FE, Staley KJ. EEG spike activity precedes epilepsy after kainate-induced status epilepticus. Epilepsia. 2010; 51(3):371–83. Epub 2009/10/23. doi: EPI2339 [pii] doi: 10.1111/j.1528-1167.2009.02339.x PMID: 19845739.

72. Tan HO, Reid CA, Single FN, Davies PJ, Chiu C, Murphy S, et al. Reduced cortical inhibition in a mouse model of familial childhood absence epilepsy. Proc Natl Acad Sci U S A. 2007; 104(44):17536– 41. Epub 2007/10/20. doi: 0708440104 [pii] doi: 10.1073/pnas.0708440104 PMID: 17947380.

73. D'Ambrosio R, Hakimian S, Stewart T, Verley DR, Fender JS, Eastman CL, et al. Functional definition of seizure provides new insight into post-traumatic epileptogenesis. Brain. 2009; 132(Pt 10):2805–21. Epub 2009/09/17. doi: awp217 [pii] doi: 10.1093/brain/awp217 PMID: 19755519.

CHAPTER III

THE HALLMARKS OF KAINATE-INDUCED EPILEPTOGENESIS: IMMUNOHISTOCHEMICAL AND BEHAVIORAL ANALYSES

Modified from a paper published in *Frontiers in Bioscience*

Sreekanth Puttachary[1B], Shaunik Sharma[1B], Achala Thippeswamy, Thimmasettappa Thippeswamy[1C]

[1]Department of Biomedical Sciences, College of Veterinary Medicine, Iowa State University, Ames IA 50011-1250, United States of America.

[A]Reprinted with permission of *Front Biosci (Elite Ed)*. 2016 Jun 1; 8:390-411.

[B]Primary researchers and authors.

[C]Author for correspondence

Abstract

We have recently demonstrated immediate epileptogenesis in the C57BL/6J mouse, the strain that is resistant to kainate-induced neurotoxicity. By using a repeated low dose of kainate, we produced mild and severe status epilepticus (SE) models. In the present study, we demonstrate the impact of mild and severe SE, and spontaneous convulsive/nonconvulsive seizures (CS/NCS) on structure and function of the hippocampus, entorhinal cortex, and amygdala at 7, 14 and 28 day post-SE. Immunohistochemistry (IHC) of brain sections confirmed reactive astrogliosis and microgliosis, neurodegeneration, and increased neurogenesis in both groups. The epileptiform spike rate was higher in the severe group during first 12 days, but they decreased thereafter. Morris water maze test confirmed cognitive deficit in both mild and severe groups at 12d post-SE. However, MRI and IHC at 18 weeks did not reveal any changes in the hippocampus. These findings suggest that in C57BL/6J mice, immediate spontaneous CS could be responsible for early brain pathology or vice versa, however, the persistent spontaneous NCS for a longterm had no impact on the brain structure in both groups.

Introduction

The C57BL/6J mouse is genetically resistant to kainate-induced acute neurotoxicity (1-4), which limited the opportunity for researchers to use this strain of mouse as a model of chronic epilepsy. The C57BL/6J mouse also serves as a background strain in the production of certain transgenic mice used in epilepsy research. Therefore, C57BL/6 wild-type mice would be the most appropriate critical control for such studies. The C57BL/6J strain, as an acute model of status epilepticus (SE), also had several disadvantages such as high mortality rate and a huge variability in seizure response to chemoconvulsants, especially for kainate (4-7). We

have recently addressed these important issues in the C57BL/6J mice by administering repeated low dose of kainate (5 mg/kg, i.p. at 30 minutes intervals) until they reached stage-3 or -5 seizures (8, 9). This method yielded consistently mild (stage-3) or severe (stage-5) SE in greater than 92 percent of the mice and the SE could last for about 2 hours with less than 7 percent mortality rate (9). Importantly, irrespective of mild or severe SE, this method of inducing SE with kainate also caused immediate epileptogenesis in the C57BL/6J mice (8).

The conventional histological methods such as cresyl violet, hematoxylin and eosin, and fluoro-jade B (FJB) staining of brain sections at early time points (less than or equal to 7 day post-SE), induced by kainate, in the C57BL/6J mouse models produced mixed results with respect to neurodegeneration in the epileptic foci of the brain (2-4, 6, 7). Perhaps, these observations led to a belief that these mice are unlikely to develop epilepsy due to lack of a significant number of neuronal cell loss in the epileptic foci of the brain, unlike in the rat kainate models (10-13). In addition to hippocampal neurodegeneration, subtle changes in the neuronal population in the hilus and the subgranular zone of the dentate gyrus, reactive gliosis in the hippocampus and in other epileptic foci, and neurogenesis and aberrant migration of neuroblasts, could all contribute to epileptogenesis (14-20). The other reason for the dearth of reports on immediate epileptogenesis in C57BL/6J mice is inadequate seizure monitoring (21-25). Using continuous (24/7) remote video-EEG telemetry system, we have recently demonstrated that repeated low dose of kainate injection method induces consistent mild or severe SE (9), and immediate epileptogenesis in the C57BL/6J mice (8). The unique feature of this model is that the maximum numbers (27 plus or minus 4) of spontaneous convulsive seizures (CS) were observed during the first 4-6 weeks of the SE, in the severe SE group, and they decreased thereafter to less than 5 seizures/month for up to 18 weeks (the maximum

recording period) (8). The mild SE also induced immediate epileptogenesis but the numbers of spontaneous CS were less than 5 episodes during the first 4 weeks of the SE and 1 or 2 seizure/month was observed during the remaining recording period. Interestingly, the numbers of spontaneous electrographic NCS were about 20 per day/night cycle in both the severe and the mild SE groups throughout the 18 weeks period (8). Based on these observations, our hypotheses were that i) the severity of the SE will induce hyperexcitability of neurons (increased spike rate), reactive gliosis and neurodegeneration in the epileptic foci of the brain, and will also increase neurogenesis in the dentate gyrus to cause spontaneous CS and NCS during the first 4 weeks ii) these changes in the hippocampus will lead to cognitive dysfunction during this period, and iii) these changes will begin to decrease by 4 weeks to promote recovery from spontaneous CS. In this study, we tested these hypotheses to understand some of the plausible neurobiological reasons for spontaneous CS and recovery. We compared the elements of epileptogenesis such as EEG correlates, reactive astrogliosis and microgliosis (using glial fibrillary acidic protein (GFAP) and ionized calcium binding adaptor molecule 1 (IBA1), neurodegeneration (FJB + neuronal nuclear antibody, NeuN) and doublecortin (DCX) immunostaining (to label neuroblasts, an indicator of neurogenesis) at 7, 14 and 28 days post-SE. In addition, the impact of immediate epileptogenesis on their cognitive function was assessed using the Morris water maze test. At 18 weeks, the mice were subjected to MRI prior to euthanasia and the brains were processed for histology. The findings from these studies are presented and discussed.

Materials and Methods

Animal source and ethics statement

The C57BL/6J male mice, 7-8 weeks old, were purchased from the Jackson Laboratory, ME, USA and maintained under controlled environmental conditions (19°C – 23°C, 12h light: 12h dark), with ad libitum access to food and water in the Laboratory of Animal Resources at ISU. All experiments were carried out in accordance with the Institutional Animal Care and Use Committee, ISU, USA (protocol no. 10-12-7446-MR). The surgery was performed under isoflurane anesthesia and aseptic conditions. Appropriate postoperative care was undertaken to minimize pain and discomfort to animals.

Chemicals and reagents

Kainate (Abcam, USA) was prepared fresh in sterile distilled water at a concentration of 2mg/ml. For perfuse fixation we used: phosphate buffered saline (PBS, all chemicals from Sigma, USA), sodium sulfide perfusate solution in deionized water (48.3 mM sodium sulfide nonhydrate, Sigma, USA; 87mM sodium phosphate monobasic monohydrate, Fisher Chemicals, USA), and 4 percent paraformaldehyde (PFA, Acros Organics, NJ, USA). The primary antibodies and concentration used were as follows: NeuN (1:400, rabbit, EMD Millipore, USA); IBA1 (1:500, goat, Abcam, USA); GFAP (1:400, mouse, Sigma, USA); DCX (1:500, goat, Santa Cruz, USA). Appropriate secondary antibodies tagged with fluorescent dyes (CY3 1:300 or FITC, 1:100) or biotinylated antibodies (1:500) or 4', 6-diamidino-2-phenylindole (DAPI at 0.0001 percent) (all from Jackson ImmunoResearch Laboratories, USA) were used. The chemicals used for preparing the diluting solution in phosphate buffer saline (PBS) for antibodies (0.1 percent Triton X-100, 2.5 percent donkey serum and 0.25

percent sodium azide) were purchased from Sigma, USA. The fluorochrome conjugates of streptavidin were diluted in PBS alone.

Mild and severe SE induction with kainate and the experimental groups

We used 70 male mice in this study. Six mice received no drug and they served as control for all time points for immunohistochemistry (IHC) and another 16 mice were used as control for Morris water maze. Further 8 mice were implanted with radiotelemetric device for continuous (24/7) video-EEG recording for 18 weeks, and for MRI, after the induction of SE with kainate. Four mice were used for sham surgery for MRI study. The remaining 36 mice, including the mice that were implanted with the radiotransmitter, were administered a low dose of kainate (5mg/kg, i.p.) which was repeated at 30 minutes intervals to induce mild or severe SE as described previously (8, 9). The seizures during the SE were classified as nonconvulsive seizures (NCS; Racine scale/stage-1 and -2) or CS (Racine scale/stage 3-5). The behavioral seizure quantification during the SE, video-EEG recording procedures, and EEG analyses to detect spontaneous behavioral CS and electrographic NCS have been described in our recent publication (8).

All the mice that received kainate, irrespective of the dose, had continuous stage 1 or 2 seizures (NCS) for greater than 40 minutes. Since C57BL/6J mice response to KA is highly variable, we titrated each mouse with repeated low doses for the development of mild or severe seizures (9). Our previous studies from the C57BL/6J mice have shown that there was no correlation between the doses of KA and the severity of the SE or epileptogenesis or frequency of spontaneous recurrent CS (8, 9). To classify them as mild or severe SE group, we considered total duration of the CS stages during the 2h established SE (8, 9). All those mice that

experienced stage-3 seizures (rearing and forelimb clonus) for less than 10 minutes were considered as the mild SE group. These mice never reached stage 4 or 5 seizure. The severe SE group had several episodes of stage 3-5 seizures (rearing and continuous forelimb clonus, repeated rearing and falling, tonic clonic seizures including wild running and jumping) for greater than10 minutes (8). The behavior of all animals during the period of SE was video recorded and further verified to score offline for the severity of the SE by two more personnel who were unaware of the experimental groups. The telemetry mice were video-EEG recorded continuously for up to 18 weeks to identify the spontaneous CS and electrographic NCS as described previously (8). These experiments were done in parallel with the mild and severe SE group mice that were not implanted with the radiotransmitter. The telemetry mice and four surgery control (sham) mice were euthanized at 18 week, after acquiring MRI images, by perfusion fixation with sodium sulfide and paraformaldehyde under terminal anesthesia with an overdose of pentobarbital sodium (100 mg/kg, i.p.). The remaining mice were euthanized similarly at 7, 14 and 28 days post-SE. During the course of the experiments, the mice were subjected to Morris water maze to investigate the impact of seizures on their cognitive function.

1. Cortical EEG acquisition with continuous video EEG monitoring and analysis

The mice were implanted with a telemetric radiotransmitter (Physiotel and Multiplus ETA-F20, Data Science International (DSI), MN, USA), subcutaneously, 8–10 days before the induction of SE with KA. The electrodes were placed bilaterally on the cortical dura mater through the burr holes (2.5 mm caudal to Bregma and 2 mm lateral to the midline) as described previously (8, 9). The EEG acquisition (Dataquest ART) and analysis were carried out using NeuroScore (DSI) software. The post-SE EEG signals were normalized with the baseline EEG

from the same mouse. The epileptiform spikes, the normal baseline spikes, and the spikes due to electrical or mechanical artifacts were distinguished based on individual spike characteristics such as amplitude, duration, frequency, and inter-spike intervals (9). We have previously described different types of epileptiform spikes and CS in this model (8). The raw EEG signal, after manually excluding artifacts, was split into 10 s epochs for fast-fourier transformation (FFT) to generate power bands. The spontaneous recurrent CS were identified based on the EEG, power spectral characteristics, and video recordings for behavior (8). The mean plus/minus standard error values were pooled from 10 s epochs for spike counts, the average spike frequency per day was calculated for the first four weeks of post-SE, and the values were compared between the mild and the severe groups using two-way analysis of variance (ANOVA).

Morris Water Maze test and quantification

1. Fixed platform cue learning in Morris water maze

We used Morris water maze to evaluate the hippocampal dependent spatial learning and reference memory (27, 28) for mice that had mild or severe SE to test the effects of seizures on spatial navigation. The apparatus consisted of a galvanized stock tank of 1.15 meters in diameter filled with clear tap water maintained at room temperature before starting the tests. A clear circular plexi glass cylinder with a diameter of 11.2 cm was used as a platform. Two identical cues were used in this study: one cue was positioned directly above the platform zone (referred as “right cue”) and the second cue was positioned in the zone without platform (referred as “false cue”). Both cues were placed constantly at the same place throughout all the trials. Both cues were raised 15 cm above the water level to maintain visibility for the

swimming mice. A non-toxic white colored tempera paint was used to make water opaque to mask the platform during the submerged trials. When the platform was submerged, it was 1 cm below the water level, sufficient for mice to stand and raise above the water level. The mice were trained or tested at a fixed time during the day. Five trials were conducted per day during training and each mouse had at least a 30-45 min gap between trials in a single day. The mice had the same starting position for each trial during the training period or submerged trials and later, the starting position was randomized for the subsequent trials on that day. A single probe trial was performed keeping a constant starting position for all mice. The mice were constantly monitored during the experiments. The video acquisition and analysis were performed using Any-Maze software (Stoelting Company, USA). For those mice which were unable to identify the platform within a minute were gently placed on the platform for 30 seconds after each test.

2. Training

The three groups of mice, 16 mice from the control group and 6 mice each from the mild and the severe SE groups, were trained for 5 days in Morris water maze. The training was started at 7d post-SE (day 1) to test the effects of seizures on learning and memory. On day 1, the mice were trained to identify the exposed platform (0.5 cm) above the water level. Five trials, each trial lasting for one minute, were performed per mouse on day 1. “The right and the false cues” were presented at the same position at all times in the clear and transparent water during the training period. These zones (true and false platform zone) had a diameter equivalent to the diameter of the plexi glass platform was considered for time spent during average of 1minute trials (Figure 11C). The training was repeated on day 2 (i.e., 8d post-SE) but with the platform was submerged under the clear water. From day 3 to 5 (i.e., 9-11d post-SE), the mice

were trained similarly but in the opaque water to identify the submerged platform, as did on the day 2 training. The right and the false cues were maintained at the same position as in day 1 and 2 training. We chose 8 random starting points (such as east, west, north, south, northeast, north-west, south-east, south-west) around the periphery of the tank during the training period as did on the day 1.

3. **Probe trial**

A single probe trial of one minute/mouse was performed on day 6 (12d post-SE) in opaque water. The platform was removed but the right and false cues were left at the same position. A random starting position was selected for the mice for the probe trial too, and they were allowed to swim for one minute to identify the right or false cues. The amount of time spent (in seconds) during the one minute probe in the "right cue zone or true platform zone" and the "false cue zone or false platform zone" were calculated for each moue. Any-Maze mice tracking software was used to calculate the time spent by each mice (in seconds) at the right cue or false cue zones during training periods (average values of all trials conducted per day) or during single probe trial. Since we chose random starting points for training and probe trials, we did not consider the path efficiency parameter in this study. Prior to the second probe trial on day 20 post-SE, the mice were re-trained on day 19 in the submerged platform (1 trial in clear water and 4 trials in opaque water). The results were recorded and quantified as we did for the previous trials.

MRI and quantification

T2-weighted MRI scans of coronal and horizontal planes were acquired from the sham control and epileptic mice, at 18 weeks post-SE, under isoflurane anesthesia using a small bore MRI system (Varian Unity/Inova 4.7. T, Varian Inc. CA) at the University of Iowa. The slice thickness (spacing) for imaging was 300 microns and had a depth of 16 bit. The images were analyzed using image-J (29). The ratio of area in pixels outlining both hippocampi with their respective cortex were determined for each sections to analyze the volume changes. The ratio of the area of the hippocampi to the cortex was determined for each coronal section of the MRI image of a mouse. An average ratio of the hippocampi to the cortex for each mouse was determined. The changes in the average ratios between the control mice, the mild SE and the severe SE groups were compared using Mann-Whitney test.

Tissue processing for histology and IHC

The brains were collected soon after perfuse fixation, post-fixed with 4 percent PFA for 4h at 4°C, and were gelatin-embedded as described previously (30, 31). The coronal sections (15µm) were cut on a cryostat (Cryostar NX70, ThermoScientific, MA, USA), and thawmounted sequentially onto chrome-alum-gelatin coated slides in such a way that each slide had four sections, 450µm apart, to represent the hippocampus, entorhinal cortex and amygdala from rostral to caudal aspect. This method of sampling for rat hippocampus has been described previously (32). A modified version of tissue sampling for mouse brain, to obtain sections at 225µm intervals, and slide selection for quantification after immunostaining are illustrated in the Figure 1.

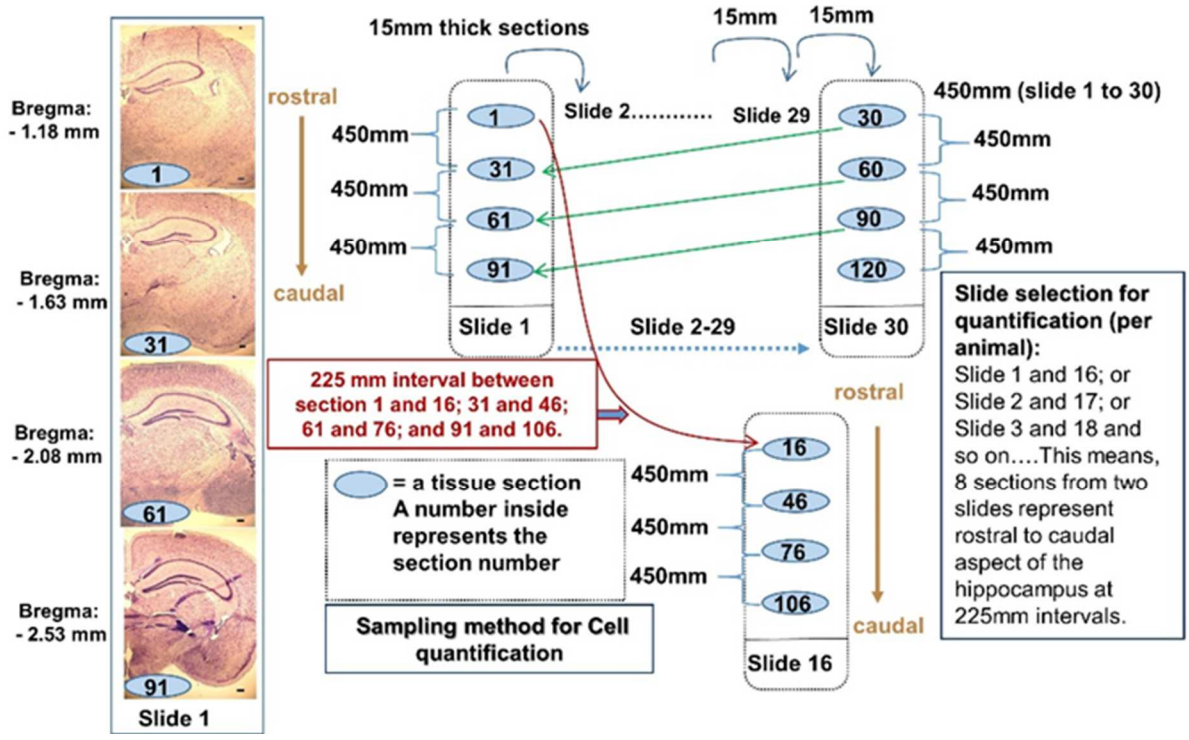

Figure 1. The method to sample the coronal brain sections, at 225 micrometer intervals, to represent the hippocampus from rostral to caudal for cell quantification. The 15µm serial sections (starting from rostral most part of the hippocampus- approximately at -1.1.8mm from Bregma, about 120 sections per mouse brain) were thaw mounted onto 30 slides sequentially in four rows starting from slide 1 to 30, as shown in the schematic diagram. The first 30 sections were placed on the first row of each slide serially followed by the 2nd, the 3rd and the 4th row. This method of sampling yielded sections on a single slide, separated by 450µm apart between sections, with a representative regions of the hippocampus, the entorhinal cortex and the amygdala from rostral to caudal. For example 1st and 31st sections, on the slide 1 are 450 micrometer apart represent the anterior region, the 61st section on the same slide represents the middle region, and the 91st section represents the posterior region of the hippocampus. A panel of photomicrographs of histology sections stained with cresyl violet and their approximate location from the Bregma is given on the left side of the images. For immunostaining, at least two slides (for example, slide 1 and 16) were selected in such a way that the gap between the corresponding sections on each slide is about 225 micrometers. For example, the distance between the 31st section on the slide number 1 and the 46th section on the slide number 16 is 225 micrometers. The immunopositive cell counts were carried out on all 8 sections bilaterally from two slides per animal and the average number of immuno-positive cells were calculated per animal. Scale bars, all 100 microns.

The brain sections for NeuN, GFAP, IBA1 and DCX were processed for double or triple IHC as described previously (31). Omission of primary antibody step served as a negative control for all antibodies, while morphology of neurons and their known location or glial cells

morphology served as internal positive controls (e.g. profusely branched astrocytes irrespective of their reactive or normal state for GFAP; pyramidal neurons in CA regions of the hippocampus and granule cells of the dentate gyrus for NeuN). Following overnight incubation with the primary antibodies at 4o C, the sections were washed with PBS and treated with appropriate secondary antibodies (biotinylated or CY3/FITC conjugated) for 1h at room temperature. After further washes, the sections that were incubated with the biotinylated anti-species and later treated with streptavidin-CY3 (1:300 for CY3 and 1:100 for FITC, Vector Laboratories, USA) for 1h, washed thoroughly in PBS, rinsed in distilled water to prevent salt crystal deposits on sections, and cover-slipped with vectashield-with DAPI® (Vector Laboratories, USA). The sections were viewed under the Zeiss inverted microscope (Axiovert 200) and photographed with Hamamatsu digital camera (Model C-10600-10B) using HCImage live (version 4.1.2.) software. For cell quantification, photographs were taken at 20x magnification (10x for Figures) keeping exposure time constant for all images.

In order to identify degenerating neurons in the hippocampus, the entorhinal cortex, and the amygdala the brain sections were processed for NeuN and FJB double staining. The sections were first stained for NeuN antibody as described above. Later, these sections were processed for FJB staining using a modified protocol from previously published method (11, 33-35). The sections on the slides were rehydrated sequentially in descending grades of ethanol starting with 100 percent for 3 min, followed by a 1 min each in 70 percent ethanol and distilled water. The slides were then transferred to 0.06 percent potassium permanganate solution for 10 min with slow shaking. After rinsing with distilled water for 1 min, the slides were transferred to 0.004 percent FJB (Histo-Chem Inc., AR) in 0.1 percent acetic acid for 30 min with slow shaking in dark. The sections were later rinsed three times in distilled water and air

dried in dark for 4h. Later the sections were dehydrated in ascending grades of alcohol, cleared in xylene, and mounted with distyrene plasticizer xylene (DPX, Electron Microscopy Sciences, PA) or acrytol (Surgipath, Leica biosystems, IL) mounting medium.

1. Immunopositive cell quantification

Procedure for cell counting has been described in our previous publications (30, 31, 36). ImageJ software (29) was used to measure the counting area (square microns) and the person counting cells was blind to the experimental groups. The cell counting area from each section was kept constant for all the experimental groups and controls. Bilateral counts were made from a minimum of eight sections per animal as described previously (30-32). The NeuN was used to mark neurons and the average number of neurons expressing FJB in each region was calculated. Microglia (IB1A), astrocyte (GFAP), and neuroblast (doublecortin (DCX)) cell markers were counterstained with DAPI and only those cells positive for cell marker and with a visible nucleus were counted from CA regions of the hippocampus, the dentate gyrus, the entorhinal cortex and the amygdala. The normal and reactive glial cells were distinguished based on their morphology.

Statistics

The average (mean plus/minus standard error) numbers of immuno-positive cells from 8 sections from 2 slides containing anterior, middle and posterior regions of the brain were calculated for each mouse within the group. To derive statistical differences (p less than 0.05) between the groups, Mann-Whitney test was applied. Likewise we compared the group performance in Morris water maze, and volumetric parameter from MRI images.

Results

The epileptiform spike rate and the frequency of spontaneous CS increase with the severity of SE during the first two weeks after the SE

As described previously, the behavioral cumulative seizure severity index during the SE was used to classify the mice as the mild or the severe SE group (8, 9). Our previous studies have demonstrated that both mild and severe SE induce immediate epileptogenesis, however the only difference was that the severe group experienced more numbers of spontaneous recurrent CS during the first four weeks of the SE (8). We further extended this study to quantify and compare the epileptiform spiking during the first four weeks between the two groups. Following termination of the behavioral SE with diazepam, no behavioral seizures were observed during the first 18 hours, however the electrographic NCS and epileptiform spiking continued to persist (Figure 2).

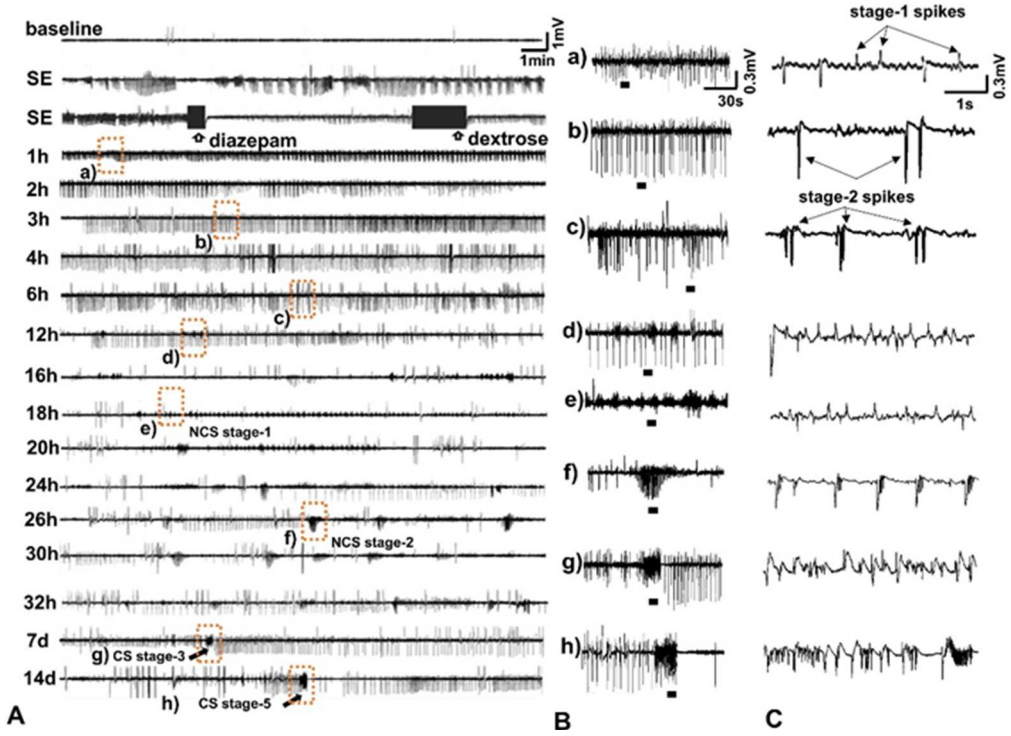

Figure 2. Representative EEG traces from a severe group mouse after terminating the behavioral SE with diazepam, and during the first 14 days of post-SE period. Each EEG trace in panel A

represents 20min of duration. The panels in B represent the expanded 2 min EEG traces shown in the boxes in A. The black bars below the EEG traces in B is further expanded as 5second traces in C. The SE was terminated by diazepam 2h after the onset of stage 3 (mild) or stage 5 (severe) seizure and dextrose normal saline injection was given thereafter. Although behavioral seizures stopped, epileptiform spikes continued to occur. These spikes organized into distinct patterns during epileptogenesis before developing into spontaneous recurrent convulsive seizures by 7d (stage-3) and by 14d (stage-5). The electrographic events during epileptogenesis include: (i) a transient decrease in the amplitude of epileptiform spiking soon after the diazepam injection (seen in trace 'a') (ii) initiation of newly formed epileptiform spike trains (seen in the trace 'b') (iii) progression of spike trains into spikes clustering (seen in the traces 'c' and 'd') leading to evolution of spontaneous recurrent NCS (as seen in the trace NCS stage-1 in 'e' and NCS stage-2 in 'f'). (iv) first spontaneous recurrent CS (stage 3, seen in the trace 'g') occurred on day 7, and (v) after several episodes of stage 3 CS, a first spontaneous recurrent CS stage-5-5 developed (as seen in the trace 'h').

The spontaneous behavioral CS and electrographic NCS, and interictal epileptiform spikes were present throughout the 28 days in all the mice irrespective of the severity of SE. There were about 16 plus or minus 3 (Mean plus or minus SEM) spontaneous CS in 4 weeks in the severe group and about 4 plus or minus 1 in the mild group. The spike frequency per minute (spike rate) was significantly higher in the severe group during the first 12 days post-SE when compared to the mild group (Figure 3, $p=0.0007$, Two-way ANOVA, $F=11.89$ with 1-140 degrees of freedom). However, after the day 12 the spike frequency was less than 5 spikes/minute in both groups.

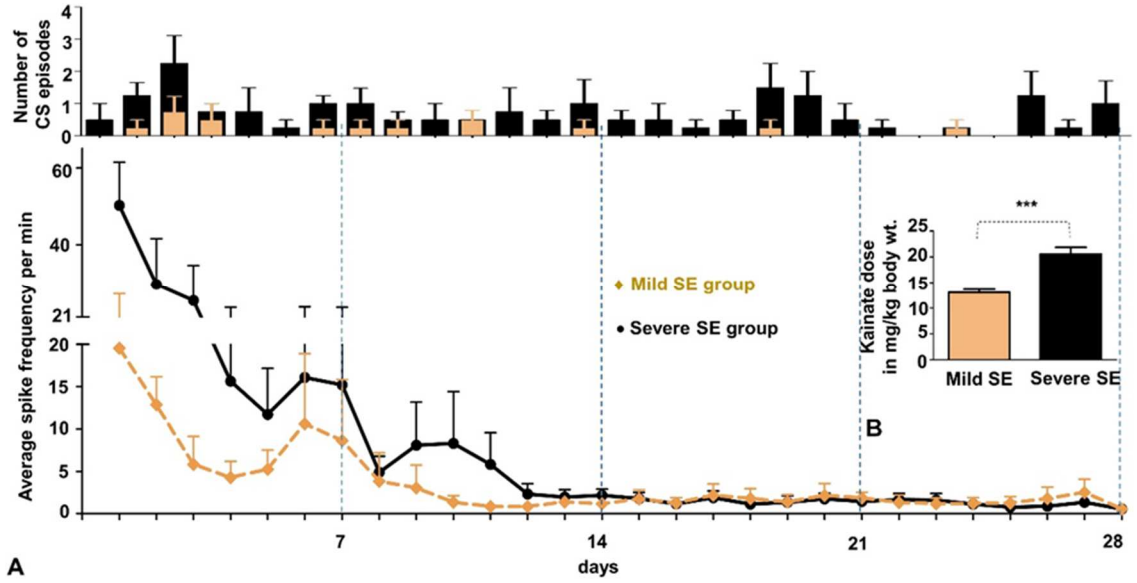

Figure 3. Comparison of the average epileptiform spike frequency in 1 day epochs during the first four weeks after the SE in the mild and the severe groups. A. The severe SE group had a higher spike frequency during the first 12 days and reached to the same level as the mild group thereafter (p=0.0007, Two-way ANOVA, F=11.89 with 1-140 degrees of freedom, n=4). A bar graph above shows the number of CS episodes/day in mild (n=4) and severe (n=4) SE groups. B. An inset bar graph showing a significant difference between the amount of kainate received by the mild and the severe SE groups (p=0.0.001, n=16 each, Mann-Whitney test) to achieve stage 3 or stage 5 seizures, respectively, during the SE. On an average, the mild SE group mice required 3 doses of 5mg/kg to achieve stage less than or equal to 3 seizures, while the severe group required 4-5 doses to achieve stage-5 seizures.

Electrographic features of epileptogenesis: Characteristics of post-diazepam EEG, pre-, post-, inter-ictal spikes, and NCS clusters during the first two weeks of post-SE

In the mild or the severe SE group, after diazepam administration, the behavioral seizures stopped. The electrographic seizures persisted although the amplitude of the epileptiform spikes reduced briefly (Figure 2B, a) during the first 20-30 minutes and reached the basal level by 16h (Figure 2A). We classified the non-convulsive interictal spikes and or episodes, and convulsive episodes based on the individual spike characteristics observed during the SE (8, 9). After the first 3h post SE, the high amplitude epileptiform spikes (predominantly stage-2 spikes) began to appear in trains lasting for 15-30 minutes with an

interspike intervals of 0.3-3 seconds (0.3-3 hertz, Hz, Figure 2B, a). The stage-2 spike trains started clustering by 6 hours (Figure 2B, c). Thereafter, stage-1 epileptiform spiking (0.2 -0.6 Hz) emerged along with stage-2 spike activity (Figure 2B, d). Later, stage-1 started to appear independently as "a string of pearls" referred to as stage-1 non-convulsive episodes (Figure 2B, e). The spiking pattern subsequently developed into a high amplitude stage-2 non-convulsive episodes with an increase in their duration (15-25s episode duration, Figure 2B, f). By 7d post-SE nonconvulsive episodes gradually evolved to culminate in stage-3 CS episode (Figure 2B, g). By 14d post-SE, several stage-3 convulsive episodes occurred before the stage-5 CS episode (Figure 2B, h).

Impact of epileptiform spiking and spontaneous CS on brain pathology at 7, 14 and 28 day post-SE

We quantified reactive gliosis to investigate time-dependent effects of the mild and the severe SE in the hippocampus, entorhinal cortex, and amygdala at 7, 14, and 28 days. Reactive astroglia and microglia were identified based on IHC using GFAP and IBA1 as cell markers for astroglia and microglia cells, respectively. The reactive astrocytes were characterized by thick cytoplasmic processes with intense GFAP staining (Figure 4). We have previously

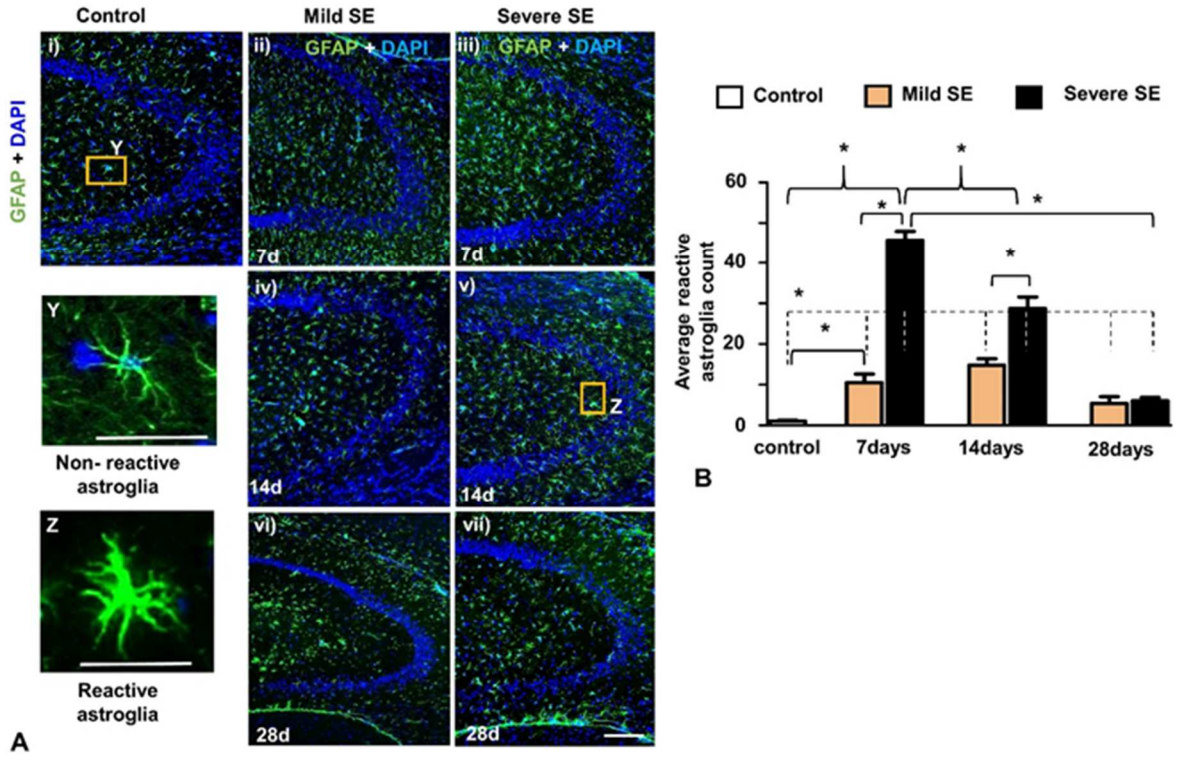

Figure 4. Reactive astrogliosis in the severe and the mild SE groups at 7d, 14d and 28d time points in CA3 region of the hippocampus. A. 10x magnified photomicrographs showing GFAP positive astrocytes (green; DAPI for nucleus, blue). Representative magnified images of normal (boxed in the panel 3Ai, marked as Y) and reactive astrocytes (boxed in the panel 3Av, marked as Z) are shown separately (Y and Z). Scale bars, all 100 microns. B. The reactive astrocytes in and around the stratum pyramidale were counted from CA regions of the hippocampus and the dentate gyrus at all three time points. There were significantly higher numbers of reactive astrocytes in the severe SE group at 7d and 14d post-SE when compared to the mild SE and the control groups (n=4 each, *p=0.029 control vs 7d mild, *p=0.029 control vs 7d severe, *p=0.028 mild vs severe 7d groups, *p=0.0294 mild vs severe 14d groups, Mann-Whitney test). There was significant reduction in reactive astrogliosis in the severe group from 7d to 28d time points (*p less than 0.05, severe 7d vs 14d and 7d vs 28d, 14d vs. 28d, Mann-Whitney test). The reactive astrogliosis was reduced at 28 day post-SE, but were significantly higher in both groups when compared with the control (*p=0.0286, control vs. mild 28d, and control vs, severe 28d, Mann-Whitney test).

shown that both reactive astrogliosis and microgliosis occurs as early as three days post-SE in the C57BL/6J mouse kainate model (31). The reactive astrogliosis and microgliosis were found in and around the cornu ammonis-3 (CA3) region of the hippocampus at 3d post-SE (31). In the present study, a similar pattern but more diffused reactive astrogliosis was observed in all

CA regions of the hippocampus, the hilus and the molecular layers of the dentate gyrus at all the time points (Figures 4). There was a significant increase in reactive astrogliosis in both the mild and the severe SE groups at 7 day when compared to the control in CA1, CA3 and dentate gyrus (Figure 4B, p less than 0.05, Mann-Whitney test). Further, severe SE group had significantly higher numbers of reactive astroglia cells at both 7d and 14d time points when compared to the mild SE group (Figure 4B, p less than 0.05, Mann-Whitney test). Likewise, reactive astrogliosis was also observed in the entorhinal cortex and the amygdala (Figure 5; p less than 0.05, Mann-Whitney test, n=5).

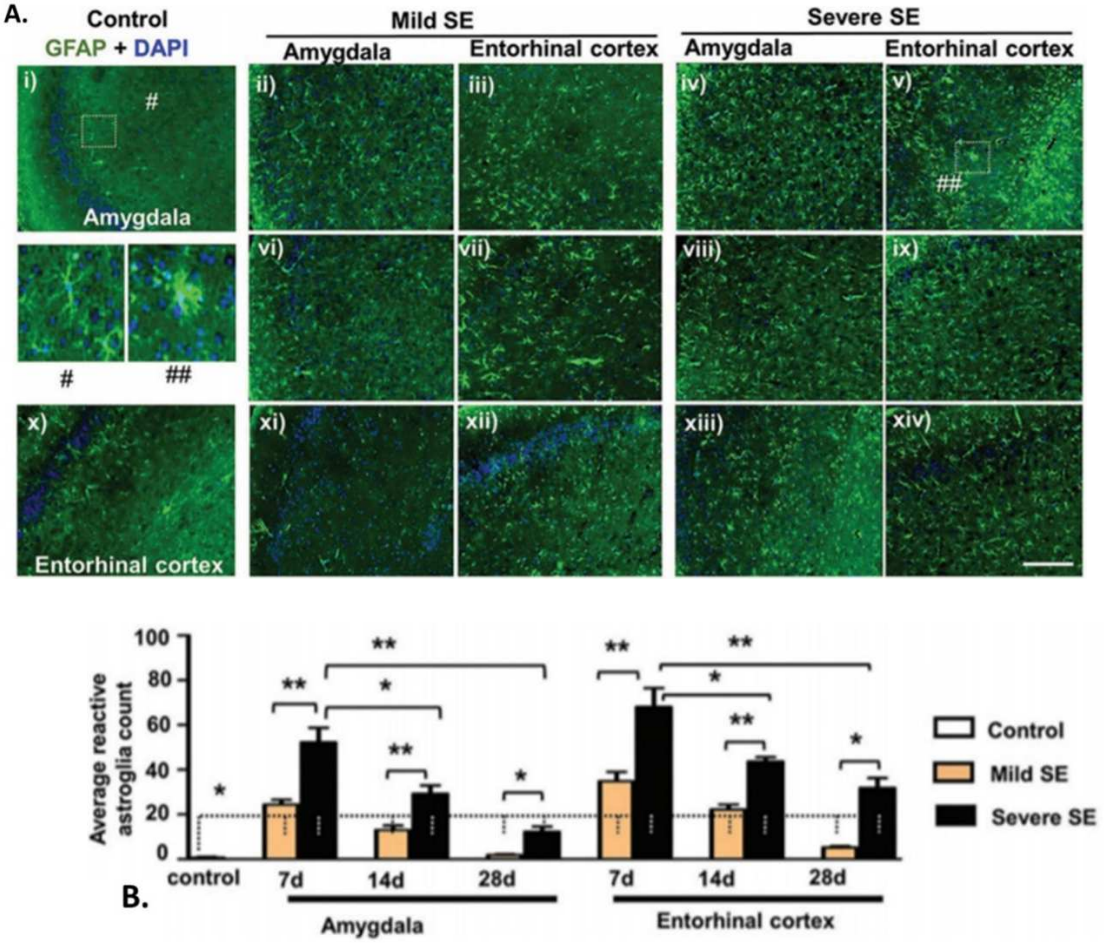

Figure 5. Reactive astrogliosis in the entorhinal cortex and the amygdala of the severe and the mild SE groups at 7d, 14d and 28d post-SE time points. A. 10x magnified photomicrographs showing GFAP positive astrocytes (green; DAPI for nucleus, blue). B. Cell quantification. The reactive astroglia significantly increased in both the mild and severe groups when compared to the naïve controls

at all the time points (p less than 0.05, Mann-Whitney test, n=5 each). The severe SE group had significantly higher reactive astroglia compared to the mild SE group at all time points, however a siginificant reduction in their numbers was observed at 14d and 28d time points when compared to 7d post SE (p less than 0.05, Mann-Whitney test). Magnified images of astrocytes shown in # (normal) and ## (reactive astrocyte). Scale bars, all 100 microns.

The reactive microglia cells were also quantified based on their morphology. They were hypertrophic and had a few thick but short cytoplasmic processes resembling pseudopodia and often amoeboid with several nuclei (Figures 6A and B) (37, 38). The reactive microglial cells were concentrated in and around the pyramidal cell layers in the CA3 and CA1 regions more frequently in the severe group than in the mild group at 7d post-SE (Figures 6A and B). In the severe SE group, the microglial cells were large and contained several nuclei suggesting their phagocytic nature, and their processes were frequently found to surround the NeuN positive cells (Figure 6B, iii, Z).

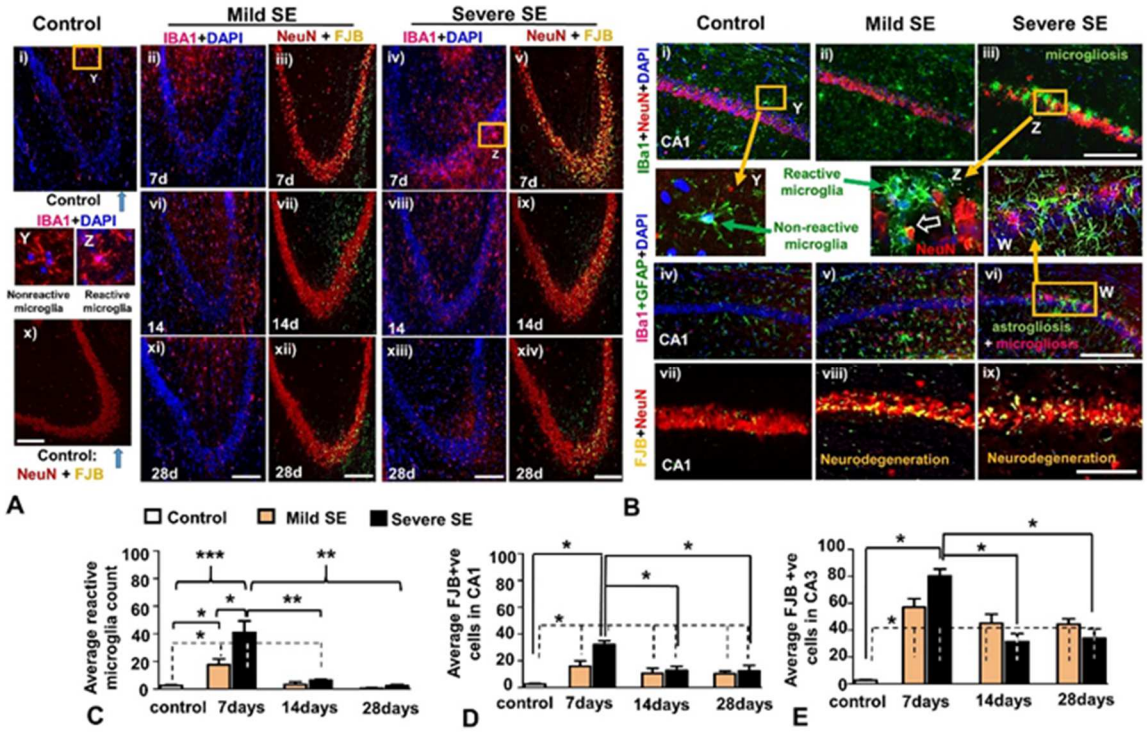

Figure 6. Reactive microgliosis and neurodegeneration in the hippocampus in the mild and the severe SE groups at 7d, 14d and 28d time points. A. 10x magnified photomicrographs showing IBA1 positive microglial cells containing nucleus. The reactive microglial cells were concentrated more in

and around the stratum pyramidale at 7d in the severe group (iv). A magnified images of normal (boxed in i) and labeled as Y) and reactive microglia (boxed in iv and labeled as Z) are shown in the panel Y and Z, respectively. The slides containing adjacent brain sections were processed for NeuN+FJB immunostaining to reveal neurodegeneration. At 7d post-SE in the severe SE group, the NeuN+FJB positive neurons were concentrated in the CA3 region (v) wher the reactive microglial cells were also present (iv), and these changes were moderate at 14d and 28d. In the mild SE group, reactive microgliosis and neurodegeneration were mild at 7d post-SE and they decreased further later on (ii and iii; vi and vii; xi and xii). B. The photomicrographs presented in B are from CA1 region- taken from the same sections as in the panel A from 7d post-SE group. The CA1 hippocampus too showed hypertrophied phagocytic reactive microglia (green cells in iii; the red cells are NeuN positive) in the severe SE group. The boxed area in (iii) is enlarged to show the morphology of reactive microglia cells that contain several nuclei (panel Z) when compared to the normal microglia from the control (i, the boxed area is enlarged- panel Y). Reactive microglia cells frequently wrapped the NeuN positive neurons (red, indicated by an open arrow in the panel Z). The parallel sections were also double stained for IBA1 and GFAP to understand the relationship between microglia and astrocytes at the site of neurodegeneration. The GFAP positive reactive astrocytes (green, iv to vi, and W) were frequently observed in close proximity with the reactive microglia cells (pink, iv to vi, and W) with no NeuN positive cells around suggesting the neuronal loss in that area. Those neurons undergoing degenerative changes were stained for FJB and NeuN (yellow stained cells in the panel vii to ix). The healthy neurons were stained by NeuN only. Those cells that stained for both FJB and NeuN were counted from CA1 and CA3 region of the hippocampus. Scale bar, all 100 microns. C-E. Cell quantification. There were significantly higher microglia cell counts in both the mild and the severe SE groups at 7d post-SE when compared to the control group (*p=0.017 control vs mild 7d, ***p=0.0006 control vs severe 7d, *p=0.0.38 mild vs severe 7d groups, Mann-Whitney test, n=5 each). The reactive microgliosis significantly reduced at 14 and 28d time points in the severe groups when compared to the 7d time point (**p=0.0028 severe 7d vs 14d and severe 7d vs 28d, Mann-Whitney test). There were significantly higher numbers of FJB positive cells in both CA1 and CA3 regions at 7, 14 and 28d post-SE in the severe groups when compared to the controls. There was a significant difference between controls and 28d mild group at CA1 and CA3 regions (*p=0.0286, Mann-Whitney test). However, there was a significant reduction in the number of FJB positive cells in the severe SE group at 14 and 28d time points when compared to 7d time point at CA1 and CA3 regions (*p=0.0286, severe 7d vs 14d or 28d, Mann-Whitney test, n=4 each).

The number of NeuN positive cells were fewer around the vicinity of the reactive microglial cells at 7d post-SE (Figure 6B, Z). The reactive astrocytes were also frequently found in the stratum pyramidale where the neurons were missing (Figure 6B, W, Z). The reactive microglia counts were also higher in the severe SE group than in the mild SE group at 7d, but not at 14d time point (Figure 6C, p less than 0.05, Mann-Whitney test). A similar pattern

of increased reactive microgliosis at 7d post-SE was also observed in the entorhinal cortex and the amygdala (as shown in Figure 7).

Overall, the reactive astroglia and microglia cell counts significantly reduced in both the severe and the mild groups after 7d time points in the hippocampus (p< less than 0.05, Mann-Whitney test, n=5), the entorhinal cortex (p less than 0.05, Mann-Whitney test, n=5) and the amygdala (p less than 0.05, Mann-Whitney test, n=5). However, when compared to the control, there was a persistent increase in reactive astrogliosis at all three time points and in all three brain regions, while the reactive microglial cell counts reached the basal level by 28d post-SE (Figures 6C and 7B).

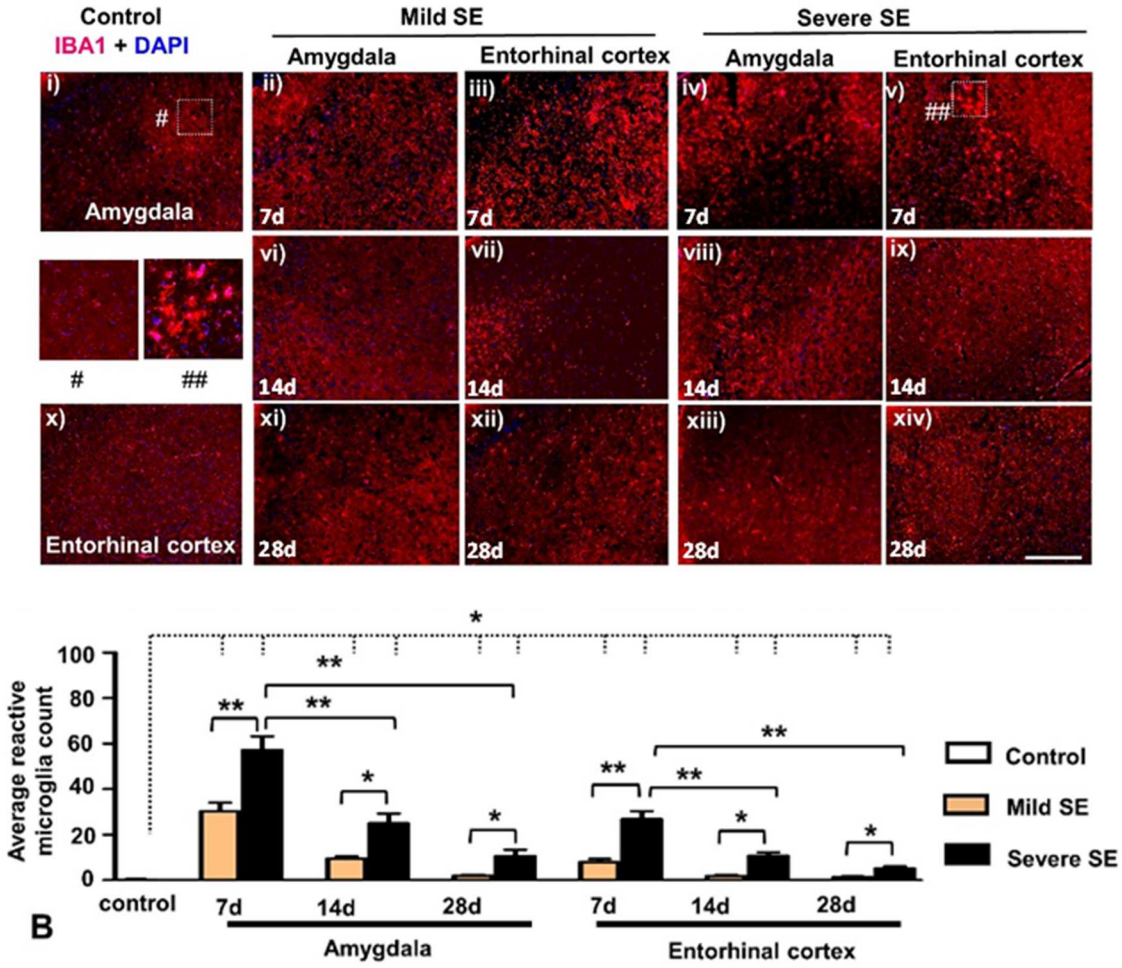

Figure 7. Reactive microgliosis in the entorhinal cortex and the amygdala of the severe and the mild SE groups at 7d, 14d and 28d time points. A. 10x magnified photomicrographs showing IB1A

positive microglia (red; DAPI for nucleus, blue). B. Cell quantification. The reactive microglia significantly increased when compared to the naïve controls at all the time points (p less than 0.05, Mann-Whitney test, n=5 each). The severe SE group had significantly higher reactive microglia compared to the mild SE group at all time points while a siginificant reduction was observed at 14d and 28d time points when compared to the 7d post-SE groups (p less than 0.05, Mann-Whitney test). Magnified images of microglia shown in # (normal) and ## (reactive microglia). Scale bars all 100 microns.

At 7 day post-SE the reactive microglial cells continued to dominate the CA3 and CA1 regions of the hippocampus (Figures 6A and B), the entorhinal cortex and the amygdala (Figure 7A). This observation, coupled with increased brain electrical activity (Figure 2 and 3) at this time point, prompted us to investigate whether neurodegeneration occurred during this period. FJB+NeuN staining revealed significant neurodegenerative changes in the same areas where there were a large numbers of reactive microglial cells. A large numbers of FJB positive cells were found in the hippocampus, the entorhinal cortex and the amygdala at 7 and 14 days in both the severe and the mild groups when compared to the control (Figures 6 and 8). However, at 28d their number declined in both groups, in all three regions, when compared to the 7d post-SE (Figures 6D and E, 8) which were similar to the patterns observed in reactive microglia and astroglia cell counts (Figures 4B and 6C).

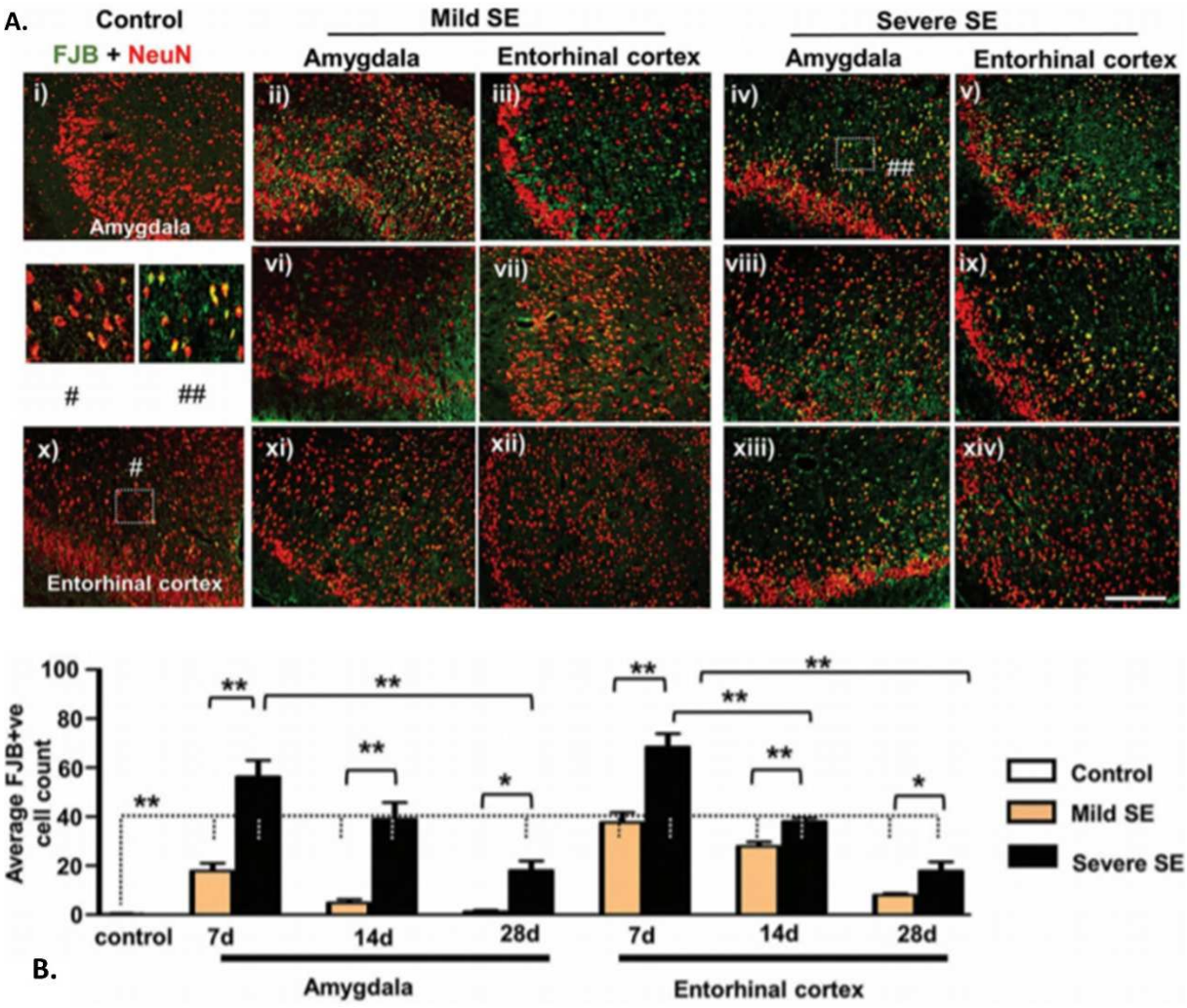

Figure 8. Neurodegeneration in the entorhinal cortex and the amygdala of the severe and the mild SE groups at 7d, 14d and 28d time points. A. 10x magnified photomicrographs showing FJB and NeuN positive cells (yellow; Green- FJB, red- NeuN, DAPI for nucleus, blue). B. Cell quantification. The number of FJB positive cells significantly increased when compared to the naïve controls at all the time points except 28d time point in amygdala (p less than 0.05, Mann-Whitney test, n=5 each). The severe SE group had significantly higher FJB positive cells when compared to the mild SE group at all time points while a siginificant reduction in their number was observed at 14d and 28d time points when compared to the 7d post-SE groups (p less than 0.05, Mann-Whitney test). Magnified images of neurons shown in # (normal) and ## (FJB positive neurons). Scale bars all 100 microns.

Having observed dramatic changes in reactive microglia and astrocytes, and neurodegeneration at 7 and 14 days, and recovery, to some extent, by 28 days in all three brain regions, we focused our investigation on the dentate gyrus. At 7d post-SE, we observed reactive astrogliosis in the hilus with thick (GFAP positive) astrocytic processes penetrating

through the dentate granule cells in both the mild and the severe groups (Figures 9A and 10A). The NeuN immunostaining revealed a significant reduction in the number of hilar neurons in both the mild and the severe SE groups at 7d post-SE when compared to the control group (Figure 9B). The NeuN+FJB double staining of the adjacent sections revealed that a large numbers of hilar neurons were FJB positive in both the mild and the severe groups suggesting an increase in neurodegeneration in the hilus of the dentate gyrus (Figure 9C; p=0.0286, Mann-Whitney test). At 14 and 28 days their numbers were reduced, the similar trend as for the reactive gliosis (data not shown).

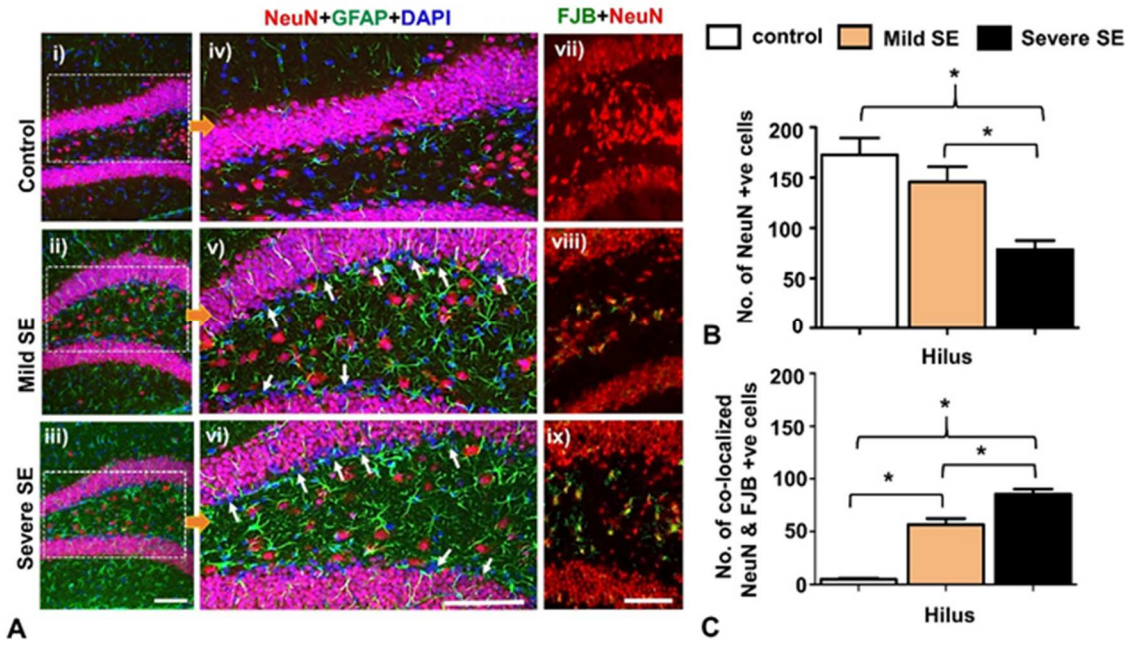

Figure 9. Neurodegeneration and reactive astrogliosis in the hilus of the dentate gyrus at 7d post-SE in the severe and the mild SE groups. A. 10x photomicrographs (i-iii) from 7d post-SE brain sections labeled for astrocytes (GFAP, bright green), neurons (NeuN, bright red/pink) and nucleus (DAPI labeled in blue). These images were further magnified in the panel iv-vi to show the subgranular zone and the cells in the hilus. The thick processes of the reactive astrocytes passing through the dentate granular cells were observed in both the groups. The white arrows in the panel v-vi (A) point to the subgranular zone are the DAPI positive cells that did not stain for NeuN or GFAP suggested that these cells were neither neurons nor astrocytes. These cells were DCX positive neuroblasts (shown in the Figure 10A). The NeuN and FJB double stained neurons in the hilus are shown in the panel vii-ix. Scale bar, all 100 microns. B-C. Cell quantification. There was a significant reduction in the NeuN positive cells in the hilus region in the severe SE groups when compared to the control or mild SE group when

compared to severe SE. C. The graph showing an increase in co-localization of NeuN and FJB positive cells in the hilus in the mild SE and the severe SE groups when compared to the control.

Interestingly, in both the mild and the severe groups we found a large numbers of DAPI positive cells that were neither positive for NeuN nor for GFAP in the subgranular zone (SGZ) of the dentate gyrus (Figure 9A). Based on our previous observation in the rat kainate model (32), we predicted that these cells could be neuroblasts. A double cortin (DCX) immunostaining was done to confirm this (Figure 10A). When compared with the control, the cell counts revealed a significant increase in the number of DCX positive cells in the SGZ at all the time points in both the mild (except at 28d) and the severe SE groups (Figure 10B). In the granule cell layer too, the DCX positive cells were higher at 7d and 14d when compared to the control in both the mild and the severe groups. In the hilus, such increase was found at 7d in the severe group only (Figure 10B). However, by 18 weeks, MRI revealed no significant changes in the ration of volume of the hippocampus to the rest of the volume of the brain in the severe and the mild groups or when compared to the control group (Figures 10C and D).

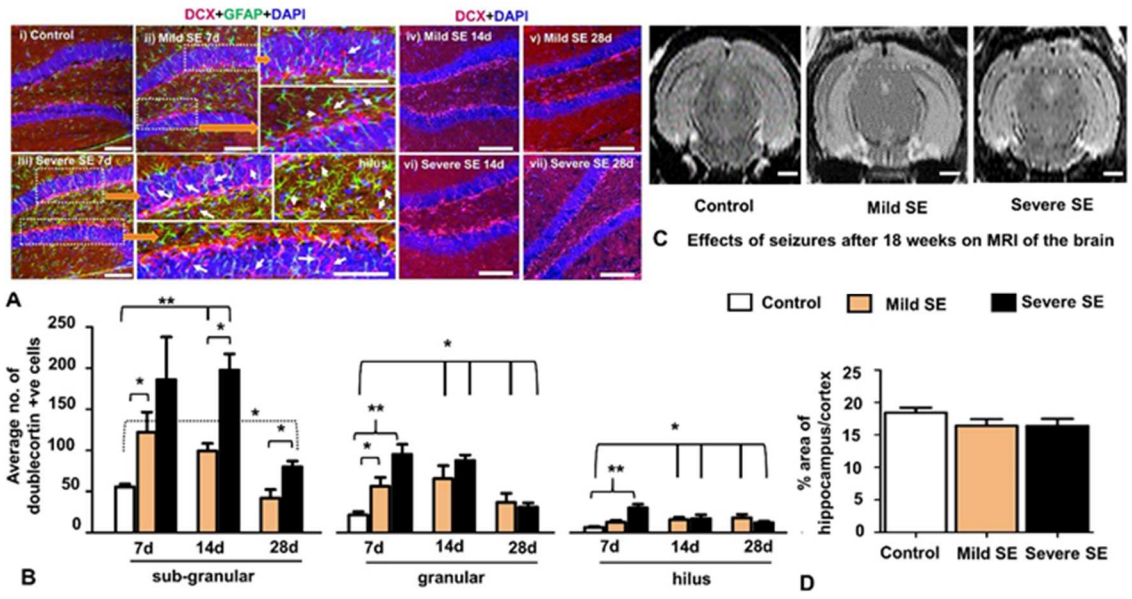

Figure 10. Neurogenesis at 7d, 14d and 28d post-SE in the severe and the mild SE groups and MRI at 18 week post-SE. A. The photomicrographs of the brain sections immunolabeled for astrocytes

(GFAP, green) and doublecortin (DCX, pink/red), and counterstained with DAPI (blue). A further magnified images from ii) and iii), indicated by large orange arrows, to demonstrate DCX positive cells in the hilus, subgranular and granular zones. The panel iv) to vii) represent DCX staining in the dentate gyrus from the mild (iv, v) and the severe (vi-vii) at 14 and 28d post-SE. Scale bar, all 100 microns. B. Cell quantification. There was an overall increase in the DCX positive cells in the subgranular and the dentate granule cell layer, and the hilus in both the severe and the mild SE groups when compared to controls at all the time points (except at 28d time points and in the subgranular zone at 28d in the mild group) (*p less than 0.05, Mann-Whitney test, n=5). At 7d post-SE there was a significant increase in the DCX positive cells in the subgranular zone which were neither NeuN nor GFAP positive as shown in the Figure 9A. An increase in the DCX positive cells (indicated by white arrows in 7d post-SE group) in the granule cell layer suggest their migration from the subgranular zone, and also in hilus in the severe and the mild SE groups than the control (A- indicated by white arrows) (*p less than 0.05, Mann-Whitney test, n=5). There was an overall decreasing trend in DCX positive cells at 28d time point compared to other time points in all three regions of the dentate gyrus. C-D. The MRI images of the control, mild and severe SE groups at 18 week did not show any morphological or volumetric changes in the hippocampus. 1mm scale bar for all images in C.

Further, cresyl violet staining of brain sections of mice that had persistent electrographic NCS for 18 weeks (evident from continuous video-EEG recording) did not reveal significant differences in morphological changes between the groups (data not shown).

Impact of epileptiform spiking, spontaneous CS and electrographic NCS, and brain pathology on hippocampal dependent discriminatory learning and memory

The Morris water maze test was performed to investigate the effects of the severity of seizures on discriminatory learning and memory. Considering the impact of the seizures on the hippocampus with respect to reactive gliosis, neurodegeneration, and neurogenesis, it was anticipated that the cognitive function could have been compromised in the epileptic mice. The mice were tested between 7-20 days post-SE, the period during which maximum pathology was observed. There were no differences between the control and the mild SE group with respect to the amount of time required to find the exposed platform on the day 7 (Figure 11A).

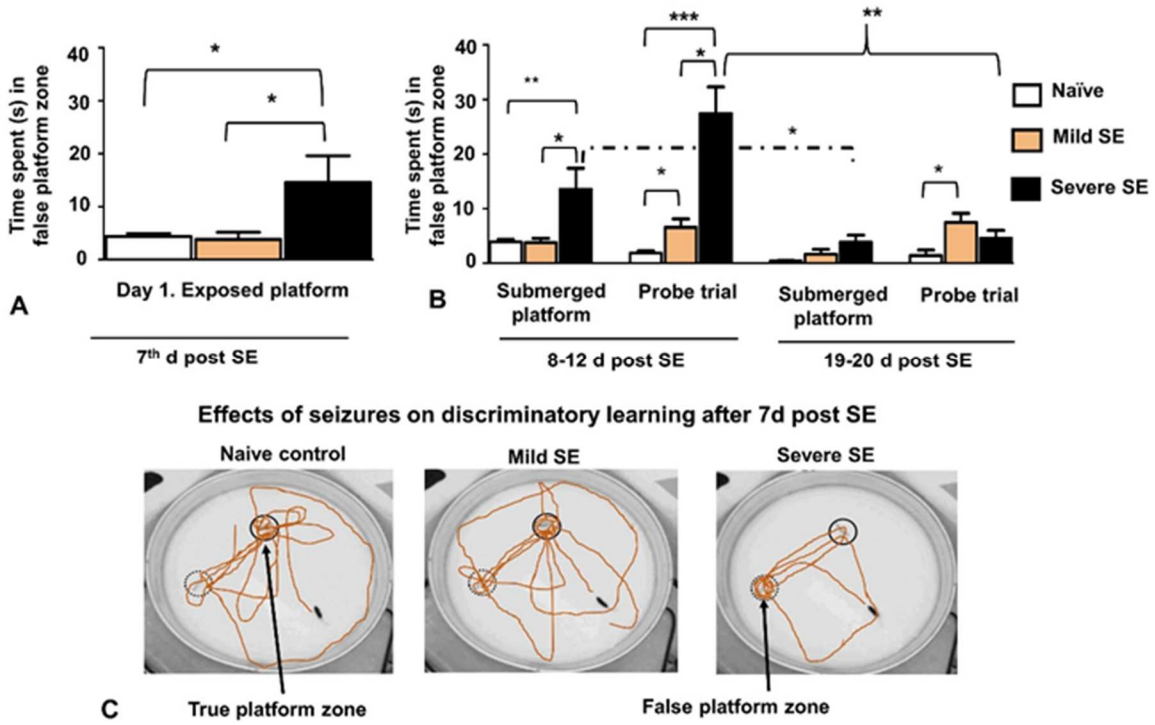

Figure 11. The impact of seizure severity, epileptiform spikes, reactive gliosis, neurodegeneration and neurogenesis on discriminatory learning behavior during the 7-20 days post-SE. The hippocampal dependent spatial learning was tested using the Morris Water Maze. A. The training was started for all three groups at 7th d post-SE to identify the exposed platform (5 trials). There were no differences between the control and the mild SE group in time spent to find the exposed platform. The severe SE group spent significantly more time at the false platform zone (incorrect learning) when compared to the mild SE and the control groups (n=16 for control, and 6 each for the severe and mild group; *p=0.026 for the control and *p=0.029 for the mild group, Mann-Whitney test). B. During the submerged platform trails (5 trials/animal each day for 4 days) from day 8 to 11 post-SE, the severe SE group continued to spend more time to find the submerged platform than the mild and the control groups (p=0.0018, Mann-Whitney test). Later, the single probe trial performed on the 12th day revealed that both the mild SE group spent a significant amount of time at the false zone than the control group (p less than 0.05, Mann-Whitney test). The severe group had further reinforced their incorrect learning behavior by spending more time at the false zone when compared with the control and the mild group (p=0.0018, Mann-Whitney test). On the day 19d, a brief re-training (5 trials) was given to all the three groups to find the submerged platform and a single probe trial was performed on the day 20. At 19d and 20d tests, there was a significant reduction in the time spent in the false platform zone in the severe group when compared to the earlier time points (p=0.002, Mann-Whitney test) suggesting an improvement in their discriminatory learning behavior. There was a small but significant increase in time spent in the false platform between the control and the mild SE mice (p=0.036, Mann-Whitney test) also suggesting a decline in their discriminatory learning behavior. C. The tracks of representative mice from each group travelled during the probe trail is presented.

However, the mild SE group mice spent more time at the false zone during the probe trails on day 12 and 20 post-SE suggesting the loss of memory. An interesting observation on the day 7 (training/learning trials) was that the severe SE group mice had a tendency to learn incorrectly i.e. they learned to choose the false zone instead of the exposed platform in contrast to the control and the mild SE groups. The incorrect learning was further reinforced during the submerged platform trials (day 8-11 post-SE) and the probe trial at 12d post-SE. However, after a gap of 7 days there was an improvement in the correct learning (i.e. choosing the true platform zone) after a short training in the submerged platform trials in the severe group (p less than 0.05, Mann-Whitney test). The tracks of representative mice from each group travelled during the probe trail is presented in Figure 11C.

Discussion

In the present study we demonstrate the effects of initial seizure severity during the SE and subsequent epileptiform spiking activity, in the C57BL/6J mouse kainate model, on the neurobiological changes in the hippocampus, the entorhinal cortex, and the amygdala during the early stage of epilepsy. The EEG recording and the IHC of brain sections from the mild and the severe SE groups revealed increased spiking activity with distinct pattern of EEG footprints of epileptogenesis, increased reactive astrogliosis and microgliosis, increased neurodegeneration and a concomitant increase in neurogenesis at 7 and 14 days post-SE. Most of these changes were reduced at 28 day post-SE. These early changes caused a significant reduction in the water maze performance in both groups indicating a cognitive decline during the early epileptic phase. Our findings from this study also seems to suggest that increased neurogenesis between 7-14 days and decreased reactive gliosis and neurodegeneration by 28 day may be responsible for reducing spontaneous CS after 4 weeks in the C57BL/6J mouse

model of epilepsy. However at a longer time point (18 weeks post-SE), neither MRI nor histology (data not shown) showed any gross changes in the brain between the groups suggesting that a different mechanism exists for the persistent spontaneous NCS that were observed in both the mild and the severe SE groups (8). The C57BL/6J mice are resistant to kainateinduced toxicity via the i.p. route (1, 2). Moreover their response to a single high dose of kainate was highly variable between different batches of mice and between different suppliers (8, 9, 39, 40). Also, an increased mortality rate was reported with a single high dose of kainate (normally greater than 20 mg/kg, i.p.) (2, 5, 6, 41). To overcome variability in seizure response to kainate and to reduce mortality rate, we demonstrated an alternate method of repeated low dose of kainate (5mg/kg, i.p.) given at 30 minutes intervals (9). This method is useful to titrate mice to a varying degree of severity based on the Racine scale (26). This method induced immediate epileptogenesis irrespective of the severity of seizures during the SE (8). We also further demonstrated a method of quantifying severity of the SE (cumulative seizure severity indices) based on real-time behavioral seizures and their corresponding EEG characteristics (8, 9). In the present study, we compared the long term effects of severe and mild SE on the brain electrical activity, pathology and the functional outcome. The studies from McKhann et al (3) and Yang et al (4), using repeated dose of kainate at different concentrations and intervals in the C57BL/6J mouse model, also reported increased seizure severity and decreased variability in seizure response. Since these were short term studies, the long term impact of severity of SE on epileptogenesis and neurobiological changes in the brain were not reported. In our studies, in addition to quantifying behavioral and electrographic SE, we further quantified the EEG for epileptiform spike rate with EEG patterns of epileptogenesis during the first four weeks (Figure 2 and 3) and spontaneous CS and electrographic NCS for

18 weeks post-SE (8). The epileptiform spikes detected during the post-SE period resembled inter ictal spikes and periodic epileptiform discharges as described for the C57BL/6J mouse kainate model (25, 31) and the rat kainate model (42). Further, it has been demonstrated that the inter ictal spike frequency could be a strong predictor of chronic epilepsy (43). A similar observation was made from our present and the previous studies from the C57BL/6J mouse chronic model of complex seizures (8).

SE causes neuroinflammation as a delayed effect (8, 44-49). SE disrupts the blood-brain-barrier (BBB) irrespective of severity of seizures (4, 50-53). The loss of BBB integrity causes infiltration of leukocytes and serum albumin in the extracellular space and increases GFAP content in astrocytes which results in reactive gliosis in the hippocampus and other brain regions (31, 45, 51, 52, 54). Until recently it was unclear whether the reactive astrogliosis in the epileptic foci was a cause or a consequence of epileptiform spiking activity (15-17, 20, 55, 56). We had demonstrated reactive astrogliosis in the hippocampus in the C57BL/6J mouse kainate model at 3 day post-SE (31). In the present study, the reactive astrogliosis and neurodegeneration persisted for up to 28 days, and reactive microgliosis for up to 14 days after the SE in the hippocampus, the entorhinal cortex, and the amygdala. Continuous video-EEG monitoring after inducing the SE revealed maximum number of spontaneous CS during the first 4 weeks when compared to the rest of the 18 weeks study (8). A recent study from a mouse model has shown that a deletion of integrin-beta1 causes widespread reactive astrogliosis and SRS during the first six weeks of postnatal life (57). Several other studies also support the view that reactive astrocytes contribute to epileptogenesis and SRS (15, 17, 20, 56). The astrocytes under a physiological condition prevent hyperexcitability of neurons by re-uptake of extracellular glutamate and ions at the synaptic terminal, which is compromised in reactive

glial cells (58-62). By 28 day post-SE in the present study, there was a reduction in the reactive astrogliosis that also coincided with the reduction in the spontaneous CS suggesting possible role for reactive astrocytes in hyperexcitability of neurons and SRS at earlier time points.

The reactive microglial cells were also increased in the hippocampus during the first 2 week of the SE in this study. At day 3 of post-SE in the C57BL/6J mice we had shown that the stratum pyramidale of the CA regions were invaded by reactive microglial cells with no evidence of neurodegenerative changes (31). At 7 day post-SE in the present study, a similar pattern of the reactive microglial cells invading the stratum pyramidale was evident in the CA3 region of the hippocampus (Figure 6A, iv), and the microglial cells were hypertrophic, which coincided with the neurodegenerative changes observed in the similar area of the hippocampus (Figure 6A, v). It has been shown that the downstream of SE-induced reactive gliosis increases the production of pro-inflammatory cytokines, chemokines and inducible nitric oxide (NO) synthase (30, 46, 63-65). In an organophosphate model of SE, an increased NO metabolites levels by 4-8 folds and a concomitant decreased ATP levels by 34-60 percent were reported in the hippocampus, and these levels persisted for up to 3 days post-SE (66, 67). These factors seems to exacerbate hyperexcitability of neurons during early epileptogenesis which was evident from the increased spiking activity on the EEG in the present study (Figure 2). Excessive amounts of reactive oxygen and nitrogen species, hyperexcitability of neurons and reactive gliosis are all known to cause neurodegeneration (8, 66-70). In the present study, we have demonstrated increased neurodegeneration in the hippocampus and the hilus of the dentate gyrus, the entorhinal cortex and the amygdala during the first few weeks of the SE (Figures 6 and 8).

The unique feature of the C57BL/6J mouse kainate model of epilepsy is that the frequency of spontaneous CS decreases after 4 weeks but the electrographic NCS persist beyond this period for up to 18 weeks (8). Other studies have also reported the impact of the severity of SE on hippocampal neurogenesis, aberrant migration of neuroblasts, and SRS in the Swiss mouse kainate, and the rat electroconvulsive and kainate models (4, 71-76). In the present study, both mild and severe SE increased reactive gliosis, neurodegeneration and DCX positive neuroblasts in the subgranular cell layer, the hilus and the dentate granule cell layer at 7 and 14 days post-SE. These changes were also coincided with an increase in the frequency of epileptiform spiking and spontaneous CS during this period (Figure 2). At 28d post-SE, these neurobiological changes were significantly reduced (Figure 10) and also the spontaneous CS (8). The role of enhanced neurogenesis during early post-SE is controversial whether it exacerbate or mitigate spontaneous seizures (14, 36, 47, 77). A recent study demonstrated a direct link between aberrant hippocampal neurogenesis, epilepsy and cognitive decline (78). In the nerve agent (soman) induced SE rat model, diazepam and valproic acid treatment increased neurogenesis and reduced spontaneous seizures (47). In the rat pilocarpine model with severe SE, an increased neurogenesis was reported in the hippocampus at 3 and 7 day post-SE (76), which supports our current findings (Figure 10). Triple immunostaining of brain sections at 7 day post-SE for GFAP, NeuN and DAPI indicated that a subpopulation of SGZ cells were neither GFAP nor NeuN positive (Figure 9A), which were indeed the neuroblasts stained for DCX (Figure 10A). The DCX positive cells were also found in the hilus and dentate granule cell layers. It has been reported that the newborn dentate granule cells synchronize with the host dentate granule cell layer (79, 80). However, aberrant migration of neuroblasts could lead to epileptogenesis (76, 78). Whether the DCX positive cells in the hilus assuming

that they originated from the subgranular zone (14, 81, 82), or they migrated from the medial ganglionic eminence (83, 84) needs further investigation.

The neurobiological evidence of hippocampal reactive gliosis and neurodegeneration resulting from the seizures, or vice versa, whether mild or severe, are most likely to have an impact on hippocampus mediated learning and memory tasks. Seizures are known to affect cognitive function (78, 85-87). In the present study, both mild and severe groups showed a significant impairment in learning and memory during the first 1-3 weeks post-SE. This coincided with increased reactive gliosis, neurodegeneration and epileptiform spiking. Epileptiform spiking is known to cause cognitive impairment (88-91). In the present study, although the epileptiform spiking on the EEG persisted for a longer period, the cognitive impairment was more pronounced during the first two weeks of the SE. We did not test the cognitive function beyond 28 days in the present study since the spontaneous seizures were reduced after 4 weeks post-SE (8).

In summary, we were able to detect the neurobiological changes such as gliosis and neurodegeneration in early epileptic phase in C57BL/6J mice that were correlated with the increased spike frequency on the EEG and cognitive dysfunction. A recovery from spontaneous CS, but not from spontaneous electrographic NCS, in this unique regressive mouse model of epilepsy also coincided with a reduction in gliosis, neurodegeneration, decreased spike rate at 28 day post-SE, which was preceded by an increased neurogenesis at 7 and 14 day post-SE. Since, these neurobiological changes occurs in less than four weeks of SE, the C57BL/6J mouse kainate model provides an earliest opportunity to test the effect of intervention drugs while, reducing the cost and duration of experiments when compared to rat models of epilepsy.

References

1. P. E. Schauwecker: The effects of glycemic control on seizures and seizure-induced excitotoxic cell death. BMC Neurosci, 13, 94 (2012) DOI: 10.1186/1471-2202-13-94.

2. P. E. Schauwecker and O. Steward: Genetic determinants of susceptibility to excitotoxic cell death: implications for gene targeting approaches. Proc Natl Acad Sci U S A, 94(8), 4103-8 (1997) DOI: 10.1073/pnas.94.8.4103.

3. G. M. McKhann, 2nd, H. J. Wenzel, C. A. Robbins, A. A. Sosunov and P. A. Schwartzkroin: Mouse strain differences in kainic acid sensitivity, seizure behavior, mortality, and hippocampal pathology. Neuroscience, 122(2), 551-61 (2003) DOI: 10.1016/S0306-4522(03)00562-1.

4. J. Yang, B. Houk, J. Shah, K. F. Hauser, Y. Luo, G. Smith, E. Schauwecker and G. N. Barnes: Genetic background regulates semaphorin gene expression and epileptogenesis in mouse brain after kainic acid status epilepticus. Neuroscience, 131(4), 853-69 (2005) DOI: 10.1016/j.neuroscience.2004.09.064.

5. P. E. Schauwecker: Genetic basis of kainateinduced excitotoxicity in mice: phenotypic modulation of seizure-induced cell death. Epilepsy Res, 55(3), 201-10 (2003) DOI: 10.1016/S0920-1211(03)00115-3.

6. S. A. Benkovic, J. P. O'Callaghan and D. B. Miller: Regional neuropathology following kainic acid intoxication in adult and aged C57BL/6J mice. Brain Res, 1070(1), 215-31 (2006) DOI: 10.1016/j.brainres.2005.11.065.

7. M. C. McCord, A. Lorenzana, C. S. Bloom, Z. O. Chancer and P. E. Schauwecker: Effect of age on kainate-induced seizure severity and cell death. Neuroscience, 154(3), 1143-53 (2008) DOI: 10.1016/j.neuroscience.2008.03.082.

8. S. Puttachary, S. Sharma, K. Tse, E. Beamer, A. Sexton, J. Crutison and T. Thippeswamy: Immediate Epileptogenesis after KainateInduced Status Epilepticus in C57BL/6J Mice: Evidence from Long Term Continuous Video-EEG Telemetry. PLoS One, 10(7), e0131705 (2015) DOI: 10.1371/journal.pone.0131705.

9. K. Tse, S. Puttachary, E. Beamer, G. J. Sills and T. Thippeswamy: Advantages of Repeated Low Dose against Single High Dose of Kainate in C57BL/6J Mouse Model of Status Epilepticus: Behavioral and Electroencephalographic Studies. PLoS One, 9(5), e96622 (2014) DOI: 1371/journal.pone.0096622.

10. P. S. Buckmaster and A. L. Jongen-Relo: Highly specific neuron loss preserves lateral inhibitory circuits in the dentate gyrus of kainate-induced epileptic rats. J Neurosci, 19(21), 9519-29 (1999).

11. M. S. Rao, B. Hattiangady, D. S. Reddy and A. K. Shetty: Hippocampal neurodegeneration, spontaneous seizures, and mossy fiber sprouting in the F344 rat model of temporal lobe epilepsy. J Neurosci Res, 83(6), 1088-105 (2006) DOI: 10.1002/jnr.20802.

12. A. P. Le and W. J. Friedman: Matrix metalloproteinase-7 regulates cleavage of pro-nerve growth factor and is neuroprotective following kainic acid-induced seizures. J Neurosci, 32(2), 703-12 (2012) DOI: 10.1523/JNEUROSCI.4128-11.2012.

13. K. M. Chiu, C. C. Wu, M. J. Wang, M. Y. Lee and S. J. Wang: Protective effects of bupivacaine against kainic acid-induced seizure and neuronal cell death in the rat hippocampus. Biol Pharm Bull, 38(4), 522-30 (2015) DOI: 10.1248/bpb.b14-00633.

14. J. M. Parent and D. H. Lowenstein: Seizureinduced neurogenesis: are more new neurons good for an adult brain? Prog Brain Res, 135, 121-31 (2002) DOI: 10.1016/S0079-6123(02)35012-X.

15. D. K. Binder and C. Steinhauser: Functional changes in astroglial cells in epilepsy. Glia, 54(5), 358-68 (2006) DOI: 10.1002/glia.20394.

16. M. L. Olsen and H. Sontheimer: Functional implications for Kir4.1. channels in glial biology: from K+ buffering to cell differentiation. J Neurochem, 107(3), 589-601 (2008) DOI: 10.1111/j.1471-4159.2008.05615.x.

17. J. Wetherington, G. Serrano and R. Dingledine: Astrocytes in the epileptic brain. Neuron, 58(2), 168-78 (2008) DOI: 10.1016/j.neuron.2008.04.002.

18. W. Zhang, R. Yamawaki, X. Wen, J. Uhl, J. Diaz, D. A. Prince and P. S. Buckmaster: Surviving hilar somatostatin interneurons enlarge, sprout axons, and form new synapses with granule cells in a mouse model of temporal lobe epilepsy. J Neurosci, 29(45), 14247-56 (2009) DOI: 10.1523/JNEUROSCI.3842-09.2009.

19. N. C. de Lanerolle, T. S. Lee and D. D. Spencer: Astrocytes and epilepsy. Neurotherapeutics, 7(4), 424-38 (2010) DOI: 10.1016/j.nurt.2010.08.002.

20. G. Seifert, G. Carmignoto and C. Steinhauser: Astrocyte dysfunction in epilepsy. Brain Res Rev, 63(1-2), 212-21 (2009) DOI: 10.1016/j.brainresrev.2009.10.004.

21. J. Kessler and H. J. Markowitsch: Different neuropathological effects of intrahippocampal injections of kainic acid and tetanus toxin. Experientia, 39(8), 922-4 (1983) DOI: 10.1007/BF01990440.

22. W. A. Turski, E. A. Cavalheiro, Z. A. Bortolotto, L. M. Mello, M. Schwarz and L. Turski: Seizures produced by pilocarpine in mice: a behavioral,

electroencephalographic and morphological analysis. Brain Res, 321(2), 237-53 (1984) DOI: 10.1016/0006-8993(84)90177-X.

23. Y. Ben-Ari and R. Cossart: Kainate, a double agent that generates seizures: two decades of progress. Trends Neurosci, 23(11), 580-7 (2000) DOI: 10.1016/S0166-2236(00)01659-3.

24. I. Knuesel, V. Riban, R. A. Zuellig, M. C. Schaub, R. M. Grady, J. R. Sanes and J. M. Fritschy: Increased vulnerability to kainateinduced seizures in utrophin-knockout mice. Eur J Neurosci, 15(9), 1474-84 (2002) DOI: 10.1046/j.1460-9568.2002.01980.x.

25. C. Huneau, P. Benquet, G. Dieuset, A. Biraben, B. Martin and F. Wendling: Shape features of epileptic spikes are a marker of epileptogenesis in mice. Epilepsia, 54(12), 2219-27 (2013) DOI: 10.1111/epi.12406.

26. R. J. Racine: Modification of seizure activity by electrical stimulation. II. Motor seizure. Electroencephalogr Clin Neurophysiol, 32(3), 281-94 (1972) DOI: 10.1016/0013-4694(72)90177-0.

27. R. Morris: Developments of a water-maze procedure for studying spatial learning in the rat. J Neurosci Methods, 11(1), 47-60 (1984) DOI: 10.1016/0165-0270(84)90007-4.

28. C. V. Vorhees and M. T. Williams: Morris water maze: procedures for assessing spatial and related forms of learning and memory. Nat Protoc, 1(2), 848-58 (2006) DOI: 10.1038/nprot.2006.116.

29. C. A. Schneider, W. S. Rasband and K. W. Eliceiri: NIH Image to ImageJ: 25 years of image analysis. Nat Methods, 9(7), 671-5 (2012) DOI: 10.1038/nmeth.2089.

30. A. S. Cosgrave, J. S. McKay, V. Bubb, R. Morris, J. P. Quinn and T. Thippeswamy: Regulation of activity-dependent neuroprotective protein (ADNP) by the NO-cGMP pathway in the hippocampus during kainic acid-induced seizure. Neurobiol Dis, 30(3), 281-92 (2008) DOI: 10.1016/j.nbd.2008.02.005.

31. E. Beamer, J. Otahal, G. J. Sills and T. Thippeswamy: N (w) -propyl-L-arginine (L-NPA) reduces status epilepticus and early epileptogenic events in a mouse model of epilepsy: behavioural, EEG and immunohistochemical analyses. Eur J Neurosci, 36(9), 3194-203 (2012) DOI: 10.1111/j.1460-9568.2012.08234.x.

32. A. S. Cosgrave, J. S. McKay, R. Morris, J. P. Quinn and T. Thippeswamy: The effects of nitric oxide inhibition prior to kainic acid treatment on neuro- and gliogenesis in the rat dentate gyrus in vivo and in vitro. Histol Histopathol, 25(7), 841-56 (2010).

33. L. C. Schmued and J. F. Bowyer: Methamphetamine exposure can produce neuronal degeneration in mouse hippocampal remnants. Brain Res, 759(1), 135-40 (1997) DOI: 10.1016/S0006-8993(97)00173-X.

34. L. C. Schmued and K. J. Hopkins: FluoroJade B: a high affinity fluorescent marker for the localization of neuronal degeneration. Brain Res, 874(2), 123-30 (2000) DOI: 10.1016/S0006-8993(00)02513-0.

35. M. S. Todorovic, M. L. Cowan, C. A. Balint, C. Sun and J. Kapur: Characterization of status epilepticus induced by two organophosphates in rats. Epilepsy Res, 101(3), 268-76 (2012) DOI: 10.1016/j.eplepsyres.2012.04.014.

36. A. S. Cosgrave, J. S. McKay and T. Thippeswamy: Differential regulation of vasoactive intestinal peptide (VIP) in the dentate gyrus and hippocampus via the NO-cGMP pathway following kainic acidinduced seizure in the rat. J Mol Neurosci, 42(3), 359-69 (2010) DOI: 10.1007/s12031-010-9353-x.

37. M. J. Carson, J. Crane and A. X. Xie: Modeling CNS microglia: the quest to identify predictive models. Drug Discov Today Dis Models, 5(1), 19-25 (2008) DOI: 10.1016/j.ddmod.2008.07.006.

38. D. S. Davis and M. J. Carson: An introduction to CNS-Resident Microglia: Definitions, Assays and Functional Roles in Health and Disease. Springer Press, (2013).

39. V. C. Kurschner, R. L. Petruzzi, G. T. Golden, W. H. Berrettini and T. N. Ferraro: Kainate and AMPA receptor binding in seizure-prone and seizure-resistant inbred mouse strains. Brain Res, 780(1), 1-8 (1998) DOI: 10.1016/S0006-8993(97)01081-0.

40. J. P. McLin, L. M. Thompson and O. Steward: Differential susceptibility to striatal neurodegeneration induced by quinolinic acid and kainate in inbred, outbred and hybrid mouse strains. Eur J Neurosci, 24(11), 3134-40 (2006) DOI: 10.1111/j.1460-9568.2006.05198.x.

41. P. E. Schauwecker: The relevance of individual genetic background and its role in animal models of epilepsy. Epilepsy Res, 97(1-2), 1-11 (2011) DOI: 10.1016/j.eplepsyres.2011.09.005.

42. P. A. Williams, A. M. White, S. Clark, D. J. Ferraro, W. Swiercz, K. J. Staley and F. E. Dudek: Development of spontaneous recurrent seizures after kainate-induced status epilepticus. J Neurosci, 29(7), 2103-12 (2009) DOI: 10.1523/JNEUROSCI.0980-08.2009.

43. K. J. Staley, A. White and F. E. Dudek: Interictal spikes: harbingers or causes of epilepsy? Neurosci Lett, 497(3), 247-50 (2011) DOI: 10.1016/j.neulet.2011.03.070.

44. D. M. de Groot, E. P. Bierman, P. L. Bruijnzeel, P. Carpentier, B. M. Kulig, G. Lallement, B. P. Melchers, I. H. Philippens and A. H. van Huygevoort: Beneficial effects of TCP on soman intoxication in guinea pigs: seizures, brain damage and learning behaviour. J Appl Toxicol, 21 Suppl 1, S57-65 (2001) DOI: 10.1002/jat.812.

45. T. Ravizza, M. Rizzi, C. Perego, C. Richichi, J. Veliskova, S. L. Moshe, M. G. De Simoni and A. Vezzani: Inflammatory response and glia activation in developing rat hippocampus after status epilepticus. Epilepsia, 46 Suppl 5, 113-7 (2005) DOI: 10.1111/j.1528-1167.2005.01006.x.

46. A. Vezzani, T. Ravizza, S. Balosso and E. Aronica: Glia as a source of cytokines: implications for neuronal excitability and survival. Epilepsia, 49 Suppl 2, 24-32 (2008) DOI: 10.1111/j.1528-1167.2008.01490.x.

47. M. de Araujo Furtado, F. Rossetti, S. Chanda and D. Yourick: Exposure to nerve agents: from status epilepticus to neuroinflammation, brain damage, neurogenesis and epilepsy. Neurotoxicology, 33(6), 1476-90 (2012) DOI: 10.1016/j.neuro.2012.09.001.

48. J. Jiang, M. S. Yang, Y. Quan, P. Gueorguieva, T. Ganesh and R. Dingledine: Therapeutic window for cyclooxygenase-2 related antiinflammatory therapy after status epilepticus. Neurobiol Dis, 76, 126-36 (2015) DOI: 10.1016/j.nbd.2014.12.032.

49. G. M. Arisi, M. L. Foresti, K. Katki and L. A. Shapiro: Increased CCL2, CCL3, CCL5, and IL-1beta cytokine concentration in piriform cortex, hippocampus, and neocortex after pilocarpine-induced seizures. J Neuroinflammation, 12(1), 129 (2015) DOI: 10.1186/s12974-015-0347-z.

50. P. Carpentier, I. S. Delamanche, M. Le Bert, G. Blanchet and C. Bouchaud: Seizure-related opening of the blood-brain barrier induced by soman: possible correlation with the acute neuropathology observed in poisoned rats. Neurotoxicology, 11(3), 493-508 (1990).

51. R. Kovacs, U. Heinemann and C. Steinhauser: Mechanisms underlying blood-brain barrier dysfunction in brain pathology and epileptogenesis: role of astroglia. Epilepsia, 53 Suppl 6, 53-9 (2012) DOI: 10.1111/j.1528-1167.2012.03703.x.

52. U. Heinemann, D. Kaufer and A. Friedman: Blood-brain barrier dysfunction, TGFbeta signaling, and astrocyte dysfunction in epilepsy. Glia, 60(8), 1251-7 (2012) DOI: 10.1002/glia.22311.

53. H. J. Shin, H. Kim, R. W. Heo, H. J. Kim, W. S. Choi, H. M. Kwon and G. S. Roh: Tonicity-responsive enhancer binding protein haplodeficiency attenuates seizure severity and NF-kappaB-mediated neuroinflammation in kainic acid-induced seizures. Cell Death Differ, 21(7), 1095-106 (2014) DOI: 10.1038/cdd.2014.29.

54. F. Frigerio, A. Frasca, I. Weissberg, S. Parrella, A. Friedman, A. Vezzani and F. M. Noe: Longlasting pro-ictogenic effects induced in vivo by rat brain exposure to serum albumin in the absence of concomitant pathology. Epilepsia, 53(11), 1887-97 (2012) DOI: 10.1111/j.1528-1167.2012.03666.x.

55. L. A. Shapiro, M. J. Korn, Z. Shan and C. E. Ribak: GFAP-expressing radial glia-like cell bodies are involved in a one-to-one relationship with doublecortin-immunolabeled newborn neurons in the adult dentate gyrus. Brain Res, 1040(1-2), 81-91 (2005) DOI: 10.1016/j.brainres.2005.01.098.

56. M. B. Gibbons, R. M. Smeal, D. K. Takahashi, J. R. Vargas and K. S. Wilcox: Contributions of astrocytes to epileptogenesis following status epilepticus: opportunities for preventive therapy? Neurochem Int, 63(7), 660-9 (2012) DOI: 10.1016/j.neuint.2012.12.008.

57. S. Robel, S. C. Buckingham, J. L. Boni, S. L. Campbell, N. C. Danbolt, T. Riedemann, B. Sutor and H. Sontheimer: Reactive astrogliosis causes the development of spontaneous seizures. J Neurosci, 35(8), 3330-45 (2015) DOI: 10.1523/JNEUROSCI.1574-14.2015.

58. A. Bordey and H. Sontheimer: Passive glial cells, fact or artifact? J Membr Biol, 166(3), 213-22 (1998) DOI: 10.1007/s002329900463.

59. A. Bordey, S. A. Lyons, J. J. Hablitz and H. Sontheimer: Electrophysiological characteristics of reactive astrocytes in experimental cortical dysplasia. J Neurophysiol, 85(4), 1719-31 (2001).

60. A. Volterra and J. Meldolesi: Astrocytes, from brain glue to communication elements: the revolution continues. Nat Rev Neurosci, 6(8), 626-40 (2005) DOI: 10.1038/nrn1722.

61. C. Steinhauser and G. Seifert: Astrocyte dysfunction in epilepsy. Brain Res Rev, 63 (1-2), 212-21 (2010) DOI: 10.1016/j.brainresrev.2009.10.004.

62. T. Eid, N. Tu, T. S. Lee and J. C. Lai: Regulation of astrocyte glutamine synthetase in epilepsy. Neurochem Int, 63(7), 670-81 (2013) DOI: 10.1016/j.neuint.2013.06.008.

63. F. J. Perez-Asensio, O. Hurtado, M. C. Burguete, M. A. Moro, J. B. Salom, I. Lizasoain, G. Torregrosa, J. C. Leza, E. Alborch, J. Castillo, R. G. Knowles and P. Lorenzo: Inhibition of iNOS activity by 1400W decreases glutamate release and ameliorates stroke outcome after experimental ischemia. Neurobiol Dis, 18(2), 375-84 (2005) DOI: 10.1016/j.nbd.2004.10.018.

64. M. Jafarian-Tehrani, G. Louin, N. C. Royo, V. C. Besson, G. A. Bohme, M. Plotkine and C. Marchand-Verrecchia: 1400W, a potent selective inducible NOS inhibitor,

improves histopathological outcome following traumatic brain injury in rats. Nitric Oxide, 12(2), 61-9 (2005) DOI: 10.1016/j.niox.2004.12.001.

65. E. Aronica, U. S. Sandau, A. Iyer and D. Boison: Glial adenosine kinase--a neuropathological marker of the epileptic brain. Neurochem Int, 63(7), 688-95 (2013) DOI: 10.1016/j.neuint.2013.01.028.

66. R. C. Gupta, D. Milatovic and W. D. Dettbarn: Depletion of energy metabolites following acetylcholinesterase inhibitor-induced status epilepticus: protection by antioxidants. Neurotoxicology, 22(2), 271-82 (2001) DOI: 10.1016/S0161-813X(01)00013-4.

67. R. C. Gupta, D. Milatovic and W. D. Dettbarn: Nitric oxide modulates high-energy phosphates in brain regions of rats intoxicated with diisopropylphosphorofluoridate or carbofuran: prevention by N-tert-butyl-alphaphenylnitrone or vitamin E. Arch Toxicol, 75(6), 346-56 (2001) DOI: 10.1007/s002040100249.

68. H. Ischiropoulos: Biological tyrosine nitration: a pathophysiological function of nitric oxide and reactive oxygen species. Arch Biochem Biophys, 356(1), 1-11 (1998) DOI: 10.1006/abbi.1998.0755.

69. M. J. Bianchetta, T. T. Lam, S. N. Jones and M. A. Morabito: Cyclin-dependent kinase 5 regulates PSD-95 ubiquitination in neurons. J Neurosci, 31(33), 12029-35 (2011) DOI: 10.1523/JNEUROSCI.2388-11.2011.

70. C. Liu, Y. Li, P. J. Lein and B. D. Ford: Spatiotemporal patterns of GFAP upregulation in rat brain following acute intoxication with diisopropylfluorophosphate (DFP). Curr Neurobiol, 3(2), 90-97 (2012).

71. J. M. Parent, R. C. Elliott, S. J. Pleasure, N. M. Barbaro and D. H. Lowenstein: Aberrant seizure-induced neurogenesis in experimental temporal lobe epilepsy. Ann Neurol, 59(1), 81-91 (2006) DOI: 10.1002/ana.20699.

72. J. M. Parent, T. W. Yu, R. T. Leibowitz, D. H. Geschwind, R. S. Sloviter and D. H. Lowenstein: Dentate granule cell neurogenesis is increased by seizures and contributes to aberrant network reorganization in the adult rat hippocampus. J Neurosci, 17(10), 3727-38 (1997).

73. P. Mohapel, C. T. Ekdahl and O. Lindvall: Status epilepticus severity influences the long-term outcome of neurogenesis in the adult dentate gyrus. Neurobiol Dis, 15(2), 196-205 (2004) DOI: 10.1016/j.nbd.2003.11.010.

74. F. Yang, J. C. Wang, J. L. Han, G. Zhao and W. Jiang: Different effects of mild and severe seizures on hippocampal neurogenesis in adult rats. Hippocampus, 18(5), 460-8 (2008) DOI: 10.1002/hipo.20409.

75. V. Bouilleret, V. Ridoux, A. Depaulis, C. Marescaux, A. Nehlig and G. Le Gal La Salle: Recurrent seizures and hippocampal sclerosis following intrahippocampal kainate injection in adult mice: electroencephalography, histopathology and synaptic reorganization similar to mesial temporal lobe epilepsy. Neuroscience, 89(3), 717-29 (1999) DOI: 10.1016/S0306-4522(98)00401-1.

76. Y. W. Hung, D. I. Yang, P. Y. Huang, T. S. Lee, T. B. Kuo, C. H. Yiu, Y. H. Shih and Y. Y. Lin: The duration of sustained convulsive seizures determines the pattern of hippocampal neurogenesis and the development of spontaneous epilepsy in rats. Epilepsy Res, 98(2-3), 206-15 (2012) DOI: 10.1016/j.eplepsyres.2011.09.015.

77. P. Jiruska, A. B. Shtaya, D. M. Bodansky, W. C. Chang, W. P. Gray and J. G. Jefferys: Dentate gyrus progenitor cell proliferation after the onset of spontaneous seizures in the tetanus toxin model of temporal lobe epilepsy. Neurobiol Dis, 54, 492-8 (2013) DOI: 10.1016/j.nbd.2013.02.001.

78. K. O. Cho, Z. R. Lybrand, N. Ito, R. Brulet, F. Tafacory, L. Zhang, L. Good, K. Ure, S. G. Kernie, S. G. Birnbaum, H. E. Scharfman, A. J. Eisch and J. Hsieh: Aberrant hippocampal neurogenesis contributes to epilepsy and associated cognitive decline. Nat Commun, 6, 6606 (2015) DOI: 10.1038/ncomms7606.

79. H. E. Scharfman, J. H. Goodman and A. L. Sollas: Granule-like neurons at the hilar/ CA3 border after status epilepticus and their synchrony with area CA3 pyramidal cells: functional implications of seizureinduced neurogenesis. J Neurosci, 20(16), 6144-58 (2000).

80. B. L. Murphy, R. Y. Pun, H. Yin, C. R. Faulkner, A. W. Loepke and S. C. Danzer: Heterogeneous integration of adult-generated granule cells into the epileptic brain. J Neurosci, 31(1), 105-17 (2011) DOI: 10.1523/JNEUROSCI.2728-10.2011.

81. H. E. Scharfman, A. E. Sollas, R. E. Berger, J. H. Goodman and J. P. Pierce: Perforant path activation of ectopic granule cells that are born after pilocarpine-induced seizures. Neuroscience, 121(4), 1017-29 (2003) DOI: 10.1016/S0306-4522(03)00481-0.

82. S. C. Danzer, X. He, A. W. Loepke and J. O. McNamara: Structural plasticity of dentate granule cell mossy fibers during the development of limbic epilepsy. Hippocampus, 20(1), 113-24 (2009) DOI: 10.1002/hipo.20589.

83. L. Danglot, A. Triller and S. Marty: The development of hippocampal interneurons in rodents. Hippocampus, 16(12), 1032-60 (2006) DOI: 10.1002/hipo.20225.

84. K. W. Henderson, J. Gupta, S. Tagliatela, E. Litvina, X. Zheng, M. A. Van Zandt, N. Woods, E. Grund, D. Lin, S. Royston, Y. Yanagawa, G. B. Aaron and J. R. Naegele: Long-term seizure suppression and optogenetic analyses of synaptic connectivity in

epileptic mice with hippocampal grafts of GABAergic interneurons. J Neurosci, 34(40), 13492-504 (2014) DOI: 0.1523/JNEUROSCI.0005-14.2014.

85. J. N. Lugo, J. W. Swann and A. E. Anderson: Early-life seizures result in deficits in social behavior and learning. Exp Neurol, 256, 74-80 (2014) DOI: 10.1016/j.expneurol.2014.03.014.

86. J. A. Witt and C. Helmstaedter: Cognition in the early stages of adult epilepsy. Seizure, 26, 65-8 (2015) DOI: 10.1016/j.seizure.2015.01.018.

87. A. P. Jellett, K. Jenks, M. Lucas and R. C. Scott: Standard dose valproic acid does not cause additional cognitive impact in a rodent model of intractable epilepsy. Epilepsy Res, 110, 88-94 (2015) DOI: 10.1016/j.eplepsyres.2014.11.005.

88. A. R. Brooks-Kayal, K. G. Bath, A. T. Berg, A S. Galanopoulou, G. L. Holmes, F. E. Jensen, A. M. Kanner, T. J. O'Brien, V. H. Whittemore, M. R. Winawer, M. Patel and H. E. Scharfman: Issues related to symptomatic and diseasemodifying treatments affecting cognitive and neuropsychiatric comorbidities of epilepsy. Epilepsia, 54 Suppl 4, 44-60 (2013) DOI: 10.1111/epi.12298.

89. J. K. Kleen, R. C. Scott, G. L. Holmes, D. W. Roberts, M. M. Rundle, M. Testorf, P. P. Lenck-Santini and B. C. Jobst: Hippocampal interictal epileptiform activity disrupts cognition in humans. Neurology, 81(1), 18-24 (2013) DOI: 10.1212/WNL.0b013e318297ee50.

90. G. L. Holmes: EEG abnormalities as a biomarker for cognitive comorbidities in pharmacoresistant epilepsy. Epilepsia, 54 Suppl 2, 60-2 (2013) DOI: 10.1111/epi.12186.

91. G. L. Holmes: Cognitive impairment in epilepsy: the role of network abnormalities. Epileptic Disord, 17(2), 101-16 (2015).

CHAPTER IV

INVESTIGATING THE NEUROPROTECTIVE AND ANTIEPILEPTOGENIC MCHANISMS OF 1400W, A HIGHLY SELECTIVE INOS INHIBITOR IN THE RAT KAINATE MODEL OF TEMPORAL LOBE EPILEPSY

Modified from a paper published in *Neurobiology of Disease*

Sreekanth Puttachary[1B], Shaunik Sharma[1B], Saurabh Verma, Yuan Yang, Marson Putra, Achala Thippeswamy, Diou Luo, Thimmasettappa Thippeswamy[1C]

[1]Department of Biomedical Sciences, College of Veterinary Medicine, Iowa State University, Ames IA 50011-1250, United States of America.

[A]Reprinted with permission of *Neurobiol Dis*. 2016 Sep; 93:184-200.

[B]Primary researchers and authors.

[C]Author for correspondence

Abstract

Status epilepticus (SE) initiates epileptogenesis to transform normal brain to epileptic state which is characterized by spontaneous recurrent seizures (SRS). Prior to SRS, progressive changes occur in the brain soon after SE, for example, loss of blood–brain barrier (BBB) integrity, neuronal hyper-excitability (epileptiform spiking), neuroinflammation [reactive gliosis, high levels of reactive oxygen/nitrogen species (ROS/RNS)], neurodegeneration and synaptic re-organization. Our hypothesis was that modification of early epileptogenic events will alter the course of disease development and its progression.We tested the hypothesis in the rat kainate model of chronic epilepsy using a novel disease modifying drug, 1400W, a highly selective inhibitor of inducible nitric oxide synthase (iNOS/NOS-II). In an *in vitro* mouse brain slice model, using a multi-electrode array system, co-application of 1400W with kainate significantly suppressed kainate-induced epileptiform spiking. In the rats, *in vivo*, 4 h after the induction of SE with kainate, 1400W (20 mg/kg, i.p.) was administered twice daily for three days to target early events of epileptogenesis. The rats were subjected to continuous (24/7) video-EEG monitoring, remotely, for six months from epidurally implanted cortical electrodes. The 1400W treatment significantly reduced the epileptiform spike rate during the first 12–74 h post-SE, which resulted in >90% reduction in SRS in long-term during the six month period when compared to the vehicle-treated control group (257 ± 113 versus 19 ± 10 episodes). Immunohistochemistry (IHC) of brain sections at seven days and six months revealed a significant reduction in; reactive astrogliosis and microgliosis (M1 type), extravascular serum albumin (a marker for BBB leakage) and neurodegeneration in the hippocampus, amygdala and entorhinal cortex in the 1400W-treated rats when compared to the vehicle control. In the seven day group, hippocampal Western blots revealed downregulation

of inwardly-rectifying potassium (Kir 4.1) channels and glutamate transporter-1 (GLT-1) levels in the vehicle group, and 1400W treatment partially reversed Kir 4.1 levels, however, GLT-1 levels were unaffected. In the six month group, a significant reduction in mossy fiber staining intensity in the inner molecular layer of the dentate gyrus was observed in the 1400W-treated group. Overall these findings demonstrate that 1400W, by reducing the epileptiform spike rate during the first three days of post-insult, potentially modifies epileptogenesis and the severity of chronic epilepsy in the rat kainate model of TLE.

Introduction

The status epilepticus (SE) due to exposure to chemoconvulsants or environmental toxins or head trauma initiates a series of overlapping changes in the brain. Chemoconvulsants cross blood–brain barrier (BBB) with ease and bind to the receptors on the neurons and in some glial cells, for example, kainate (KA) binds to the KA and the AMPA receptors (Ben-Ari, 2012; Ben-Ari and Cossart, 2000; Zhang and Zhu, 2012). This results in hyper-excitability of neurons, measured by changes in the electrical activity, and altered glial cell behavior such as modification of astrocytic end-feet at the BBB and loss of its function (Heinemann et al., 2012; Marchi and Lerner-Natoli, 2013; Tomkins et al., 2011; van Vliet et al., 2007). Compromised selective permeability of BBB causes infiltration of leukocytes and extravasation of serum albumin in the brain parenchyma to initiate reactive gliosis (Marchi et al., 2015; van Vliet et al., 2007; Weissberg et al., 2015) and downregulation of glutamate transporter and potassium channels in astrocytes (David et al., 2009; Takaki et al., 2013; Wang et al., 2003). The activated microglia, especially M1-type, and astrocytes are known to produce proinflammatory cytokines and inducible nitric oxide synthase (iNOS/NOS-II) (Cherry et al.,

2014; Chhor et al., 2013; Hirai et al., 2013; Hu et al., 2013; Kigerl et al., 2009; Liu et al., 2016; Zhao et al., 2015). These glial changes will ultimately increase the production of reactive oxygen and nitrogen species (ROS/RNS) to cause neurodegeneration (Tang and Le, 2015). The microglia become chronically activated due to neuronal death which in turn exacerbate hyperexcitability and neurodegeneration, thus establishing a potential self-perpetuating vicious cycle to maintain low seizure threshold to increase the probability of developing into an established epileptic state (Loane et al., 2013; Lull and Block, 2010; Papageorgiou et al., 2014; Waldbaum and Patel, 2009). The neurodegenerative changes coupled with persistent reactive glia produce pro-inflammatory cytokines, for example, interleukin-1 beta (IL-1β), and iNOS-mediated NO continue to excite neurons during the post-SE period i.e. the period of epileptogenesis (Kaushik et al., 2013; Kim et al., 2006; Vezzani et al., 2012). These factors persistently sensitize neurons to lower seizure threshold (Vezzani et al., 2012; Vezzani and Baram, 2007). Therefore, our hypothesis is that the drug that targets glial cells to reduce some of these factors during the early post-SE period could modify epileptogenesis to impact long-term suppression of spontaneous recurrent seizures (SRS).

The current antiepileptic drugs (AEDs) target neurons to suppress hyperexcitability by modulating ion channels at the pre- and/or postsynaptic terminals or the extra-synaptic membranes (Galanopoulou et al., 2013; Meldrum and Rogawski, 2007; Rogawski and Loscher, 2004). However, 1/3 of the people with epilepsy are refractory to the current AEDs (Kwan and Brodie, 2000; Kwan et al., 2011; Treiman, 2010). Therefore, the drugs that target sensitizers of neurons mediated by glia could be therapeutically useful to modify the processes of epileptogenesis and to retard/halt the progression of the disease. We tested this idea in the established rat model of temporal lobe epilepsy (TLE) induced by a conventional neurotoxin,

KA. KA-induced SE initiates neuroinflammation and neurodegeneration as early as 24 h (Drexel et al., 2012; Noe et al., 2013; Ryan et al., 2014; Ravizza et al., 2005; Vezzani et al., 2000). In the rat KA model of TLE, iNOS and IL-1β mRNA expression levels were significantly increased at 2 h post-SE and persisted for several weeks thereafter (De Simoni et al., 2000). In another rat KA study, it was shown that NO production peaks at 8 h post-SE in the hippocampus and the increased levels persisted for up to 6 weeks (Ryan et al., 2014). We have also previously demonstrated a significant increase in iNOS mRNA at 3 h and protein synthesis in microglial cells at 3 day post-SE in the rat KA model (Cosgrave et al., 2008). These findings suggest that upregulation of RNS and pro-inflammatory cytokines during early epileptogenesis could be a potential target for modification. Therefore, we treated the rats with a highly specific iNOS inhibitor, 1400W, at 12 h intervals for 3 days starting 2 h after administering diazepam to stop behavioral seizures. The 1400W is a slow, tight binding and highly selective pharmacological inhibitor of iNOS with a Kd value of 7 nM. It is N5000 and N200 fold selective for iNOS versus endothelial NOS (eNOS) and neuronal NOS (nNOS), respectively (Garvey et al., 1997; Jafarian-Tehrani et al., 2005; Parmentier et al., 1999; Staunton et al., 2013). The 1400W is biologically active *in vivo* and it has no pulmonary or cardiovascular side effects, and the physiological activities mediated by eNOS and nNOS are not compromised at the optimal dose (Boer et al., 2000; Pigott et al., 2013). We present the results from six months continuous (24/7) video-EEG surveillance, and the mechanistic pathway mediated by 1400W in disease modification in epilepsy. The 1400W treatment significantly reduced the epileptiform spike rate during the first 12-74 h post-SE, which caused >90% reduction in the number of SRS and prolonged the inter-seizure intervals in long-term during the six month continuous video-EEG study. Furthermore, 1400W treatment attenuated

BBB impairment by reducing the serum albumin levels in the brain parenchyma, suppressed reactive gliosis, neurodegeneration and mossy fiber sprouting. It partially ameliorated the downregulation of astrocytic inwardly-rectifying potassium (Kir 4.1) channels in the hippocampus. These results are discussed in the context of a plausible anti-epileptogenic properties of 1400W and disease modification in epilepsy.

Materials and Methods

Animal source and ethics statement

We used young adult male Sprague Dawley rats (Charles River, USA) for *in vivo* and 7–8 weeks old C57BL/6J male mice (Jackson labs, USA) for brain slice experiments. These animals were maintained at Laboratory of Animal Resources, Iowa State University (LAR, ISU), with ad libitum access to food and water under controlled environmental conditions (19 °C–23 °C, 12 h light:12 h dark). All experiments were carried out in accordance with the Institutional Animal Care and Use Committee, ISU (protocol numbers: 10-12-7446-MR, 9-15-8090-MR). The surgery was performed under aseptic conditions under general anesthesia (isoflurane) and, later appropriate postoperative care was given to minimize pain and discomfort to the animals.

Chemicals and reagents

KA (Abcam, USA) was prepared fresh in sterile distilled water at a concentration of 5 mg/ml. The 1400W (Tocris bioscience, USA) was dissolved in sterile distilled water (DW) at a concentration of 20 mg/ml. The chemicals for phosphate buffered saline (PBS) were purchased from Sigma, USA. Sodium sulfide perfusate ingredients (48.3 mM sodium sulfide nonahydrate 87 mM sodium phosphate monobasic monohydrate) were bought from Sigma and

Fisher Scientific, USA. Flurojade-B (FJB) was purchased from Histochem Inc. USA. Paraformaldehyde (PFA) was purchased from Acros Organics, NJ, USA.

Brain slice electrophysiology using multi-electrode arrays to investigate the effects of KA and 1400W

Under terminal general anesthesia, four C57BL/6J mice were decapitated to remove the brain for multi-electrode array (MEA) electrophysiology to test the effects of 1400W on KA-induced neuronal hyperexcitability before it was tested in *in vivo* in rats. Fresh coronal sections of 400 μm thickness were cut using a vibratome (series 1000, TPI, MO, USA) using chilled (2–5 °C) sucrose slicing solution (26 mM NaHCO3, 1 mM KCl, 9 mM MgCl2, 1 mM CaCl2, 248 mM sucrose and 10 mM D-glucose (Le Duigou et al., 2008). Later these sections were transferred to recording solution (124 mM NaCl, 4.5 mM KCl, 1 mM NaH2PO4, 26 mM NaHCO3, 2 mM CaCl2, 2 mM MgCl2, 10 mM glucose with an osmolarity of 300 mosmol per liter) at 32–35 °C. The slices were constantly exposed to carbogen (95% O_2 and 5% CO_2) when they were in slicing or recording solution. The recording chamber included an integrated planar MEA chamber (60-MEA500 series, Multichannel systems, USA). The data acquisition components included MEA1060 amplifiers, desktop computer with MC Rack software (Multichannel systems, MCS GmbH, USA). Using suction, the brain slices were carefully positioned on the 60 electrodes in the MEA chamber to encompass dentate granule cell layers, the hilus of the dentate gyrus, and cornu ammonis (CA) regions of the hippocampus (CA1, CA3, and CA4). The slices were incubated in the recording solution at 35 °C for 10–15 min in the MEA bath chamber. The position of electrodes on the hippocampus and dentate gyrus regions during each recording, and for each slice, was photographed. We used two fresh brain

slices per mouse (8 slices from four mice). The baseline recording was set at an amplitude of <25 μV. The threshold for spontaneous spikes was set at an amplitude of 35 μV for KA and KA + 1400W applications to determine changes in epileptiform spike frequency. The baseline spiking was recorded initially and later, the drugs prepared in the recording solution were perfused over the slices in the MEA bath chamber. After a 2 min of initial baseline recording, the slices were exposed to KA (1 μM) for 2 min and later KA perfusion was continued along with 1400W (5 μM) for a further 2 min. The recordings were later analyzed using MC Rack software to quantify the epileptiform spike frequency per second (Hertz, Hz) to compare baseline spiking with KA or KA with 1400W. These results were compared using paired Student t-tests.

Seven day post-SE in vivo experiments: SE induction with KA and treatment with diazepam and 1400W

We used 40 rats for this experiment to investigate the impact of 1400W on the early stage of epileptogenesis. Twenty rats served as naïve controls for all time points for immunohistochemistry (IHC) and Western blots. The remaining twenty rats were administered with KA to induce SE. We followed a refined repeated-low-dose method of KA administration to; i) titrate animals according to the development of behavioral SE, ii) to minimize mortality due to KA-induced SE, iii) to achieve a fair consistency in seizure severity during SE, and iv) to minimize animal-to-animal and group-to-group variabilities in neurodegeneration and SRS frequency (Beamer et al., 2012; Glien et al., 2001; Hellier et al., 1998; Puttachary et al., 2015a,b; Tse et al., 2014). The rats were initially treated with a low dose of KA at 5 mg/kg via intraperitoneal (i.p.) route and a second dose was given 30 min later. After the first two doses

of KA, the dose of KA was set at 2.5 mg/kg at 30 min intervals to reduce mortality. KA injection was stopped once the rats reached stage-5 seizure (starting point of "2 h established SE") and 2 h later behavioral seizures were terminated by administering diazepam (10 mg/kg, i.p., the end point of "2 h established SE") to keep the duration of SE constant between animals. After terminating behavioral SE, all rats received supportive fluid therapy (1 ml Ringers lactate subcutaneous route for the next 3 days) and were later randomized into two groups. In this study, the duration of the established SE was 2 h. During the 2 h established SE, the behavioral seizures were scored live based on modified Racine scale, by direct observations and also verified later from remote videos by two experimenters, as described previously (Beamer et al., 2012; Cosgrave et al., 2008; Puttachary et al., 2015a, b; Tse et al., 2014). Seizures were classified as non-convulsive seizures (stage-1 and -2 on Racine scale) or convulsive seizures (stages 3–5 on Racine scale) (Racine, 1972), and the exact duration of each stage of seizure was scored and expressed in minutes. During the 2 h of established SE, the rats had continuous seizures ranging from stage-1 to stage-5. After administering diazepam, the rats were divided into two groups based on similar convulsive seizure severity scores and the total amount of KA they had received. The groups were code numbered to keep the experimenters blinded to the treatment. Two hours after administering diazepam, one group of rats received six injections of 1400W (20 mg/kg, i.p.) or vehicle (equal volume of sterile DW) at 12 h intervals. The animals were euthanized at 7 day post-SE. Some animals were perfuse fixed with 4% PFA in PBS for IHC or without PFA for Western blotting.

BBB integrity experiment

To understand the effects of KA and 1400W on BBB integrity, rats (n = 15) were administered with 25 µl of 4% hydroxy-stilbamidine (Fluro-Gold, Colorado, USA, Molecular

Weight 472.54) intraperitoneally 2 h prior to the induction of SE with KA (Molecular Weight, 213.23) or vehicle. Five rats without KA served as control, five rats each were treated with a single dose of 1400W (20 mg/kg, i.m., Molecular Weight 250.17) or its vehicle 1 h prior to the induction of SE as described above. Two hours after the onset of the first stage-5 seizure, the rats were deeply anaesthetized and perfuse fixed with 4% PFA. The brains were processed for histology to assess BBB integrity.

Telemetry device implantation, induction of SE by KA, intervention by 1400W, and continuous long-term video-EEG monitoring for 6 months

Twenty one male rats were used for this study. Five rats were used as sham controls. The remaining 16 rats were implanted with radio-transmitter (Physiotel and Multiplus CTA-F40, Data Science International, DSI, MN, USA) subcutaneously, 10 days before the induction of SE with KA. The electrode leads were placed bilaterally on the cortical dura mater through the burr holes (4 mm caudal to Bregma and 3 mm lateral to the midline) as described previously for mice (Beamer et al., 2012; Puttachary et al., 2015a, b; Tse et al., 2014). The video-EEG acquisition was started immediately, after the rats recovered from anesthesia, using Dataquest ART 4.3.2 and later the offline analyses were carried out using NeuroScore 3.2.0 (DSI) software. The implanted radiotransmitter had a built-in thermal module that relayed body temperature in real-time. The rats were regularly monitored for their bodyweight, body temperature and their overall activity. Nails were trimmed as required if the skin at the surgery site or transmitter site was found scratched. We acquired ~260 h of baseline EEG data, which included at least 10 day–night cycles, to normalize the post-SE EEG signal from the same animal. SE was induced with KA as described above. Two hours after behavioral SE was terminated with diazepam, the rats were randomly grouped and treated with 1400W or vehicle,

as described in Section 2.4, and subjected to continuous (24 h per day and 7 days a week) video-EEG monitoring for six months. At the end of the study, the animals were euthanized by terminal anesthesia using pentobarbital sodium (100 mg/kg, i.p.), perfuse fixed, and the brains were processed for histology and IHC.

EEG analyses

The EEG recordings were analyzed to determine the numbers of SRS during the six months continuous study, and the average spike frequency (per min) per day was determined for the first 4 weeks of post-SE and expressed as standard error mean (±SEM) values. The EEG signals from post-SE were normalized to the baseline EEG from the same animal to observe epileptiform spiking/seizures. The normal baseline spikes, epileptiform spikes and clusters, and the spikes arising from electrical or mechanical artifacts were distinguished based on the video and the individual spike characteristics on EEG (spike amplitude, duration, frequency, and inter-spike intervals) as described previously for mice (Puttachary et al., 2015a, b; Tse et al., 2014) and rats (Williams et al., 2009; White et al., 2010). The raw EEG signal was subjected to fast-Fourier transformation (FFT) to generate power bands, after manually excluding artifacts. The epileptiform spiking, power spectral characteristics, and real-time behavioral video recordings were used to identify SRS. The spike frequency across 4 weeks from the experimental groups was compared using a two-way analysis of variance (ANOVA). The numbers of SRS were compared using Mann– Whitney tests.

Tissue processing for histology and IHC, and cell quantification

The procedures for perfusion fixation of rodent brains, gelatin-embedding, cryo-sectioning to obtain coronal sections (15 μm), immunostaining, imaging and immunopositive

cell counting has been described in our previous papers (Puttachary et al., 2016; Beamer et al., 2012; Cosgrave et al., 2009, 2010; Thippeswamy et al., 2007). The primary antibodies for IHC were incubated overnight at 4°C immediately after 1 h blocking step with 10% normal donkey serum to prevent nonspecific antibody binding. The primary antibodies used were; neuronal nuclear antibody (NeuN, 1:400, rabbit, EMD Millipore, USA), Ionized calcium binding adaptor molecule-1 (IBA1, 1:500, goat, Abcam, USA), Glial fibrillary acidic protein (GFAP, 1:400, mouse, Sigma, USA), 3-nitrotyrosine (3-NT, 1:250, rabbit, Millipore, USA), Kir 4.1 (1:250, rabbit, Alomone labs, Jerusalem, Israel), anti-serum albumin (SA, 1:250, chicken, Sigma, USA), anti-glial glutamate transporter-1 (GLT-1, 1:500, Millipore, USA). A combination of several secondary antibodies (all from Jackson Laboratories, USA) conjugated with fluorescent dyes (CY3 1:300 or FITC, 1:100) or biotin (1:500) or 4′,6-diamidino-2-phenylindole (DAPI at 0.0001%) were used for double or triple staining. The primary antibodies were diluted in solution (0.1% Triton X-100, 2.5% donkey serum and 0.25% sodium azide, Sigma, USA) and streptavidin conjugates (CY3 or FITC) were diluted in PBS alone. The brain sections without primary antibodies treatment served as negative control. All primary antibodies were titrated by serial dilution to derive optimum concentration and a limited neutralizing antibodies step was included to confirm antibody specificity. The normal/resting and reactive glial cells were distinguished based on their morphology. In order to identify degenerating neurons in the hippocampus, the entorhinal cortex, and the amygdala in the brain sections, we used the modified method of NeuN and FJB double staining as described in the literature (Schmued and Hopkins, 2000; Puttachary et al., 2016; Todorovic et al., 2012). The immunopositive cells with visible nuclei (DAPI stained) were counted bilaterally from eight sections per animal containing anterior, middle and posterior regions of

the hippocampus. We used ImageJ software (Schneider et al., 2012) to determine the counting area (square microns) from each section that was kept constant for all the experimental groups. The counting was carried out by research staff and students who were blind to the experimental groups. The rats from six month study were perfuse fixed with sodium sulfide and 4% PFA at the end of the study for Timm's staining as described in the literature (Buckmaster et al., 2002; Danscher, 1981; Rao et al., 2006; Shetty et al., 2005). ImageJ software was used to determine the grey scale intensity of mossy fiber staining (silver staining) in the inner molecular layer of the dentate gyrus. The pooled data was compared between the treatment groups using Mann–Whitney test.

Western blotting

The fresh hippocampal tissues harvested from rats were lysed on wet ice (4°C) using Tissue Ruptor (Qiagen, USA) in RIPA buffer with a cocktail of protease and phosphatase inhibitors (Thermo-Scientific, USA). These lysates were later normalized for equal amounts of protein using the Bradford protein assay kit (Biorad, USA). Equal amounts of protein (25 µg per sample) from the lysates were loaded per lane on 12% Tris glycine precast gels along with molecular weight marker (Biorad, USA). After separation, proteins were transferred overnight on to a nitrocellulose membrane. After the protein transfer, nonspecific binding sites were blocked for 1 h at room temperature using blocking buffer for fluorescent Western blotting (Rockland Immunochemicals, USA). Later, the membranes were incubated with Kir 4.1 or GLT-1 (both 1:1000) and beta actin (1:10,000, Sigma, USA) primary antibodies for overnight at 4 °C. After incubation, the membranes were washed 5 times with PBS containing 0.05% Tween 20, and then appropriate anti-species secondary antibodies tagged to IR-680 or

IR-800 dyes (1:10,000, LiCor, USA) were added. The antibody binding was detected using the Odyssey IR imaging system (LiCor, USA). Antibodies to beta actin were used as loading controls. ImageJ software was used to normalize the intensity of the beta actin with the intensity of the desired bands within each sample. The pooled data was later was compared between the treatment groups using Mann-Whitney test.

Methodological rigor, power calculation, and statistical analyses

For all experimental groups, the group size was calculated based on the preliminary data. For telemetry experiments, we started off with 4 animals per group in the preliminary study for a couple of weeks of continuous video-EEG recording. The data from the preliminary study group was analyzed on weekly basis. Since the results were encouraging it prompted us to continue for up to six months. Based on the six month continuous video-EEG data we worked out the group sizes. Based on the preliminary data and power calculation, we estimated 5–6 rats for IHC and 6–8 rats for other assays to demonstrate statistical significance ($p \leq 0.05$) at 80% power. We had consulted biostatistician, Dr. C. Wang at Iowa State University.

All animals were randomized before the treatment protocols began after diazepam was administered. The experimenters were blinded to the treatment groups until the data analyses were completed. As per the pre-determined criteria set for the study, we excluded 6 rats since 3 of them did not respond to the predetermined KA dose range (15 ± 2.5 mg/kg) and 3 rats were euthanized during the course of the 6 month study. We had taken measures to minimize variables by: i) randomization of animals based on predetermined weight and age range before the start of the experiment, ii) the animals were grouped for interventional studies, after diazepam treatment, based on seizure severity score during the SE, and the KA dose range, so that each group contained fairly same number of animals of similar seizure severity and the

amount of KA, iii) we acquired ~260 h of baseline EEG data, covering at least 10 day-night cycles, to normalize post-SE EEG from the same animal, and iv) we implemented the first two of the three principles of reduction, refinement, and replacement (3Rs) by testing 1400W in brain slices *in vitro*, and by adopting a refined method of SE induction which reduced mortality rate. We compared statistical differences between the post-diazepam treatment groups i.e., the vehicle versus the 1400W groups using Student's t-tests, Mann–Whitney tests or two way ANOVA tests, and the p-value < 0.05 between the groups was considered significant.

Results

1400W reduced KA-induced spike frequency in brain slices

To investigate the effect of 1400W on the brain tissue and also in view of reducing the number of animals required for *in vivo* experiments, we initially tested KA and 1400W in mouse brain slices. The brain slices were carefully positioned on 60 electrodes to encompass dentate gyrus, the hilus, and CA regions of the hippocampus. Two minutes of baseline recording showed spontaneous spiking activity. The epileptiform spike frequency increased from 2 ± 0.98 Hz to 6.6 ± 3.1 Hz when 1 μM KA was perfused for 2 min (Fig. 1, #$p = 0.054$).

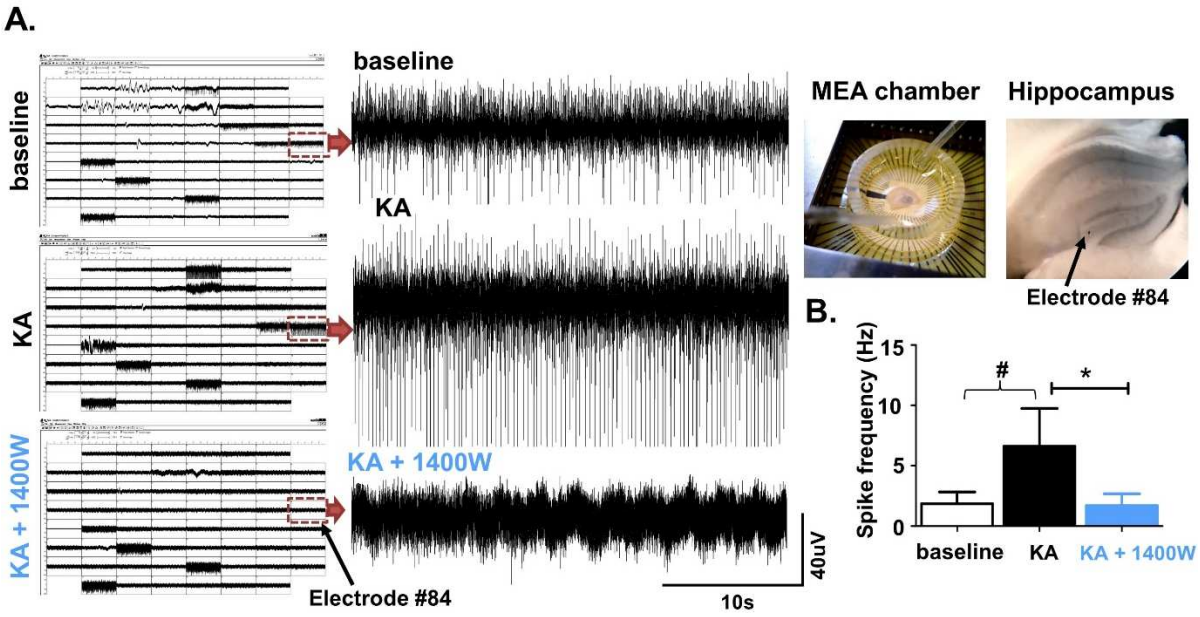

Fig. 1. Multi-electrode array system to record electrical field potential differences between 1400W and KA responses from the mouse brain slices. A) The electrographic recordings from 60 electrodes in the presence or absence of 1400W in KA-perfused brain slices in the MEA chamber. The brain slice was positioned on 60 electrodes to encompass the dentate gyrus, the hilus, and CA regions of the hippocampus to acquire electrical field potentials. The boxed recordings from the same electrode from CA region (electrode #84) are further expanded to reveal spiking during baseline, KA, and KA + 1400W applications. The arrow points to the electrode #84 on the hippocampus. B) The epileptiform spike frequency comparison of pooled recordings from 8 slices from the electrodes overlying the hippocampus and the dentate gyrus. The KA perfusion increased the epileptiform spike rate. Co-application of 1400W significantly reduced KA-induced epileptiform spiking activity (*p = 0.0487, paired t-test, 8 slices from 4 mice). Later, when 5 µM 1400W was co-applied with 1 µM KA for another 2 min, there was a significant suppression of KA-induced epileptiform spiking from 6.6 ± 3.1 Hz to 1.7 ± 0.97 Hz (Fig. 1; p = 0.0487, n = 8 slices from 4 mice, paired t-test) demonstrating an inhibitory effect of 1400W on KA-induced spike frequency.

1400W suppressed epileptiform spike rate during the first 12–74 h and the rest of the first 4 weeks of post-SE in vivo

A refined repeated-low-dose method of SE induction by KA reduced mortality and increased consistency in seizure severity during the SE (Hellier et al., 1998; Puttachary et al., 2015a, b, 2016; Tse et al., 2014). The Fig. 2A illustrates the experimental design for induction of SE by repeated-low-dose of KA and post-treatment with 1400W or the vehicle. In this study,

from all the experimental groups that involved KA-induced SE, there was <5% mortality. As described for mice in our recent publications (Puttachary et al., 2015a, b, 2016; Tse et al., 2014), we utilized integrated video-EEG analyses (Fig. 2B) to determine precise seizure severity score based on the exact duration of convulsive seizures and the electrographic seizures during the SE (Fig. 2C). It is important to note that the animals grouped for the 1400W or the vehicle treatment, after diazepam administration, had no significant differences in their behavioral or electrographic seizures during the SE or in the total amount of KA administered to achieve the severity of SE (Fig. 2C).

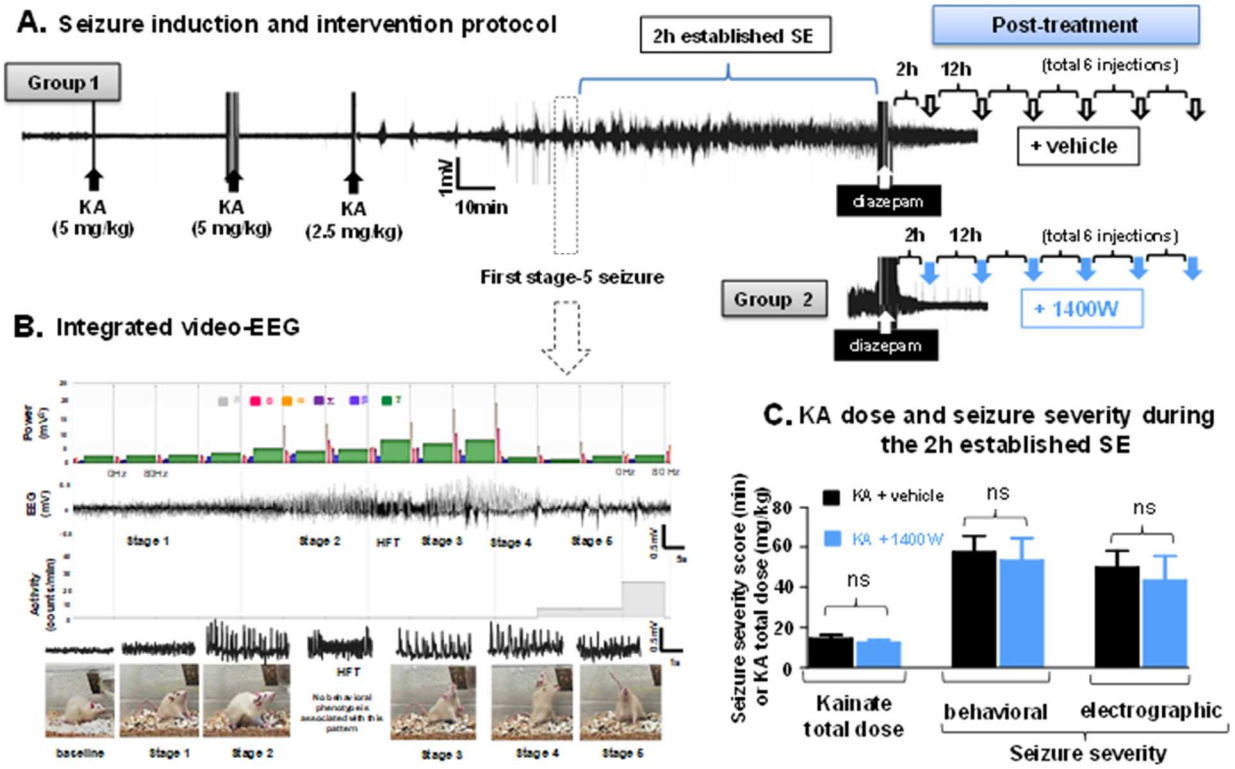

Fig. 2. SE induction by repeated-low-dose of KA to test the efficacy of 1400W in real-time when it was administered as post-SE treatment. A) EEG trace recorded during SE induction by RLD of KA. The behavioral SE was terminated by administering DZP 2 h after the onset of first stage-5 seizure. 2 h after the DZP treatment, six injections of 1400W or vehicle were given at 12 h intervals during the first 3 days of post-SE to investigate immediate and long-term effects on epileptogenesis and epilepsy. B) The first stage-5 seizure segment of the EEG is expanded to reveal epileptiform spike characteristics and the corresponding behavioral correlates. As the seizures progressed from non-convulsive to convulsive, the gamma power spectrum increased. The behavioral seizures were typically correlated

with the EEG characteristics during the entire 2 h established SE. Gamma spectrum decreased to the basal level or below when the animal showed rigidity during the seizure episode. Activity counts (shown below the EEG trace in panel B) also increased as a result of uncoordinated and exaggerated movement (generalized tonic-clonic convulsions followed by a brief rigidity) observed at the end of the seizure episode. C) The animals that were grouped for post-treatment with the vehicle or the 1400W received similar doses of KA and also had fairly similar seizure severity scores (behavioral and electrographic) during the 2 h established SE. The behavioral and electrographic seizures severity during the 2 h established SE and the amount of KA received by each animal in the groups were compared, and found no significant differences between the groups.

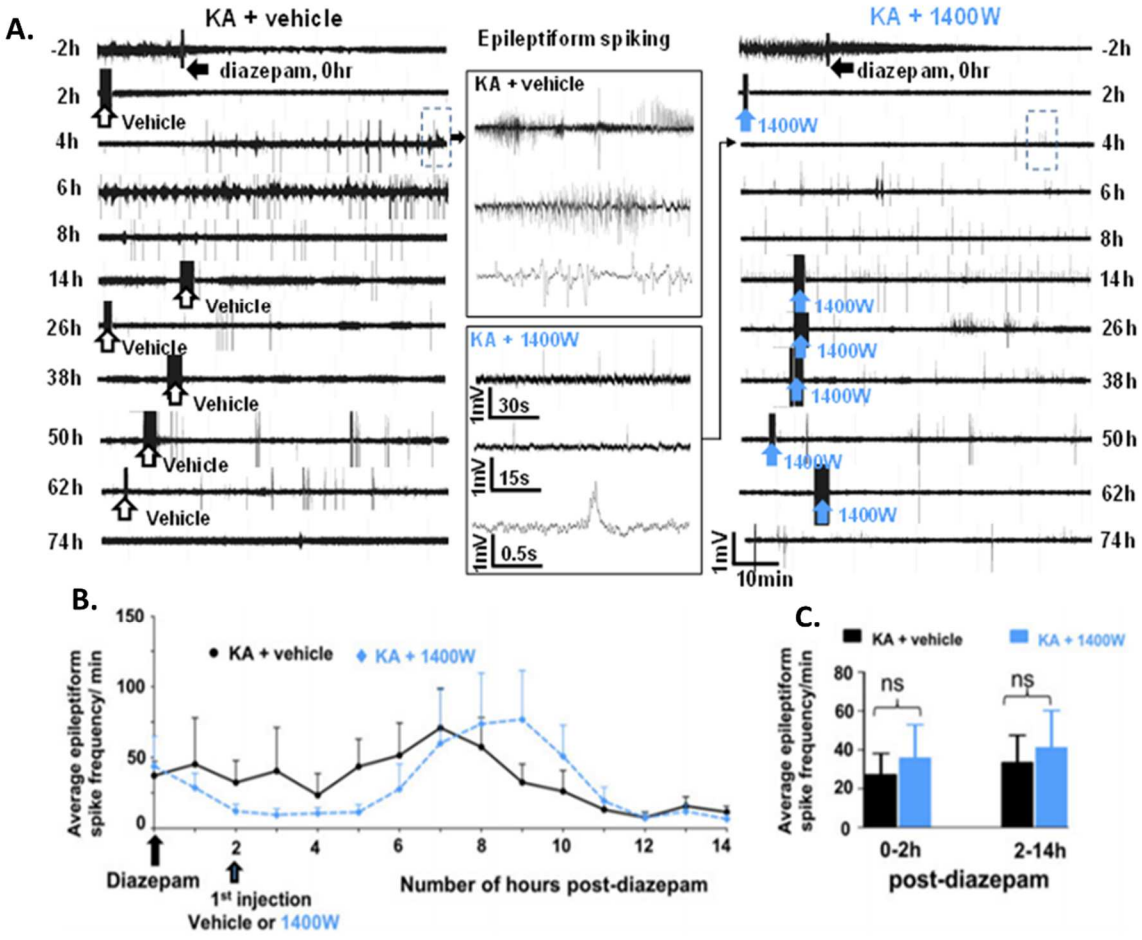

Fig. 3. Average epileptiform spike frequency after RLD of KA and 1400W treatment. A) Representative EEG traces during the post-SE treatment with the vehicle and the 1400W. Expanded representative EEG traces are shown in the boxes. B) The average epileptiform spike frequency is represented at 1 h epochs for the first 14 h of post-diazepam/SE. C) The cumulative epileptiform spike frequency was compared between the vehicle and the 1400W treated groups before treating with 1400W (0–2 h post-SE) and after the first dose of 1400W (2–14 h post-SE). There were no significant differences between the groups either at 0–2 h or 2–14 h post-SE.

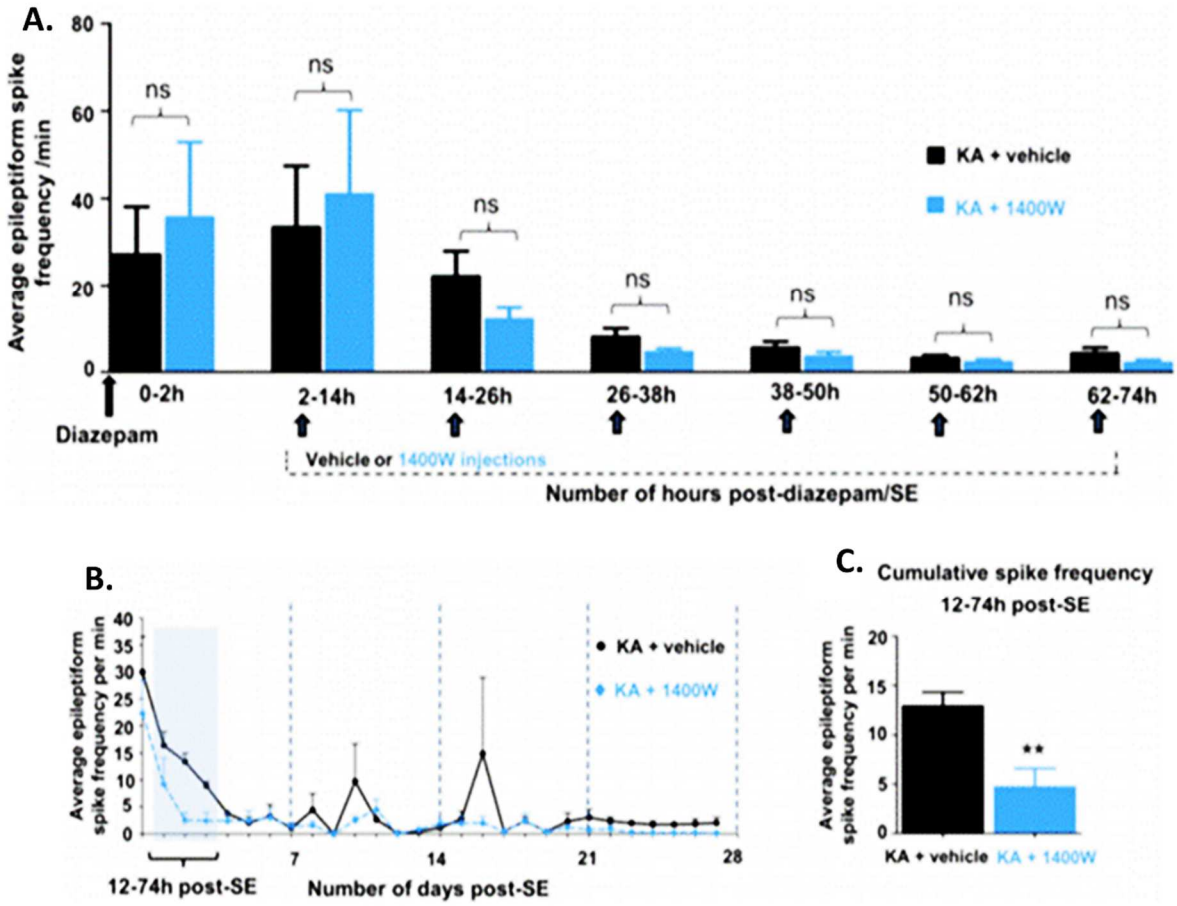

Fig. 4. 1400W suppressed epileptiform spikes during the first three days of epileptogenesis. A) Comparison of the epileptiform spike frequency at 12 h epochs after each dose of the 1400W or the vehicle treatment. The first 2 h post diazepam data is also included for comparison. There were no significant differences at any time point between the drug and the vehicle treatment. B) The average epileptiform spike frequency is represented at 1 day epochs for the first four weeks. The 1400W significantly reduced epileptiform spike frequency when compared to the vehicle treated group during the first four weeks ($p = 0.0005$, $n = 6–7$, two way ANOVA, $F = 12.87$ between 1 and 140 degrees of freedom). C) The 1400W significantly suppressed epileptiform spikes during the first 3 days of epileptogenesis i.e. during the treatment period (the shaded area in H represents the treatment duration of the 1400W or the vehicle). The cumulative epileptiform spike frequency was compared between the vehicle and the 1400W treated groups ($p = 0.002$, Mann– Whitney test, $n = 6–7$).

Since an increased epileptiform spike rate contributes to epileptogenesis, we compared the impact of the 1400W on epileptiform spike rate during: 0–2 h and 2–14 h post-SE at 1 h epochs for the first dose of the 1400W (Fig. 3B, C); each subsequent dose of the 1400W or the

vehicle at 12 h epochs (Fig. 4A); 12 and 74 h post-SE for cumulative dose effect of the 1400W (Fig. 4B, C); the first 4 weeks of post-SE at 1 day epochs (Fig. 4B). A detailed epileptiform spike frequency analysis during the immediate post-diazepam period revealed no significant differences in the spike rate either before the first dose of the 1400W (0–2 h post-diazepam/SE) or after the dosing (2–14 h post-diazepam/SE) when compared to the vehicle treated group (Fig. 3B, C). This suggests that the first dose of 1400W had no impact on epileptiform spike frequency. We further analyzed the effect of each subsequent dose of the 1400W or the vehicle, and plotted the graphs as cumulative epileptiform spike rate for the duration of 12 h (Fig. 4A) to understand the overall impact. The 2nd to 6th dose of 1400W showed a tendency to reduce epileptiform spike rate in the 1400W group, especially the 2nd and the 3rd dose, in contrast to the vehicle treated group, however they were also not statistically significant. Interestingly, when the cumulative spike frequency was calculated for all the doses together, except the first dose, between 12 and 74 h post-SE, it revealed a significant reduction in the spike rate in the 1400W treated group (Fig. 4B and C). During this 3 day post-SE period, 1400W significantly reduced spike frequency from 12.9 ± 1.4 to 4.7 ± 1.9 spikes per min (Fig. 4C, $p = 0.002$, Mann–Whitney test, n = 6–7). After 7 days, although spike frequency was reduced in both groups, there were periods of burst in spikes on the 9th, 11th and 17th day in the vehicle group when compared to the 1400W group (Fig. 4B). Overall, there was a significant reduction in epileptiform spike frequency by 1400W during this critical phase of epileptogenesis when compared to the vehicle treated group (Fig. 4B; $p = 0.0005$, n = 6 for vehicle and n = 7 for 1400W group, two way ANOVA, $F = 12.87$ between 1 and 140 degrees of freedom).

1400W suppressed neuroinflammation and neurodegeneration at 7 day post-SE

Increased epileptiform spike rate, reactive gliosis (neuroinflammation) and neurodegeneration are the hallmarks of epileptogenesis (Arabadzisz et al., 2005; Benkovic et al., 2006; Rao et al., 2006; White et al., 2010). Since we found that 1400W reduced epileptiform spiking induced by KA in brain slices (Fig. 1) and it also reduced epileptiform spike rate during the first week of post-SE *in vivo* (Fig. 3A–C), we predicted that 1400W will suppress reactive gliosis and neurodegeneration during this period. To investigate this, we processed the 7 day post-SE brain sections for IHC from the rats that were treated with 1400W or the vehicle. Reactive gliosis was found in all regions of the hippocampus, dentate gyrus, amygdala, and entorhinal cortex. Representative images from CA1 hippocampus are shown in the Fig. 5A. The 1400W significantly suppressed both reactive microgliosis (Fig. 5A and C) and reactive astrogliosis (Fig. 5A and B) in all regions of interest when compared to the vehicle treated control group (*p < 0.05, **p < 0.01, ***p < 0.001, n = 5, Mann–Whitney test).

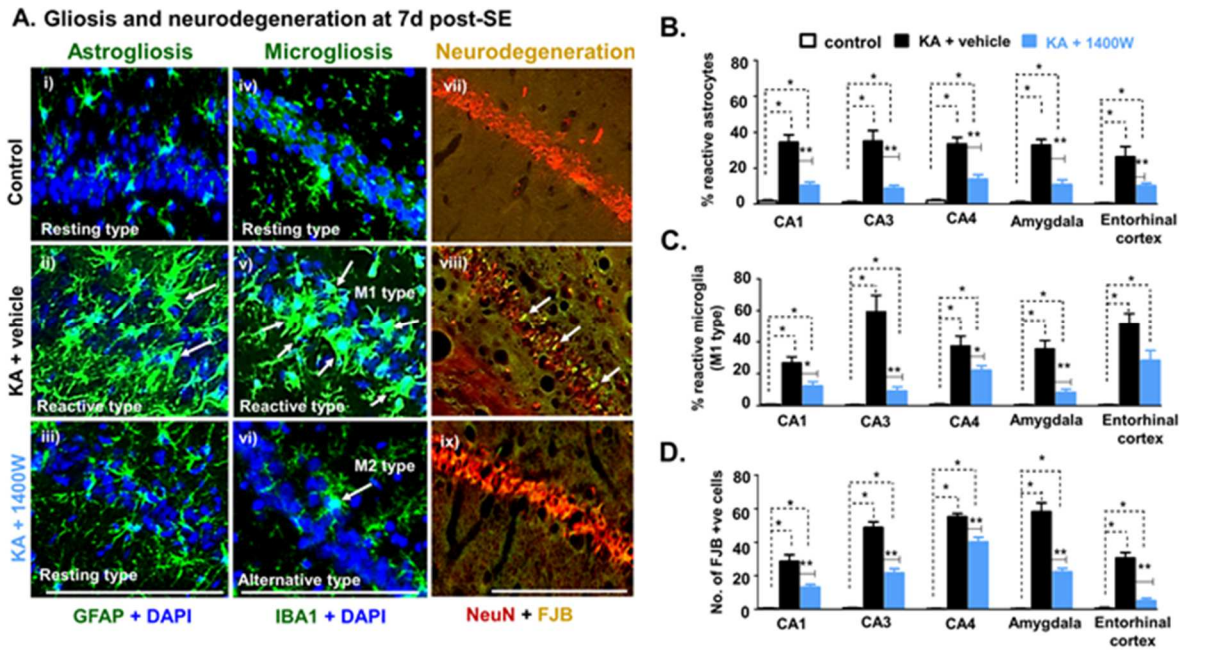

Fig. 5. The 1400W suppressed SE-induced reactive gliosis and neurodegeneration at 7 d post-SE. A. Representative images to demonstrate cellular morphology of glial cells and degenerating neurons.

Green labelled cells are GFAP (i to iii) or IBA1 (iv to vi) or FJB (vii to ix), red labelled cells are neurons (NeuN, vii to ix), and DAPI was used to label nuclei in blue in panels i) to vi). GFAP and IBA1 IHC revealed resting type glial cells, reactive astroglia, and M1 and M2 type microglia cells (a few examples are indicated by arrows). These types of cells were found throughout the hippocampus, amygdala and entorhinal cortex. The parallel brain sections processed for FJB and NeuN (panels, vii–ix) co-staining revealed neurodegeneration (A, viii, examples are shown by white arrows in the CA1 region) in these regions in the vehicle treated group. Scale bars for all: 100 μm. B–D: Cell quantification comparison between naïve control, the vehicle, and the 1400W treated groups. The 1400W treatment significantly reduced reactive astrogliosis (B), reactive microgliosis (C), and neurodegeneration (D) in the hippocampus, amygdala, and entorhinal cortex when compared to the vehicle treated group. The total number of GFAP or IBA1 or FJB positive cells was counted from a predetermined area. The percentage of reactive astrocytes and reactive microglia were calculated from the total number of glial cells (GFAP or IBA1 positive cells) (*$p < 0.05$, **$p < 0.01$, ***$p < 0.001$, $n = 5$, Mann–Whitney test).

Importantly, the microglial morphology revealed M1 and M2 types, and there was a significant reduction in M1 type (reactive) microglial cells in the 1400W treated group (Fig. 5C). The parallel sections stained for FJB and NeuN revealed a significant increase in neurodegeneration in CA regions of the hippocampus, the hilus of the dentate gyrus, amygdala, and entorhinal cortex, in the vehicle treated group when compared to the 1400W treated group (Fig. 5A and D, *$p < 0.05$, **$p < 0.01$, ***$p < 0.001$, $n = 5$, Mann–Whitney test).

1400W protected BBB integrity, reduced extravasation of serum albumin in the brain parenchyma, reduced 3-NT levels, and partly reversed Kir 4.1 levels at 7 d post-SE

The BBB integrity is compromised during seizures and/or soon after a prolonged SE (Abbott et al., 2006; David et al., 2009; Heinemann et al., 2012; Marchi et al., 2015; Morin-Brureau et al., 2011; Seiffert et al., 2004; Tomkins et al., 2011; van Vliet et al., 2007). We tested this in our model by treating the rats with a high molecular weight (472.54) fluorescent chemical, hydroxy-stilbamidine (Fluro-Gold) 2 h prior to the induction of SE with KA. In these experiments, we tested the effects of vehicle and 1400W administered 1 h prior to the induction of SE with KA. Fluro-Gold has about twice the molecular weight when compared to KA

(213.23) or 1400W (250.17). As expected, significantly high levels of Fluro-Gold deposits were found in the extracellular space at 2 h post-SE in the vehicle treated group (Fig. 6A, ii), while it was restricted to the capillaries in the naïve control (Fig. 6A, i).

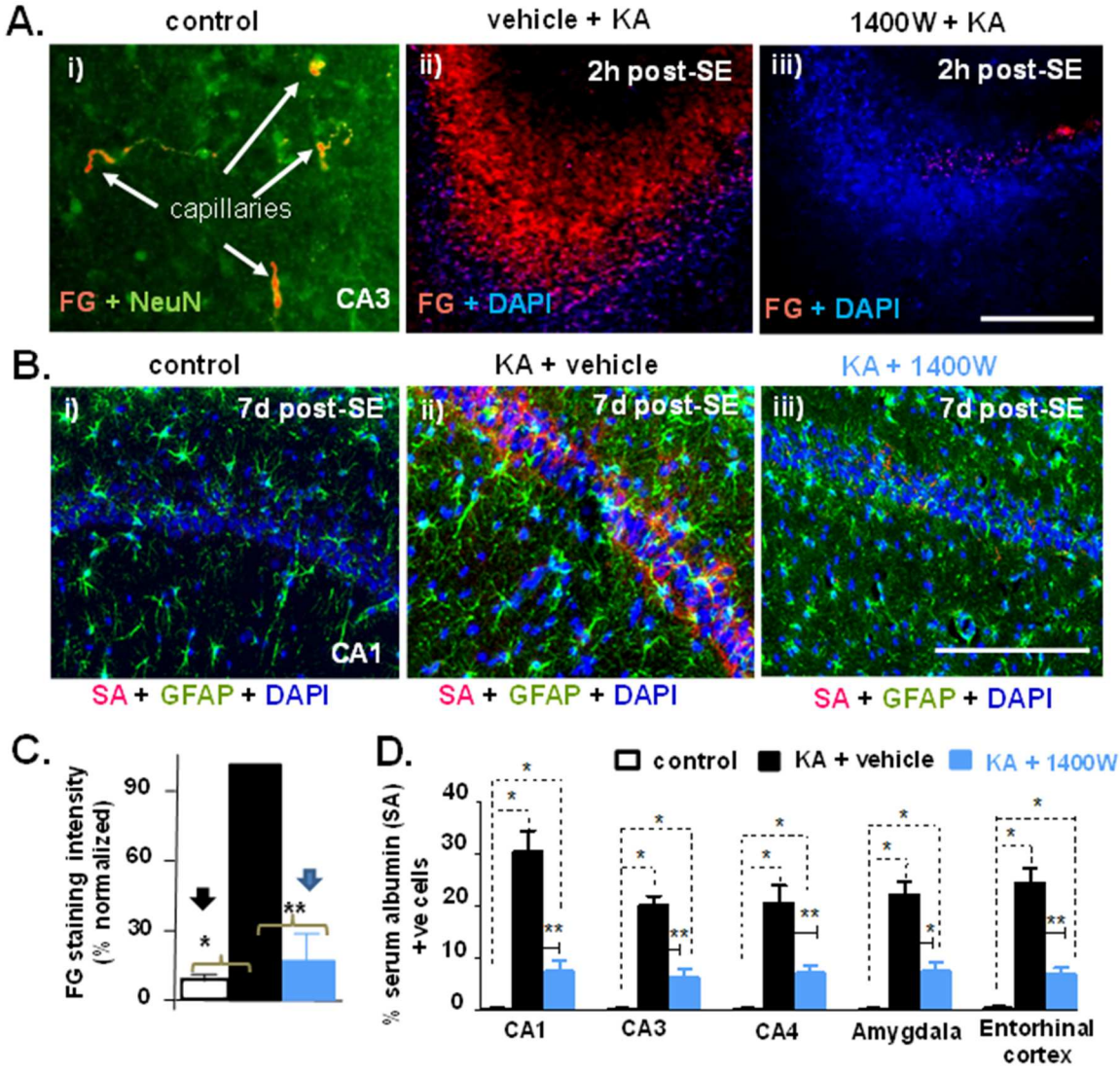

Fig. 6. The 1400W protects BBB integrity and reduces serum albumin positive neurons and astrocytes. A) The 1400W protects BBB integrity. Fluro-Gold (FG) was administered 2 h prior to SE followed by treatment with the 1400W or the vehicle 1 h prior to the induction of SE with KA. The animals were euthanized immediately at the end of "2 h established SE". The SE caused loss of BBB integrity as revealed by the FG in the extracellular space (pseudo colored red in panel A-ii) and in some neurons and glial cells, which was largely prevented in the 1400Wtreated group (A-iii). In the control, without kainate injections, (A-i), FG was restricted to the capillaries and it was neither in the interstitial space nor taken up by neurons or glial cells (green cells). B) Serum albumin IHC at 7 d post-SE. In this case, the 1400W was given as post-treatment (twice daily for three days). Serum albumin

immunostaining (pink or red) was observed in both reactive astrocytes and in some neurons in the vehicle treated, but it was suppressed by the 1400W. C) Relative quantification of the intensity of FG staining in A (i–iii). n = 5, *p < 0.05, **p < 0.01, ***p < 0.001, Mann–Whitney test. D) Quantification of serum albumin positive cells (*p < 0.05, **p < 0.01, ***p < 0.001, n = 4–5 each group, Mann–Whitney test). Scale, all 100 μm.

In the 1400W pre-treated rats, there was a significant reduction in extracellular Fluro-Gold deposits (Fig. 6A, iii, C; *p < 0.05, **p < 0.01, n = 5, Mann–Whitney test). This demonstrates that 1400W protects the BBB integrity. Similar results were also observed in 7 d post-SE groups that received treatment with the 1400W or the vehicle at 4 h post-SE. At 7 d post-SE, we found that serum albumin containing astrocytes (and also in some neurons) in the hippocampus, amygdala, and entorhinal cortex were significantly increased in the vehicle treated rats (Fig. 6B). When 1400W was administered in six doses at 12 h intervals after SE induction, it significantly suppressed serum albumin containing cells in all the regions (Fig. 6B and D, *p < 0.05, **p < 0.01, ***p < 0.001, n = 5, Mann–Whitney test). Serum albumin uptake by astrocytes is known to affect their function, especially, potassium and glutamate clearance from extracellular milieu (David et al., 2009; Weissberg et al., 2015). We found a significant reduction in potassium channel, Kir 4.1 protein levels at 7 d post-SE which was partially reversed by 1400W (Fig. 7A and B, **p = 0.0095, n = 4–6, Mann–Whitney test). However, the suppressed glutamate transporter-1 (GLT-1) levels by KA-induced SE were not reversed by 1400W (Fig. 7C–D, # = 0.067, n = 4–6, Mann–Whitney test).

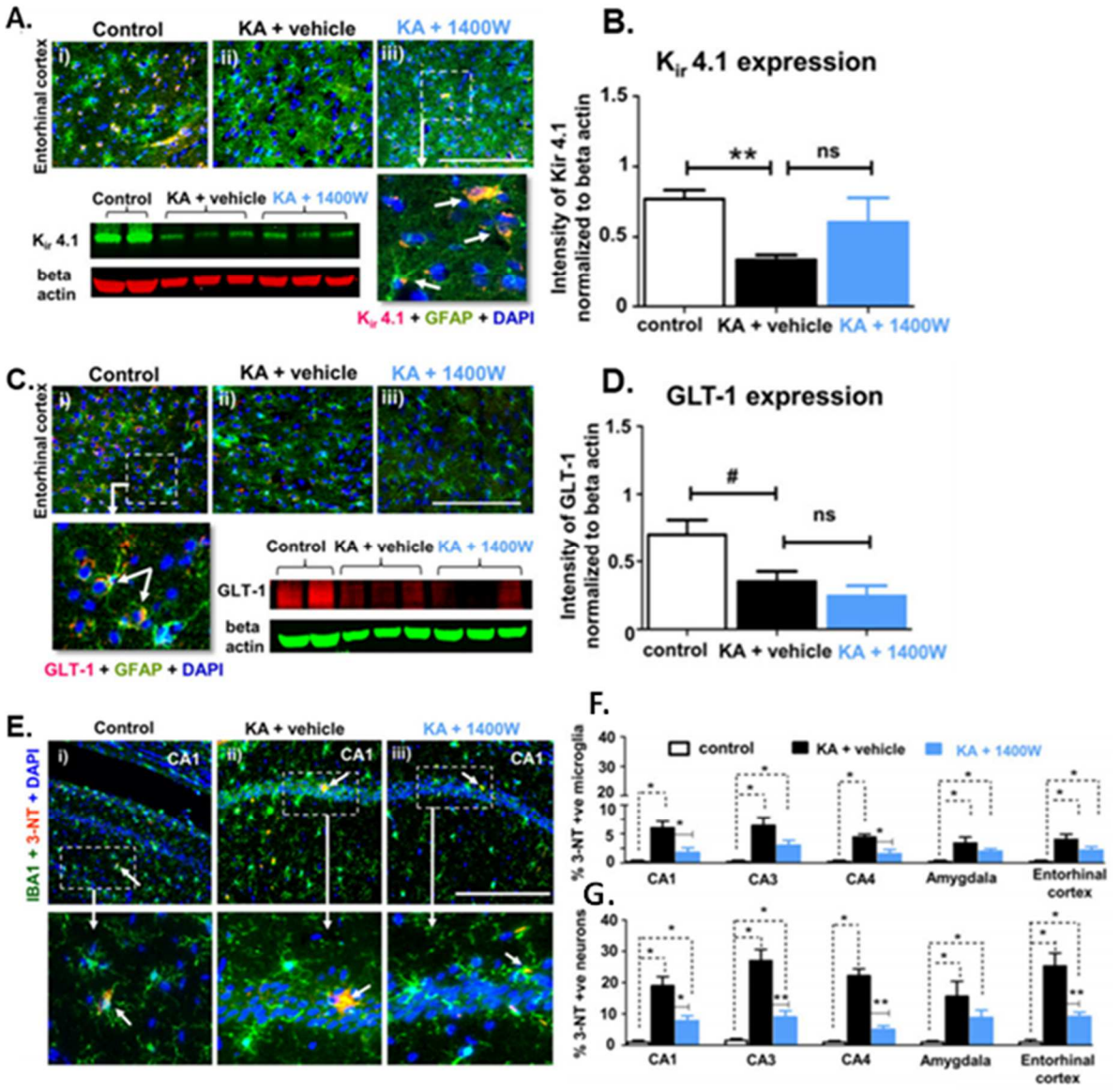

Fig. 7. Kir 4.1, GLT-1, and 3-NT levels at 7 d post-SE in the 1400W and the vehicle treated groups. Western blots and IHC images (A and C) at 7 d post-SE from naïve control, the vehicle and the 1400W treated animals. B and D represent quantified results of Western blots in A and C. Astrocytic Kir 4.1 channels (A and B, **p = 0.0095, n = 4–6, Mann–Whitney test) and GLT-1 transporters (C and D, #p = 0.066, n = 4–6, Mann–Whitney test) were down regulated at 7 d post-SE in the vehicle treated animals. The 1400W treated groups showed a partial recovery in Kir 4.1 levels, but not GLT-1 levels. IHC revealed their localization with GFAP positive astrocytes in the hippocampus, amygdala, and entorhinal cortex (representative images are from the entorhinal cortex). E–G) The 3-NT IHC and cell quantification. The 3-NT immunoreactivity was found in both microglial cells and neurons. Their numbers significantly increased in the vehicle treated group and the 1400W reversed the effects (n = 4–5, *p < 0.05, **p < 0.01, Mann–Whitney test). Boxed regions in panels A, C and E are further magnified to show co-localization. Scale, all 100 μm.

SE-induced neuroinflammation increases iNOS in M1 type reactive microglial cells and excessive NO production nitrosylates proteins on tyrosine residues, 3-nitrotyrosine (3-NT), which serves as a marker of RNS that can be identified in both neurons and glial cells (Rao et al., 2003; Yi et al., 2000). At 7 d post SE, we observed a significant increase in 3-NT containing microglia and neurons in the hippocampus, amygdala and entorhinal cortex (Fig. 7E–G, *p b 0.05, n = 4–6, Mann–Whitney test). The 1400W significantly suppressed 3-NT levels in microglia (*p < 0.05, n = 4–6, Mann–Whitney test) and in neurons (*p < 0.05, **p < 0.01 n = 4–6, Mann–Whitney test). A similar trend was observed in other regions of the brain.

1400W significantly reduced the number of SRS episodes and the disease progression in the six month continuous study

As per the pre-determined criterion, the animals that did not complete the full course of the study were eliminated from the analyses. We used 8 animals each for 1400W and the vehicle treatments. Two rats from the vehicle group were euthanized before the completion of the study due to complications of severe SRS, while one rat from the 1400W group was euthanized due to foreign body (bedding material) obstruction in the trachea. The number of SRS episodes for each rat that completed the 6 month study is represented in the Fig. 8A and B. All the rats in the vehicle group had several hundreds of SRS episodes, while the 1400W treated rats had <70 episodes in the six months (Fig. 8A, B). Out of 7 rats in the 1400W group, one rat had experienced only one SRS episode (stage-3 on the day 9 post-SE), another rat had two SRS episodes (stage-5, on the days 59 and 117 post-SE), and the remaining five rats had 7 to 65 SRS episodes during the 6 month continuous recording.

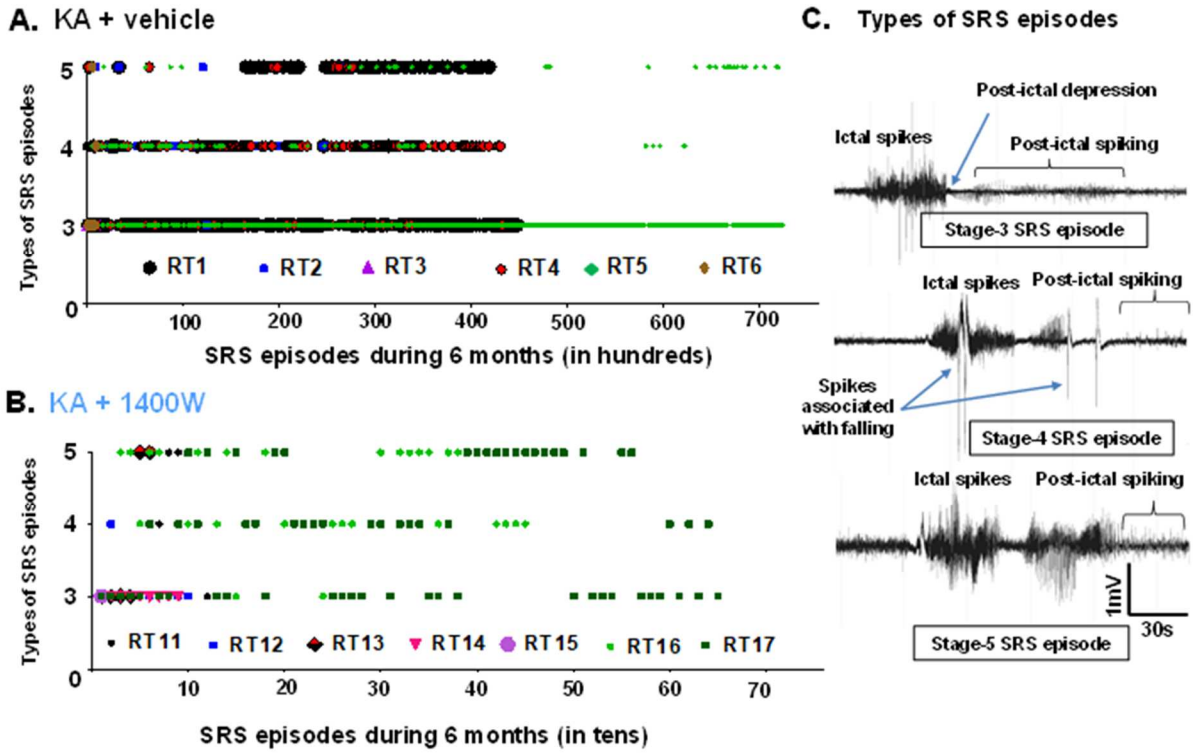

Fig. 8. Comparison of SRS episodes occurrence between individual animals during the six month period between the vehicle (A) and the 1400W (B) treated groups, and representative EEG samples of the types of convulsive SRS. Each colored spot in both A and B represents an SRS episode (rats RT1–6 in the vehicle group, RT11–17 in the 1400W group). Y-axis represents the stages of spontaneous recurrent convulsive seizures on the Racine scale. Rearing with fore limb clonus in stage-3, rearing and falling in stage-4, and generalized tonic-clonic convulsions with rigidity in stage-5 episodes. All of the SRS episodes during the six months period were verified for behavioral correlates which were similar to the episodes observed during the SE as illustrated in the Fig. 2B. The types of SRS with post-ictal patterns lasting for N15–20 min were the most common features in the vehicle treated group. In the 1400W-treated group, in a vast majority of SRS episodes the post-ictal pattern lasted for <5 min.

All rats, in both vehicle and 1400W treated groups had several episodes of electrographic non-convulsive seizures, including the two rats that had 1 or 2 SRS episodes in the 1400W group, therefore we considered all of them as epileptic. The types of convulsive SRS episodes observed in these animals are represented in the Fig. 8C. The convulsive SRS types were classified based on the Racine scale; stage-3 type which showed rearing and

forelimb clonus, stage-4 type with rearing and falling, and stage-5 type with generalized tonic–clonic convulsions (Fig. 8C). When all the SRS episodes (stage-3 to stage-5) were plotted as cumulative seizures occurred in a month, it revealed a clear progression of the disease during six months in the vehicle treated group (Fig. 9A– C).

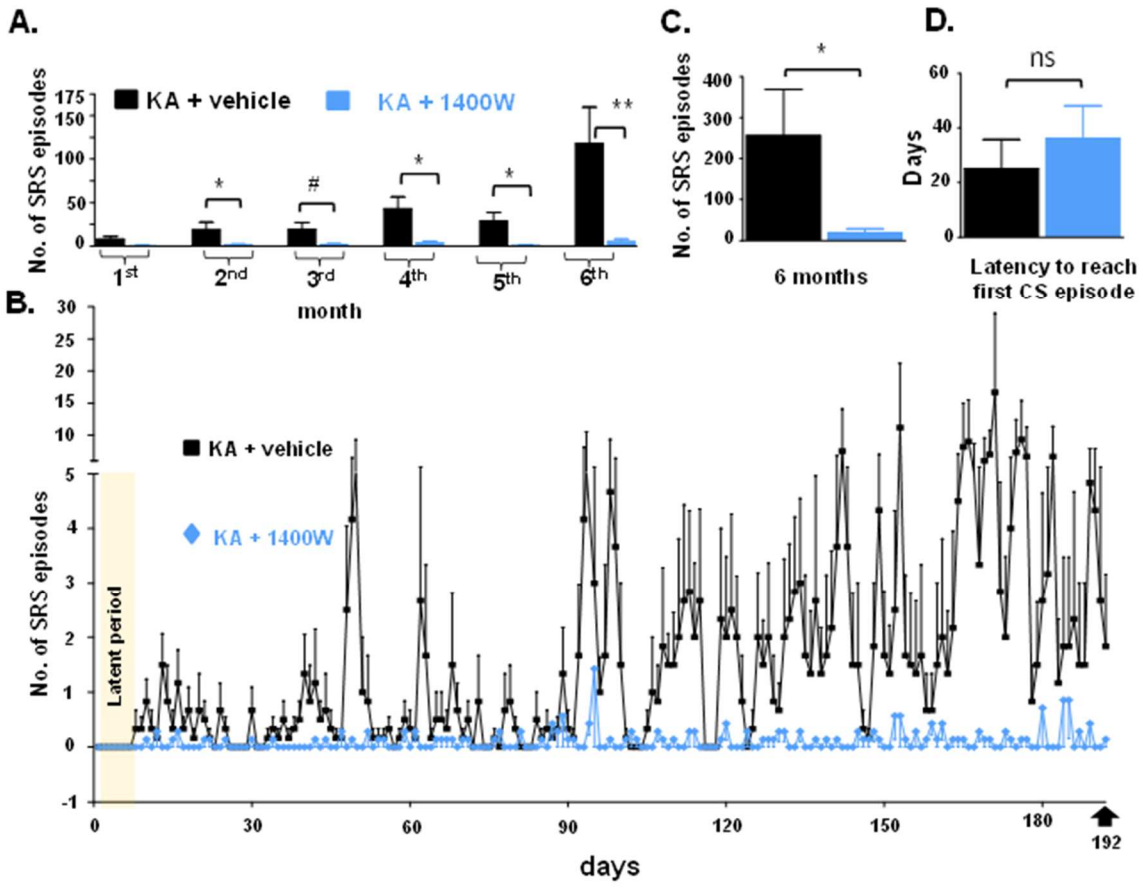

Fig. 9. The 1400W significantly decreased the number of convulsive SRS during the six month period. A) There was a progressive increase in the number of SRS episodes over time and the 1400W significantly reduced their numbers (*p = 0.043, 2nd month; *p = 0.026, 4th month; *p = 0.03, 5th month; and **p = 0.0095, 6th month; n = 6 for the vehicle and n = 7 for the 1400W, Mann–Whitney test). B) Comparison between the number of SRS episodes per day between the vehicle and the 1400W treated groups during the entire study period of six months. There was a significant reduction in the number of seizure episodes in the 1400W-treated group when compared to the vehicle control ($p \leq 0.0001$, n = 6–7, two way ANOVA, F = 122 between 1 and 2112 degrees of freedom). C) Cumulative SRS episodes occurred in six months revealed a significant difference between the groups (*p = 0.022, n = 6–7, Mann–Whitney test). There was 92% reduction in the number of SRS episodes in the 1400W treated group. D) There were no significant differences between the groups on latency to the onset of the first spontaneous seizure or the average duration of the individual convulsive seizure episodes.

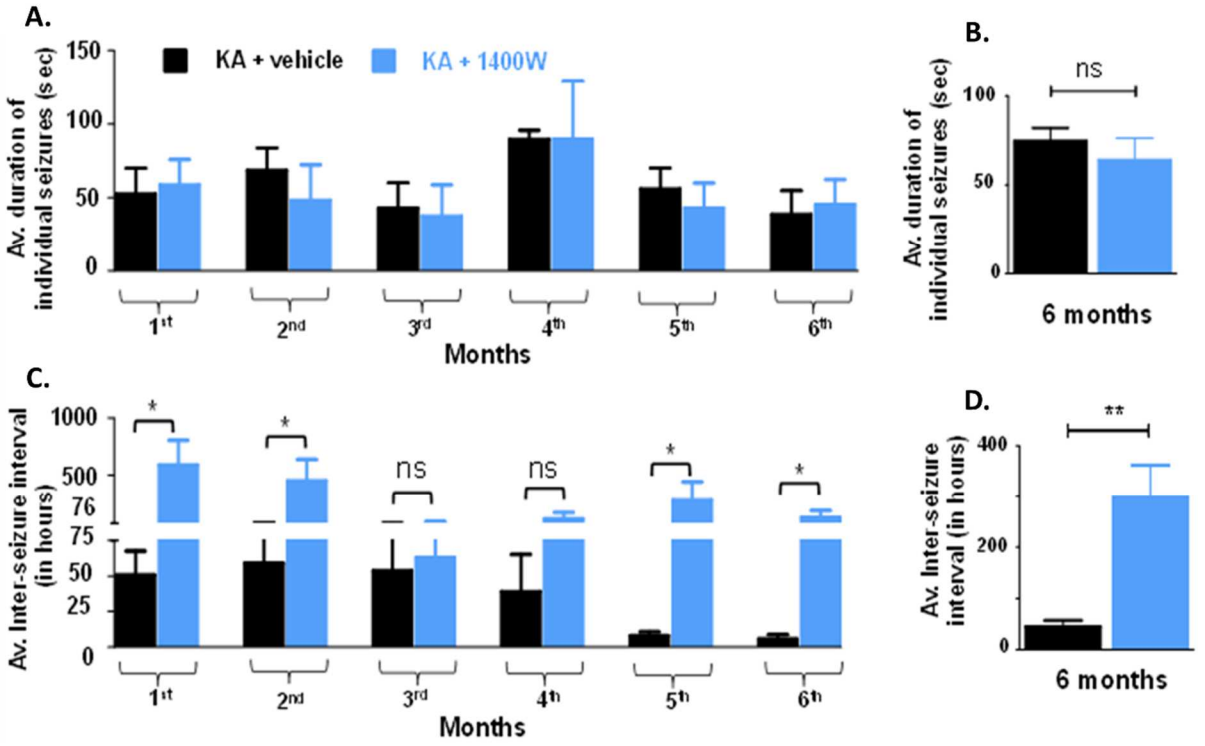

Fig. 10. 1400W significantly reduced the number of interictal events during the six month period. A, B) The inter-ictal intervals significantly reduced in the 1400W treated group when compared to the vehicle control (C, *p = 0.029, 1st month; *p = 0.032, 2nd month; p = 0.016, 5th month; and 0.028 during 6th month). The average inter-seizure intervals during entire six month period significantly increased in the 1400W treated group when compared to the vehicle treated group (D, **p = 0.0022, Mann–Whitney test, n = 6 for the vehicle, n = 7 for the 1400W).

In the 1400W-treated group, there was a significant reduction in the disease progression during the 2nd month (*p = 0.042), 3rd month (#p = 0.06), 4th month (*p = 0.026), 5th month (*p = 0.032), and 6th month (*p = 0.0095, n = 6–7, Mann–Whitney test). The cumulative SRS episodes occurred in six months showed a dramatic (92% reduction) and a significant reduction in the number of episodes in the 1400W group when compared with the vehicle control group (Fig. 9B; $p \leq 0.0001$, n = 6–7, two way ANOVA, F = 122 between 1 and 2112 degrees of freedom, Fig. 9C; *p = 0.022, n = 6–7, Mann–Whitney test). However, there were no significant differences in the latency to the onset of first SRS (Fig. 9D) and the average duration of individual seizures during six months between the two groups (Fig. 10A–B). Further

analysis revealed a significant increase in inter-seizure intervals in the 1400W treated group in contrast to the vehicle group during 1st (*p = 0.028) and 2nd (*p = 0.032) month, 5th (*p = 0.015) and 6th month (*p = 0.028, Mann–Whitney test, n = 6–7 each group). An increase in inter-seizure intervals was also significant during the entire six months in the 1400W group when compared to the vehicle treated group (Fig. 10D; **p = 0.0022, Mann–Whitney test, n = 6–7 each group).

1400W treatment suppressed reactive gliosis, neurodegeneration, and aberrant mossy fiber sprouting at six month post-SE

IHC of the rat brain sections from the long-term telemetric studies for neuroinflammation and neurodegeneration also revealed similar results as observed at 7 d post-SE (Fig. 5). Representative images from the CA3 region of the hippocampus are shown in the Fig. 11A. Cell quantification revealed a significant reduction in reactive astroglia (Fig. 11A i–iii, B), reactive microglia (Fig. 11A, iv–vi, C), and neurodegeneration (Fig. 11A, vii–ix, D) in the 1400W treated group in the hippocampus, amygdala, and entorhinal cortex when compared with the vehicle treated group (Fig. 11B–D; *p < 0.05, **p < 0.01, n = 5 each group, Mann–Whitney test).

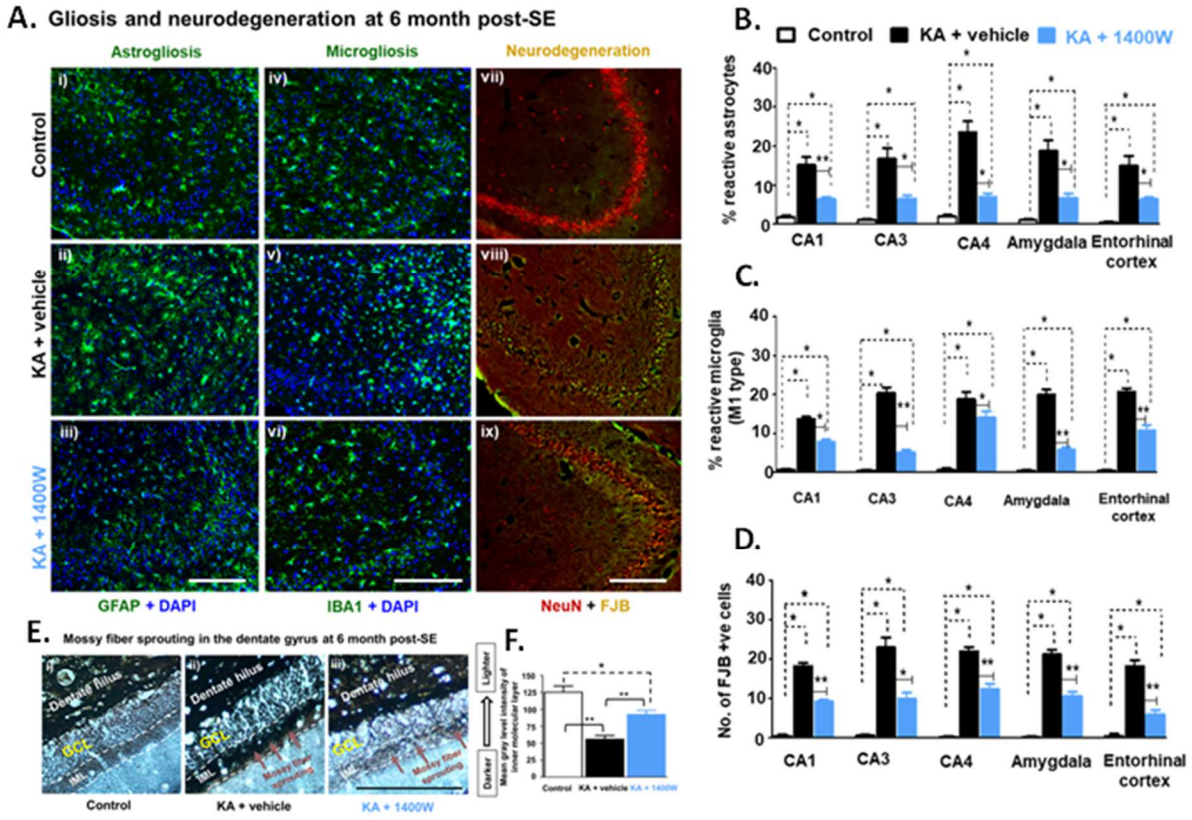

Fig. 11. The 1400W treatment immediately after the SE had long-term indirect effects on reactive gliosis, neurodegeneration and mossy fiber sprouting at 6 month. As observed at 7 d postSE, there was a significant reduction in reactive astrocytes (GFAP) and reactive microglia (IBA1) and FJB positive cells in CA1, CA3, CA4, amygdala, and entorhinal cortex regions (A–D) in the 1400W-treated group in contrast to the vehicle group (*p b 0.05, **p b 0.01, ***p b 0.001, n = 4–5 each group, Mann–Whitney test). A representative images from the CA3 region are presented for astrogliosis (A, i–iii), microgliosis (A, iv–vi) and neurodegeneration (FJB + ve cells, A, vii–ix). E). In Timm's stained sections, the inner molecular layer (IML) of the dentate gyrus showed intense dark staining for mossy fiber sprouting in the vehicle treated animal (E, ii), when compared to the naive controls (E, i) and the 1400W treated animals (E, iii). The grey level intensity of IML is quantified using ImageJ to determine the mossy fiber staining intensity. In the vehicle treated animals there was a significant decrease in the grey intensity levels in IML (seen as a dark band) when compared to the 1400W treated group (*p < 0.05, **p < 0.01, n = 6–7 each group, Mann–Whitney test). Scale, all 100 μm.

Discussion

In this study, we demonstrate a novel disease modifying property of a highly selective pharmacological inhibitor of iNOS, 1400W that targets neuroinflammatory mediators

produced by reactive glial cells. A vast majority of currently available AEDs target neurons at their excitatory synaptic terminals to suppress hyperexcitability or to promote the function of inhibitory neurons (Galanopoulou et al., 2013; Meldrum and Rogawski, 2007; Rogawski and Loscher, 2004). According to a report, 47 drugs targeting ion channel receptors and their downstream effector proteins, after an epileptogenic insult, have failed in human clinical trials (Temkin, 2001). In spite of several newly discovered AEDs, >30 drugs altogether, >50% of people with epilepsy (PWE) presented with first seizure do not become seizure-free with the first AED, and about 17% of PWE require 2–3 or multiple AEDs (Kwan and Brodie, 2000). Importantly, about 1/3 of PWE do not respond to any of the current AEDs (Kwan and Brodie, 2000; Kwan et al., 2011). Although AEDs control symptomatic seizures in the remaining 2/3 of PWE, they do not cure epilepsy or significantly modify the disease process (Camfield et al., 2002; Loscher, 2011; Moshe et al., 2014; Varvel et al., 2015). Therefore we focused our investigation on the combination of drugs that have different mechanisms of action and targets to modify the events that occur during early epileptogenesis, and to understand their long-term impact on the disease process. We tested a single moderate dose of diazepam (10 mg/kg), the conventional benzodiazepine derivative of an AED to target GABAergic signaling to stop acute seizures, and a novel anti-neuroinflammatory and neuroprotectant, 1400W (6 doses at 12 h intervals, started 2 h after diazepam) to target the disease promoters such as glial-mediated neuroinflammation and neurodegeneration that occur after SE insult. This approach modulated the key early epileptogenic events, it; i) suppressed epileptiform spiking activity (Fig. 4B–C) during the first 12-74 h post-SE, ii) restored BBB integrity (Fig. 6A and C), iii) reduced extracellular serum albumin and its uptake by glia and neurons (Fig. 6B and D), iv) promoted glial protective functions by modulating Kir 4.1 and 3-NT levels (Fig. 7), and v) polarized

microglia from M1 to M2 type (Fig. 5A, iv–vi and C). These early effects of 1400W had a remarkable long-term impact on reducing SRS by >90% (Fig. 9, 10), a sustained functional recovery over time and thus it altered the course of the disease.

To test long-term disease modifying effects of 1400W, we chose an established chronic rat KA model of TLE for two reasons; i) the early epileptogenic hallmark events such as reactive gliosis (neuroinflammation) and neurodegeneration (Bertram et al., 1990; Jorgensen et al., 1993; Rao et al., 2006; Vezzani, 2014; Vezzani and Granata, 2005) mediated by KA in rats are reproducible (Figs. 3A and 8A), and ii) the symptomatic SRS is progressive in nature (Rao et al., 2006; Williams et al., 2007, 2009) and also reproducible (Fig. 9). These factors are measurable and therefore useful to quantify the disease modifying effects mediated by 1400W. Since the severity of SE influences disease progression (Bortel et al., 2010; Klitgaard et al., 2002; Suchomelova et al., 2006), we employed repeated-low-dose method of KA injections to titrate all the rats to achieve stage-5 seizures and to achieve a fair seizure severity score during the SE (Fig. 2C). The duration of the established SE (2 h) was kept constant between all animals by terminating the behavioral SE with diazepam. A continuous video-EEG monitoring for 6 months facilitated real-time assessment of 1400W's immediate, acute, and long-term effects after the drug withdrawal on the day 3 of post-SE.

The 1400W is a small molecule (MW 250.17), BBB permeable, water soluble, and biologically active. It suppressed abnormal levels of NO in rodent disease models (Garvey et al., 1997; Parmentier et al., 1999; Perez-Asensio et al., 2005). We have further tested 1400W in rodents (20 mg/kg, optimum dose) using echocardiogram in M-mode for cardiac function and flexiVent method for lung function, and confirmed that it had no adverse effects on heart and lungs (data not shown). 1400W is 100-fold potent than other iNOS inhibitors (ED50 =

~0.3 mg) in reducing delayed vascular injury in the rat LPS model (Garvey et al., 1997). Importantly, rats tolerated a dose of 120 mg/day for a 7-day period when 1400W was administered as intravenous infusion, however, it was lethal at 50 mg/kg when given as a single intravenous bolus (Garvey et al., 1997). This is an important finding considering the reported controversial roles of NO in brain pathology (Chung et al., 2005; Dawson and Snyder, 1994; Dawson and Dawson, 1998; Hobbs et al., 1999; Moncada and Erusalimsky, 2002; Puttachary et al., 2015a; Thippeswamy et al., 2006). The controversies could be due to inappropriate use of NOS inhibitors with respect to selectivity, dose and time of treatment (pre- or post-insult), solvents used as vehicle and method of reconstitution, and route/method of administration (Beamer et al., 2012; Cosgrave et al., 2008; Hagioka et al., 2005; Kato et al., 2005; Kovacs et al., 2009; Takei et al., 2001). We always prepared 1400W fresh in sterile DW and the first dose was administered 2 h after treating the SE with diazepam for the long-term study.

The production of disease promoting pro-inflammatory mediators begins soon after the insult (2-8 h post-SE), with concomitant rapid activation of microglial cells (Davalos et al., 2005; Nimmerjahn et al., 2005; Ransohoff and Cardona, 2011; Ravizza et al., 2005; Vezzani et al., 2008b), and their levels persist for several weeks (Ryan et al., 2014; Vezzani et al., 2000; Vezzani et al., 2008b). In a recent study it was shown that the RNS marker, 3-NT levels were elevated in CA3 pyramidal cells at 24 h post-SE and persisted throughout the epileptic phase (Ryan et al., 2014). Excessive 3-NT levels promote neurodegeneration (Boje and Arora, 1992; Rao et al., 2003; Vincent et al., 1998). Elevated levels of IL1β and NO enhance seizure susceptibility, spontaneous seizures and neurodegeneration (Noe et al., 2013; Ravizza et al., 2005; Vezzani et al., 2008a; Vezzani and Baram, 2007). It is important to note that the nuclear factor kappa B (NF-κB), a common transcription factor for both IL-1β and iNOS, is also up-

regulated in reactive glial cells during the post-SE period (Kim et al., 2006; Vezzani and Baram, 2007). In a neuron-glia co-culture model, 1400W significantly suppressed lipopolysaccharide-induced neuroinflammation and neurodegeneration by restoring neuronal respiration and by preventing glutamate release (Bal-Price and Brown, 2001). Therefore, our hypothesis was that targeting reactive gliosis by 1400W will ameliorate hyperexcitability and neurodegeneration to modify epileptogenesis. The 1400W significantly suppressed hyperexcitability of neurons [evident from reduced epileptiform spike rate (Fig. 3A–C)], and reduced neurodegeneration [evident from decreased FJB positive neurons (Fig. 5A, D)] during the first week of epileptogenesis. The morphology of microglia and astrocytes also confirmed a significant reduction in reactive types, especially M1 type, and an increase in M2 type microglial cells (Fig. 5). M1 type microglia cells are the predominant glial cell type observed during neuroinflammation and they produce proinflammatory cytokines TNFα and IL-1β, and iNOS (De Simoni et al., 2000; Engel et al., 2013). We found increased iNOS activity at 7 d time point as evident from a significant increase in 3-NT positive M1 type microglia cells in the hippocampus, amygdala, and entorhinal cortex (Fig. 7E–G), which was suppressed in the 1400W treated group. It is plausible that an inhibition of iNOS by 1400W could have polarized M1 to M2 type microglia to cause a reduction in epileptiform spike rate and neurodegeneration during the first week of post-SE (Fig. 4B; Fig. 5A, vii–ix and C). Recent articles highlight the therapeutic importance of drugs that polarize glial cells from reactive to non-reactive or "alternate state" (Binder and Carson, 2013; Franco and Fernández-Suárez, 2015; Taetzsch et al., 2014; Zamanian et al., 2012). "Alternate state or non-reactive" gliosis has been implicated in neuroprotection (Carson et al., 2008; Pekny et al., 2014; Rathbone et al., 1999).

It has been suggested that an increased levels of IL-1β and iNOS during neuroinflammation could compromise BBB integrity and function by downregulating endothelial zonula occludens-1 (HernandezRomero et al., 2012; Librizzi et al., 2012; Morin-Brureau et al., 2011; Obermeier et al., 2014). Increased BBB dysfunction and permeability can impair brain function due to altered metabolic function, infiltration of leucocytes, extravasation of serum albumin to cause hyperexcitability of neurons and further activation of glia to decrease seizure threshold (Librizzi et al., 2012; Morin-Brureau et al., 2011). NOS inhibitors have been shown to mitigate BBB dysfunction by upregulating zonula occludens-1 (Leal et al., 2007; Librizzi et al., 2012; Morin-Brureau et al., 2011; Yang et al., 2013). The 1400W treatment prevented BBB leakage and reduced serum albumin positive cells in the hippocampus (Fig. 6) suggesting 1400W's protective role in re-establishing BBB integrity. To test this function, we used higher molecular mass fluorescent dye or Fluro-Gold (hydroxy-stilbamidine, 472.54 Da), which has ~50% greater molecular mass than 1400W and KA. The average molecular mass of CNS active drug is 357 Daltons (Da) (Pardridge, 2003). Water soluble therapeutic small molecules generally cross the BBB with ease if the molecular mass of a drug is b400 Da (Fischer et al., 1998; Lipinski, 2000; Pardridge, 2003). Therefore, water soluble 1400W with low molecular mass (250.2) has a therapeutic advantage. Rat serum albumin molecular mass is >65 kDa and hence it is impossible for it to cross the BBB under normal conditions. Seizures disrupt BBB, therefore we found Fluro-Gold in the extracellular space at 2 h post-SE, and at 7 d post-SE there was a significant increase in serum albumin containing neurons and astrocytes (Fig. 6). It has also been shown that serum albumin uptake by astrocytes, mediated by transforming growth factor beta receptors, impairs astrocytes' buffering ability to clear extracellular potassium ions and glutamate, which could result in

hyper-excitability of neurons (Cacheaux et al., 2009; David et al., 2009; Ivens et al., 2007). Of particular interest, Kir 4.1 and GLT-1 are involved in clearing excessive potassium and glutamate from the extracellular space (Ivens et al., 2007; Petr et al., 2015). These two protein levels were downregulated in the hippocampus at 7 d post-SE (Fig. 7A–D). The 1400W partially reversed Kir 4.1 levels, however, GLT-1 levels were unaffected (Fig. 7A–D) suggesting that 1400W's protective mechanisms are predominantly mediated by targeting the glial source of pro-neuroinflammatory mediators. Further *in vitro* studies are required to address detailed mechanistic pathway of 1400W-mediated anti-neuroinflammatory and neuroprotective roles.

Having known 1400W's modulation of the disease promoters during the early epileptogenic phase, we focused our investigation on its long-term effects by employing continuous video-EEG surveillance for six months to understand whether 1400W can ultimately modify the disease outcome. The quantification of SRS from the vehicle and the 1400W treated groups revealed a remarkable disease modifying effects of 1400W (Fig. 9, 10). It is important to note that the 1400W was only given during the first three days of post-SE. Hence, 1400W qualifies as a disease modifying agent since it produced a sustained and highly significant improvement in functional recovery by reducing spontaneous convulsive seizures by >90%. Furthermore, IHC of brain sections at six month confirmed a significant reduction in reactive gliosis and neurodegeneration which could be due to a reduction in convulsive seizure activity. Aberrant MFS is expected in the IML of the dentate gyrus of chronic epileptic brains in humans and animal models (Buckmaster et al., 2002; Sutula et al., 1989; Sutula and Dudek, 2007; Wenzel et al., 1997). We also observed a well-defined MFS in the IML of the dentate gyrus in the vehicle treated group (Fig. 11E, ii). In the 1400W-treated group there was

a significant reduction in the grey levels intensity (reduced the dark band of sprouted axonal fibers) in the IML when compared to the vehicle group (Fig. 11E–F). Several studies have correlated the degree of MFS with seizure frequency in animal models of chronic epilepsy (Lemos and Cavalheiro, 1995; Masukawa et al., 1992; Mathern et al., 1996a, b; Patrylo et al., 1999). However, MFS is not mandatory for SRS occurrence (Buckmaster, 2012; Buckmaster, 2014; Buckmaster and Lew, 2011; Heng et al., 2013; Lew and Buckmaster, 2012). Aberrant MFS could be pro- or anti-epileptic depending on their synapse with excitatory dentate granule cells or inhibitory neurons (Okazaki et al., 1995; Okazaki et al., 1999; Sloviter, 1992; Wuarin and Dudek, 1996). In our study, the decreased staining intensity of MFS could be due to reduced SRS episodes in the 1400W treated group.

In summary, our results reveal the disease modifying property of 1400W, by significantly reducing the epileptiform spiking activity during the first 12–74 h post-SE, when it was administered twice daily for three days after the diazepam treatment in the rat KA model of TLE. Whether a first seizure is appropriately treated or untreated, or the second seizure is treated with AEDs, they do not reduce the probability of seizure freedom in long-term (Camfield et al., 1996; Camfield et al., 2002; Musicco et al., 1997). Therefore, a combination of an AED and an anti-neuroinflammatory or neuroprotectant drug given within three days of acute insult could be an effective strategy to alter the course of the disease in acquired epilepsy. Further experiments are required to investigate whether 1400W could be a potential anti-epileptogenic or an antiepileptic agent by administering it during the late phase of epileptogenesis or after the occurrence of SRS when the disease is established.

References

1. Abbott, N.J., et al., 2006. Astrocyte–endothelial interactions at the blood–brain barrier. Nat. Rev. Neurosci. 7, 41–53.

2. Arabadzisz, D., et al., 2005. Epileptogenesis and chronic seizures in a mouse model of temporal lobe epilepsy are associated with distinct EEG patterns and selective neurochemical alterations in the contralateral hippocampus. Exp. Neurol. 194, 76–90.

3. Bal-Price, A., Brown, G.C., 2001. Inflammatory neurodegeneration mediated by nitric oxide from activated glia-inhibiting neuronal respiration, causing glutamate release and excitotoxicity. J. Neurosci. 21, 6480–6491.

4. Beamer, E., et al., 2012. N(w)-propyl-L-arginine (L-NPA) reduces status epilepticus and early epileptogenic events in a mouse model of epilepsy: behavioural, EEG and immunohistochemical analyses. Eur. J. Neurosci. 36, 3194–3203.

5. Ben-Ari, Y., 2012. Kainate and Temporal Lobe Epilepsies: 3 Decades of Progress. Ben-Ari, Y., Cossart, R., 2000. Kainate, a double agent that generates seizures: two decades of progress. Trends Neurosci. 23, 580–587.

6. Benkovic, S.A., et al., 2006. Regional neuropathology following kainic acid intoxication in adult and aged C57BL/6J mice. Brain Res. 1070, 215–231.

7. Bertram, E.H., et al., 1990. The hippocampus in experimental chronic epilepsy: a morphometric analysis. Ann. Neurol. 27, 43–48.

8. Binder, D.K., Carson, M.J., 2013. Glial cells as primary therapeutic targets for epilepsy. Neurochem. Int. 63, 635–637.

9. Boer, R., et al., 2000. The inhibitory potency and selectivity of arginine substrate site nitric-oxide synthase inhibitors is solely determined by their affinity toward the different isoenzymes. Mol. Pharmacol. 58, 1026–1034.

10. Boje, K.M., Arora, P.K., 1992. Microglial-produced nitric oxide and reactive nitrogen oxides mediate neuronal cell death. Brain Res. 587, 250–256.

11. Bortel, A., et al., 2010. Convulsive status epilepticus duration as determinant for epileptogenesis and interictal discharge generation in the rat limbic system. Neurobiol. Dis. 40, 478–489.

12. Buckmaster, P.S., 2012. Mossy Fiber Sprouting in the Dentate Gyrus. Buckmaster, P.S., 2014. Does mossy fiber sprouting give rise to the epileptic state? Adv. Exp. Med. Biol. 813, 161–168.

13. Buckmaster, P.S., Lew, F.H., 2011. Rapamycin suppresses mossy fiber sprouting but not seizure frequency in a mouse model of temporal lobe epilepsy. J. Neurosci. 31, 2337–2347.

14. Buckmaster, P.S., et al., 2002. Axon sprouting in a model of temporal lobe epilepsy creates a predominantly excitatory feedback circuit. J. Neurosci. 22, 6650–6658.

15. Cacheaux, L.P., et al., 2009. Transcriptome profiling reveals TGF-beta signaling involvement in epileptogenesis. J. Neurosci. 29, 8927–8935.

16. Camfield, C., et al., 1996. Does the number of seizures before treatment influence ease of control or remission of childhood epilepsy? Not if the number is 10 or less. Neurology 46, 41–44.

17. Camfield, P., et al., 2002. Long-term outcome is unchanged by antiepileptic drug treatment after a first seizure: a 15-year follow-up from a randomized trial in childhood. Epilepsia 43, 662–663.

18. Carson, M.J., et al., 2008. Modeling CNS microglia: the quest to identify predictive models. Drug Discov Today Dis Models. 5, 19–25.

19. Cherry, J.D., et al., 2014. Neuroinflammation and M2 microglia: the good, the bad, and the inflamed. J. Neuroinflammation 11, 98.

20. Chhor, V., et al., 2013. Characterization of phenotype markers and neuronotoxic potential of polarised primary microglia in vitro. Brain Behav. Immun. 32, 70–85.

21. Chung, K.K., et al., 2005. Nitric oxide, S-nitrosylation and neurodegeneration. Cell. Mol. Biol. (Noisy-le-Grand) 51, 247–254.

22. Cosgrave, A.S., et al., 2008. Regulation of activity-dependent neuroprotective protein (ADNP) by the NO-cGMP pathway in the hippocampus during kainic acid-induced seizure. Neurobiol. Dis. 30, 281–292.

23. Cosgrave, A.S., et al., 2009. Nitric oxide regulates activity-dependent neuroprotective protein (ADNP) in the dentate gyrus of the rodent model of kainic acid-induced seizure. J. Mol. Neurosci. 39, 9–21.

24. Cosgrave, A.S., et al., 2010. The effects of nitric oxide inhibition prior to kainic acid treatment on neuro- and gliogenesis in the rat dentate gyrus in vivo and in vitro. Histol. Histopathol. 25, 841–856.

25. Danscher, G., 1981. Histochemical demonstration of heavy metals. A revised version of the sulphide silver method suitable for both light and electronmicroscopy. Histochemistry 71, 1–16.

26. Davalos, D., et al., 2005. ATP mediates rapid microglial response to local brain injury in vivo. Nat. Neurosci. 8, 752–758.

27. David, Y., et al., 2009. Astrocytic dysfunction in epileptogenesis: consequence of altered potassium and glutamate homeostasis? J. Neurosci. 29, 10588–10599.

28. Dawson, V.L., Dawson, T.M., 1998. Nitric oxide in neurodegeneration. Prog. Brain Res. 118, 215–229.

29. Dawson, T.M., Snyder, S.H., 1994. Gases as biological messengers: nitric oxide and carbon monoxide in the brain. J. Neurosci. 14, 5147–5159.

30. De Simoni, M.G., et al., 2000. Inflammatory cytokines and related genes are induced in the rat hippocampus by limbic status epilepticus. Eur. J. Neurosci. 12, 2623–2633.

31. Drexel, M., et al., 2012. Sequel of spontaneous seizures after kainic acid-induced status epilepticus and associated neuropathological changes in the subiculum and entorhinal cortex. Neuropharmacology 63, 806–817.

32. Dudek, F.E., Shao, L.R., 2004. Mossy fiber sprouting and recurrent excitation: direct electrophysiologic evidence and potential implications. Epilepsy Curr. 4, 184–187.

33. Engel Jr., J., et al., 2013. Epilepsy biomarkers. Epilepsia 54 (Suppl. 4), 61–69. Fischer, H., et al., 1998. Blood–brain barrier permeation: molecular parameters governing passive diffusion. J. Membr. Biol. 165, 201–211.

34. Franco, R., Fernández-Suárez, D., 2015. Alternatively activated microglia and macrophages in the central nervous system. Prog. Neurobiol. 131, 65–86.

35. Galanopoulou, A.S., et al., 2013. Epilepsy therapy development: technical and methodologic issues in studies with animal models. Epilepsia 54 (Suppl. 4), 13–23.

36. Garvey, E.P., et al., 1997. 1400W is a slow, tight binding, and highly selective inhibitor of inducible nitric-oxide synthase in vitro and in vivo. J. Biol. Chem. 272, 4959–4963.

37. Glien, M., et al., 2001. Repeated low-dose treatment of rats with pilocarpine: low mortality but high proportion of rats developing epilepsy. Epilepsy Res. 46, 111–119.

38. Hagioka, S., et al., 2005. Effects of 7-nitroindazole and N-nitro-L-arginine methyl ester on changes in cerebral blood flow and nitric oxide production preceding development of hyperbaric oxygen-induced seizures in rats. Neurosci. Lett. 382, 206–210.

39. Heinemann, U., et al., 2012. Blood–brain barrier dysfunction, TGFbeta signaling, and astrocyte dysfunction in epilepsy. Glia 60, 1251–1257.

40. Hellier, J.L., et al., 1998. Recurrent spontaneous motor seizures after repeated low-dose systemic treatment with kainate: assessment of a rat model of temporal lobe epilepsy. Epilepsy Res. 31, 73–84.

41. Heng, K., et al., 2013. High-dose rapamycin blocks mossy fiber sprouting but not seizures in a mouse model of temporal lobe epilepsy. Epilepsia 54, 1535–1541.

42. Hernandez-Romero, M.C., et al., 2012. Peripheral inflammation increases the deleterious effect of CNS inflammation on the nigrostriatal dopaminergic system. Neurotoxicology 33, 347–360.

43. Hirai, T., et al., 2013. The prevalence and phenotype of activated microglia/macrophages within the spinal cord of the hyperostotic mouse (twy/twy) changes in response to chronic progressive spinal cord compression: implications for human cervical compressive myelopathy. PLoS One 8, e64528.

44. Hobbs, A.J., et al., 1999. Inhibition of nitric oxide synthase as a potential therapeutic target. Annu. Rev. Pharmacol. Toxicol. 39, 191–220.

45. Hu, X., et al., 2013. Microglia/macrophage polarization dynamics reveal novel mechanism of injury expansion after focal cerebral ischemia. Stroke 43, 3063–3070.

46. Ivens, S., et al., 2007. TGF-beta receptor-mediated albumin uptake into astrocytes is involved in neocortical epileptogenesis. Brain 130, 535–547.

47. Jafarian-Tehrani, M., et al., 2005. 1400W, a potent selective inducible NOS inhibitor, improves histopathological outcome following traumatic brain injury in rats. Nitric Oxide 12, 61–69.

48. Jorgensen, M.B., et al., 1993. Microglial and astroglial reactions to ischemic and kainic acid-induced lesions of the adult rat hippocampus. Exp. Neurol. 120, 70–88.

49. Kato, N., et al., 2005. Sequential changes of nitric oxide levels in the temporal lobes of kainic acid-treated mice following application of nitric oxide synthase inhibitors and phenobarbital. Epilepsy Res. 65, 81–91.

50. Kaushik, D.K., et al., 2013. Interleukin-1beta orchestrates underlying inflammatory responses in microglia via Kruppel-like factor 4. J. Neurochem. 127, 233–244.

51. Kigerl, K.A., et al., 2009. Identification of two distinct macrophage subsets with divergent effects causing either neurotoxicity or regeneration in the injured mouse spinal cord. J. Neurosci. 29, 13435–13444.

52. Kim, Y.J., et al., 2006. IL-1beta, an immediate early protein secreted by activated microglia, induces iNOS/NO in C6 astrocytoma cells through p38 MAPK and NF-kappaB pathways. J. Neurosci. Res. 84, 1037–1046.

53. Klitgaard, H., et al., 2002. Pilocarpine-induced epileptogenesis in the rat: impact of initial duration of status epilepticus on electrophysiological and neuropathological alterations. Epilepsy Res. 51, 93–107.

54. Kovacs, R., et al., 2009. Endogenous nitric oxide is a key promoting factor for initiation of seizure-like events in hippocampal and entorhinal cortex slices. J. Neurosci. 29, 8565–8577.

55. Kwan, P., Brodie, M.J., 2000. Epilepsy after the first drug fails: substitution or add-on? Seizure 9, 464–468. Kwan, P., et al., 2011. Drug-resistant epilepsy. N. Engl. J. Med. 365, 919–926.

56. Le Duigou, C., et al., 2008. Epileptiform activities in slices of hippocampus from mice after intra-hippocampal injection of kainic acid. J. Physiol. 586, 4891–4904.

57. Leal, E.C., et al., 2007. Inducible nitric oxide synthase isoform is a key mediator of leukostasis and blood-retinal barrier breakdown in diabetic retinopathy. Invest. Ophthalmol. Vis. Sci. 48, 5257–5265.

58. Lemos, T., Cavalheiro, E.A., 1995. Suppression of pilocarpine-induced status epilepticus and the late development of epilepsy in rats. Exp. Brain Res. 102, 423–428.

59. Lew, F.H., Buckmaster, P.S., 2012. Is there a critical period for mossy fiber sprouting in a mouse model of temporal lobe epilepsy? Epilepsia 52, 2326–2332.

60. Librizzi, L., et al., 2012. Seizure-induced brain-borne inflammation sustains seizure recurrence and blood–brain barrier damage. Ann. Neurol. 72, 82–90.

61. Lipinski, C.A., 2000. Drug-like properties and the causes of poor solubility and poor permeability. J. Pharmacol. Toxicol. Methods 44, 235–249.

62. Liu, X., et al., 2016. Interleukin-4 is essential for microglia/macrophage M2 polarization and long-term recovery after cerebral ischemia. Stroke 47, 498–504.

63. Loane, D.J., et al., 2013. Progressive neurodegeneration after experimental brain trauma: association with chronic microglial activation. J. Neuropathol. Exp. Neurol. 73, 14–29.

64. Loscher, W., 2011. Critical review of current animal models of seizures and epilepsy used in the discovery and development of new antiepileptic drugs. Seizure 20, 359–368.

65. Lull, M.E., Block, M.L., 2010. Microglial activation and chronic neurodegeneration. Neurotherapeutics 7, 354–365.

66. Marchi, N., Lerner-Natoli, M., 2013. Cerebrovascular remodeling and epilepsy. Neuroscientist 19, 304–312.

67. Marchi, N., et al., 2015. Blood–brain barrier, bulk flow, and interstitial clearance in epilepsy. J. Neurosci. Methods 260, 118–124.

68. Masukawa, L.M., et al., 1992. The functional relationship between antidromically evoked field responses of the dentate gyrus and mossy fiber reorganization in temporal lobe epileptic patients. Brain Res. 579, 119–127.

69. Mathern, G.W., et al., 1996a. Aberrant hippocampal mossy fiber sprouting correlates with greater NMDAR2 receptor staining. Neuroreport 7, 1029–1035.

70. Mathern, G.W., et al., 1996b. Severe seizures in young children are associated with hippocampal neuron losses and aberrant mossy fiber sprouting during fascia dentata postnatal development. Epilepsy Res. Suppl. 12, 33–43.

71. Meldrum, B.S., Rogawski, M.A., 2007. Molecular targets for antiepileptic drug development. Neurotherapeutics 4, 18–61.

72. Moncada, S., Erusalimsky, J.D., 2002. Does nitric oxide modulate mitochondrial energy generation and apoptosis? Nat. Rev. Mol. Cell Biol. 3, 214–220.

73. Morin-Brureau, M., et al., 2011. Epileptiform activity induces vascular remodeling and zonula occludens 1 downregulation in organotypic hippocampal cultures: role of VEGF signaling pathways. J. Neurosci. 31, 10677–10688.

74. Moshe, S.L., et al., 2014. Epilepsy: new advances. Lancet 385, 884–898. Musicco, M., et al., 1997. Treatment of first tonic-clonic seizure does not improve the prognosis of epilepsy. First Seizure Trial Group (FIRST Group). Neurology 49, 991–998.

75. Nimmerjahn, A., et al., 2005. Resting microglial cells are highly dynamic surveillants of brain parenchyma in vivo. Science 308, 1314–1318.

76. Noe, F.M., et al., 2013. Pharmacological blockade of IL-1beta/IL-1 receptor type 1 axis during epileptogenesis provides neuroprotection in two rat models of temporal lobe epilepsy. Neurobiol. Dis. 59, 183–193.

77. Obermeier, B., et al., 2014. Development, maintenance and disruption of the blood–brain barrier. Nat. Med. 19, 1584–1596.

78. Okazaki, M.M., et al., 1995. Hippocampal mossy fiber sprouting and synapse formation after status epilepticus in rats: visualization after retrograde transport of biocytin. J. Comp. Neurol. 352, 515–534.

79. Okazaki, M.M., et al., 1999. Recurrent mossy fiber pathway in rat dentate gyrus: synaptic currents evoked in presence and absence of seizure-induced growth. J. Neurophysiol. 81, 1645–1660.

80. Papageorgiou, I.E., et al., 2014. Widespread activation of microglial cells in the hippocampus of chronic epileptic rats correlates only partially with neurodegeneration. Brain Struct. Funct. 220, 2423–2439.

81. Pardridge, W.M., 2003. Blood–brain barrier drug targeting: the future of brain drug development. Mol. Interv. 3 (90–105), 51.

82. Parmentier, S., et al., 1999. Selective inhibition of inducible nitric oxide synthase prevents ischaemic brain injury. Br. J. Pharmacol. 127, 546–552.

83. Patrylo, P.R., et al., 1999. Abnormal responses to perforant path stimulation in the dentate gyrus of slices from rats with kainate-induced epilepsy and mossy fiber reorganization. Epilepsy Res. 36, 31–42.

84. Pekny, M., et al., 2014. The dual role of astrocyte activation and reactive gliosis. Neurosci. Lett. 565, 30–38.

85. Perez-Asensio, F.J., et al., 2005. Inhibition of iNOS activity by 1400W decreases glutamate release and ameliorates stroke outcome after experimental ischemia. Neurobiol. Dis. 18, 375–384.

86. Petr, G.T., et al., 2015. Conditional deletion of the glutamate transporter GLT-1 reveals that astrocytic GLT-1 protects against fatal epilepsy while neuronal GLT-1 contributes significantly to glutamate uptake into synaptosomes. J. Neurosci. 35, 5187–5201.

87. Pigott, B., et al., 2013. On the selectivity of neuronal NOS inhibitors. Br. J. Pharmacol. 168, 1255–1265.

88. Puttachary, S., et al., 2015a. Seizure-induced oxidative stress in temporal lobe epilepsy. Biomed. Res. Int. 2015, 745613.

89. Puttachary, S., et al., 2015b. Immediate epileptogenesis after kainate-induced status epilepticus in C57BL/6J mice: evidence from long term continuous video-EEG telemetry. PLoS One 10, e0131705.

90. Puttachary, S., et al., 2016. Immediate epileptogenesis: impact on brain in C57BL/6J mouse kainate model. Frontiers in Bioscience, Elite 8, 390–411.

91. Racine, R.J., 1972. Modification of seizure activity by electrical stimulation. II. Motor seizure. Electroencephalogr. Clin. Neurophysiol. 32, 281–294.

92. Ransohoff, R.M., Cardona, A.E., 2011. The myeloid cells of the central nervous system parenchyma. Nature 468, 253–262.

93. Rao, S.D., et al., 2003. Disruption of glial glutamate transport by reactive oxygen species produced in motor neurons. J. Neurosci. 23, 2627–2633.

94. Rao, M.S., et al., 2006. Hippocampal neurodegeneration, spontaneous seizures, and mossy fiber sprouting in the F344 rat model of temporal lobe epilepsy. J. Neurosci. Res. 83, 1088–1105.

95. Rathbone, M.P., et al., 1999. Trophic effects of purines in neurons and glial cells. Prog. Neurobiol. 59, 663–690.

96. Ravizza, T., et al., 2005. Inflammatory response and glia activation in developing rat hippocampus after status epilepticus. Epilepsia 46 (Suppl. 5), 113–117.

97. Rogawski, M.A., Loscher, W., 2004. The neurobiology of antiepileptic drugs. Nat. Rev. Neurosci. 5, 553–564.

98. Ryan, K., et al., 2014. Temporal and spatial increase of reactive nitrogen species in the kainate model of temporal lobe epilepsy. Neurobiol. Dis. 64, 8–15.

99. Schmued, L.C., Hopkins, K.J., 2000. Fluoro-Jade: novel fluorochromes for detecting toxicant-induced neuronal degeneration. Toxicol. Pathol. 28, 91–99.

100. Schneider, C.A., et al., 2012. NIH image to ImageJ: 25 years of image analysis. Nat. Methods 9, 671–675.

101. Seiffert, E., et al., 2004. Lasting blood–brain barrier disruption induces epileptic focus in the rat somatosensory cortex. J. Neurosci. 24, 7829–7836.

102. Shetty, A.K., et al., 2005. Repair of the injured adult hippocampus through graft-mediated modulation of the plasticity of the dentate gyrus in a rat model of temporal lobe epilepsy. J. Neurosci. 25, 8391–8401.

103. Sloviter, R.S., 1992. Possible functional consequences of synaptic reorganization in the dentate gyrus of kainate-treated rats. Neurosci. Lett. 137, 91–96.

104. Staunton, C., et al., 2013. Inducible nitric oxide synthase inhibitor, 1400W dihydrochloride, reduces neuropathic pain in a rodent model. British Neuroscience Meeting Abstract, PI-C-108.

105. Suchomelova, L., et al., 2006. Treatment of experimental status epilepticus in immature rats: dissociation between anticonvulsant and antiepileptogenic effects. Pediatr. Res. 59, 237–243.

106. Sutula, T.P., Dudek, F.E., 2007. Unmasking recurrent excitation generated by mossy fiber sprouting in the epileptic dentate gyrus: an emergent property of a complex system. Prog. Brain Res. 163, 541–563.

107. Sutula, T., et al., 1989. Mossy fiber synaptic reorganization in the epileptic human temporal lobe. Ann. Neurol. 26, 321–330.

108. Taetzsch, T., et al., 2014. Redox regulation of NF-kappaB p50 and M1 polarization in microglia. Glia 63, 423–440.

109. Takaki, J., et al., 2013. L-Glutamate released from activated microglia downregulates astrocytic L-glutamate transporter expression in neuroinflammation: the 'collusion' hypothesis for increased extracellular L-glutamate concentration in neuroinflammation. J. Neuroinflammation 9, 275.

110. Takei, Y., et al., 2001. Different effects between 7-nitroindazole and L-NAME on cerebral hemodynamics and hippocampal lesions during kainic acid-induced seizures in newborn rabbits. Brain Dev. 23, 406–413.

111. Tang, Y., Le, W., 2015. Differential roles of M1 and M2 microglia in neurodegenerative diseases. Mol. Neurobiol. 53, 1181–1194.

112. Tauck, D.L., Nadler, J.V., 1985. Evidence of functional mossy fiber sprouting in hippocampal formation of kainic acid-treated rats. J. Neurosci. 5, 1016–1022.

113. Temkin, N.R., 2001. Antiepileptogenesis and seizure prevention trials with antiepileptic drugs: meta-analysis of controlled trials. Epilepsia 42, 515–524.

114. Thippeswamy, T., et al., 2006. Nitric oxide, a biological double-faced Janus—is this good or bad? Histol. Histopathol. 21, 445–458.

115. Thippeswamy, T., et al., 2007. Nitric oxide-NGF mediated PPTA/SP, ADNP, and VIP expression in the peripheral nervous system. J. Mol. Neurosci. 33, 268–277.

116. Todorovic, M.S., et al., 2012. Characterization of status epilepticus induced by two organophosphates in rats. Epilepsy Res. 101, 268–276.

117. Tomkins, O., et al., 2011. Blood–brain barrier breakdown following traumatic brain injury: a possible role in posttraumatic epilepsy. Cardiovasc. Psychiatry Neurol. 2011, 765923.

118. Treiman, D.M., 2010. Management of refractory complex partial seizures: current state of the art. Neuropsychiatr. Dis. Treat. 6, 297–308.

119. Tse, K., et al., 2014. Advantages of repeated low dose against single high dose of kainate in C57BL/6J mouse model of status epilepticus: behavioral and electroencephalographic studies. PLoS One 9, e96622.

120. Van Vliet, E.A., et al., 2007. Blood–brain barrier leakage may lead to progression of temporal lobe epilepsy. Brain 130, 521–534.

121. Varvel, N.H., et al., 2015. Candidate drug targets for prevention or modification of epilepsy. Annu. Rev. Pharmacol. Toxicol. 55, 229–247.

122. Vezzani, A., 2014. Epilepsy and inflammation in the brain: overview and pathophysiology. Epilepsy Curr. 14, 3–7.

123. Vezzani, A., Baram, T.Z., 2007. New roles for interleukin-1 beta in the mechanisms of epilepsy. Epilepsy Curr. 7, 45–50.

124. Vezzani, A., Granata, T., 2005. Brain inflammation in epilepsy: experimental and clinical evidence. Epilepsia 46, 1724–1743.

125. Vezzani, A., et al., 2000. Powerful anticonvulsant action of IL-1 receptor antagonist on intracerebral injection and astrocytic overexpression in mice. Proc. Natl. Acad. Sci. U. S. A. 97, 11534–11539.

126. Vezzani, A., et al., 2008a. The role of cytokines in the pathophysiology of epilepsy. Brain Behav. Immun. 22, 797–803.

127. Vezzani, A., et al., 2008b. Glia as a source of cytokines: implications for neuronal excitability and survival. Epilepsia 49 (Suppl. 2), 24–32.

128. Vezzani, A., et al., 2012. Glia-Neuronal Interactions in Ictogenesis and Epileptogenesis: Role of Inflammatory Mediators.

129. Vincent, V.A., et al., 1998. Production, regulation and role of nitric oxide in glial cells. Mediators Inflamm. 7, 239–255.

130. Waldbaum, S., Patel, M., 2009. Mitochondria, oxidative stress, and temporal lobe epilepsy. Epilepsy Res. 88, 23–45.

131. Wang, Z., et al., 2003. Reduced expression of glutamate transporter EAAT2 and impaired glutamate transport in human primary astrocytes exposed to HIV-1 or gp120. Virology 312, 60–73.

132. Weissberg, I., et al., 2015. Albumin induces excitatory synaptogenesis through astrocytic TGF-beta/ALK5 signaling in a model of acquired epilepsy following blood–brain barrier dysfunction. Neurobiol. Dis. 78, 115–125.

133. Wenzel, H.J., et al., 1997. Ultrastructural localization of neurotransmitter immunoreactivity in mossy cell axons and their synaptic targets in the rat dentate gyrus. Hippocampus 7, 559–570.

134. White, A., et al., 2010. EEG spike activity precedes epilepsy after kainate-induced status epilepticus. Epilepsia 51, 371–383.

135. Williams, P.A., et al., 2007. Development of spontaneous seizures after experimental status epilepticus: implications for understanding epileptogenesis. Epilepsia 48 (Suppl. 5), 157–163.

136. Williams, P.A., et al., 2009. Development of spontaneous recurrent seizures after kainateinduced status epilepticus. J. Neurosci. 29, 2103–2112.

137. Wuarin, J.P., Dudek, F.E., 1996. Electrographic seizures and new recurrent excitatory circuits in the dentate gyrus of hippocampal slices from kainate-treated epileptic rats. J. Neurosci. 16, 4438–4448.

138. Yang, S., et al., 2013. Hemoglobin-induced nitric oxide synthase overexpression and nitric oxide production contribute to blood–brain barrier disruption in the rat. J. Mol. Neurosci. 51, 352–363.

139. Yi, D., et al., 2000. Quantification of 3-nitrotyrosine in biological tissues and fluids: generating valid results by eliminating artifactual formation. J. Am. Soc. Mass Spectrom. 11, 578–586.

140. Zamanian, J.L., et al., 2012. Genomic analysis of reactive astrogliosis. J. Neurosci. 32, 6391–6410.

141. Zhang, X.M., Zhu, J., 2012. Kainic acid-induced neurotoxicity: targeting glial responses and glia-derived cytokines. Curr. Neuropharmacol. 9, 388–398.

142. Zhao, H., et al., 2015. Microglia/macrophage polarization after experimental intracerebral hemorrhage. Transl. Stroke Res. 6, 407–409.

CHAPTER V

INVESTIGATING THE NEUROPROTECTIVE AND ANTIEPILEPTOGENIC MECHANISMS OF SARACATINIB (AZD0530), A SFK/FYN INHIBITOR IN THE RAT KAINATE MODEL OF TEMPORAL LOBE EPILEPSY

Some of the data in this chapter is published in *Neurobiology of Disease*

Shaunik Sharma[1B], Steve Carlson[1], Sreekanth Puttachary[1], Souvarish Sarkar[1], Lucas Showman[2], Marson Putra[1], Anumantha Kanthasamy[1], Thimmasettappa Thippeswamy[1C]

[1]Department of Biomedical Sciences, College of Veterinary Medicine, Iowa State University, Ames 50011, USA.

[2]W.M. Keck Metabolomics Research Laboratory, Iowa State University, Ames 50011, USA.

[A]Reprinted with permission of *Neurobiol Dis*. 2018 Feb; 110:102-121.

[B]Primary researcher and author.

[C]Author for correspondence

Abstract

Status epilepticus (SE) induces neuroinflammation and epileptogenesis, but the mechanisms are not yet fully delineated. The Fyn, a non-receptor Src family tyrosine kinase (SFK), and its immediate downstream target, PKCδ are emerging as potential mediators of neuroinflammation. In order to first determine the role of Fyn kinase signaling in SE, we tested the efficacy of a SFK inhibitor, saracatinib (25 mg/kg, oral) in C57BL/6J mouse and rat kainate model of acute seizures. Saracatinib pretreatment dampened SE severity and completely prevented mortality. We further utilized *fyn*$^{-/-}$ and *fyn*$^{+/+}$ mice (wildtype control for the *fyn*$^{-/-}$ mice on same genetic background), and the rat kainate model, treated with saracatinib post-SE, to validate the role of Fyn/SFK in SE and epileptogenesis. We observed significant reduction in SE severity, epileptiform spikes, and electrographic non-convulsive seizures in *fyn*$^{-/-}$ mice when compared to *fyn*$^{+/+}$ mice. Interestingly, significant reductions in phosphorylated pSrc-416 and PKCδ (pPKCδ-507) and naive PKCδ were observed in *fyn*$^{-/-}$ mice as compared to *fyn*$^{+/+}$ mice suggesting that PKCδ signaling is a downstream mediator of Fyn in SE and epileptogenesis. Notably, *fyn*$^{-/-}$ mice also showed a reduction in key proinflammatory mediators TNF-α, IL-1β, and iNOS mRNA expression; serum IL-6 and IL-12 levels; and nitro-oxidative stress markers such as 4-HNE, gp91phox, and 3-NT in the hippocampus. Immunohistochemistry revealed a significant increase in reactive microgliosis and neurodegeneration in the hippocampus and hilus of dentate gyrus in *fyn*$^{+/+}$ mice in contrast to *fyn*$^{-/-}$ mice. Interestingly, we did not observe upregulation of Fyn in pyramidal neurons of the hippocampus during post-SE in *fyn*$^{+/+}$ mice, but it was upregulated in hilar neurons of the dentate gyrus when compared to naïve control. In reactive microglia, both Fyn and PKCδ were persistently upregulated during post-SE suggesting that Fyn-PKCδ may drive

neuroinflammation during epileptogenesis. Since disabling the Fyn kinase prior to SE, either by treating with saracatinib or fyn gene knockout, suppressed seizures and the subsequent epileptogenic events, we further tested whether Fyn/SFK inhibition during post-SE modifies epileptogenesis. Telemetry-implanted, SE induced, rats were treated with saracatinib and continuously monitored for a month. At 2 h post-diazepam, the saracatinib (25 mg/kg) or the vehicle was administered orally and repeated twice daily for first three days followed by a single dose/day for the next four days. The saracatinib post-treatment prevented epileptogenesis in > 50% of the rats and significantly reduced spontaneous seizures and epileptiform spikes in the rest (one animal did not respond) when compared to the vehicle treated group, which had > 24 seizures in a month. Saracatinib post-treatment also reduced Fyn and PKCδ immunopositive reactive microglia, astrocytes and neurons at 7 day and 4 month post-SE in all the regions of the brain. Moreover, reduction in oxidative stress molecules such as 4-HNE, $gp91^{phox}$, iNOS and 3-NT and neurodegeneration was also observed along with reduction in proinflmmatory proteins and genes in the serum and hipocampal tissues after saracatinib post-treatment. Collectively, the findings suggest that Fyn/SFK is a potential mediator of epileptogenesis and a therapeutic target to prevent/treat seizures and epileptogenesis.

Introduction

Neuroinflammation and neurodegeneration are hallmarks of epileptogenesis and temporal lobe epilepsy (TLE). In human TLE, immunohistochemistry (IHC) of brain sections from temporal lobectomized patients with history of intractable seizures, from both children and adults, provide evidence for occurrence of neuroinflammation and neurodegeneration (Beach et al., 1995; Choi et al., 2009; Das et al., 2012). We have recently demonstrated a persistent reactive microgliosis and astrogliosis, and neurodegeneration at six months after the induction of status epilepticus (SE) in the rat kainate model of TLE (Puttachary et al., 2016b). Neuronal hyperexcitability during a seizure, and/or prior to its occurrence, is largely attributed to intrinsic factors such as localized ionic imbalance, receptors dysfunction, and impaired release and/or uptake of neurotransmitters at synapses (Steinhäuser et al., 2016; Vezzani et al., 2011). These past findings led to the discovery of several new antiepileptic drugs (AED) based on their action on the ion-channels (Bialer and White, 2010; Rogawaski and Loscher, 2004; Schmidt, 2009). However, the majority of the current AEDs (including 47 failed drugs in human trials) are less effective, or do not cure the disease, and some even require lifelong administration with some potential side-effects (Kwan et al., 2011; Varvel et al., 2015). This suggests the need for development of more effective drugs that target alternative pathways to prevent/treat epilepsy. This is a major unmet clinical obligation due to poor understanding of the mechanisms of epileptogenesis. Therefore, we focused our investigation on identifying a novel molecular pathway and a drugable target for epileptogenesis, and possibly as a disease modifier.

Neuroinflammation is emerging as a new mechanistic target for drug development, and it also serves as a biomarker for neuroimaging in various neurodegenerative diseases (Abi-

Dargham and Horga, 2016; Albrecht et al., 2016; French, 2016; Gershen et al., 2015). The microglia are considered as resident macrophages and they mediate neuroinflammation and hyperexcitability in neurons (Block, 2014; Davis and Carson, 2012; Devinsky et al., 2013). The reactive glia are known to produce proinflammatory cytokines, reactive oxygen and nitrogen species (ROS/RNS), lipid peroxidation, hippocampal neurodegeneration, reorganization of neural circuits, and hyper-synchronicity (Bertram, 2013; Goldberg and Coulter, 2013; Puttachary et al., 2015a; Ryan et al., 2014; Scharfman and Binder, 2013; Vezzani et al., 2011 and Vezzani et al., 2013). The microglia become reactive in response to SE insult (Avignone et al., 2008; Puttachary et al., 2016a and b). However, the mechanism of microglial activation following seizures is largely unknown. Therefore, understanding the mechanism of activation of microglia may reveal its impact on epileptogenesis.

The Fyn is a non-receptor tyrosine kinase, a member of the Src family of kinase (SFK). It is associated with both excitatory and inhibitory ion channels, and its role in the pathophysiology of synaptic transmission, plasticity, neurodevelopment, and brain injury are well known (Knox and Jiang, 2015; Kojima et al., 1998; Lu et al., 1999; Nygaard et al., 2014; Salter and Kalia, 2004). The neuronal Fyn has been known to modulate both NMDA and GABAA receptors (Kojima et al., 1998; Lu et al., 1999), and the role of Fyn in normal amygdala kindling (Cain et al., 1995) suggests its potential association with acute seizure onset. However, its role in chronic seizures is not well known. Likewise the roles of Fyn kinase and one of its downstream targets, the protein kinase C delta (PKCδ), in microglia, astrocytes and neurons that mediate neuroinflammation and epileptogenesis are also not well known. Their role in glial cells in experimental disease models is however beginning to emerge, and it has been described in Parkinson's disease (PD) models (Nygaard et al., 2015; Panicker et al.,

2015). Therefore, we hypothesized that the Fyn-PKCδ signaling pathway may also mediate microglial activation in seizures, and disabling or pharmacologically inhibiting the Fyn kinase will suppress epileptiform activity and seizures by dampening neuroinflammation and neurodegeneration. We tested the hypothesis in the fyn knockout (fyn−/−) and wildtype control mice (fyn+/+, not overexpressing Fyn) bred on the same genetic background, and the Sprague Dawley rats in kainate model using a pharmacological inhibitor of the SFK, saracatinib, which is in phase IIa clinical trial for Alzheimer's disease (Kaufman et al., 2015; Nygaard et al., 2015). Our results demonstrate that disabling and inhibiting the fyn kinase activity reduces: PKCδ, pPKCδ-507, pSrc-416, caspase-3, proinflammatory cytokines, ROS/RNS levels, reactive microgliosis and neurodegeneration, SE severity, epileptiform spikes, spontaneous electrographic non-convulsive (NCS) and convulsive seizure (CS) frequencies in the mouse and rat kainate model. In the rat kainate model, treatment with saracatinib after SE induction suppresses epileptogenesis (reduced neuroinflammation and neurodegeneration), significantly reduced epileptiform spikes and spontaneous convulsive seizures in the animals.

Methods

Animal source and ethics statement

We used young adult (8 weeks) male C57BL/6J mice from Jackson laboratory (ME, USA), young adult male Sprague Dawley rats (8 weeks) from Charles River (MA, USA) and fyn+/+ and fyn−/− mice (8 weeks) for our experiments. The fyn+/+ and fyn−/− mice were bred on C57BL/6J and Balb-c genetic background in Dr. Kanthasamy's animal breeding facility, Laboratory Animal Resources (LAR), Iowa State University (ISU). The fyn+/+ mice were used as control for fyn−/− mice. The fyn+/+ mice neither overexpress Fyn nor contain constitutively

active Fyn. The fyn−/− mice were originally obtained from Dr. Dorit Ron's laboratory (by Dr. Kanthasamy) at the University of California, San Francisco, and are now available from the Jackson Laboratory (stock #002271). The fyn−/− mice were genotyped routinely by qRT-PCR to confirm fyn knockout. The fyn−/− mice used in this study had normal phenotype and no obvious differences were observed in their sexual and exploratory behaviors, body weight, and brain structure (gross weight and histology) when compared to the wildtype control mice (fyn+/+ mice). All animals were maintained at the LAR at ISU under controlled environmental conditions (19 °C–23 °C, 12 h light: 12 h dark), with ad libitum access to food and water. Animals purchased from Jackson laboratory and Charles River were used for experiments after four days of quarantine. All experiments were carried out in accordance with Institutional Animal Care and Use Committee (IACUC), ISU, USA (protocol number 10-12-7446/8090-MR). All surgical procedures were carried out in sterile and aseptic conditions under gaseous isoflurane anesthesia. The pre- and post-operative care was given to all animals to minimize pain and discomfort during and after surgery. Animals were monitored and weighed daily after surgery until they were used in the experiments. At the end of each experiment, the animals were euthanized by intraperitoneal (i.p.) administration of 100 mg/kg pentobarbital sodium as per the recommendations of the American Veterinary Medical Association (AVMA) Guidelines for Euthanasia of Animals.

Chemicals and reagents

Kainate (Tocris) was prepared in sterile water at the concentration of 2 mg/mL. It was always prepared fresh prior to its use. Saracatinib was purchased from Selleck Chemicals, PA, USA, and was prepared fresh in 0.5% (w/v) hydroxypropyl methylcellulose (HPMC) and 0.1% tween 80 (Sigma Aldrich, USA) at the concentration of 5 mg/mL. After CMC is evenly

dispersed in sterile water at 90 °C, the temperature of the solution was decreased by adding cold sterile water and stored at 20 °C to prevent it from precipitating at higher temperature. For perfusion, we used 4% paraformaldehyde (PFA) solution (Acros Organics, USA) in 0.1 M phosphate buffer saline (PBS) at pH 7.2. The primary antibodies used in the study and their concentrations are as follows: Fyn [mouse monoclonal, 1:300 for immunohistochemistry (IHC) and 1:800 for Western blot (WB)], PKCδ (rabbit polyclonal, 1:300 for IHC and 1:1000 for WB), pPKCδ-507 (goat polyclonal, 1:1000 for WB), iNOS (rabbit polyclonal, 1:500 for WB) and lamin-B (goat polyclonal; 1:500 for WB) were all purchased from Santa Cruz, CA, USA; GFAP (mouse monoclonal, 1:400 for IHC) and GFAP (rabbit monoclonal, 1:400 for IHC) was purchased from Sigma and Novus Biologicals; pSrc-416 (rabbit polyclonal; 1:1000 for WB) and caspase-3 and cleaved caspase-3 (rabbit polyclonal, 1:1000 for WB) were purchased from Cell Signaling, MA, USA; 4-HNE (rabbit polyclonal, 1:300 for IHC and 1:1000 for WB), gp91phox (rabbit polyclonal, 1:400 for IHC and 1:1000 for WB); 3-NT (mouse monoclonal, 1:1400 for WB), IBA1 (goat polyclonal, 1:500 for IHC) and β-actin (rabbit polyclonal, 1:10,000 for WB) were purchased from Abcam, MA, USA; NeuN (rabbit polyclonal, 1:400 for IHC, EMD Millipore, USA); Fluoro-Jade B was purchased from Histochem Inc., Jefferson, AR, USA. The secondary antibodies used for IHC were tagged with either a fluorescent dye (CY3 conjugated 1:200 or FITC conjugated 1:80) or biotin (1:500). They were purchased from Jackson ImmunoResearch laboratories, PA, USA. All the primary and secondary antibodies were prepared in 2.5% donkey (neutral species) serum to prevent cross reactivity, 0.25% sodium azide and 0.1% triton in 0.1 M PBS. Streptavidin conjugates (reacts with Biotin-SP-conjugated antibodies and Biotin-SP-conjugated ChromePure proteins) were diluted in PBS alone. For WB, IRDye 680LT and 800CW donkey anti-goat or anti-mouse

or anti-rabbit secondary antibodies were used at the dilution of 1:10,000. They were purchased from LICOR Biosciences, NE, USA. The Bradford protein assay kit was purchased from Biorad, CA, USA. For qRT-PCR, high capacity cDNA reverse transcription kit was purchased from ThermoFisher Scientific, MA, USA; SYBR Green Master Mix was purchased from Applied Biosystems, CA, USA and the QuantiTect primer assays were purchased from Qiagen, CA, USA. We used bead-based multiplex assay (Milliplex mouse cytokine kit from Millipore MA, USA) for IL-6 and IL-12 for $Fyn^{-/-}$ and $Fyn^{+/+}$ experiments in mice and ELISA kits to determine TNFα, IL-6, IL-12 and IL-1β for saracatinib experiment in rats (ThermoFisher Scientific, USA) to determine serum cytokine levels in accordance with manufacturer's recommendations. Analytes such as anti-mouse IL-6 functional grade biotin (Cat. No. 36-7062-85) and anti-mouse IL-12 biotin (Cat. No. 13-7123- 85) were purchased from Affymetrix eBioscience, CA, USA. Appropriate neutralizing IgGs for all primary antibodies were purchased from the same source as the primary antibodies. Kits for biochemical assays such as Griess was purchased from Sigma (03553) and glutathione (STA-312) and ROS/RNS (STA-347) from Cell Biolabs, USA.

Experimental groups and drug treatment

We used 150 mice and 47 rats in this study. The animals were randomly chosen for experimental and control groups. The first group had 30 C57BL/6J mice for saracatinib experiment. In this experiment, 15 mice were treated with saracatinib (25 mg/kg, oral gavage as a single dose) at 4 h prior to a single high dose (SHD) of kainate (25 mg/ kg, i.p.), while the remaining 15 mice were given the vehicle [0.5% hydroxypropyl methylcellulose in 0.1% tween 80] 4 h prior to kainate. The second group of 20 mice (n = 10 each of fyn+/+ and fyn−/− mice)

were tested for effectiveness of SHD method of kainate (25 mg/kg, i.p.) administration to induce SE. We observed 80% mortality in the fyn+/+ and 40% in the fyn−/− mice with SHD of kainate, therefore for the rest of the experiments we followed a repeated low dose (RLD) method of SE induction with kainate (5 mg/kg, i.p., given at 30 min intervals until they showed convulsive seizures) as described previously (Puttachary et al., 2015b; Tse et al., 2014). The third group of mice (n = 6 each, fyn+/+ and fyn−/−) were used for video-EEG telemetry experiments. In this group, SE was induced 10 days after the transmitter implant after the animals recovered bodyweight. During the 10 day period of postsurgery, the baseline EEG was recorded continuously to cover both day and night cycles. The EEG recording during this period was used to evaluate the impact of surgery on spontaneous epileptiform spiking activity or seizures. The telemetry device has a built-in temperature monitoring module which gives information about their body temperature and its impact on EEG outcome. The fourth group had 88 animals (n = 12 each from fyn+/+ and fyn−/− per time-point for kainate, and 8 animals each from fyn+/+ and fyn−/− without kainate served as naïve control for all time-points). Animals were administered with a RLD of kainate and euthanized at 4 h, 24 h, and 7 d time-points. The last group of animals consisted of 47 rats, 13 implanted with telemetry device (6 for KA+vehicle; 7 for KA+SAR goup) 10 days prior to the induction of SE, with RLD of kainate, as described previously (Puttachary et al., 2016b). In all kainate-treated animals, the behavioral seizures were terminated with diazepam (5 mg/kg, i.p.) at 2 h after the first onset of convulsive seizure. The 2 h duration between the onset of convulsive seizure and the diazepam treatment was considered as 2 h established SE. During this period, all wildtype control mice and rats had continuous convulsive seizures for > 30 min. All kainate-treated animals received 1 mL of Ringer's lactate solution (s.c.) twice a day for three days to enable them to recover

from dehydration and the lost bodyweight due to SE. Out of 13 telemetry implanted rats, 6 rats served as vehicle control and the other 7 rats were treated with saracatinib (25 mg/kg). The saracatinib was administered orally starting at 2 h post-diazepam and repeated twice daily for the first three days followed by a single dose/day for the next four days during the first week of post-SE period. The rats were subjected to continuous video-EEG monitoring for a period of one month to quantify the impact of saracatinib post-treatment on epileptiform spikes and spontaneous seizures.

SE quantification

All animals administered with kainate were subjected to video recording. The seizures were staged and the SE was scored by direct observation of animals during the 2 h SE and the exact duration of each stage of seizure was calculated. The video recordings were used for secondary analysis and for independent verification of seizures by two different personnel who were not involved in direct scoring during the experiments. The person who performed the behavioral analysis were blind to the experimental groups. The behavioral seizures were scored based on modified Racine scale from stage 1 to 5 as described previously (Beamer et al., 2012; Puttachary et al., 2015b; Racine, 1972; Tse et al., 2014). The staging was as follows: stage 1, absence-like immobility; stage-2, hunching with facial or manual automatisms evident from brisk movement of vibrissae and repeated grooming of the face; stage 3, rearing with forelimb clonus and facial or manual automatisms; stage 4, repeated rearing with continuous forelimb clonus and falling; and stage-5, generalized tonic clonic convulsions with lateral recumbence or jumping and/or wild running followed by generalized convulsions. Stage 1 and stage 2 were categorized as non-convulsive seizures (NCS) and stage $\geq$3 as convulsive seizures (CS)

(Beamer et al., 2012; Puttachary et al., 2015b; Tse et al., 2014). The latency to the onset of CS and the duration of seizures were analyzed for each animal within a group as described previously (Puttachary et al., 2015b; Tse et al., 2014). The duration of CS is the total time spent by an animal in stage ≥3 during the 2 h of established SE until the diazepam was administered. Since very few animals reached stage 5 in the saracatinib pretreated group and in the fyn−/− mice, we considered stage ≥3 as the starting point for 2 h established SE. The data were analyzed and the severity of seizures, duration of CS, latency to CS onset, and mortality rate were compared between the groups.

Procedure for transmitter device implantation and video-EEG recording

The fyn+/+ and fyn−/− mice (n = 6 each) and rats (n = 7 each) were implanted with the ETA-F20 (for mice) or CTA-F40 (for rats) PhysioTel™ telemetry device (Data Science International, Minneapolis, USA) for video-EEG recording. The animals received analgesic buprenorphine (0.3 mg/kg, s.c.) prior to surgery. The animals were anesthetized with gaseous isoflurane and the mid-dorsal aspect of the head and neck were shaved and chlorhexidine scrub followed by 70% ethanol were applied using a Q-tip. The eyes were lubricated with artificial tears ointment during surgery. The surgery was performed under a sterile condition while the animal was placed on a heating mat. A mid-dorsal incision was made on the head extending from just above the mid-point of the eyes to the middle of the neck. The connective tissue was separated between the skin and muscles and a subcutaneous pocket was created along the spine and flank region, which was irrigated with sterile saline before the transmitter was inserted subcutaneously. The frontalis muscle was scraped off from the bone and bilateral burr holes were drilled (2.5 mm caudal to the bregma and 2 mm lateral to the midline) without damaging

the dura matter. Insulation from the tips of the electrode wires was removed, and the exposed electrodes were bent into a "V" shape and inserted into the holes to rest on the surface of the dura matter over each cerebral hemisphere. The wires were secured in place with dental cement (mixed with methyl methacrylate liquid compound, A-M systems, WA, USA), and the exposed electrodes were completely covered with dental cement to avoid them contacting the surrounding tissues. The incision was closed with sterile surgical clips. The triple antibiotic ointment, Vetropolycin, was applied, antibiotic Baytril (Bayer pharma, PA, 5 mg/ kg, s.c.) and 1 mL of dextrose normal saline were administered subcutaneously after the procedure. The nails were trimmed to prevent skin laceration. The telemetry device implanted animals were individually caged and placed on the PhysiolTel receivers RPC-1 connected to the data exchange matrix (specific to Dataquest A.R.T. system). The receivers detect previously matched transmitters and transmit information such as video-integrated EEG, body temperature, and activity counts from the receiver pads to the matrix and finally to the PC.

Quantification of epileptiform spikes, spontaneous electrographic NCS, and spontaneous CS

About 10 days of baseline EEG was recorded from each animal, prior to kainate treatment, which was used to normalize the EEG from post-SE period and to detect spontaneous spiking activity after surgery. The artifacts (electrical noise, exploratory behavior, grooming) were identified and excluded from epileptiform spike rate analysis. The epileptiform spikes were distinguished from artifacts based on the amplitude, duration of spikes and inter spike interval, as described in our previous publications on the mouse and rat models (Puttachary et al., 2015b and Puttachary et al., 2016b; Tse et al., 2014). After filtering

the artifacts, the raw EEG was divided into 10 s epochs for fastfourier transformation (FFT) to generate power bands. The epileptiform spikes that were quantified included the spikes from the spike trains and the NCS. The spike train consisted of both spike clusters and individual epileptiform spikes including isolated pre-ictal and inter-ictal spikes. The spike clusters (< 12 s) included the epileptiform spikes of various amplitudes above the baseline. The electrographic NCS (> 12 s), associated with increased theta and delta power were quantified separately and compared between the groups. The spontaneous NCS and CS were identified and verified against real-time video and power spectrum and quantified as described in our previous publications (Puttachary et al., 2015b and Puttachary et al., 2016b; Tse et al., 2014). The identified seizures were subjected to a secondary validation by two independent observers. The number of seizure episodes and the spike rate were quantified using NeuroScore 3.2.0 software and were expressed as standard error mean (SEM) values.

LC-MS for detection of saracatinib from the hippocampus

1. Tissue processing and chemical extraction

Based on the published literature, we selected the optimal dose of saracatinib for our experiment (Green et al., 2009; Hannon et al., 2010; Liu et al., 2012; Yang et al., 2010). However, to confirm whether it crossed the BBB and whether its levels persisted for a reasonable amount of time after the drug administration, we tested the brain concentrations of saracatinib at 8 h using liquid chromatography-mass spectrometry (LC-MS). The mice hippocampal tissues were homogenized in ~0.2 mL 1:1 methanol:water using bullet blender. An additional 125 µL HPLC grade water was added to the homogenized samples. This was followed by three similar successive extractions with 375 µL 3:1 acetonitrile:water. The

homogenate was sonicated for 10 min in a sonication water bath. The sample was pelleted by centrifugation at 13,000g for 7 min and the supernatant was collected after each extraction and the samples were pooled. The pooled supernatant was dried under a dry nitrogen gas stream. The dried sample was then re-suspended in 200 µL of 5% acetonitrile in water, filtered through a 0.2 µm PTFE syringe filter, and then subjected to LC-MS analysis.

2. LC-MS and data analysis

The LC-MS analysis for saracatinib was conducted using an Agilent Technologies 1290 Infinity Binary Pump UHPLC system coupled to an Agilent Technologies 6540 UHD Accurate-Mass Q-TOF mass spectrometer in high resolution mode (4Gz) and scanning m/z 100–1700. LC separations were performed with Agilent Technologies Eclipse C18 1.8 µm 2.1 mm × 50 mm analytical column using an 18 min gradient from 100% buffer A (0.1% formic acid in HPLC grade water with 1% HPLC grade acetonitrile) to 100% buffer B (0.1% formic acid in HPLC grade acetonitrile with 1% HPLC grade water) followed by a 2 min hold in 100% buffer B and a 3 min equilibration in 100% buffer A. Saracatinib was detected as [M + H]+ ions while using electrospray ionization in positive mode. Saracatinib detection is represented by extracted ion chromatogram (EIC) using a 10 ppm extraction window and was analyzed (Fig. 1E) using Agilent Mass Hunter Qualitative Analysis B.07.00 software. The X-axis on the EIC represents retention time and the Y-axis represents the abundance of ions detected. Saracatinib concentrations were observed as the area of the EIC peaks and was calculated based on the linear curve of the observed peak areas of standards. The standard concentrations ranged from 10 femtograms/ mL to 1 microgram/mL.

Tissue processing, immunohistochemistry, imaging, and cell quantification

Animals in the mice telemetry group were euthanized at the end of 4 weeks and non-telemetry group at 4h, 24h and 7 d post-SE, while rats in the telemetry group were euthanized at 4 month post-SE and non-telemetry group at 7 d post-SE. The brains were isolated and processed for IHC, WB, ELISA, biochemical assays and qRT-PCR studies. The serum samples were used for ELISA, cytokine and other biochemical assays. Serum was collected using the standard 'serum preparation protocol' from ThermoFischer Scientific. All animals were euthanized with an overdose of pentobarbital sodium (100 mg/kg, i.p.). For IHC, animals were transcardially perfused with 4% PFA in 0.1 M PBS (4% PFA in 0.1 M PBS) under terminal anesthesia. The tissues were collected and postfixed in the same solution for 4 h at 4 °C. After 4 h, they were cryopreserved in 25% sucrose solution for 3–4 days at 4 °C (Cosgrave et al., 2008). The tissues were then embedded in gelatin (15% type A gelatin, 7.5% sucrose, and 0.1% sodium azide in PBS, Sigma, MO, USA), wrapped in the cling film, and stored overnight at 4 °C. The gelatin embedded tissue blocks were prepared by snap-freezing in the liquid nitrogen, using isopentane, and were then stored in −20 °C prior to cryosectioning (Beamer et al., 2012; Cosgrave et al., 2008). The coronal brain sections, 16 μm thickness, from the tissue block were cut using CryoStar NX70 cryostat (specimen head temperature −20 °C; blade temperature −16 °C; trim section thickness 30 μm; ThermoFischer Scientific, MA, USA). The sections were collected on chrome alum gelatin (Pfaltz and Bauer, CT, USA) coated slides. The details of brain section sampling method, to represent different regions of the hippocampus (rostral to caudal) on a slide, has been described in our previous publication (Puttachary et al., 2016a). The sections were then either processed for IHC immediately or were stored in −20 °C for later use. Prior to IHC, antigen retrieval was performed on the brain sections using citrate buffer (10

mM citric acid, 0.05% tween 20, pH 6.0) for 20 min at 95–100 °C. The sections were washed with 0.1 M PBS for an hour at room temperature (RT) followed by incubation with 10% donkey serum in PBS. The sections were then incubated with primary antibodies of interest (Fyn, PKCδ, 4-HNE, $gp91^{phox}$, IBA1 and GFAP) overnight at 4 °C (48 h for NeuN). All new batches of primary antibodies were titrated to determine the optimum concentration. In addition to neutralizing IgG antibodies against primaries, primary antibody omission step was run as a negative control. Next day, the sections were washed with PBS for an hour at RT and probed with appropriate secondary antibodies (FITC or CY3 conjugated, or biotinylated), for an hour, at RT followed by subsequent washing with PBS and then treated with streptavidin CY3 (only biotinylated ones) for an hour. The sections were washed in PBS, and finally with water to remove salt crystals and coverslipped with vectashield containing 4′,6-diamidino-2-phenylindole (DAPI) for nuclear staining. To observe the extent of neurodegeneration in the hippocampus, we did FJB-NeuN double staining. The brain sections were first stained with NeuN followed by FJB staining as described earlier (Puttachary et al., 2016b; Rao et al., 2006; Todorovic et al., 2012). For FJB staining, the sections were incubated in 0.006% potassium permanganate solution for 5–10 min with slow shaking. They were thoroughly washed twice with distilled water for a minute. The slides were submerged in 0.0003% FJB-0.1% acetic acid solution for 10 min in dark followed by 3 washes for 1 min each. The slides were air-dried in the dark at RT, cleared with xylene and then mounted with surgipath acrytol (Surgipath, Leica Biosystems, IL).

For imaging, we used Axiovert 200 M Zeiss inverted fluorescence microscope equipped with Hamamatsu camera (Zeiss, Deutschland, Germany). Images were captured using HCImage live 4 software (Hamamatsu Corporation, Sewickley, PA). The software has

the capability to measure a large number of parameters related to size, shape, intensity, and position. All the images were taken at 20× magnification at 2 s exposure. ImageJ was used to quantify the cells from a known area (in square microns) (Schneider et al., 2012). Bilateral cell counts were done from minimum of four sections per animal as described in our previous publications (Beamer et al., 2012; Cosgrave et al., 2008, 2010a and 2010b; Puttachary et al., 2016a and Puttachary et al., 2016b). The areas of cell counting for all sections on a slide and from all the groups were kept constant. The NeuN positive cells with FJB staining were counted to determine neurodegeneration. IBA1, GFAP and NeuN positive cells with Fyn/ PKCδ in the nucleus and/or cytoplasm alone were quantified to determine microgliosis and astrogliosis. The DAPI staining was used to mark nuclei. Since there is no consensus on reliable and reproducible markers for reactive microglia and astrocytes, so we considered the area of cell body, the number of branches, and the junctions to distinguish reactive microglia and astrocytes (also referred by some as M1-type and A1-type microglia and astrocytes) from the resting or alternative type microglia and astrocytes (often referred by some as M2-type and A2-type) (Andersson et al., 1991; Block, 2014; Torres-Platas et al., 2014; Walker and Lue, 2015). Initially, we derived these parameters from the resting microglia and astrocytes in the control brain section from a known area (e.g. CA3 region) to compare with reactive microglia an astrocytes derived from a similar area in the kainate treated groups at various time-points. To consider a reactive microglia and atrocytes as positive for Fyn or PKCδ in the cytoplasm or in the nucleus, we first set the threshold for cytoplasm and nucleus separately. The percentage of reactive microglia and astrocytes were derived from the total number of IBA1 and GFAP positive cells. We further calculated the percentage of nuclear Fyn or PKCδ positive

reactive microglia from the total Fyn and PKCδ positive reactive microglia (for $Fyn^{-/-}$ and $Fyn^{+/+}$ experiment only).

Western blotting

The hippocampal tissues were dissected from both fyn+/+ and fyn−/− animals at 4 h, 24 h and 7 d and from rats at 7 d and 4 month time points immediately after euthanasia and were snap frozen in liquid nitrogen. The tissues were homogenized and lysed in RIPA buffer containing 1% protease and phosphatase inhibitors (ThermoFischer Scientific, USA). For cell fractionation and protein extraction from cytoplasm or nucleus, we used the kit and standard protocol from ThermoFischer Scientific (NE-PER™ Nuclear and Cytoplasmic extraction reagents; catalog number 78833). The hippocampal tissues were homogenized in 200 µl of cytoplasmic extraction reagent I (CER I). The samples were vortexed vigorously for 15 s to suspend the pellet followed by incubation in ice for 10 min. After incubation, 11 µl of cytoplasmic extraction reagent II (CER II) was added followed by repeated vortexing and ice incubation steps. The samples were then centrifuged at 16,000 xg for 5 min. The supernatant (cytoplasmic extract) was collected and the pellet was re-suspended in 100 µl of ice-cold nuclear extraction reagent (NER) followed by repeated vortexing for 15 s and ice incubation for 10 min for the total of 40 min. The samples were then centrifuged at 16,000 xg for 10 min. The supernatant (nuclear extract) was collected and stored in −80 °C for later analysis. The protein concentration from tissue lysates were determined using the Bradford assay kit (Biorad, USA). Equal amounts of protein (40 µg) was loaded in the wells of precast gels along with the molecular weight marker. The gels were run at 100 V for 1–2 h at RT until the bromophenol dye reached at least 0.5 cm from the bottom of the plate. The proteins were transferred onto

the nitrocellulose membrane and the transfer sandwich was placed into a mini transfer blot unit (Biorad, USA) at 4 °C overnight at 25 V for 14 h according to the manufacturer's instructions. Next day, the membrane was washed with PBS and 0.05% tween 20 (PBS-T) for 1 h followed by blocking with Fluorescent Western Blot blocking buffer (to avoid non-specific binding) (Rockland Immunochemicals, PA, USA) in PBS at RT. After the blocking step, the blots were washed twice for 15 min each with PBS-T and probed with primary antibodies of interest overnight at 4 °C. The following day, the membrane was incubated with IR-680 or IR-800 dyes (1:10,000, LiCor, USA) followed by further washes with PBS-T as described earlier. The β-actin was used as a loading control for cytosolic fractions and lamin-B for nuclear fractions. Fluorescent Western Blotting blocking buffer with 0.05% tween 20 was used as a diluent for both primary and secondary antibodies. The bands were identified using Odyssey IR imaging system and were quantified using image J software and normalized with the β-actin.

qRT-PCR

RNA was extracted using the trizol chloroform (ThermoFisher Scientific) extraction method as described previously (Cosgrave et al., 2008; Seo et al., 2014). One microgram of RNA was used for reverse transcription using High Capacity cDNA Reverse Transcription Kit (Applied Biosystems, CA) yielding high quality single stranded cDNA. Quantitative RT-PCR was performed for the following genes using SYBR Green Mastermix (Applied Biosystems, CA, USA) with pre-validated qPCR primers. Primers for IL-1β, iNOS, and TNF-α were purchased from QuantiTect Primer Assay (Qiagen, USA). The house keeping gene, 18S rRNA (Qiagen, MD, USA), was used in all qPCR experiments for normalization. No-template controls (NTCs) and dissociation curves were obtained for all experiments to exclude cross-

contamination. The fold change in the mRNA expression was determined using cycle threshold (Ct) values for the genes of interest and also for the housekeeping genes.

Multiplex cytokine immunoassays

Cytokine levels were assessed from the serum of Fyn knockouts and wildtype animals using Luminex assay kit as described previously (Panicker et al., 2015). A five-fold dilution of serum was made with 0.1 M PBS containing BSA. 40 µL of diluted serum was then added to the equal amount of primary antibodies, conjugated to magnetic microspheres, followed by overnight incubation at 4 °C in a clear bottom black 96-well plate. After incubation, each well was triple-washed using a magnetic washer and then incubated for an hour with secondary antibodies followed by three secondary washes. The samples were incubated for 30 min with streptavidin/phycoerythrin followed by two additional washes. All assays were done in duplicates and previously known positive control and a negative control without primary antibodies were used simultaneously with the test samples. A Bioplex reader was used to read the 96-well plates. A standard curve of all the cytokines was prepared using standard cytokines (Peprotech).

ELISA

Cytokine levels were detected in the serum of Sprague Dawley rats using ELISA kit from ThermoFischer Scientific. 100 uL of 1X coating buffer and antibody of interest was added to Nunc MaxiSorp 96 well plates and were stored for 16 hours at 4°C. The following day, contents were discarded from the well plates and washed three times with 1X PBS in 0.1% tween 20 (PBS-T). 200 uL of 1X blocking buffer was added to all the wells and incubated at

RT for 1 hour. Recombinant standards and samples were then added in duplicates using serial dilutions (only for standards) as described in the manufacturer's protocol. Standards and samples were incubated for 2 hours at RT. After 3 washes with PBS-T, detection antibody was added to all the wells and incubated for 1 hour at RT followed by 3 washes. HRP-avidin was then added to all the wells and left in the dark for 30 minutes at RT. After 5 washes, 100 uL of 1X TMB was added to all the wells. This step should be done quickly as TMB has very high reactivity towards other chemicals. After 15 minutes of TMB incubation, 50 uL of 2N H_2SO_4 was added to all the wells. Plates were read at 450 nm using SpectraMax M2 Gemini Molecular Device Microplate Reader.

Griess Assay

Griess assay was used to detect nitrite levels from the serum samples. Briefly, 6 serial two-fold dilutions of 0.1M sodium nitrite standard solution was made in triplicates to generate nitrite standard curve. 50 uL of serum (diluted or undiluted) was added in triplicates followed by equal amounts of sulfanilamide solution to all the wells. The plates were incubated for 10 minutes in the dark at RT. Next, 50 uL of NED solution was added to the mixture and was again incubated for 10 minutes at RT protected from light. Plates were read at 540 nm using Synergy 2 multi-mode microplate reader (BioTek Instruments, USA) and the averages were compared between the groups using ANOVA.

Glutathione Assay

Glutathion assay was used to quantify total glutathione content, ie., reduced and oxidized (GSH/GSSG), within the sample. Glutathione reductase converts oxidized

glutathione (GSSG) into reduced glutathione (GSH) in the presence of $NADP^+$. Chromogen attaches to the thiol group of GSH to give a coloured compound that can be detected at 405 nm. Briefly, GSH standards are prepared by dissolving stock GSSG in 0.5% MPA in 1X assay buffer. 25 uL of GSH reductase followed by equal concentration of 1X NADPH was added to each well to be tested. Serial dilutions of GSH standards were prepared in triplicates as described in the manufacturer's instruction protocol. 100 uL of standards and sample were added to the wells that were to be tested. Finally, 50 uL of 1X chromogen was added to all the wells and mixed thoroughly. Plates were read at 405 nm at 2 minute intervals for 10 minutes using Synergy 2 multi-mode microplate reader (BioTek Instruments, USA).

ROS Assay

Reactive oxygen species (ROS) assay determines the presence of total free radical in the sample. These include hydrogen peroxide, peroxyl radical, nitric oxide, peroxynitrite anion and other redox molecules. DCFH-DiOxyQ is ROS/RNS specific probe which undergoes quench priming with the help of priming solution to form DCFH-DiOxy. This molecule is then stabilized to form DCFH which is highly reactive with ROS/RNS, present in the sample. DCFH then gets oxidized to give highly fluorescent DCF. Briefly, standards, solutions and samples were prepared fresh prior to the experiment. Serial dilutions of DCF and H_2O_2 standards were prepared as described in the manufacturer's protocol. 50 uL of sample and H_20_2 standard were added to the wells. Next, 50 uL of 1X catalyst was added to each well and incubated for 5 minutes at RT. 100 uL of DCFH solution was then added to all the wells to be tested and incubated in the dark for 40 minutes. DCFH solution was prepared by mixing DCF-DiOxyQ stock with priming reagent and then diluting the mixture with 1X stabilization

solution. Plates were read at 480 nm excitation/530 nm emissin using SpectraMax M2 Gemini Molecular Device Microplate Reader.

Experimental design, methodological rigor, and statistical analyses

Medicine, Iowa State University, for experimental design and statistical analyses for this study. We chose the most appropriate control (strain of mice or the vehicle) and statistics for each set of experiments. For example, for the saracatinib experiment to determine its anti-seizure property, we used C57BL/6J mouse kainate model of seizure. For the KO experiments, the same genetic background for the fyn−/− mice and the wildtype control mice were used. To determine saracatinib's antiepileptogenic or disease modifying effects, we chose the rat kainate model and post-SE treatment regimen since pretreatment reduces SE severity and compromises epileptogenesis. In the rat kainate model, in contrast to the mouse model, occurrence of spontaneous CS is reliable and progressive (Puttachary et al., 2016b).

The experimenters were blind to the experimental groups until the data analyses were completed. Transgenic mice genotyping was done using qRT-PCR to confirm the gene knockout. We followed pre-determined criteria to exclude animals from data analyses. The criteria set were: i) if animals do not respond to the predetermined kainate dose (a maximum of six doses of 5 mg/kg in RLD method; 25 mg/kg in SHD method); ii) if animals die during the course of experiment; and, iii) in telemetry group if animals do not regain bodyweight within 8–10 days. We had taken measures to minimize variables by: i) randomizing the animals based on predetermined weight (≥20 g mice or ≥200 g rat) and age range (8 weeks) before the start of experiment; ii) seizure severity during the SE was quantified by both direct observation and offline video analysis by at least two independent observers; iii) we acquired ~260 h of

baseline EEG data, covering at least 10 day-night cycles, to normalize post-SE EEG from the same animal; iv) where appropriate, we implemented the first two of the three principles of reduction, refinement, and replacement (3Rs) by adopting a refined RLD method of SE induction, which reduced mortality rate and minimized variability in SE severity between animals and groups; and, v) we determined the optimum concentration of the primary antibodies by serial dilution and validated their specificity using neutralizing antibodies appropriate to the primary antibodies.

For statistical analyses, we compared the standard error means between the groups using the Fisher's exact test, the Mann-Whitney test, one-way ANOVA with Bonferroni multiple comparison or Tukey post-test or repeated measures (RM) two way ANOVA with Sidak or Tukey post-test where appropriate. For example, RM two-way ANOVA with appropriate degrees of freedom was used to calculate seizure frequency since they do not follow a normal distribution (Figs. 1A; 2D; 3F, I; 4B-C; 5E, K, M; 7G-I; 10G-I; 15M-N; 16D). Further information on statistical test/s for each figure is described in legends. We used the GraphPad Prism 5 and 6 and R-studio version 1.1.463 for all statistical analysis. The p-value ≤ 0.05 was considered statistically significant.

Results

The Fyn/SFK inhibitor, saracatinib significantly reduced the severity of SE and prevented mortality during SE

The saracatinib is a broad spectrum SFK inhibitor (Green et al., 2009; Hennequin et al., 2006), and is in the clinical trials for treating Alzheimer's disease (Nygaard et al., 2015). Since saracatinib also targets the hippocampus, an important ictogenic foci of the brain, we

tested it's impact on SE onset. Saracatinib (25 mg/kg) or the vehicle was administered orally as a single dose at 4 h prior to the induction of SE with kainate. The dose was selected based on the published literature (Green et al., 2009; Hennequin et al., 2006). We tested the effect of a SHD of kainate (25 mg/kg) on behavioral seizures onset, and compared the seizure severity, duration of convulsive seizures, latency, and survival rate between the groups. The studies revealed a significant reduction in seizure severity and the duration of CS, and increased latency to the onset of first CS in the saracatinib treated mice when compared to the vehicle control group during the 2 h established SE (Fig. 1A–C).

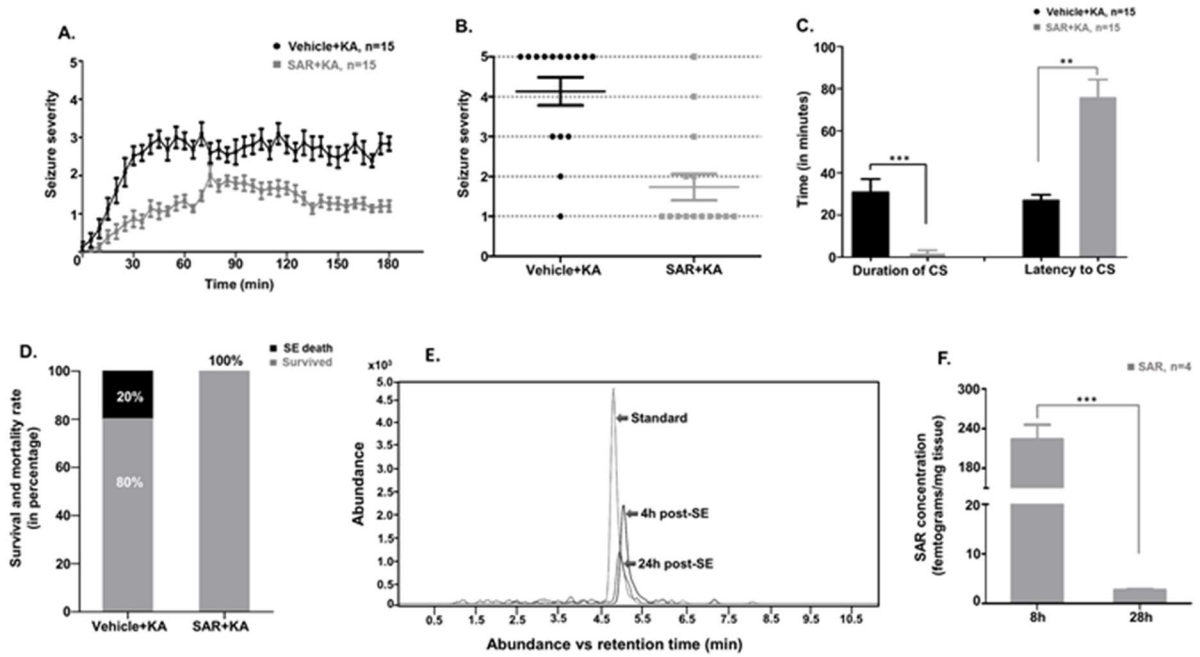

Fig. 1. The saracatinib (SAR) crossed the BBB, increased latency to seizure onset, and reduced seizure severity and mortality rate in C57BL/6J mice. The SAR (25 mg/kg) was administered orally 4 h prior to a SHD of kainate (25 mg/kg, i.p.). A, B) The comparison of the time course of behavioral SE between the groups (A) during the first 3 h after kainate injection (***$p < 0.0001$, two way ANOVA between 1 and 1271 degrees of freedom, $F = 502.65$, $n = 15$). In B, each dot represents individual animal. C) The SAR treated group showed a significant reduction in the duration of CS (***$p < 0.0001$), and a very few mice reached stage ≥3 seizure after a prolonged period when compared with the vehicle treated group (**$p < 0.01$). D) The survival and mortality rate in SAR and the vehicle treated mice (Fisher's exact test). E, F) The ion chromatogram showing the relative abundance of the SAR in the hippocampus. The LC-MS analysis confirmed that the SAR crossed the BBB and it persisted in the hippocampus at higher levels at 8 h post-SE when compared to 28 h post-administration (***$p < 0.001$). *$p < 0.05$, **$p < 0.01$, ***$p < 0.001$; Mann-Whitney test for figure B, C, and F.

There was no mortality in the saracatinib treated group due to a significant reduction in the severity of seizures. As expected, about 20% mortality occurred in the vehicle-treated control group due to severity of kainate-induced seizures (Fig. 1D). In the SHD of kainate group, 67% of the mice reached stage 5 seizure in the vehicle group, while only 7% reached stage 5 and they spent less time in CS stages in the saracatinib group (Fig. 1B) suggesting the role of Fyn and other SFK in seizure modulation. LC-MS analysis of the hippocampi confirmed that the saracatinib crossed the BBB and it persisted at high levels at 8 h (223.8 ± 22.01), and were also detected at 28 h post-administration (2.693 ± 0.1714) ($r^2 = 0.9665$; ***$p < 0.0001$) (Fig. 1E–F).

Fyn knockout reduced SE severity, mortality, epileptiform spikes, and spontaneous NCS and CS during the first 4 weeks of post-SE

Having observed a significant reduction in SE severity with saracatinib treatment, we tested further whether Fyn kinase has a role in the mechanism of seizure onset. We used fyn−/− and the wildtype control mice for SE induction. First, similar to saracatinib experiment, we used a SHD of kainate (25 mg/kg) for both fyn−/− and fyn+/+ mice. Interestingly, unlike the vast majority of C57BL/6J mice, the fyn+/+ hybrid mice did not show a progressive seizure pattern from stage 1 to 5, instead the majority of them (90%) directly reached stage 5 seizures in < 20 min of kainate administration, and 80% of them died during SE (Fig. 2A–B). In contrast, fyn−/− mice showed fewer episodes of stage 5 seizures in 30% of the mice, but mortality rate was 40% (Fig. 2B) even after diazepam administration. Animals that had severe SE, during the 2 h of established SE, excessive salivation was observed more frequently in fyn+/+ mice than in fyn−/− mice. Another interesting observation was their sensitivity to diazepam treatment. Both fyn+/+ and fyn−/− mice took longer time to recover from the

diazepam (almost 12 h) compared to C57BL/6J mice with the same dose (10 mg/kg) and they recovered in < 3 h after diazepam treatment.

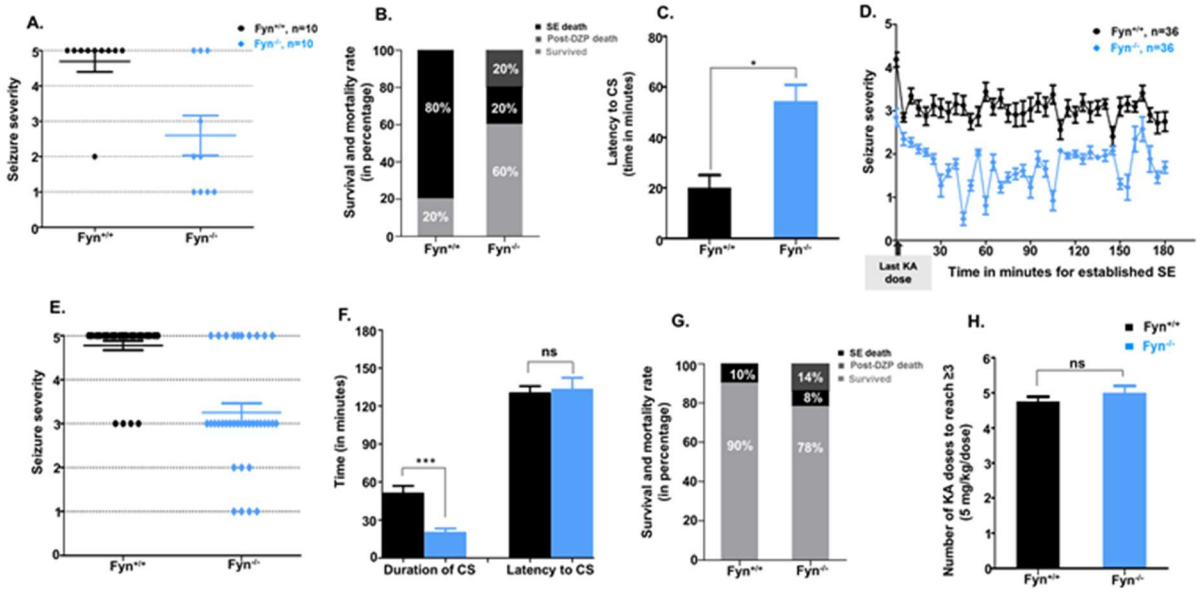

Fig. 2. Comparison of seizure severity and its duration, and mortality rate in fyn+/+ and fyn−/− mice in SHD (A–C) and RLD (D–H) of kainate treatments. A) Each dot represents individual animal. The fyn−/− mice showed a significant reduction in seizure severity compared to the fyn+/+ mice (**p < 0.01, Mann-Whitney, n = 10 for each group). B) The survival and mortality rate in fyn+/+ and fyn−/− mice (*p < 0.05, Fisher's exact test). Of the total 40% mortality, about 20% was observed after the diazepam treatment in the fyn−/− mice. C) The latency to convulsive seizures (CS) onset, following a SHD of kainate, was significantly increased in fyn−/− when compared to fyn+/+ mice (*p < 0.05, Mann-Whitney). D) The comparison of the time course of behavioral SE between the groups during 2 h established SE after mice reached first stage ≥3 seizure (***p < 0.0001, two way ANOVA between 1 and 2072 degrees of freedom, F = 839.67, n = 36 for each group). In E, each dot represents individual animal (***p < 0.0001, Mann-Whitney). FeH) The fyn−/− mice showed a significant reduction in the duration of CS (F, ***p < 0.001, Mann-Whitney), and there was no significant difference in the latency to the onset of CS. In fyn−/− mice, 22% mortality was observed (8% during the SE and 14% post-diazepam), while in the fyn+/+ mice 10% of the mice died during the SE, but none died after the diazepam treatment (G, not significant, Fisher's exact test). H) There was no significant difference in the average numbers of RLD of kainate injections (5 mg/kg per injection at 30 min intervals) given to the fyn+/+ and fyn−/− mice to achieve stage ≥3 seizure.

Since there was increased mortality rate in both fyn+/+ and fyn−/− mice with SHD of kainate, we used RLD of kainate method to reduce mortality and to understand seizure progression during SE. We pooled the SE behavioral data from all time-points in non-

telemetric groups and compared between the fyn+/+ and fyn−/− mice. Both groups received similar numbers of RLD of kainate, therefore there was no significant difference in the total amount of kainate administered between the groups to reach convulsive seizures (Fig. 2H). Also, there was no significant difference between the groups in latency to the first onset of convulsive seizure (Fig. 2F), but there was a significant reduction in the seizure severity (Fig. 3A–C). Interestingly, the mortality rate in fyn−/− mice was higher than fyn+/+ mice (22% vs. 10%; Fig. 2G) with the RLD method of SE induction with kainate, which was unexpected. Out of 22% mortality in the fyn−/−, 14% was after diazepam treatment.

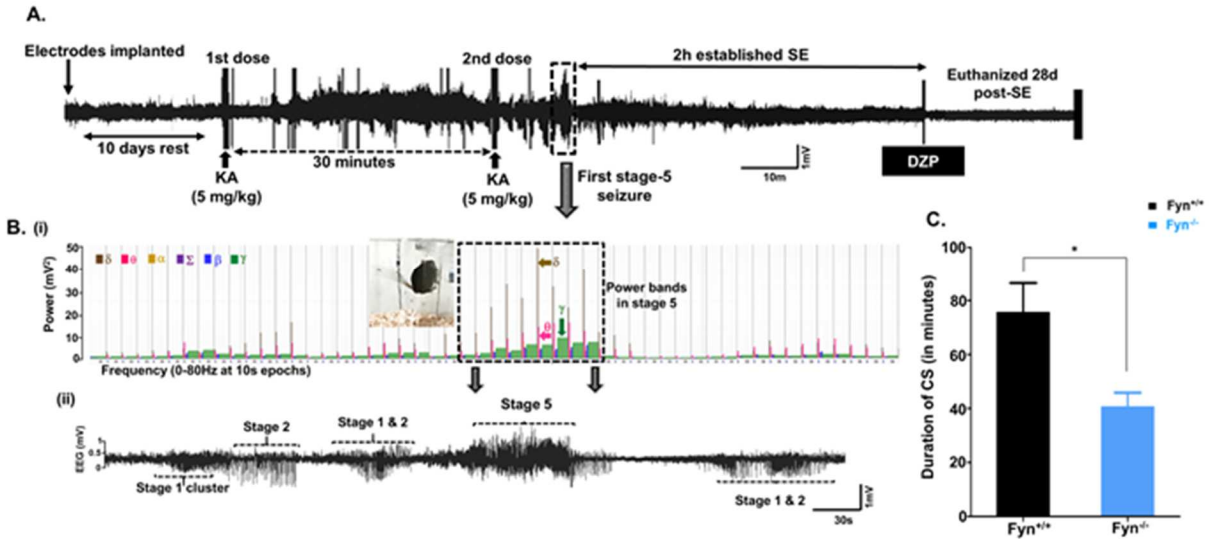

Fig. 3. Real-time video-EEG recording and duration of CS during SE. A) A representative EEG trace recorded during the SE induced by a RLD of kainate is presented. The behavioral SE was terminated by diazepam (10 mg/kg, i.p.), 2 h after the onset of first CS. B) A segment of the EEG trace covering the stages of seizures before & after the stage 5 seizure & the associated seizure stage-specific power bands are illustrated. The theta and delta power were increased in NCS, while the gamma power was increased during the stage 5 seizure, and the image represents the stage 5 behavior (jumping). C) The duration of CS for EEG seizures (stage ≥3) during the 2 h established SE was significantly lower in the fyn−/− mice when compared to the fyn+/+ mice (*$p < 0.05$, Mann-Whitney test, n = 6 for each group).

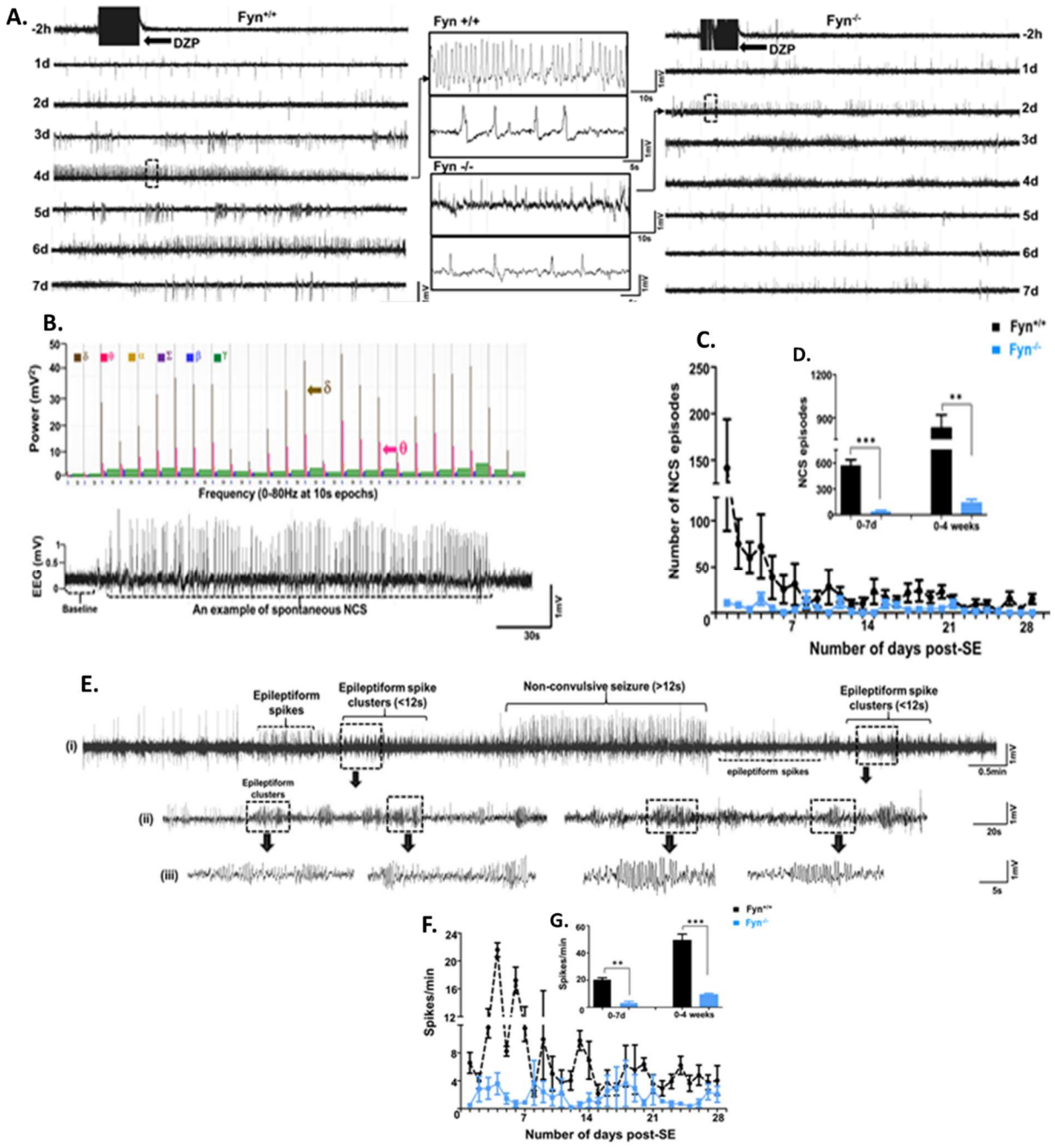

Fig. 4. Analyses of epileptiform spike and spontaneous NCS. A, B) Representative EEG traces and epileptiform spikes during the first 7 d post-SE (A), & a typical spontaneous NCS episode with associated power bands (B). C, D) The comparison of NCS frequencies between the fyn−/− and fyn+/+ mice during 28 d post-SE (C, ***$p < 0.0001$, two way ANOVA between 1 & 140 degrees of freedom, $F = 35.17$, $n = 6$ per group; D, **$p = 0.0016$, ***$p < 0.001$, Mann-Whitney). E) An example of spike trains with spike clusters (< 12 s), a typical NCS episode (> 12 s), & isolated epileptiform spikes. F–G). The comparison of epileptiform frequencies between the fyn−/− and fyn+/+ mice during 28 d post-SE.

The telemetry implanted mice were subjected to continuous (24/7) video-EEG monitoring to quantify epileptiform spikes and spontaneous seizures frequency during the first four weeks of post-SE. Prior to kainate administration, none of the mice showed epileptiform spike or seizure during the first 10 d post-surgery. A representative EEG traces during the SE (Fig. 3A) and post-SE between fyn+/+ and fyn−/− mice (Fig. 4A) are shown. Increased delta and theta powers, and decreased gamma power were correlated with the epileptiform spike characteristics on EEG in NCS (Fig. 4B). During the SE, there was about 50% reduction in the duration of CS in the fyn−/− mice when compared to the fyn+/+ mice (Fig. 3C). Unlike the C57BL/6J mice reported in our publication (Puttachary et al., 2015b), the number of spontaneous CS were very few (average 5 episodes) in the fyn+/+ and spontaneous CS were completely absent in the fyn−/− mice. Therefore, we quantified electrographic NCS and the epileptiform spike frequency in both groups as described previously in our publication (Puttachary et al., 2015b). We considered spike trains and the epileptiform spikes within seizure clusters (< 12 s duration) to determine the epileptiform spike frequency. An example of an electrographic NCS, the spike train, and spike clusters is illustrated (Fig. 4E). During the 28 d post-SE, both spontaneous electrographic NCS and the epileptiform spikes frequencies were significantly reduced in fyn−/− when compared to fyn+/+ mice (Fig. 4C–D, F–G).

CSSS index to determine severity of SE in telemetry and non-telemetry rats in KA and KA+SAR group

Repeated low doses of kainate was given to both telemetry and non-telemetry rats until convulsive seizure, ie., ≥3 was achieved as described in our previous publications (Puttachary et al., 2015b, 2016a and 2016b). The seizure severity was very similar between the groups

(Fig. 5A-C). Animals in the 7 d non-telemetry vehicle group showed almost similar seizure severity compared to animals in the 7 d non-telemetry SAR group, except at 35, 45, 60, 65, 70, 160 and 230 min (B). The electrode implantation is known to induce electrode gliosis in some animal models (Griffith and Humphrey, 2006; Polikov et al., 2005; Salatino et al., 2017), therefore, telemetry rats were given slightly lower doses of kainic acid compared to non-telemetry rats (Fig. 5D). Also, the latency to reach convulsive seizure in telemetry rats was

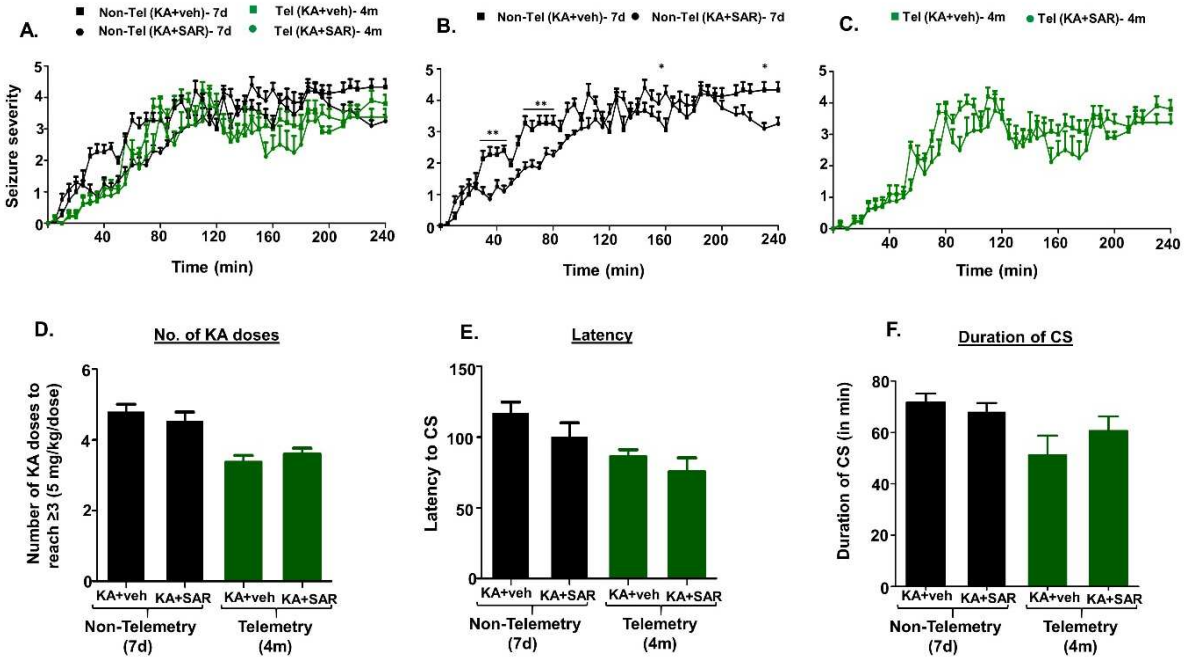

Fig. 5. Seizure severity, latency and duration of convulsive seizures during SE. A) Seizure severity between telemetry and non-telemetry groups according to the modified Racine scale. Seizure severity comparison between the 7 d non-telemetry (B) (***$p < 0.0001$, Repeated measures-two way ANOVA between 1 and 1518 degrees of freedom, $F = 44.52$, $n = 10$ for each group) and 4 month telemetry group (C). Animals with impanted electrodes required slightly lesser doses of kainate than non-telemetry animals (D) and also showed early convulsive seizures than non-telemetry group, but the differences were not statistically significant (E). Rats in non-telemetry group spent more time in convulsive seizures than the rats in telemetry group (F). **$p < 0.01$, ***$p < 0.001$, RM-two way ANOVA with Sidak's post-hoc. There were no significant differences between the groups in latency or the duration of CS.

higher compared to non-telemetry rats (Fig. 5E). The amount of time spent in convulsive seizures during 2h of SE was slightly greater in non-telemetry group, ie., >60 minutes, maybe

due to higher kainate doses, than telemetry group, but there was no significant difference between these groups (Fig. 5F) suggesting that the surgical procedure to implant electrodes may not lead to increased seizure severity, but reduced the seizure threshold.

Saracatinib suppressed epileptiform events during the first seven days of treatment

Saracatinib treatment was initiated 2 hours after DZP (5 mg/kg, i.p.). It was given twice a day for 3 days followed by once a day for 4 days (25 mg/kg, oral). Animals were euthanized at early (7 day) and late (4 month) time-points post-SE. EEG signatures of all the epileptiform events (epileptiform clusters, interictal events and epileptiform spikes) and spontaneous convulsive (CS) and non-convulsive (NCS) seizures were quantified to understand the evolution of epileptogenesis (table 1 and 2; Fig. 6A, B, Fig. 7A). Animals with severe SE (RT104, RT103, RT3, RT108, row 3 of table 1), ie., the animals that spent more time in convulsive SE, showed higher numbers of epileptiform events (preictal events and clusters, row 4 and 5 of table 1) and NCS (row 7, table 1) after SE. Animals with mild seizures (RT107 and RT4) had lower number of epileptiform events and only one animal (RT107) developed NCS in that group (row 6, table 1). Interestingly, all the animals that showed spontaneous CS later (row 13, table 1), also showed multiple spontaneous NCS (except RT4). Moreover, animals with severe SE had higher number of epileptiform events compared to mild SE (row 12, table 1). This suggests that, 1) the severity of SE determines the number of epileptiform spikes, especially interictal events, 2) Animals had several NCS prior to the onset of first CS (with the exception of one animal, ie., RT4), 3) Persistant interictal events, epileptiform clusters and spontaneous NCS are equally important components of of epileptogenesis and epilepsy (Sharma et al., 2018; table 1).

Table 1. EEG events during the latent period prior to the onset of 1st CS: KA+Vehicle group

Animal number	RT104	RT103	RT3	RT108	RT107	RT4
	KA+vehicle					
Time spent in SE (in mins)	93	80	70	68	41	32
Preictal events before 1st NCS	234	220	249	121	95	*
Number of epileptiform clusters before 1st NCS	35	219	112	89	49	*
1st NCS episode observed post-SE (number of days)	2d	3d	7d	2d	9d	*
Total number of NCS episodes before 1st CS	2	27	12	15	4	*
Number of interictal events after 1st NCS (before 1st CS)	169	160	19	190	39	79
Number of epileptiform clusters after 1st NCS (before 1st CS)	67	59	13	71	11	8
Total number of interictal events before 1st CS (includes all events)	403	380	268	311	134	79
Total number of epileptiform clusters before 1st CS (includes all clusters)	102	278	125	160	60	8
Total of all the epileptiform spikes (preictal and postictal events and epileptiform clusters)	505	658	393	471	194	87
1st CS episode post-SE (number of days)	4d	5d	7d	7d	10d	38d

Development of first spontaneous convulsive seizure after SE in the vehicle group. EEG events prior to the 1st CS development in six rats after the induction of SE. All the epileptiform events such as epileptiform clusters, interictal spikes and NCS were quantified before the onset of 1st CS. Animals that spent more than 50% of their time in convulsive SE (RT104, RT103, RT3, RT108- row 3) showed higher number of epileptiform clusters (row 11) and interictal events (row 10) than animals that spent less time in convulsive SE (RT107, RT104- row 3). The total number of these events were very high in the severe SE group than the mild seizure group (row 12). The most striking observation is that the vast majoriy of animals (5 out of 6) developed NCS (row 6) prior to the 1st CS (row 13). All the animals that showed severe seizures also showed early convulsive seizures.

Table 2. EEG events during the latent period prior to the onset of 1st CS: KA+SAR group

Animal number	RTSAR4	RTSAR5	RTSAR9
	KA+SAR		
Time spent in SE (in mins)	81	73	66
Preictal events before 1st NCS	*	115	*
Number of epileptiform clusters before 1st NCS	*	39	*
1st NCS episode observed post-SE (number of days)	*	2d	*
Total number of NCS episodes before 1st CS	0	1	0
Number of interictal events after 1st NCS or before 1st CS	101	36	177
Number of epileptiform clusters after 1st NCS (before 1st CS)	78	3	112
Total number of interictal events before 1st CS (includes all events)	101	151	177
Total number of epileptiform clusters before 1st CS (includes all clusters)	78	42	112
Total of all the epileptiform spikes (preictal and postictal events and epileptiform clusters)	179	193	289
1st CS episode post-SE (number of days)	7d	4d	11d

Development of first spontaneous convulsive seizure after SE in SAR treated group. SAR treatment was initiated 2h post diazepam and continued for twice a day for 3 days and then once a day for the next 4 days. Only 3 animals, out of 7, became epileptic in this group. The total number of epileptiform events after SAR treatment (row 12) were lower than the vehicle treated group (table 1, row 12). Only 1 animal showed NCS (just 1 NCS, row 7) in this group in contrast to vehicle treated group (between 2-27, row 7, tabl 1) prior to 1st CS, which later showed spontaneous convulsive seizure on the day 4 of post-SE (row 13).

Saracatinib post-treatment, given for the first 7 days of post-SE, reduced these epileptiform events (row 12, table 2) and the development of spontaneous NCS which was observed in only in one animal (row 6, table 2). Moreover, only 3 animals out of 7 showed spontaneous CS as shown in table 2 (row 13; Fig. 5B). Spontaneous NCS and CS were verified by power bands, EEG spike signature and video-EEG as described in our previous publications (Puttachary et al., 2015b, 2016a and 2016b) and as shown in Fig. 7A-B.

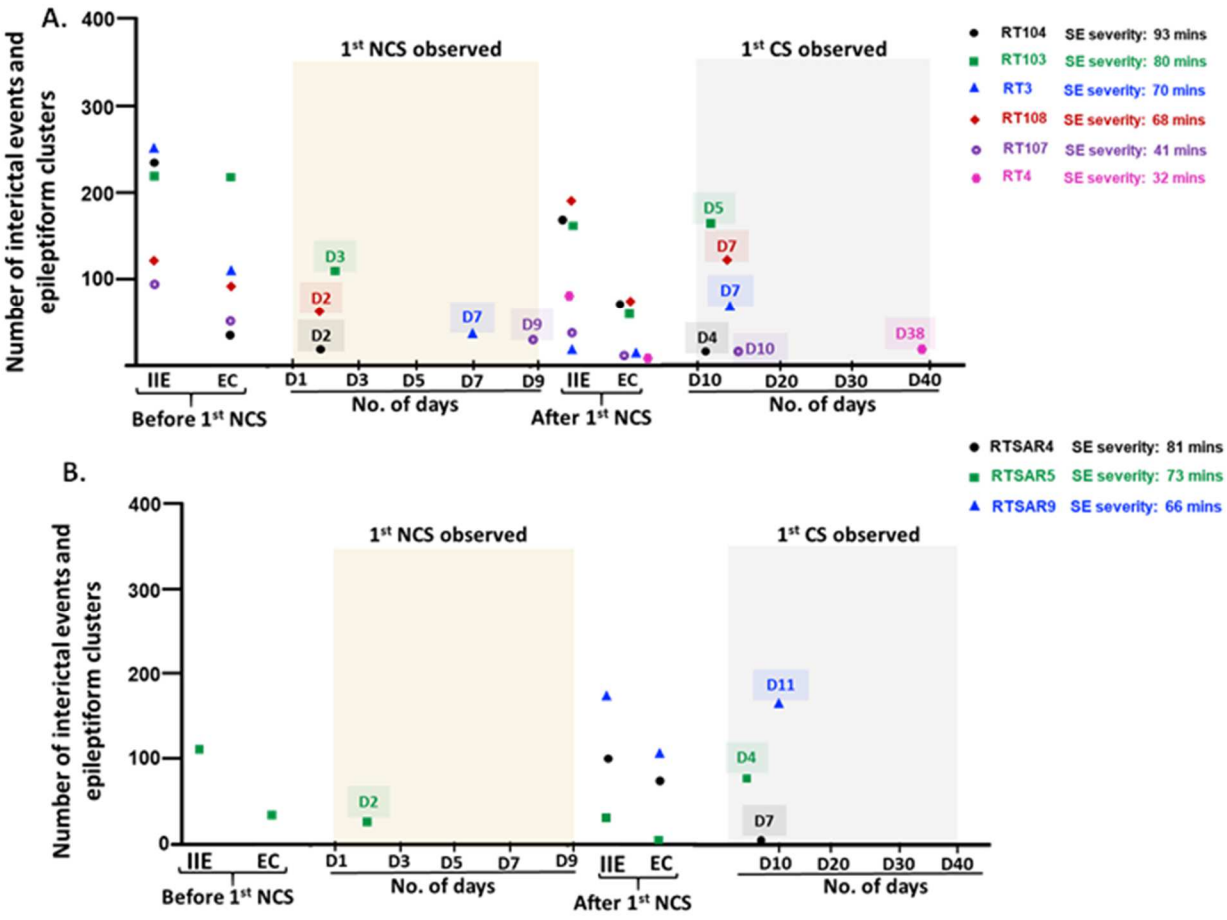

Fig. 6. Saracatinib reduced epileptiform events during 7 day of treatment. A-B) A dot plot representation of table 1 and table 2 showing the development of 1st spontaneous non-convulsive and convulsive seizure in the vehicle and SAR treated groups. All six animals became epileptic in vehicle group (A) while only 3 animals, out of 7, became epileptic in SAR group (B). Each dot represents individual animal. The number of epileptiform events such as interictal spiking and epileptiform clusters were significantly reduced in the durig the SAR treatment. The number of pre-ictal events and post-ictal events were higher in the vehicle compared to the SAR group (table 1). 5 out of 6 animals in the vehicle group showed nonconvulsive seizure while only 1 animal out of eight animals showed nonconvulsive seizure in the SAR group (table 1 and 2). For detailed description of events for figure 6A-B, see table 1 and 2 legends. Abbreviation: IIE, interictal events; EC, epileptiform clusters; NCS, spontaneous non-convulsive seizure; CS, spontaneous convulsive seizure.

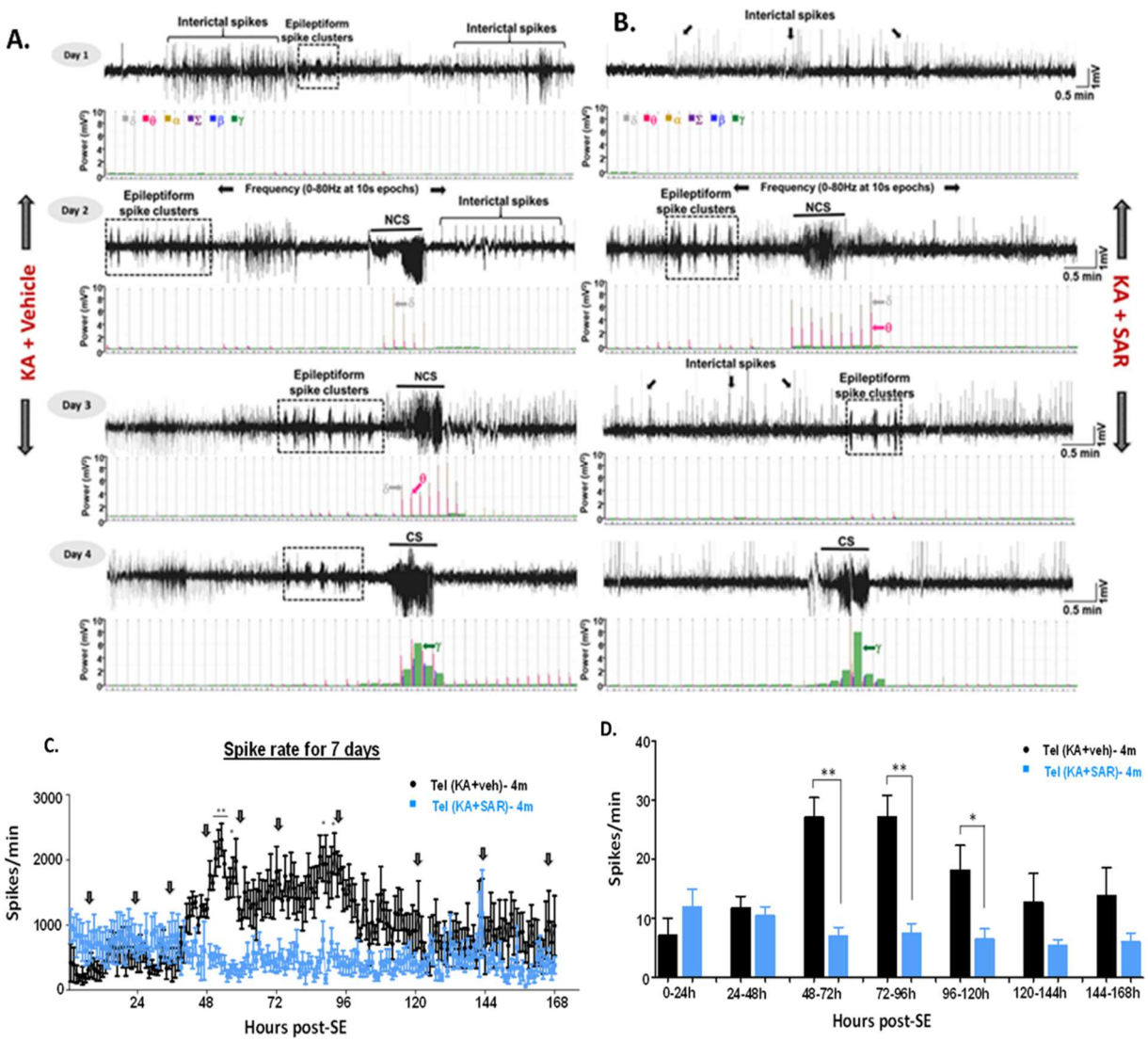

Fig. 7. Saracatinib reduced spike frequency during seven day of treatment. A-B) Epileptiform events (interictal activity and clusters) and spontaneous NCS were verified using EEG spike signatures, power bands and CS were verified against integrated videos. Interictal events lasted from 5 seconds – 150 seconds, clusters were >10 seconds and NCS and CS lasted for >12 seconds. Theta and delta were increased during NCS while gamma power bands were increased during CS with change in phenotypic activities whereas no change in behavioral activity was observed during interictal events and clusters. C-D) Spike rate comparison between vehicle and SAR group during the first week of SAR treatment. SAR post-treatment significantly reduced epileptiform spikes on day 3, 4 and 5 but not during the first two (C, ***p < 0.0001, RM-two way ANOVA between 1 and 2119 degrees of freedom, F= 118; D, *p<0.05, **p<0.01, Mann-Whitney). *p<0.05, **p<0.01, ***p < 0.001, RM two way ANOVA with Tukey post-hoc test and Mann-Whitney test.

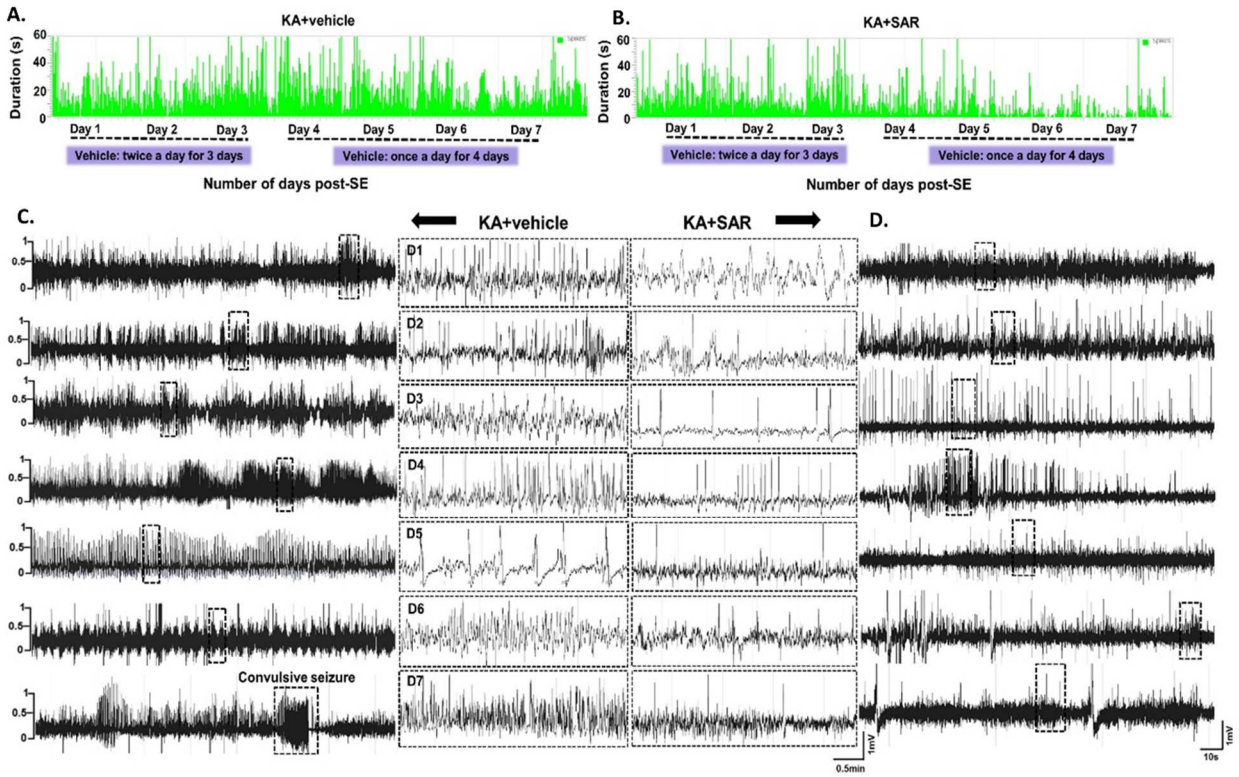

Fig. 8. Saracatinib reduced epileptiform activity during the 7 day of treatment. A-B) Seizure report comparison between the groups. Each vertical bar represent a spike train that includes interictal spikes, epileptiform clusters, NCS and CS (C-D). Representation of the daywise EEG traces between the vehicle (C) and SAR group (D).

Spontaneous NCS showed increased delta and theta activity with episode lasting for >12 seconds with behavioral arrest on video-EEG while spontaneous CS showed increased gamma bands with severe convulsive phenotypic activity. Interictal events did not show any change in the power bands with duration lasting between 5 seconds to as long as 150 seconds whereas epileptiform clusters showed a slight increase in theta bands, but this increase was much lower than theta increase in NCS, with duration >10 seconds. A normal behavioral activity such as grooming, nesting and exploratory behavior was observed during these events. Next, we determined whether saracatinib has any effect on the epileptiform activity during the 7 day dosage regimen. The first two days of administration did not have any effect on the epileptiform activity in the rats, but on days 3, 4 and 5, a significant reduction in the

epileptiform spiking activity was observed during the dosage regimen (Fig. 7C-D). A 7 day seizure report on the spike trains (Fig. 8A-B) and EEG traces of epileptiform spiking (Fig. 8C-D), both demonstrated a reduction in the epileptiform activities after saracatinib treatment.

Saracatinib reduced spike frequency and spontaneous convulsive seizures in the 4 month continuous EEG study

In our previous long-term continuos EEG studies on the rat model of TLE, we observed a rapid increase in convulsive seizure frequency after three months of post-SE (Puttachary et al., 2016b). Also, electroencephalographic studies on interictal events in animal models of epilepsy have shown that the persistant occurrence of such events and epileptiform spiking over the long periods of time can lead to severe brain damage, generation of spontaneous recurrent seizures, worsening and continuous progression of seizures and other serious neurological consequences (Berdichevsky et al., 2012; Dube et al., 2001; Hufnagel et al., 1994; Staley and Dudek, 2006; Staley et al., 2005). Therefore, we quantified all the epileptiform spikes (includes epileptiform clusters, interictal events, convulsive and nonconvulsive seizures), quantified as as spikes/minute, and the number of sponatenous convulsive seizures in the 4 month continuous video-EEG studies as shown in figure 9. All the noise such as behavioral artifacts and electrographic noise was manually removed before the analysis.

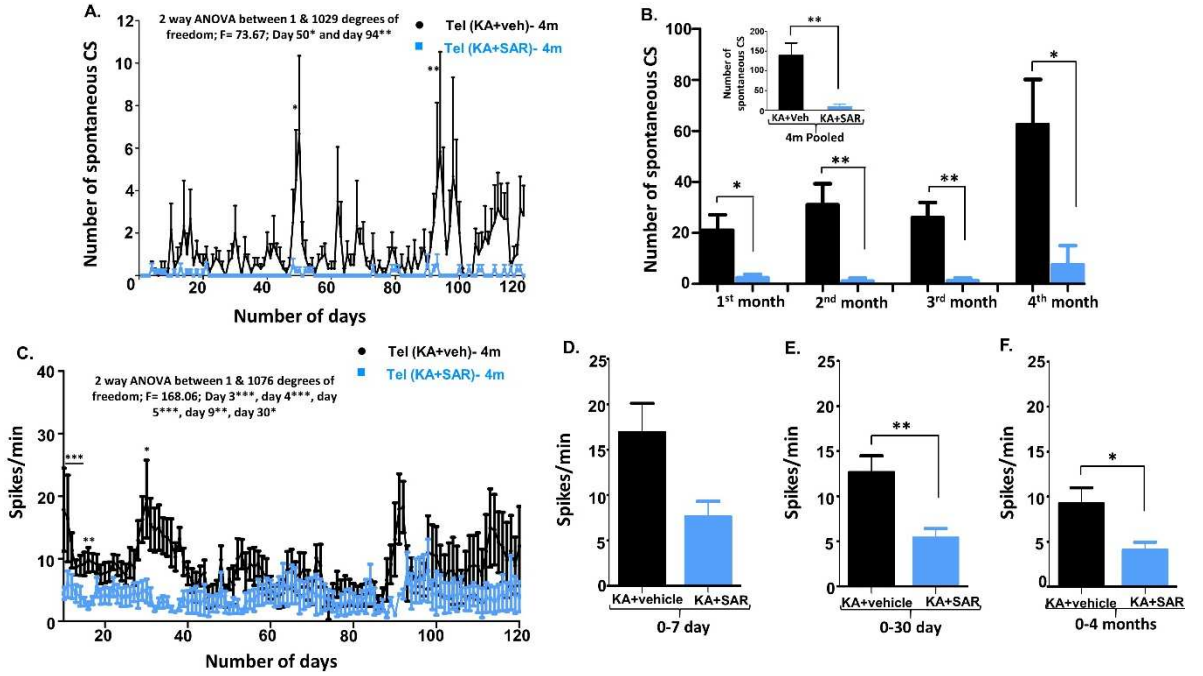

Fig. 9. Saracatinib reduced the number of spontaneous recurrent seizures and spike frequency during 4 month period. A-F) Results from the 4 month continuous video-EEG studies showing spontaneous CS (A-B) and spike frequency (C-F) between the groups. Individual and pooled data showed that SAR post-treatment significantly reduced the spike frequency (D-F) (C, ***$p < 0.0001$, RM-two way ANOVA between 1 and 1076 degrees of freedom, $F = 168.06$); D-F, *$p<0.05$, **$p<0.01$, Mann-Whitney) and the number of spontaneous CS (A-B) (A, ***$p < 0.0001$, RM-two way ANOVA between 1 and 1029 degrees of freedom, $F = 73.67$; L, *$p<0.05$, **$p<0.01$, Mann-Whitney) during 4 month of post-SE. *$p<0.05$, **$p<0.01$, ***$p < 0.001$, RM two way ANOVA with Tukey post-hoc test and Mann-Whitney test.

As rat model is a progressive model of epilepsy, we therefore observed increased spiking activity during the first, third and the fourth month of post-SE in the vehicle group (Fig. 9C-F). The number of sponatenous CS were also consistently higher from the first to fourth month of SE (Fig. 9A-B). Saracatinib post-treatment significantly reduced the spike frequency and also the number of spontaneous CS as can be observed from the pooled data (bar graphs, Fig. 9B, D-F). These results suggest that the SFKs are involved in modulating brain circuitry over time, and its early inhibition after the injury can have a long-term neuroprotective effects on the brain by suppressing abnormal spiking activity that can cause severe brain damage, if occurs persistently for longer periods.

SE significantly increased both Fyn and phosphorylated Src kinase levels in the hippocampus of fyn+/+ mice, but not in fyn−/− mice

To understand the molecular mechanism of microglial activation mediated by the Fyn kinase during epileptogenesis, we tested the levels of Fyn and phosphorylated Src (pSrc-416) in the hippocampus at 4 h, 24 h, and 7 d post-SE. The Western blot analysis revealed a significant increase in both Fyn and pSrc-416 levels at all the time points in the hippocampus of fyn+/+ mice, except the cytosolic Fyn at 4 h, when compared with naïve control (Fig. 10A–D).

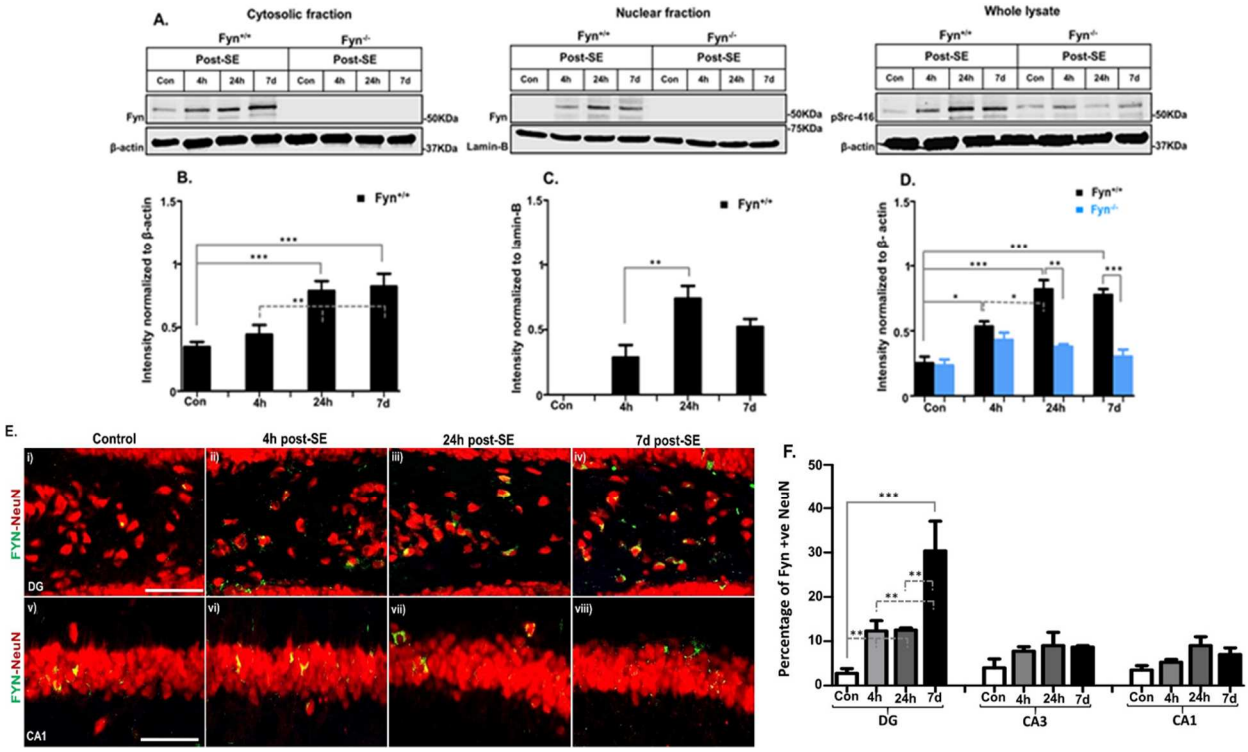

Fig. 10. Fyn and pSrc-416 levels in the hippocampus during epileptogenesis. A–D) The Western blot analysis of Fyn and pSrc-416 at 4 h, 24 h, and 7 d post-SE. The cytosolic and nuclear Fyn proteins were absent in the fyn−/− mice, while they were significantly increased at 24 h and 7 d post-SE in fyn+/+ mice when compared to the naïve control. The pSrc-416 levels also increased significantly in the fyn+/+ mice at all time points, but no significant differences were observed in the pSrc-416 levels in the fyn−/− compared to the control (D). However, when compared between the groups, it was reduced in the fyn−/− mice at 24 h and 7 d post-SE (D) *p < 0.05, **p < 0.01, ***p < 0.001; n = 5–6.

E–F): IHC images of the hilus of dentate gyrus demonstrating Fyn (yellow) co-localization in neurons in fyn+/+ mice. Fyn expression was significantly increased in the hilus of DG at all the time points when compared to the control. No significant difference was observed in CA1 and CA3 regions (**p < 0.01, ***p < 0.001).

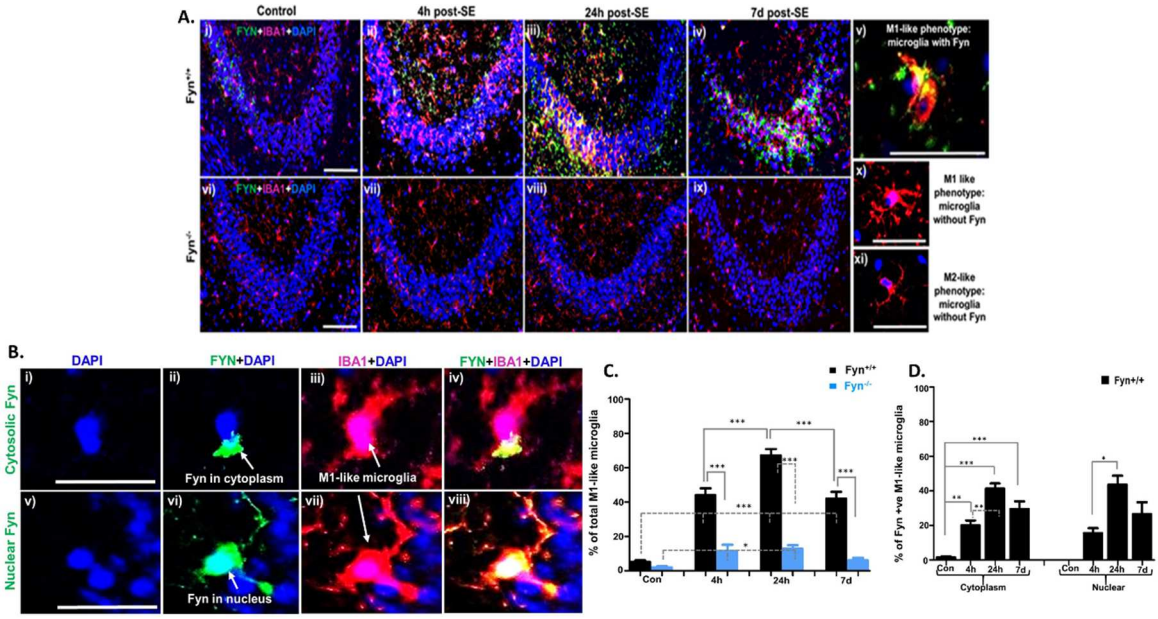

Fig. 11. Fyn levels in the hippocampus during epileptogenesis. A–C): IHC images from CA3 region of the hippocampus showing Fyn immunoreactivity at different time points (red, IBA1 for microglia; yellow/green, Fyn; blue, DAPI for nucleus). A representative high power view images (A-v, x, xi) of the microglia that resembled M1/M2-like phenotype with or without Fyn at 24 h from the fyn+/+ and fyn −/− are shown. The Images in the panel B represents Fyn immunoreactivity in the cytoplasm (i–iv) and its nuclear translocation (B, vigreen and viii-yellow) in the M1-like microglia. In the fyn+/+ mice, the microglia had M1-like phenotype with a large cell body and thick processes (B–iii, vii). In fyn−/− mice, there were also M1 like microglia, but without Fyn (A, x). I). The M1-like microglia cell quantification (C-D). Fyn+/+ mice showed a significantly higher percentage of total M1-like phenotype at all time points when compared to their respective controls. However, a similar increase was observed in the percentage of M1-like microglia in fyn−/− compared to the controls but this difference was not significant at 7 d post-SE. D) Fyn was not detected in fyn −/− mice. In fyn+/+ mice, there was a significant increase in both cytosolic and nuclear Fyn positive M1-like microglia at all the time points when compared to the control. One way ANOVA, *p < 0.05, **p < 0.01, ***p < 0.001; n = 5–6. Scale bar, all 100 μm.

As expected, total Fyn levels were not detected in fyn−/− mice, however, pSrc-416 levels were detected, but there were no significant differences between naïve control and SE groups. At 24

h and 7 d post-SE, the pSrc-416 levels were significantly lower in fyn−/− mice when compared to fyn+/+ mice (Fig. 10D). This may suggest that other members of the SFK may have a minor role in epileptogenesis. Further analysis of the fractionated samples revealed a significant increase in Fyn levels in both the cytoplasmic and nuclear fractions at all the time points in fyn+/+ mice when compared to naïve control (Fig. 10A–C).

Fyn selectively upregulated in the microglia and hilar neurons of the dentate gyrus in fyn+/+ mice during post-SE

IHC of brain sections, double stained for neuron (NeuN) or microglia marker (IBA1) and Fyn, revealed a pattern of Fyn staining in neurons, and in the cytoplasm and nuclei of reactive microglia in the hippocampus and dentate gyrus (7E–J). The pyramidal neurons in CA1 and CA3 regions of the hippocampus did not show increase in Fyn staining at any time point tested during the post-SE. However, the Fyn positive neurons in the hilus of dentate gyrus were significantly increased at all the time-points when compared to the control (Fig. 10E–F). Interestingly, we also observed an increase in the number of FJB positive neurons in the hilus at these time points in fyn+/+ mice. Moreover, a significant increase in reactive microglia was also observed at 4 h, 24 h, and 7 d in fyn+/+ mice when compared to naïve control (Fig. 11A, C). At 24 h and 7 d, intense Fyn positive microglia were found in CA1 (not shown), CA3 (Fig. 11A), and the dentate gyrus (not shown). The vast majority of these microglia resembled M1-like phenotype with thick cytoplasmic process and often multinucleated with a large cell body. In these cell types, the Fyn was localized in the nucleus (Fig. 11A–B, D). In contrast, the fyn−/− mice did not show any Fyn staining, and the vast majority of microglia had M2-like phenotype or alternatively activated type morphology with a small soma and thin cytoplasmic processes (Fig. 11A). However, there was a significant increase in reactive type microglia at 4 h and 24

h, and a marginal increase at 7 d post-SE in the fyn−/− mice was observed when compared with the naïve control (Fig. 11C). A similar pattern of Fyn staining in microglia was detected in other parts of the brain such as the entorhinal cortex, thalamus, and amygdala (not shown).

Saracatinib post-treatment also reduced Fyn nuclear translocation and its levels in reactive gliosis and neurons

Fyn translocation to the nucleus and its upreglation in glial cells and neurons has been shown to regulate the transcription of proinflammatory genes (Panicker et al., 2015; Sharma et al., 2018). Therefore, to investigate whether Fyn has any role in the maintenance of the brain inflammation, we did fractionation studies on the hippocampal tissues at 7 d and 4 month to investigate whether SAR prevents Fyn translocation to the nucleus or not. In our previous studies, we observed enhanced Fyn/PKCδ upregulation in non-microglia cells in the hippocampus of $Fyn^{+/+}$ mice (Sharma et al., 2018a). Moreover, not much is known about the role of Fyn in glial cells in different brain regions. Therefore, in this project, we investigated Fyn's expression in glial cells and neurons in six different regions of the brain which includes, DG, CA3, CA1, thalamus, ENT and amygdala.

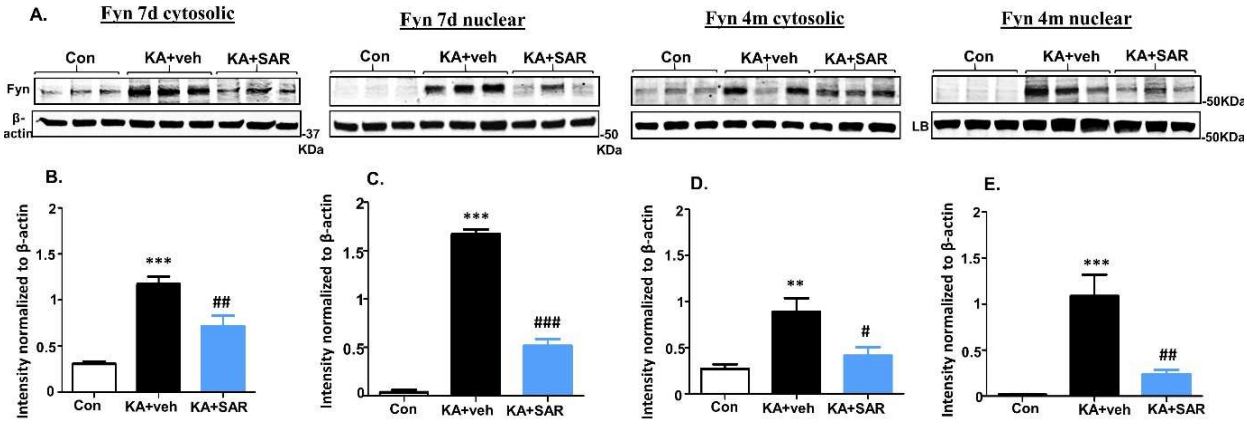

Fig. 12. Cytosolic and nuclear Fyn levels in the hippocampus at 7 d and 4 month during epileptogenesis. A-E) Western Blot results of cytosolic and nucler Fyn from the hippocampal tissues at 7 day and 4 month from the vehicle and SAR treated groups. Higher levels of Fyn was observed in

the nucleus at 7 day (A, C) but it was reduced at 4 month post-SE (A, E). SAR treatment reduced both cytosolic (A, B, D) and nuclear (A, C, E) Fyn levels to >50% (C, E) (*p<0.05, **p<0.01, ***p<0.001; One way ANOVA, n=5).

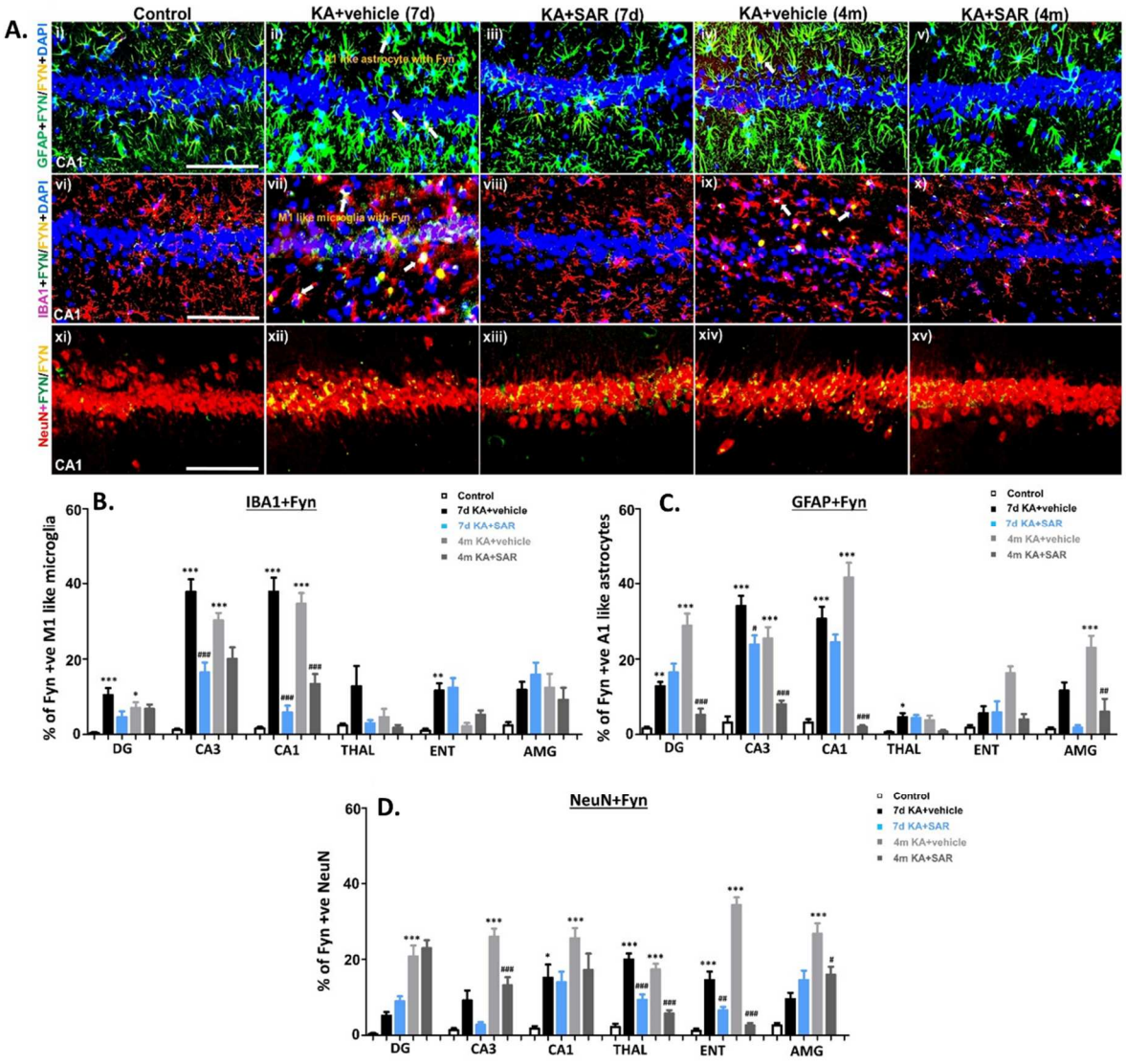

Fig. 13. Cell-specific Fyn expression in different regions of the brain during epileptogenesis. A) IHC images of CA1 region of the hippocampus is shown with Fyn expression in different cell types. Fyn (yellow in A, i-xv) expression in the astrocytes (green in A, i-v), microglia (red in A, vi-x) and neurons (red in A, xi-xv). Fyn expression in reactive astrocytes (ii, iv) and microglia (vii, ix) are shown with white arrows. B-D) Quantification and comparison of Fyn expression in reactive microglia (B), reactive astrocytes (C) and in neurons (D) in DG, CA3, CA1, thalamus, entorhinal cortex and amygdala at 7d and 4 month post-SE. *p<0.05, **p<0.01, ***p<0.001, Repeated measures with two way ANOVA with Tukey post-hoc test; n=5; Scale bar, all 100 µm.

Western Blot results from the hippocampal tissue lysates revealed increased Fyn translocation from cytosol into the nucleus at 7 day but not at 4 month post-SE (Fig. 12A-E). Saracatinib significantly reduced Fyn levels in the cytosol and also prevented its nuclear translocation at both time-points (Fig. 12A-E). IHC results from the reactive microglia (M1-like microglia) and astrocytes (A1-like astrocytes) revealed increased Fyn expression in CA3 and CA1 region of the hippocampus in the vehicle treated group when compared to the controls (Fig. 13B-C). Overall, Fyn was not much upregulated in other regions of the brain such as DG, thalamus, entorhinal cortex and amygdala compared to hippocampus, except in DG and amygdala in reactive astrocytes at 4 month post-SE (Fig. 13C). Interestingly, Fyn levels in neurons were equally higher in all the regions of the brain, especially at 4 month (Fig. 13D), but they were lower in CA3 and CA1 when compared to its levels in reactive microglia and astrocytes. Only a few studies have reported the role of Fyn in thalamus and amygdala in the development of thalamic networks and the regulation of behavior and the formation of contextual memories in the entorhinal cortex (Ge et al., 2017; Ross et al., 1988; Yagi, 1994). To our knowledge, none of the reports have discussed its role in the pathological conditions in these regions. In neurons, Fyn is responsible for the initiation of amygdala kindling but is not required for the maintenance of kindling (Cain et al., 1995). Post-treatment with saracatinib reduced Fyn levels in reactive glia and neurons in most of the brain regions at both the time-points. The suppression was maximum in reactive microglia in CA1 at 7 d and 4 month, in reactive astrocytes in DG and CA1 and in neurons of the entorhinal cortex at 4 month post-SE.

Saracatinib post-treatment reduced phosphorylated Src, iNOS and 3-NT levels in the hippocampus

Since Fyn phosphorylation at tyrosine residue 416 is important for its activation and translocation to the nucleus, we investigated whether saracatinib post-treatment has any effect on Fyn phosphorylation or not. Fyn phosphorylation (pSrc-416) was increased to more than 50% in the vehicle-treated group at both the time-points when compared to the control (Fig. 14A-B). Saracatinib treatment significantly reduced SE-induced upregulation of pSrc-416 by about two-folds when compared to the vehicle (Fig. 14A-B) suggesting a potential role of saracatinib in preventing Fyn activation and nuclear translocation.

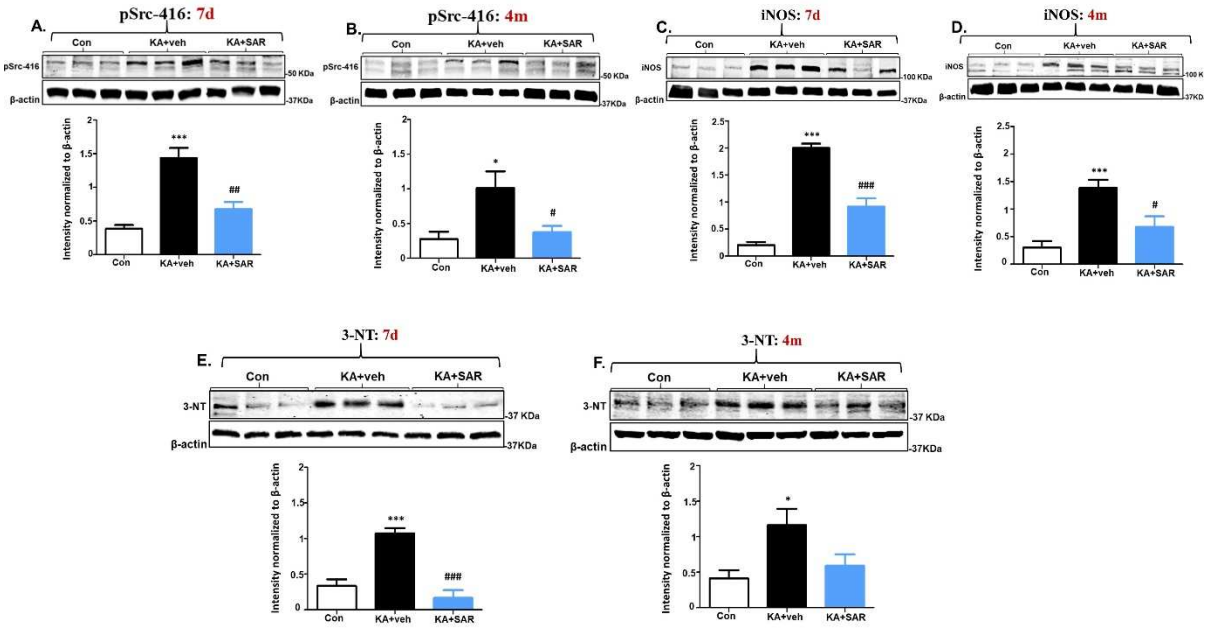

Fig. 14. SAR reduced SFK phosphorylation at Y416 and nitrosative stress in the hippocampus. Phosphorylated Src-416, iNOS and 3-NT levels in the hippocampus at 7 d and 4 month post-SE (A-F). Repeated low doses of kainate induced the activation of SFK at tyrosine 416 (A, B) and resulted in its activation and nuclear translocation. Fyn activation has been known to initiate the transcription of iNOS and post-translational modification or nitrosylation of proteins. pSrc-416 (A, B), iNOS (C, D) and 3-NT (E, F) WB analysis confirmed high levels of these proteins in the hippocampus of the vehicle group at both time-points when compared to the controls, while SAR treatment reduced their levels to about ≥ 50% compared to the vehicle (A-F) *p<0.05, **p<0.01, ***p<0.001; One way ANOVA, n=5.

Recent studies on immune cells such as microglia and macrophages and on astrocytic cultures have shown the regulatory role of Fyn in modulating iNOS activity (Gallego et al., 2011; Ko et al., 2018). Activation of Src, through stress-associated glucocorticoid receptors, have also been shown to mediate iNOS phosphorylation in breast cancer and promote tumourigenesis (Flaherty et al., 2017). In this study, we showed increased levels of iNOS in the hippocampus at 7 d and 4 month after kainate induced SE (Fig. 14C-D). Saracatinib reduced iNOS levels by two-folds suggesting the potential role of Fyn in regulating iNOS in the brain during pathological conditions. High production of iNOS can produce increased amounts of peroxynitrites through the interaction of superoxides with NO. This generates higher oxides of nitrogen dioxide causing nitration of proteins generating 3-nitrotyrosine (Puttachary et al., 2015a; Syslova et al., 2014). Like iNOS, 3-NT levels were also upregulated in the vehicle group at these time-points (Fig. 14E-F). This may suggest the iNOS mediated upregulation of 3-NT in the hippocampus which continues to persist over the period of 4 months after the initial insult. After the pharmacological inhibition of SFK, 3-NT levels were significantly reduced at 7 d and were also downregulated, although not significantly, at 4 month of post insult (Fig. 14E-F).

SE significantly increased naïve and phosphorylated PKCδ levels in the hippocampus of fyn+/+ mice when compared to fyn−/− mice

It was known that phosphorylated SFK (pSrc-416) activates PKCδ and translocates to the nucleus of microglia in cell culture and animal models of PD (Panicker et al., 2015; Saminathan et al., 2011). Therefore, we speculated that a similar mechanism may exist in the kainate model of epileptogenesis. In the fyn+/+ mice, the Western blot analysis of proteins

from the hippocampus revealed a significant increase in both the naïve full-length PKCδ and phosphorylated PKCδ (pPKCd-507) at 4 h, 24 h, and 7 d post-SE when compared with the control (Fig. 15A–D).

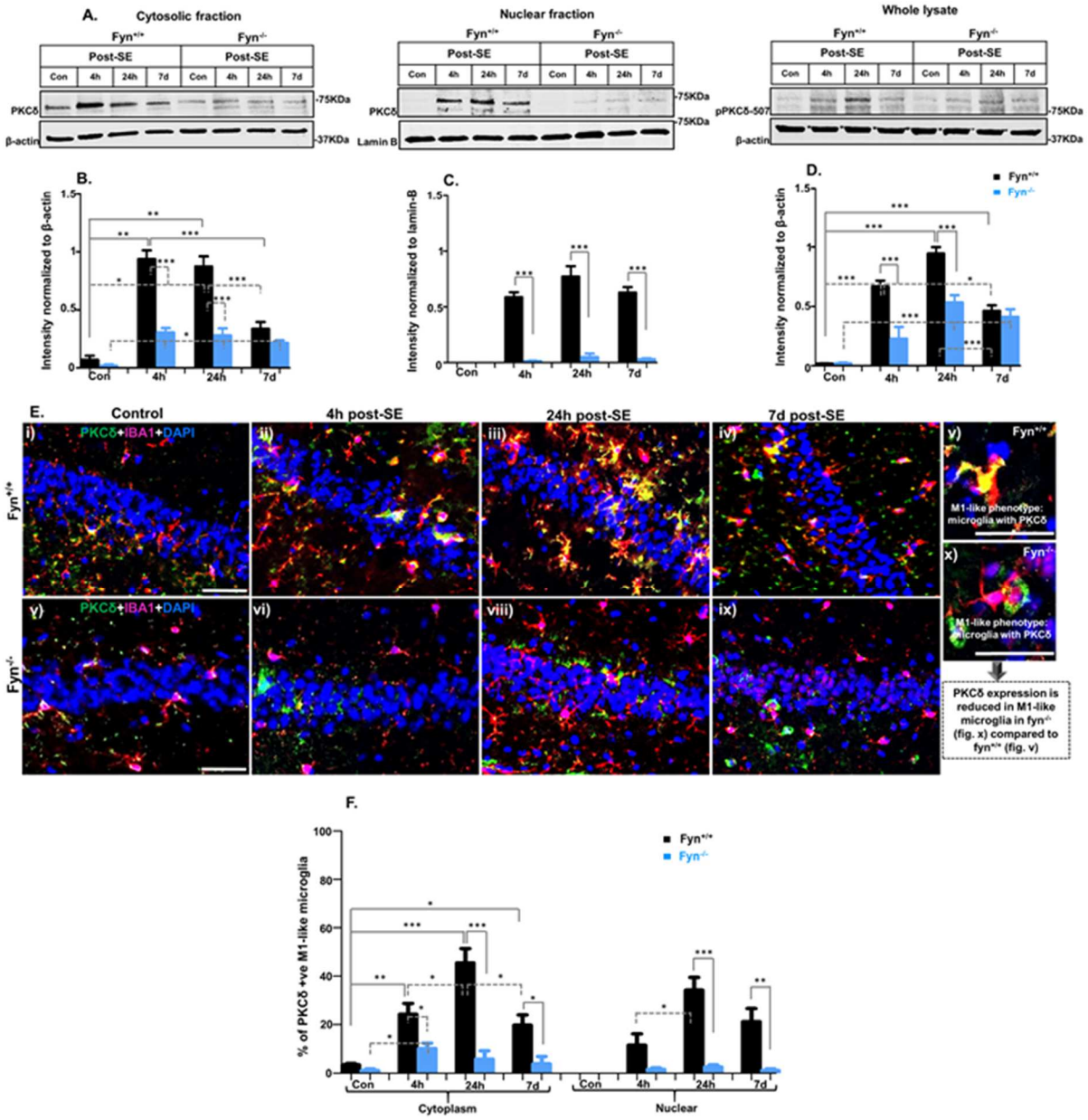

Fig. 15. The PKCδ (cytosolic and nuclear), and pPKCδ-507 protein levels in the hippocampus during epileptogenesis. A–D): The Western blot analysis showed a significant increase in both the cytosolic and nuclear PKCδ levels, and also pPKCδ, in fyn+/+ at all the time points compared to the control. The cytosolic PKCδ levels were relatively decreased at 7 d post-SE, but the nuclear PKCδ levels remained at the same levels at all the time points. In fyn−/− mice, the cytosolic PKCδ levels were increased significantly at all time points, while pPKCδ-507 levels were increased significantly at 24 h

and 7 d when compared to the control. However, their levels were significantly lower than the levels observed in fyn+/+ mice (*p < 0.05, **p < 0.01, ***p < 0.001). Nuclear translocation of PKCδ in fyn−/− was marginally increased, but this increase was much lower when compared to fyn+/+ mice. E–F): Immunohistochemistry images of CA1 region of the hippocampus showing PKCδ (green or yellow) immunoreactivity in the M1-like microglia (red). In the fyn+/+ mice, there were significant increase in the numbers of both cytoplasmic and nuclear PKCδ immunoreactive microglia at all time points when compared to the control. In fyn−/− mice, there was a significant reduction in their numbers, at all time points, in both the nuclei and cytoplasm (and also the intensity of staining) of the M1-like microglia when compared to fyn+/+ mice (*p < 0.01, **p < 0.01, ***p < 0.001). A high power view of the images show intense PKCδ staining in the nucleus and cytoplasm of M1-like microglia in fyn+/+ and fyn−/− mice (E–v, x). One way ANOVA, *p < 0.05, **p < 0.01, ***p < 0.001; n = 5–6. Scale bar, 100 μm.

Since pSrc-416 levels were detected in fyn−/− mice, we also observed an increase in the levels of both full-length PKCδ and pPKCδ-507 at all-time points. Further analysis of the nuclear fractions from the hippocampus, revealed a significant increase in PKCδ levels in the fyn+/+ mice, but not in the fyn−/− mice (Fig. 15C). In concurrence with the Western blot results, IHC of the brain sections revealed a significant increase in both the numbers of PKCδ positive microglia as well as increase in intensity of staining in the nuclei of the reactive microglia in the hippocampus at 4 h, 24 h, and 7 d time points (Fig. 15E–F) in the fyn+/+ mice. In the fyn−/− mice, there was a marginal increase in microglial cytoplasmic PKCδ over time, but there was no significant increase in the nuclear PKCδ (Fig. 15E–F).

Saracatinib reduced PKCδ nuclear translocation and its levels in reactive gliosis and neurons

Phosphorylation of Fyn either directly translocates to the nucleus or activates and phosphorylates PKCδ at tyrosine 311 (Panicker et al., 2015). Phosphoryation of PKCδ stimulates MAP kinase that results in NFkB translocation into the nucleus transcribing activation of proinflammatory genes and iNOS (Panicker et al., 2015; Sharma et al., 2018). PKCδ translocation into the nucleus and its upreglation in glial cells and neurons has also been

shown to regulate the transcription of proinflammatory genes (Panicker et al., 2015; Sharma et al., 2018). Also, PKCδ phospshorylation and cleavage is essential for the production and generation of reactive oxygen and nitrogen species (Panicker et al., 2015; Sharma et al., 2018). The fractionation studies on hippocampal tissue lysates, similar to Fyn, were conducted to investigate whether PKCδ translocates to the nucleus or not. We also investigated the expression of PKCδ in microglia, astrocytes and neurons, similar to Fyn, in DG, CA3 and CA1 of hippocampus, thalamus, entorhinal cortex and amygdala.

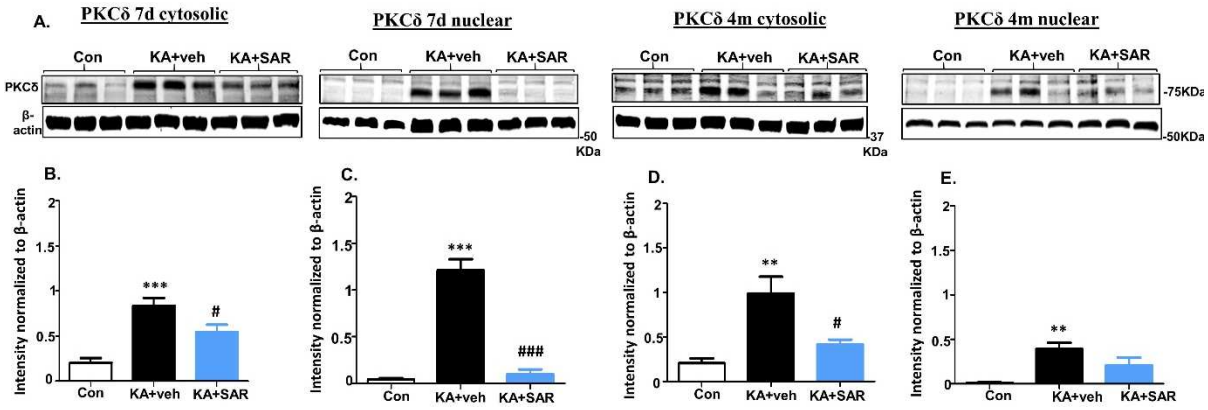

Fig. 16. Cytosolic and nuclear Fyn levels in the hippocampus at 7 d and 4 month during epileptogenesis. A-E) Western Blot results of cytosolic and nucler PKCδ from the hippocampal tissues between vehicle and SAR treated groups at 7 day and 4 month post-SE. Increased levels of cytosolic and nuclear PKCδ was observed at both 7 d and 4 month post-SE in the vehicle group compared to the control. PKCδ nuclear translocation increased to two-folds by 7 d (A, C) and reduced to almost half by 4 month post-SE (A, E). This may suggest that PKCδ is involed in the early progression of the disease but may not be involved in the late maintenanace of the disease. SAR treatment significantly reduced cytosolic PKCδ (A, B, D), and also nuclear PKCδ (A, C) to >90% by 7 d and mildly by 4 month post-SE (A, E) which suggests its protective role during epileptogenesis and in epilepsy (*p<0.05, **p<0.01, ***p<0.001; One way ANOVA, n=5).

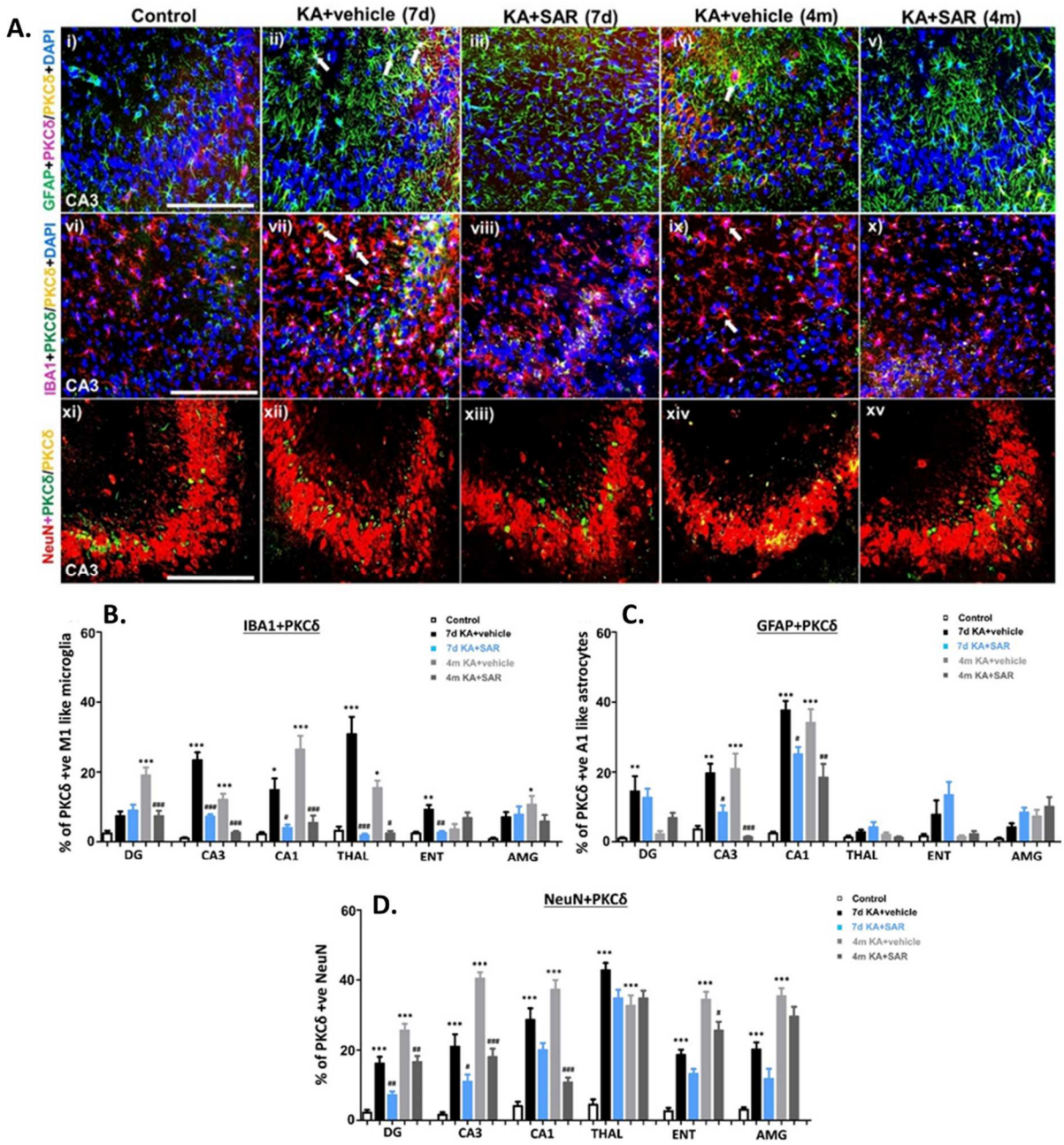

Fig. 17. PKCδ levels in the hippocampus, thalamus, entorhinal cortex and amygdala during epileptogenesis and epilepsy. A) IHC images of CA3 region of the hippocampus is shown with PKCδ expression in different cell types. PKCδ (yellow in A, i-xv) expression in the astrocytes (green in A, i-v), microglia (red in A, vi-x) and neurons (red in A, xi-xv). PKCδ expression in reactive astrocytes (ii, iv) and microglia (vii, ix) is shown with white arrows. B-D) Quantification and comparison of PKCδ expression in reactive microglia (B), reactive astrocytes (C) and in neurons (D) of DG, CA3, CA1, thalamus, entorhinal cortex and amygdala at 7d and 4 month post-SE. *p<0.05, **p<0.01, ***p<0.001, Repeated measures with two way ANOVA with Tukey post-hoc test; n=5; Scale bar, all 100 μm.

Western Blot results from the hippocampal tissue lysates revealed increased PKCδ translocation into the nucleus at 7 day, and the trnslocation was reduced to half by 4 month post-SE (Fig. 16A-E). SFK inhibitor saracatinib significantly reduced PKCδ levels in the cytosol at 7 d and 4 month and >90% in the nucleus at 7 d (Fig. 16C). PKCδ levels were marginally reduced at 4 month post-SE (Fig. 16E). IHC results from M1-like microglia revealed increased PKCδ expression in CA3, CA1 and thalamus and in DG at 4 month in the vehicle treated group when compared to the control (Fig. 17A). In reactive astrocytes, PKCδ levels were higher in CA3 and CA1. In entorhinal cortex and amygdala, PKCδ levels were consistently lower in reactive glia. Interestingly, PKCδ levels in neurons were very high in all the regions of the brain at both time-points (Fig. 17D) when compared to its levels in reactive microglia and astrocytes. Highest PKCδ levels were observed in CA3, CA1, entorhinal cortex and amygdala at 4 month and in thalamus at 7 d post-SE. Post-treatment with saracatinib reduced PKCδ in these cells in most of the regions. The suppression was maximum in reactive microglia in thalamus at both the time-points, in reactive astrocytes in CA3 and in the neurons of CA1 at 4 month post-SE (Fig. 17B-D).

SE significantly increased caspase-3 and cleaved caspase-3 levels in the hippocampus of fyn+/+ mice when compared to fyn−/− mice

The PKCδ is cleaved by caspase-3 to cause neuronal death (Kaul et al., 2003; Kato et al., 2009; Kitazawa et al., 2005), therefore we tested the caspase-3 and cleaved caspase-3 levels in the hippocampus.

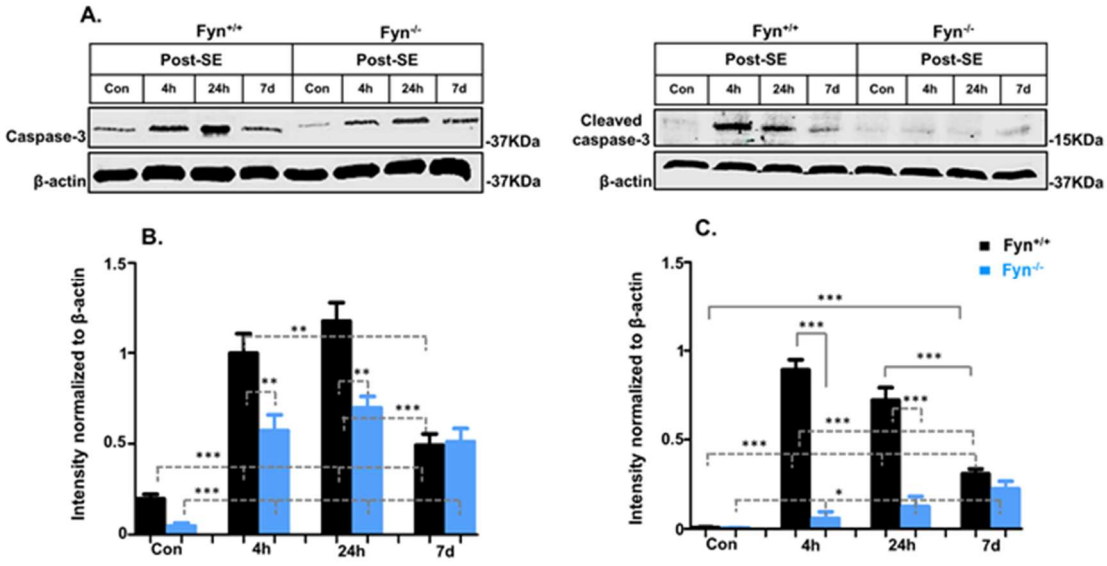

Fig. 18. The caspase-3 and cleaved caspase-3 levels in the hippocampus of fyn+/+ and fyn−/− mice during epileptogenesis. In both groups, the caspase-3 levels were significantly increased at all time points. B) At 4 h and 24 h, the caspase-3 levels were significantly lower in fyn−/− in contrast to the fyn+/+ mice. C) The cleaved caspase-3 levels also significantly increased at all time points in fyn+/+ when compared to the control, and when compared to the fyn−/− mice, except at 7 d postSE. In fyn−/− mice, cleaved caspase-3 levels also increased over time compared to the control, but their levels were significantly lower in fyn+/+ mice at 4 h and 24 h time points. One way ANOVA, *p < 0.05, **p < 0.01, ***p < 0.001; n = 5–6.

There was an increase in the caspase-3 and cleaved caspase-3 levels at all time points in both fyn+/+ and fyn−/− mice groups when compared with the respective controls (Fig. 18A–C). However, in the fyn−/− mice, the caspase-3 and cleaved caspase-3 levels were significantly lower at 4 h and 24 h post-SE when compared with the fyn+/+ mice (Fig. 18A–C).

Key proinflammatory cytokine profile during epileptogenesis in fyn+/+ and fyn−/− mice It has been demonstrated that PKCδ translocation to the nucleus initiates transcription of proinflammatory cytokines and iNOS in M1- like microglia (Bujor et al., 2011; Gordon et al., 2016). Since we found the PKCδ translocation to the nucleus in microglia, which also had M1- like phenotype (large cell body, thick cytoplasmic process), we further

investigated whether it has an effect on proinflammatory cytokines in the hippocampus and serum.

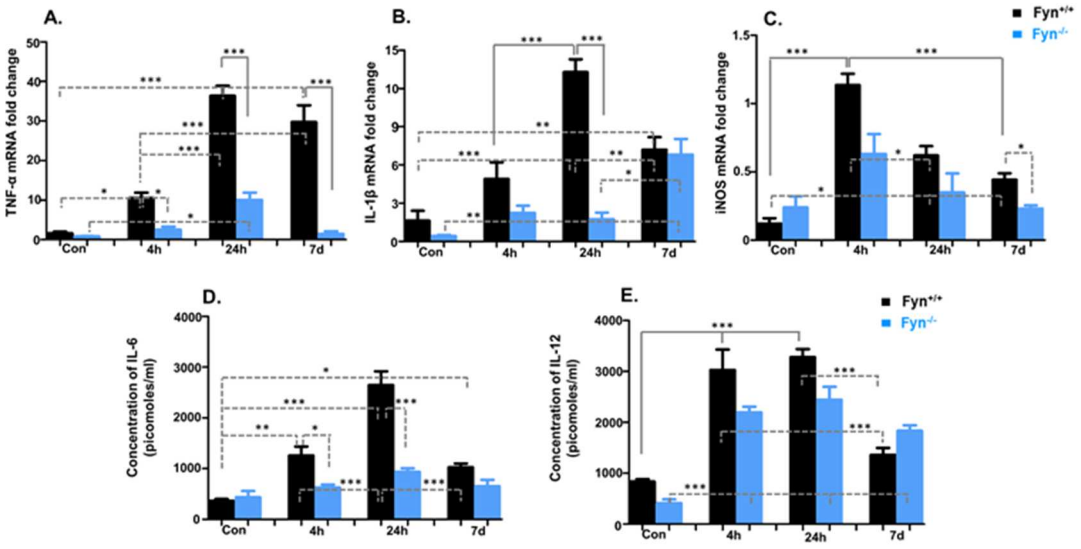

Fig. 19. TNF-α, IL-1β, and iNOS mRNA expression levels in the hippocampus, and serum IL-6 and IL-12 levels in fyn+/+ and fyn−/− mice during epileptogenesis. A–C): In fyn+/+ mice, the TNF-α mRNA levels were significantly increased at all the time points, while the IL-1β mRNA levels were increased at 24 h and 7 d post-SE when compared to the controls. In fyn−/− mice, the TNF-α mRNA levels were significantly reduced at all time points, and IL-1β levels at 24 h post-SE when compared to the fyn+/+ mice. *p < 0.05, **p < 0.01, ***p < 0.001; n = 5–6. The iNOS mRNA levels were increased at all time points in fyn+/+ mice when compared to the control, especially at 4 h post-SE, while its levels did not change significantly in fyn−/− mice when compared to the control. However, there was a significant reduction in mRNA levels at 7 d post-SE when compared between fyn+/+ and fyn−/− mice. D–E): The serum IL-6 and IL-12 levels were significantly higher, except IL-12 at 7 d post-SE, in fyn+/+ mice when compared to the controls at all time points. In fyn−/− mice, the IL-6 levels were marginally increased at 24 h, while the IL-12 levels were significantly higher at all time points when compared to the controls. When their levels were compared between the groups at various time points, there was a reduction in the IL-6 levels at 4 h and 24 h post-SE, but there were no significant differences in IL-12 levels between the groups. One way ANOVA, *p < 0.05, **p < 0.01, ***p < 0.001; n = 5–6.

We utilized quantitative RT-PCR for mRNA assay for the hippocampus and multiplex cytokine assay for the serum. We found an increase in the TNF-α, IL-1β, and iNOS mRNA levels in the fyn+/+ mice when compared to the control at 4 h, 24 h, and 7 d time points (Fig. 19A–C). In the fyn−/− mice, the IL-1β mRNA was significantly increased at 7 d, and TNF-α mRNA at 24 h post-SE, however iNOS mRNA expression levels did not change significantly

(Fig. 19A–C). However, when compared between the groups, the TNF-α expression was significantly higher at all the time points, while the IL1β at 24 h and the iNOS at 7 d post-SE. Multiplex cytokine assay of the serum revealed a significant increase of both IL-6 and IL-12 levels at all the time points in the fyn+/+ mice when compared with the control (Fig. 19D–E). Interestingly, in the fyn−/− mice, the IL-12 levels were upregulated at all time points, but the IL-6 levels were marginally increased at 24 h post-SE (Fig. 19D–E). When their levels were compared between the groups, IL-6 levels, but not IL-12, were significantly reduced in the fyn−/− mice when compared to the fyn+/+ mice at 4 h and 24 h post-SE (Fig. 19D–E). Other cytokines mRNA or proteins levels were undetectable at all three time points.

Saracatinib reduced proinflammatory cytokines during epileptogenesis

TNFα and IL-1β are the key regulators of inflammation in the brain. IL-1β regulated NR2B subunit activation of NMDA receptors through SFKs are known to play an important role in glutamate-mediated neurotoxicity (Viviani et al., 2013). Moreover, SFK-stimulated TNFα production generates superoxides that results in tissue damage possibly through neutrophil recruitment and increased nitric oxide signaling in the immune cells (Leu et al., 2006; Xing et al., 2001; Yan and Novak, 1999). Therefore, we further investigated proinflammatory cytokine gene expression (qRT-PCR) in the hippocampal tissues, and also assayed the serum using ELISA. All the cytokines increased significantly in the serum of the epileptic animals at both the time-points, except IL-1β at 4 month post-SE, when compared to the controls. Among these cytokines, TNFα levels were the highest while IL-1β were the lowest in the vehicle group. At 4 month post-SE, all the cytokines reduced to almost half compared to their levels at 7 d (Fig. 13A, D).

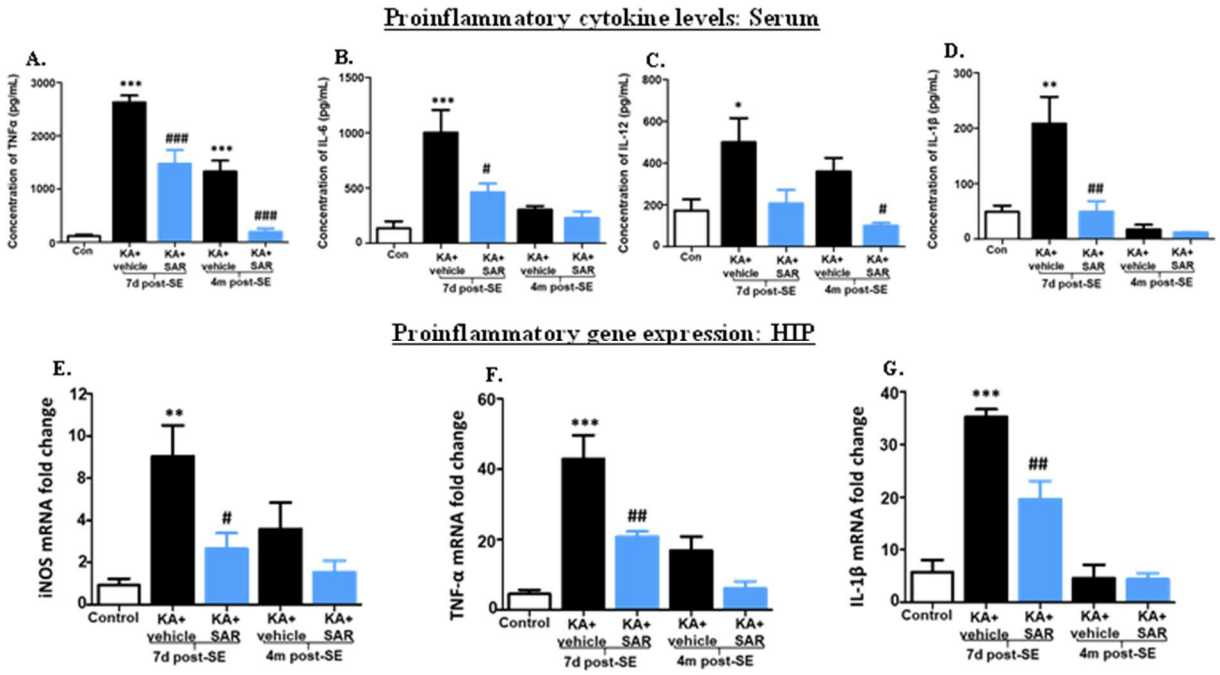

Fig. 20. Proinflammatory cytokines and gene expression in the rat hippocampus and serum during epileptogenesis. A-D) Proinflammatory cytokines were detected in the serum of vehicle and SAR treated rats using ELISA. All the cytokines in the vehicle group were increased at both time-points, except IL-1β at 4 month, when compared to the controls. Among these cytokines, TNFα levels were the highest (A) while IL-1β (D) were the lowest in the vehicle group. About 50% decrease in the cytokine levels were observed in the vehicle group by 4 month compared to 7 d. SAR treatment reduced all the cytokine levels but had little or no effect on IL-6 and IL-1β at 4 month post-SE. E-G) The mRNA gene expression pattern of proinflammatory genes was slightly similar to that observed in the serum. The expression of all the proinflammatory genes were increased in the vehicle group at both the time-points, except IL-1β at 4 month, when compared to controls. Of the three proinflamamtory genes investigated, TNFα expression was the highest (F) while iNOS expression was the lowest (E) in the vehicle group, and their expression was reduced to about ≥ 50% by 4 month post-SE (E-G). SAR treatment significantly suppressed TNFα, IL-1β and iNOS expression at 7 d and also at 4 month, but this difference was not significant. One way ANOVA, *$p < 0.05$, **$p < 0.01$, ***$p < 0.001$; $n = 5$.

Saracatinib treatment significantly reduced these cytokines in the serum at both the time-points. The maximum reduction (more than two-fold) was observed with TNFα and IL-12 at 4 month and IL-1β at 7 d post-SE.

The role of Fyn and PKCδ in regulating the transcription of proinflammatory genes and iNOS has already been well described (Panicker et al., 2015; Sharma et al., 2018a). Therefore, we further investigated the mRNA gene expression of two proinflammatiry cytokines, TNFα

and IL-1β, and iNOS in the hippocampal tissues using quantitative real-time PCR. The gene expression of TNFα, IL-1β and iNOS increased in the vehicle group, at both the time-points, when compared to the controls, except IL-1β where no change was observed at 4 month post-SE. Moreover, similar to serum proinflammatory levels, the expression of cytokines TNFα and IL-1β and iNOS reduced to half by 4 month when compared to 7 d (Fig. 20E-G). Saracatinib treatment suppressed the expression of these cytokines and iNOS, except IL-1β at 4 month. The maximum suppression was observed with iNOS expression at 7 d. These results suggest that the increased expression of Fyn and PKCδ might be responsible for the upregulation of proinflammatory cytokines at early time-point (7 day) and partially at later time-point (4 month). Therefore, it is possible that other proinflammatory factors/events might be involved in regulating epileptogenesis at later time-points.

The saracatinib post-treatment reversed oxidant and anti-oxidant levels during epileptogenesis

Disabling the Fyn kinase, either by pretreatment with saracatinib or Fyn KO, prior to SE induction impacts the initial severity of SE and thus compromises the epileptogenic events. Therefore, we tested whether saracatinib treatment altered the levels of oxidants such as nitrite and reactive oxygen species (ROS) and anti-oxidant glutathione (GSH) during epileptogenesis. The Griess assay for nitrite estimation, ROS for measuring the presence of total free radical and GSH for total GSH concentration were performed on the serum.

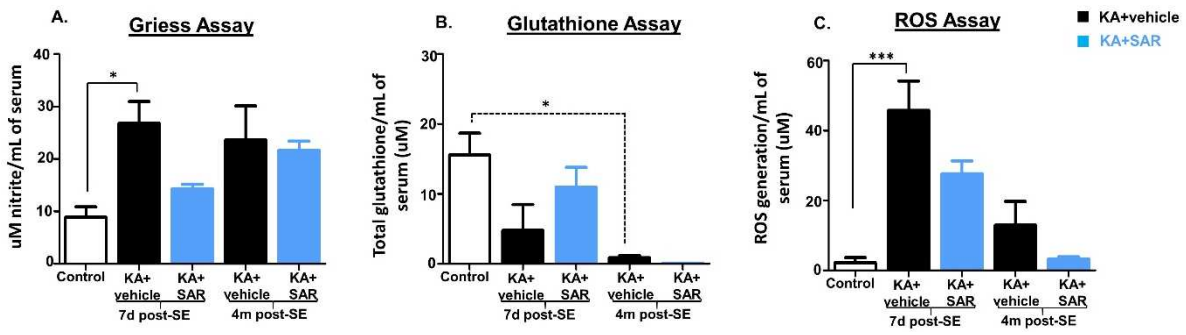

Fig. 21. Saracatinib post-treatment reduced nitrite and ROS and increased glutathione levels in the serum. Griess and ROS assays were performed to determine the amount of nitrites and total reactive oxygen and nitrogen species in the serum of epileptic rats. Kainate treatment increased nitrite and ROS levels in the vehicle at both time-points compared to controls (A, C). However, ROS levels decreased to > 50% in vehicle at 4 month post-SE (C) whereas nitrite did not change (A). Anti-oxidant glutathione was reduced at both 7 d (not significant) and 4 month in vehicle when compared to controls (B). SAR post treatment reduced nitrite levels at 7d, ROS at both 7 d and 4 month and restored glutathione at 7 d post-SE. One way ANOVA, *$p < 0.05$, **$p < 0.01$, ***$p < 0.001$; $n = 5–6$. Scale bar, all 100 μm.

Nitrite and ROS levels were significantly higher in the vehicle treated group at 7 d when compared to the controls. Similar increase in these oxidants was observed at 4 month but the increase was not significant. ROS were decreased to two-folds at 4 month in the vehicle group but nitrite levels were unchanged (Fig. 21A, C). Saracatinib post-treatment mitigated oxidant levels to almost two folds by 7 d and 4 month but had no effect on the nitrite levels at 4 month post-SE (Fig. 21A). Anti-oxidant glutathione helps the cell from the damage from the oxidative stress by neutralizing reactive oxygen and nitrogen species and helps the cell with their metabolic and biochemical functions (Kidd, 1997; Lobo et al., 2010; Singh, 2002). The production of proinflammatory mediators after kainate induction may destabilize the balance between oxidants and anti-oxidants producing higher amounts of highly reactive species. Therefore, we performed glutathione assay to measure whether anti-oxidant glutathione levels are affected during epileptogenesis or not and whether saracatinib treatment recovered their levels. We observed that kainate treatment decreased GSH in the serum at 7 d and 4 month

compared to the control, and saracatinib post-treatment restored its levels (Fig. 21B), especially at 7 d suggesting its protective role against oxidative damage during epileptogenesis.

Nitro-oxidative stress markers in the hippocampus in fyn+/+ and fyn−/− mice, and the impact of saracatinib post-treatment during epileptogenesis

Phosphorylated PKCδ activates $p47^{phox}$, the cytosolic subunit of NOX2, which forms a functional complex with the membrane associated $gp91^{phox}$ to activate NOX2 signaling pathway and drives ROS and RNS production (Bedard and Krause, 2007; Fontayne et al., 2002). In this study, we quantified nitro-oxidative stress markers; $gp91^{phox}$, 4- HNE, and 3-NT levels from the hippocampus by employing IHC and WB methods.

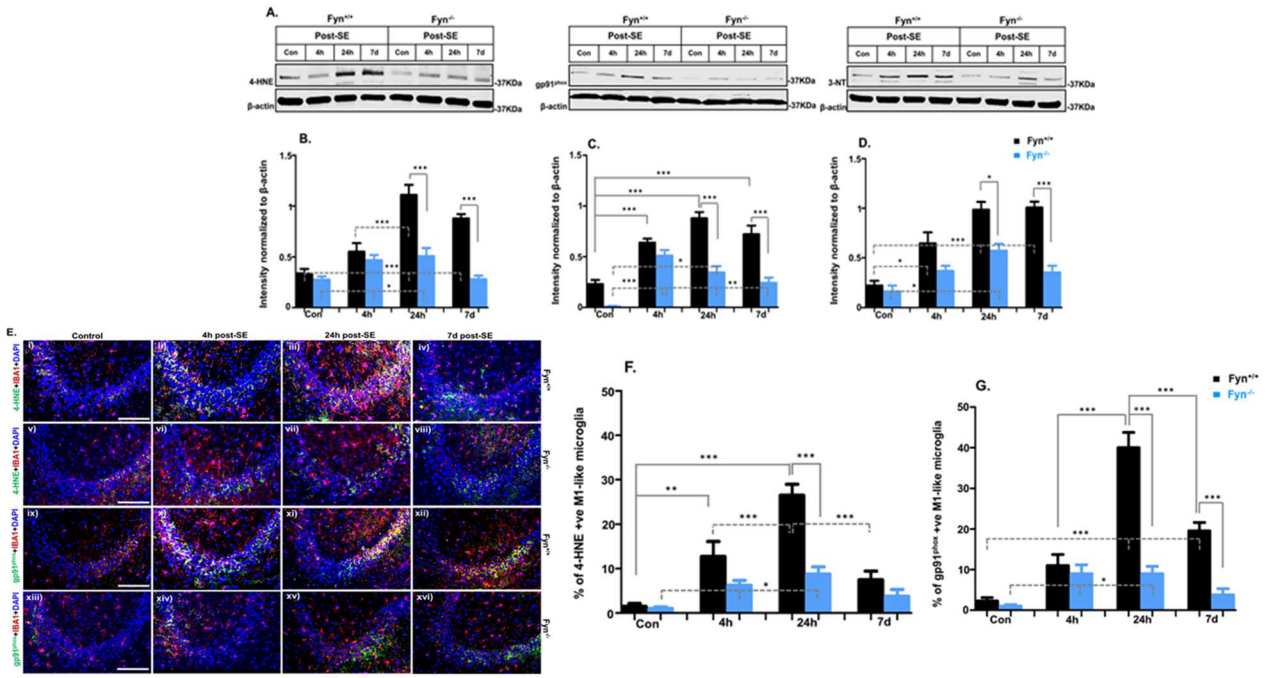

Fig. 22. IHC & Western blot analysis of 4-HNE, $gp91^{phox}$ and 3-NT in the hippocampus of fyn+/+ and fyn−/− mice and SAR/vehicle-treated Sprague Dawley rats during epileptogenesis. A–D, H-K) Increased levels 4-HNE and $gp91^{phox}$ were observed in the hippocampus at all the time points, in both groups (except at 7 d for 4-HNE in fyn−/−), when compared to their respective controls. The 3-NT levels were also increased at all the time points in both fyn−/− and fyn+/+ mice when compared to their respective controls. At 24 h and 7 d post-SE, 4-HNE, $gp91^{phox}$ and 3-NT levels were significantly reduced in fyn−/− mice in contrast to fyn+/+ mice. *p < 0.05, **p < 0.01, ***p < 0.001; n = 5–6.

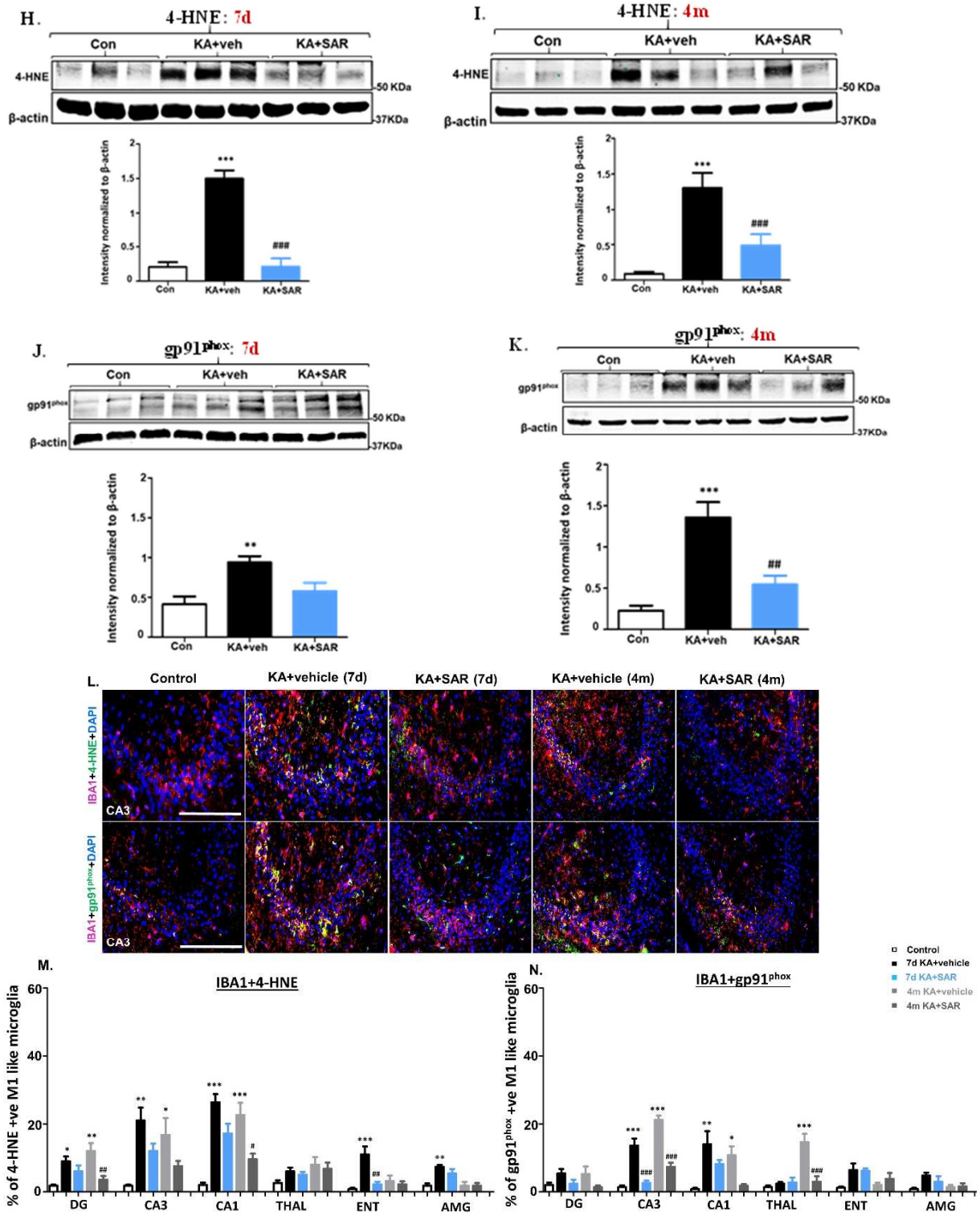

Fig. 22 continued. E): Immunohistochemistry images of CA3 region of the hippocampus showing the 4-HNE and gp91^{phox} immunoreactive cells [IBA1 (red) and DAPI (blue) in all panels; 4-HNE (green/yellow) in panels i) to viii) in 'E' and i) to v) in 'L' and gp91^{phox} (green/ yellow) in panels ix) to xvi) in 'E' and vi) to x) in 'L'). Scale bar, all 100 µm. F–G, M-N): Cell quantification. The IBA1 positive microglial processes that were in close proximity to the pyramidal cell membranes in the CA3

region were counted. The 4-HNE and gp91^{phox} immunopositive cells were increased at all time points in fyn+/+ mice and Sprague Dawley rats compared to the control. The maximum increase was observed at 24 h post-SE in fyn+/+ mice (F, G) and at 7 d and 4 month in CA3 and CA1 of hippocampus in Sprague Dawley rats (M, N). A significant reduction was observed in the gp91^{phox} positive microglia, but not the 4-HNE, at 7 d post-SE in fyn−/− when compared to fyn+/+mice. In fyn−/− mice, there was a significant increase in both 4-HNE and gp91^{phox} positive cells at all time point, except at 7 d, compared to controls. In rats, low levels of 4-HNE and gp91^{phox} immunopositive reactive microglia were observed in thalamus, entorhinal cortex and amygdala (M, N). The levels of these stress markers were significantly lower in M1 like microglia in SAR group in most of the regions of brain. One way ANOVA, *$p < 0.05$, **$p < 0.01$, ***$p < 0.001$; $n = 5–6$. Scale bar, all 100 μm.

The 4-HNE and gp91^{phox} levels were significantly increased at 24 h and 7 d in the fyn+/+ mice (Fig. 22A-B) and at 7d and 4 month in Sprague Dawley rats (Fig. 22H-K), while gp91phox and 3-NT levels were upregulated in both fyn+/+ and fyn−/− mice at all time points when compared with their respective controls (Fig. 22A–D). All three markers were significantly decreased at 24 h and 7 d post-SE in the fyn−/− mice when compared with the fyn+/+ mice and at 7 d and 4 month in saracatinib group when compared to KA group (Fig. 22A-D, H-K). At cellular level, their expression was predominantly in the microglia (Fig. 22E-G, L-N), however, neurons and a few astrocytes were also immunoreactive to these markers (data not shown). When compared between the groups at 24 h and 7 d post-SE in mice and at 7 d and 4 month in rats, we observed a large number of gp91^{phox} containing reactive microglia in the hippocampus in the fyn+/+ mice and in rats (Fig. 22E, M-N). Their numbers significantly reduced in the fyn−/− mice and after saracatinib treatment (Fig. 22G, N). Likewise, the numbers of 4-HNE and 3-NT positive neurons were also changed between the groups in the entorhinal cortex, amygdala, and the thalamus (data not shown).

The FJB positive neurons increased in the hippocampus and other regions during epileptogenesis in both fyn+/+ and fyn−/− mice and Sprague Dawly rats

Having observed increased levels of nitro-oxidative stress markers, proinflammatory cytokines, cleaved caspase-3, and increased expression of Fyn and PKCδ levels in microglia and other cells of the hippocampus and other regions during epileptogenesis, we were interested to find out the extent of neurodegeneration in the hippocampus and other brain regions. We confirmed this by staining the brain sections with FJB and NeuN.

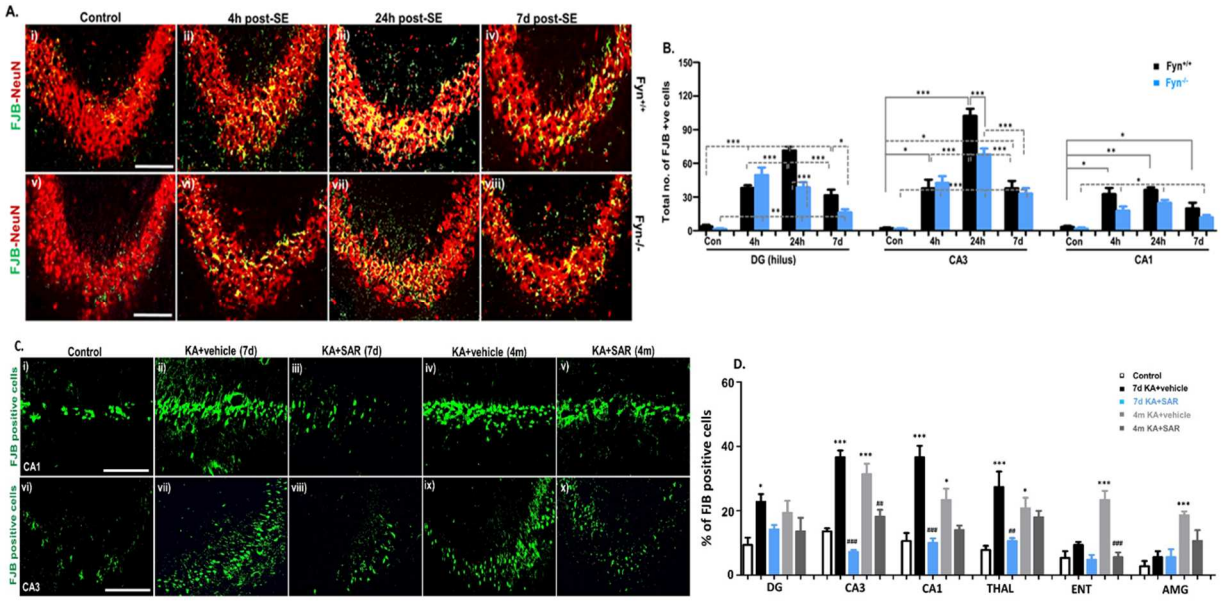

Fig. 23. Neurodegeneration. FJB-NeuN co-staining in CA3 (A) and FJB positive cells in CA1 (C) region of hippocampus. FJB positive cells (yellow in A,B and green in C) were observed in the neurons (red) of the pyramidal cell layer of CA3 (A) in both fyn+/+ and fyn−/− mice and CA1 (C) region of hippocampus at all time points. The maximum neurodegeneration was observed in CA3 and hilus in both the groups at 24 h post-SE (A, iii and vii, and B) and also in CA3 and CA1 of hippocampus and thalamus in rats at 7 d and 4 month (D). A significant difference in the number of FJB positive cells was observed in the DG and in other areas of the brain at all time points in fyn+/+ and fyn−/− and rats when compared to their respective controls. Higher number of FJB positive cells were observed at 24 h post-SE in fyn+/+ in CA3 (A, iii) but they were reduced at 7 d post-SE. Similar results were observed in fyn−/− where the neurodegeneration was diminished at 7 d post-SE compared to other time points. In fyn−/− mice, there was increased neurodegeneration in pyramidal layer of CA3 (A, viii) but this was significantly lower compared to fyn+/+ mice. In rats, fewer number of FJB positive cells were observed in the entorhinal cortex and amygdala (D). Maximum effect of SAR was observed in CA3 and CA1 at 7 d and 4 month and thalamus at 4 month post-SE, where the maximum suppression was observed (D). Overall, neurodegeneration was reduced in fyn−/− compared to fyn+/+ especially at 24

h and 7 d post-SE and in all areas of hippocampus and also in SAR group at all time points. One way ANOVA, *p < 0.05, **p < 0.01, ***p < 0.001; n = 5–6. Scale bar, all 100 μm.

There were significantly more numbers of degenerating neurons in the hippocampus at all time points in both groups when compared to their respective controls (Fig. 23A–D). This suggests that Fyn alone has little impact on neurodegeneration during epileptogenesis. FJB positive cells were also observed in higher numbers in thalamus at 7 d and 4 month and also in entorhinal cortex and amygdala at 4 month (Fig. 23D). Although the numbers of FJB positive neurons decreased at 7 d post-SE in both groups in mice, overall they were significantly lower in fyn−/− mice at 24 h post-SE in CA3 region of the hippocampus and the dentate gyrus when compared with the fyn+/+ mice (Fig. 23B). Saracatinib treatment reduced the number of FJB positive cells in all the regions at both time-points, except at 7 d in amygdala (Fig. 23D).

Discussion

In the present study, we provide evidence for the role of Fyn-PKCδ signaling as a novel mechanism of microglial activation during epileptogenesis in the kainate model of TLE. The role of neuronal Fyn in synaptic transmission and plasticity, LTP, epileptiform activity, neurodevelopment, and ischemic brain injury have been well known (Kaufman et al., 2015; Kojima et al., 1998; Lu et al., 1999; Nakazawa et al., 2001; Nygaard et al., 2014). However, its role in neuroinflammation-mediated epileptogenesis is unknown. We demonstrate that the Fyn upregulation occurs in the microglia, astrocytes and in the neurons of the hilus of dentate gyrus, CA3 and CA1 of hippocampus, thalamus, entorhinal cortex and amgdala during epileptogenesis. For the first time we demonstrate the role of Fyn and PKCδ in reactive microglia, astrocytes and neurons and their impact on proinflammatory cytokines, nitro-oxidative stress biomarkers, and neurodegeneration in the mouse and rat kainate model of TLE.

Furthermore, a continuous (24/7) video-EEG monitoring provided real-time evidence for epileptiform spiking and spontaneous seizure occurrence as functional readouts for the assessment of the lack of fyn gene during SE and epileptogenesis, and the impact of inhibiting Fyn function during post-SE on epileptogenesis. As a proof-of-concept for translational purpose, a pharmacological inhibitor of the SFK, saracatinib was tested in the mouse and rat models of TLE to demonstrate its anti-seizure and antiepileptogenic or disease modifying properties.

The targeted deletion of Fyn showed resistance or slower rate of epileptogenesis (Cain et al., 1995; Kojima et al., 1998). In transgenic mice, overexpressing a constitutively active form of Fyn showed decreased seizure threshold and higher mortality (Kojima et al., 1998). In our study, a SHD of kainate (25 mg/kg) caused 80% mortality in fyn+/ + mice. These mice are normal wildtype bred on a similar genetic background as fyn−/−mice, and they do not overexpress Fyn. The RLD method of SE induction with kainate (Tse et al., 2014) reduced mortality during the SE in both fyn+/+ and fyn−/− groups. However, in fyn−/− mice, mortality was higher after the diazepam administration (Fig. 2G), which could be due to abnormal GABAA receptor activity in the absence of Fyn kinase (Boehm, 2004; Jurd et al., 2010; Knox and Jiang, 2015; Lu et al., 1999). It has been shown that Fyn deletion can cause abnormal GABAergic synaptic transmission resulting in behavioral, functional, and developmental abnormalities in different brain regions (Knox and Jiang, 2015). However, the extent of morphological abnormality in the hippocampus and functional deficits in the fyn KO mice depend on strains/genetic background (Grant et al., 1992; Kojima et al., 1998; Lu et al., 1999). The fyn−/− mice developed on C57BL/6J and Balb-c background, used in this study, did not show morphological changes in the hippocampus. In contrast, fyn−/− mice bred on C57BL/ 6J

× S129 background showed varying degree of hydrocephalus (unpublished). The increased mortality in the fyn−/− mice in this study could also be due to the residual effects of kainate in the brain. The RLD method of kainate administration was chosen with the intention of achieving severe SE and to reduce mortality. It is important to note that the kainate levels persisted in the hippocampus for > 24 h (unpublished). It is likely that the first dose of kainate increases the BBB permeability (Puttachary et al., 2016b), which allows large quantities of kainate into the brain with subsequent dosing. It has been shown that RLD of kainate induces mGluR5 receptor expression in astrocytes (Umpierre et al., 2016), which could impact synaptic function. The mGluR5 is also associated with Fyn signaling (Nygaard et al., 2014), and it facilitates both ionotropic glutamate and GABAA receptors at central synapses (Xiao et al., 2006). Therefore, the activation of the receptors in the absence of Fyn may have a different outcome such as the diazepam-induced death in this study.

The chemoconvulsant-induced SE leads to the development of epilepsy (Buckmaster, 2004; Puttachary et al., 2016b; Williams et al., 2009). The most common features of epileptogenesis are increased epileptiform spike rate, reactive gliosis, neurodegeneration, and altered synaptic plasticity (Han et al., 2016; Puttachary et al., 2016a; Rattka et al., 2013; Robel et al., 2015; Sutula, 2004; White et al., 2010). It is still unclear which of these processes starts first, and which cell types play critical role at different stages of epileptogenesis. The role of both GABAA and NMDA receptors in the onset of acute seizures has been well known, and several AEDs have been discovered to modulate these receptors to prevent seizure onset (Bialer and White, 2010; Loscher, 2002; Rogawaski and Loscher, 2004; Schmidt, 2009). These receptors' activity at the postsynaptic terminal can also be modified by the signaling molecules associated with the PSD, for example, PSD-95, SFK including Fyn, neuronal NOS, tau, and

several other molecules. The role of NMDAR in pyramidal neuronal excitation during SE and epileptogenesis has been well described in several experimental models of epilepsy (Dingledine et al., 1990; Gataullina et al., 2017; Ghasemi and Schachter, 2011; Moussa et al., 2001; Naylor et al., 2013; Rice and DeLorenzo, 1998). Studies have shown an increased SFK mediated tyrosine phosphorylation of NMDAR complexes after experimentally induced seizures in animals (Kojima et al., 1998; Moussa et al., 2001; Nakazawa et al., 2001; Salter and Kalia, 2004; Zheng et al., 1998). The role of neuronal Fyn in modulating GABAA and NMDA receptor function is well known (Cain et al., 1995; Knox and Jiang, 2015; Lu et al., 1999; Kojima et al., 1998). Neuronal Fyn involvement in normal amygdala kindling has also been known for more than two decades (Cain et al., 1995). However, Fyn is not required for maintenance of kindling implying that neuronal Fyn may be limited to acute seizure onset. Our results from Fyn/SFK inhibitor, saracatinib pretreatment experiment in the mouse kainate model of acute seizures confirm that disabling Fyn/SFK prior to SE induction dampens the severity of seizures (Fig. 1A–B). IHC of brain sections from the wildtype control animals that had severe SE confirmed that Fyn was mildly upregulated in the excitatory pyramidal neurons of the hippocampus in mice, but highly in the hilar neurons of the dentate gyrus at 4 h, 24 h and 7 d post-SE (Fig. 10E–F). It has been known that the neurons in the hilus of dentate gyrus contain GABA, calbindin, somatostatin, neuropeptide-Y, cholecystokinin, and parvalbumin (Hofmann et al., 2016; Houser, 2007; Long et al., 2011; Marx et al., 2013; Megahed et al., 2015; Sik et al., 1997; Sun et al., 2007; Sundstrom et al., 2001). SE has been known to cause the loss of such inhibitory neurons in the hilus (Hofmann et al., 2016; Long et al., 2011; Marx et al., 2013; Pitkanen et al., 2007; Sun et al., 2007). The flurojade B and NeuN co-staining confirmed a significant increase in the FJB/NeuN positive neurons in the hilus of dentate gyrus

(Fig. 23) suggesting that the loss of inhibitory neurons during post-SE partly contributes to epileptogenesis.

The role of microglia in epileptogenesis and the time of their activation following SE is intriguing. Earlier studies, based on morphology, have reported that microglia become reactive after 24–36 h post-SE in animal models (Andersson et al., 1991; Avignone et al., 2008; Beamer et al., 2012; Sabilallah et al., 2016). However, the two-photon real-time brain imaging, *in vivo*, has revealed that the microglia become activated in < 30 min of post-insult and they engage in pruning the dendritic spines and synaptic re-organization. Activated microglia also produce trophic factors as an early protective mechanism (Parkhurst et al., 2013; Szalay et al., 2016; Vezzani et al., 2011). The microglia are highly mobile and dynamic cells. The chemokines and fractalkines facilitate their migration to the site of hyper-excited neurons (Eyo et al., 2017; Harrison et al., 1998). Though the Fyn has been shown to play a role in astrocytes and microglia migration in response to a signal from neurons (Dey et al., 2008; Stuart et al., 2007), its role in microglial and astrocytic activation in response to seizures is unknown. Since we found a significant increase in the Fyn and pSrc-416 levels during the early phase of epileptogenesis, and an increase in the numbers of reactive microglia and astrocytes in the hippocampus and other regions of the brain (Fig. 13), we speculated that Fyn also mediates neuroinflammatory response during epileptogenesis in addition to the loss of hilar neurons in the dentate gyrus. The microglia are resident immune cells of the brain which mediate innate immune response (Davis and Carson, 2012; Kettenmann et al., 2011). In the peripheral immune system, Fyn activates mast cells and lymphocytes and drives proinflammatory cytokines production (Tamura et al., 2001; Thomas and Brugge, 1997). The hippocampus and cortex contain a large amount of the SFK including Fyn (Salter and Kalia, 2004). Dysregulation of

SFK in mast cells offers resistance to epileptogenesis in an epilepsy-resistant variant of mouse originating from epilepsy-prone EL mice colony (Kitaura et al., 2006). Therefore, we speculated that a similar mechanism may exist in the kainate model of epileptogenesis. The Western blot and IHC analysis revealed a significant increase in nuclear Fyn and PKCδ levels in the hippocampus at 24 h, and 7 d post-SE in the fyn+/+ mice (Figs. 4, 5, 7-11), which provide evidence for increased Src kinase activity during epileptogenesis. As expected, Fyn was completely absent in the fyn−/− mice, however, we observed a marginal increase in pSrc-416 levels, which may suggest a partial role of other SFK (e.g. cAbl tyrosine kinase) in epileptogenesis. The c-Abl has been implicated in reactive microgliosis and in neurodegeneration (Gonfloni et al., 2012; Maiani et al., 2011).

In concurrence with the Western blot results, we found a significant increase in Fyn and PKCδ staining in nuclei of microglia in the hippocampus during epileptogenesis in fyn+/+ mice (Figs. 7G-H,J, 5E–F). In a cell culture and animal model of PD, it has been shown that phosphorylated Fyn activates PKCδ in microglia, which in turn translocates to the nucleus (Saminathan et al., 2011) and initiates transcription of proinflammatory cytokines either directly or in association with c-Abl or NFkB signaling components (Bujor et al., 2011; Gordon et al., 2016). It was shown that shRNA-mediated knockdown or genetic ablation of PKCδ in primary microglia abolished inflammogens-induced proinflammatory response in microglia, suppressed ROS and RNS production, and proinflammatory cytokines release (Gordon et al., 2016). Phosphorylated PKCδ also activates cytoplasmic subunit of the NOX2, which forms a functional complex with the membrane associated gp91phox to activate NOX2 signaling pathway and drives ROS and RNS production (Bedard and Krause, 2007; Fontayne et al., 2002; Gordon et al., 2016). In our studies, since we observed PKCδ staining in the reactive

microglia in fyn+/+ mice reactive microglia and astrocytes and neurons and and a reduction in seizure threshold as evident from EEG analysis, we speculated that proinflammatory cytokines and nitro-oxidative stress markers are also upregulated. As predicted, the proinflammatory mediators TNF-α, IL-1β, IL-6, and IL-12 were upregulated in fyn+/+ mice and KA rats. Likewise, the nitrooxidative stress markers such as 4-HNE, gp91phox and 3-NT levels were also upregulated. In the fyn−/− mice and saracatinib group, their levels were significantly reduced suggesting the proinflammatory role of Fyn in epileptogenesis. However, we found an increase in M1-like reactive microglia during post-SE in the fyn−/− mice, in contrast to the control, suggesting a partial role of other signaling pathways. For example, toll-like receptor and HMGB1, IkB kinase complex induced pathways involving Wnt signaling transduction pathway, and cytokine signaling via JAK/STAT involving IFN-α and IFN-β in microglial activation (Gesuete et al., 2014; Kaminska et al., 2016; Walker et al., 2017).

It has also been suggested that Fyn KO may compensate the loss of SFK protein levels by upregulating the other members of SFK such as Yes and c-Abl (Grant et al., 1995; Lowell et al., 1994). We have not tested this concept in our study. However, the pre- and post- SE treatment regimen with saracatinib, in this study, was expected to target all members of the SFK to achieve robust anti-seizure and antiepileptogenic effects.

Increased levels of proinflammatory cytokines and nitro-oxidative stress molecules are known to cause neurodegeneration (Glass et al., 2010; Vezzani et al., 2011 and Vezzani et al., 2013), altered synaptic plasticity, and decreased seizure threshold in epilepsy models (Bozzi et al., 2011; Reddy and Kuruba, 2013). As described previously (Puttachary et al., 2016a), we used FJB and NeuN co-staining to confirm neurodegeneration in our model. There was a significant increase in neurodegeneration in the fyn+/+ mice and KA rat when compared to the

fyn−/− mice and saracatinib treated rats (Fig. 23) suggesting Fyn's contribution to neurodegeneration during epileptogenesis. However, there was also increased neurodegeneration in the fyn−/− mice, when compared to the control, which may suggest the role of other SFKs and/or different mechanisms of neurodegeneration. The SFKs are known to mediate NMDAR-mediated hyperexcitability, which could have contributed to a moderate increase in neurodegeration in fyn−/− mice during post-SE. We did not test the compensatory mechanism in this study. However, to test whether Fyn KO alone has any impact on the hyperexcitability of neurons, measured by epileptiform spike rate and chronic seizures, a continuous video-EEG recording for 28 d post-SE was undertaken. The results revealed a significant reduction in epileptiform spiking and spontaneous NCS in the fyn−/−, in contrast to fyn+/+ mice, confirming the partial role of Fyn in epileptogenesis. Collectively, these results suggest that SFK is a potential target for achieving an anti-epileptogenic and/or a disease modifying effect.

Previous studies have shown that SFK inhibitor, PP2 reduces frequency of epileptiform discharges in the hippocampal in *in vitro* model (Salter and Kalia, 2004; Sanna et al., 2000). We used saracatinib in our *in vivo* studies. It is more potent than other SFK inhibitors, and has been in clinical trials for AD (Nygaard et al., 2015) and breast cancer (Gucalp et al., 2011). Saracatinib is an anilinoquinazoline compound which has high specificity for the tyrosine kinase domains of SFK (Hennequin et al., 2006). In these enzymes, an adenine moiety of ATP is bound to Src kinase domains through hydrogen bond networks. This allows chlorobenzo dioxide moiety of quinazoline compounds to sit deep inside the hydrophobic pocket of SFK making number of hydrophobic contacts forming stronger inhibitor-enzyme complex. Moreover, the presence of C5 position on the quinazoline ring, which fits well into enzyme's

ribose pocket, makes them even more selective for SFK thereby increasing their binding affinity and potency (Ballard et al., 2005; Gibson et al., 2002; Hennequin et al., 2006). Furthermore, the SFK has enzyme residues present at the entrance of their pocket site, also known as gatekeepers, is another potential feature for the selectivity of quinazolines as inhibitors of SFK. In contrast to SFK, the ribose pocket in other kinases is open to wide range of compounds that makes them less selective in nature (Hennequin et al., 2006). In our experiments, saracatinib significantly reduced severity and duration of SE in the mouse kainate model suggesting its seizure modulatory effect (Fig. 1). We further tested this in the rat kainate model of TLE and observed an anti-epileptogenic effect in four rats and a reduction in the numbers of spontaneous CS in others in contrast to the vehicle treated rats (Fig. 6-8, 9), which all became epileptic and had > 24 spontaneous CS in a month. These results imply that SFK play an important role in epileptogenesis and saracatinib could be a potential disease modifying agent for epilepsy.

In conclusion, the Fyn and PKCδ were upregulated in the microglia in hippocampus during epileptogenesis. Concurrently, proinflammatory cytokines and nitro-oxidative stressors were also upregulated to cause neurodegeneration, increased epileptiform spiking, and electrographic NCS. These changes were significantly reduced in the fyn−/− mice and saracatinib rats suggesting the role of Fyn in epileptogenesis. The saracatinib pretreatment significantly reduced SE severity and the post-treatment modified epileptogenesis suggesting its therapeutic potential in seizure modulation and modification of epileptogenesis. Further experiments using cell specific deletion of Fyn would help reveal the direct effect of glial and neuronal dependent neuroinflammatory processes in epileptogenesis.

References

1. Abi-Dargham, A., Horga, G., 2016. The search for imaging biomarkers in psychiatric disorders. Nat. Med. 22, 1248–1255.

2. Albrecht, D.S., Granziera, C., et al., 2016. In vivo imaging of human neuroinflammation. ACS Chem. Neurosci. 7, 470–483.

3. Andersson, P.-B., et al., 1991. The kinetics and morphological characteristics of the macrophage-microglial response to kainic acid-induced neuronal degeneration. Neuroscience 42, 201–214.

4. Avignone, E., et al., 2008. Status epilepticus induces a particular microglial activation state characterized by enhanced purinergic signaling. J. Neurosci. 28, 9133–9144.

5. Ballard, P.G., et al., 2005. Inhibitors of epidermal growth factors receptor tyrosine kinase: identification of novel C-5 substituted anilinoquinazolines designed to target the ribose pocket. Bioorg. Med. Chem. Lett. 15, 4226–4229.

6. Beach, T., et al., 1995. Reactive microglia in hippocampal sclerosis associated with human temporal lobe epilepsy. Neurosci. Lett. 191, 27–30.

7. Beamer, E., et al., 2012. N w -Propyl- l -arginine (L-NPA) reduces status epilepticus and early epileptogenic events in a mouse model of epilepsy: behavioural, EEG and immunohistochemical analyses. Eur. J. Neurosci. 36, 3194–3203.

8. Bedard, K., Krause, K.H., 2007. The NOX family of ROS-generating NADPH oxidases: physiology and pathophysiology. Physiol. Rev. 87, 245–313.

9. Berdichevsky, Y., et al., 2012. Interictal spikes, seizures and ictal cell death are not necessary for post-traumatic epileptogenesis in vitro. Neurobiol Dis. 45, 774-85.

10. Bertram, E.H., 2013. Neuronal circuits in epilepsy: do they matter? Exp. Neurol. 244, 67–74. Bialer, M., White, H.S., 2010. Key factors in the discovery and development of new antiepileptic drugs. Nat. Rev. Drug Discov. 9, 68–82.

11. Block, M.L., 2014. Neuroinflammation: modulating mighty microglia. Nat. Chem. Biol. 19, 988–989.

12. Boehm, S.L., 2004. Deletion of the Fyn-kinase gene alters sensitivity to GABAergic drugs: dependence on 2/3 GABAA receptor subunits. J. Pharmacol. Exp. Ther. 309, 1154–1159.

13. Bozzi, Y., et al., 2011. Cell signaling underlying epileptic behavior. Front. Behav. Neurosci. 5, 45.

14. Buckmaster, P.S., 2004. Laboratory animal models of temporal lobe epilepsy. Comp. Med. 54, 473–485.

15. Bujor, A.M., et al., 2011. The c-Abl tyrosine kinase controls protein kinase Cδ-induced Fli1 phosphorylation in human dermal fibroblasts. Arthritis Rheum. 63, 1729–1737.

16. Cain, D.P., et al., 1995. Fyn tyrosine kinase is required for normal amygdala kindling. Epilepsy Res. 22, 107–114.

17. Choi, J., et al., 2009. Cellular injury and neuroinflammation in children with chronic intractable epilepsy. J. Neuroinflammation 6, 38.

18. Cosgrave, A.S., et al., 2008. Regulation of activity-dependent neuroprotective protein (ADNP) by the NO-cGMP pathway in the hippocampus during kainic acid-induced seizure. Neurobiol. Dis. 30, 281–292.

19. Cosgrave, A.S., et al., 2010a. The effects of nitric oxide inhibition prior to kainic acid treatment on neuro- and gliogenesis in the rat dentate gyrus in vivo and in vitro. Histol. Histopathol. 25, 841–856.

20. Cosgrave, A.S., et al., 2010b. Differential regulation of vasoactive intestinal peptide (VIP) in the dentate gyrus and hippocampus via the NO-cGMP pathway following kainic acid-induced seizure in the rat. J. Mol. Neurosci. 42, 359–369.

21. Das, A., et al., 2012. Hippocampal tissue of patients with refractory temporal lobe epilepsy is associated with astrocyte activation, inflammation, and altered expression of channels and receptors. Neuroscience 220, 237–246.

22. Davis, D.S., Carson, M.J., 2012. An introduction to CNS-resident microglia: definitions, assays, and functional roles in health and disease. In: Neural-Immune Interactions in Brain Function and Alcohol Related Disorders, pp. 3–29.

23. Devinsky, O., Vezzani, A., et al., 2013. Glia and epilepsy: excitability and inflammation. Trends Neurosci. 36, 174–184.

24. Dey, N., et al., 2008. The protein phosphatase activity of PTEN regulates Src family kinases and controls glioma migration. Cancer Res. 68, 1862–1871.

25. Dingledine, R., et al., 1990. Excitatory amino acid receptors in epilepsy. Trends Pharmacol. Sci. 11, 334–338.

26. Dube et al., 2001. Relationship between neuronal loss and interictal glucose metabolism during the chronic phase of the lithium-pilocarpine model of epilepsy in the immature and adult rat. Exp Neurol. 167, 227-41.

27. Eyo, U.B., et al., 2017. Microglia-neuron communication in epilepsy. Glia 65, 5–18.

28. Fontayne, A., et al., 2002. Phosphorylation of p47phox sites by PKC alpha, beta II, delta, and zeta: effect on binding to p22phox and on NADPH oxidase activation. Biochemistry 41, 7743–7750.

29. French, J.A., 2016. Imaging brain inflammation: if we can see it, maybe we can treat it. Epilepsy Curr. 16, 24–26.

30. Flaherty, R.L., et al., 2017. Glucocorticoids induce production of reactive oxygen species/reactive nitrogen species and DNA damage through an iNOS mediated pathway in breast cancer. Breast Cancer Res. 19, 35.

31. Gallego, C., et al., 2011. Toll-Like Receptors Participate in Macrophage Activation and Intracellular Control of *Leishmania (Viannia) panamensis*. Infect Immun. 79, 2871-2879.

32. Gataullina, S., et al., 2017. The role of altered NMDA receptors expression in the epilepsy related to Tuberos Sclerosis Complex. Eur. J. Paediatr. Neurol. 21 (Supp 1), e8.

33. Gershen, L.D., et al., 2015. Neuroinflammation in temporal lobe epilepsy measured using positron emission tomographic imaging of translocator protein. JAMA Neurol. 72, 882–888.

34. Gesuete, R., et al., 2014. Toll-like receptors and ischemic brain injury. J. Neuropathol. Exp. Neurol. 73, 378–386.

35. Ghasemi, M., Schachter, S.C., 2011. The NMDA receptor complex as a therapeutic target in epilepsy: a review. Epilepsy Behav. 22, 617–640.

36. Gibson, A.E., et al., 2002. Probing the ATP ribose-binding domain of cyclin-dependent kinases 1 and 2 with O6 -substituted guanine derivatives. J. Med. Chem. 45, 3381–3393.

37. Glass, C.K., et al., 2010. Mechanisms underlying inflammation in neurodegeneration. Cell 140, 918–934.

38. Goldberg, E.M., Coulter, D.A., 2013. Mechanisms of epileptogenesis: a convergence on neural circuit dysfunction. Nat. Rev. Neurosci. 14, 337–349.

39. Gonfloni, S., et al., 2012. Oxidative stress, DNA damage, and c-Abl signaling: at the crossroad in neurodegenerative diseases? Int. J. Cell Biol. 2012, 1–7.

40. Gordon, R., et al., 2016. Protein kinase Cδ upregulation in microglia drives neuroinflammatory responses and dopaminergic neurodegeneration in experimental models of Parkinson's disease. Neurobiol. Dis. 93, 96–114.

41. Grant, S.G., et al., 1992. Impaired long-term potentiation, spatial learning, and hippocampal development in Fyn mutant mice. Science 258, 1903–1910.

42. Grant, S.G., et al., 1995. Focal adhesion kinase in the brain: novel subcellular localization and specific regulation by Fyn tyrosine kinase in mutant mice. Genes Dev. 9, 1909–1921.

43. Green, T.P., et al., 2009. Preclinical anticancer activity of the potent, oral Src inhibitor AZD0530. Mol. Oncol. 3, 248–261.

44. Griffith, R.W., Humphrey, D.R. (2006). Long-term gliosis around chronically implanted platinum electroides in the rhesus macaque motor cortex. Neurosci Lett. 406(1-2):81-6.

45. Gucalp, A., et al., 2011. Phase II trial of Saracatinib (AZD0530), an oral SRC-inhibitor for the treatment of patients with hormone receptor-negative metastatic breast cancer. Clin. Breast Cancer 11, 306–311.

46. Han, T., et al., 2016. Seizure induced synaptic plasticity alteration in hippocampus mediated by IL-1β receptor through PI3K/Akt pathway. Am. J. Transl. Res. 8, 4499–4509.

47. Hannon, R.A., et al., 2010. Effects of the Src kinase inhibitor saracatinib (AZD0530) on bone turnover in healthy men: a randomized, double-blind, placebo-controlled, multiple-ascending-dose phase I trial. J. Bone Miner. Res. 25, 463–471.

48. Harrison, J.K., et al., 1998. Role for neuronally derived fractalkine in mediating interactions between neurons and CX3CR1-expressing microglia. Proc. Natl. Acad. Sci. 95, 10896–10901. Hennequin, L.F., et al., 2006. N-(5-chloro-1,3-benzodioxol-4-yl)-7-[2-(4-methypiperazin1-yl)ethoxy]-5-(tetrahydro-2H-pyran-4-yloxy)quinazolin-4-amine, a novel, highly selective, orally available, dual-specific c-Src/Abl kinase inhibitor. J. Med. Chem. 49, 6465–6488.

49. Hofmann, G., et al., 2016. Hilar somatostatin interneuron loss reduces dentate gyrus inhibition in mouse model of temporal lobe epilepsy. Epilepsia 57, 977–983.

50. Houser, C.R., 2007. Interneurons of the dentate gyrus: an overview of cell types, terminal fields and neurochemical identity. Prog. Brain Res. 163, 217–232.

51. Hufnagel et al., 1994. Prognostic significance of ictal and interictal epileptiform activity in temporal lobe epilepsy. Epilepsia. 35, 1146-53.

52. Jurd, R., et al., 2010. Fyn kinase contributes to tyrosine phosphorylation of the GABAA receptor γ2 subunit. Mol. Cell. Neurosci. 44, 129–134.

53. Kaminska, B., et al., 2016. Signal transduction and epigenetic mechanisms in the control of microglia activation during neuroinflammation. Biochim. Biophys. Acta 1862, 339–351.

54. Kato, K., et al., 2009. Caspase-mediated protein kinase C-cleavage is necessary for apoptosis of vascular smooth muscle cells. Am. J. Physiol. Heart Circ. Physiol. 297, 2253–2261.

55. Kaufman, A.C., et al., 2015. Fyn inhibition rescues established memory and synapse loss in Alzheimer mice. Ann. Neurol. 77, 953–971.

56. Kaul, S., et al., 2003. Caspase-3 dependent proteolytic activation of protein kinase C delta mediates and regulates 1-methyl-4-phenylpyridinium (MPP)-induced apoptotic cell death in dopaminergic cells: relevance to oxidative stress in dopaminergic degeneration. Eur. J. Neurosci. 18, 1387–1401.

57. Kettenmann, H., et al., 2011. Physiology of microglia. Physiol. Rev. 91, 461–553.

58. Kidd, P.M., 1997. Glutathione: Systemic protectant against oxidative and free radical damage. Alternative Medicine Review. 2, 155-176.

59. Kitaura, J., et al., 2006. Dysregulation of Src family kinases in mast cells from epilepsyresistant ASK versus epilepsy-prone EL mice. J. Immunol. 178, 455–462.

60. Kitazawa, M., et al., 2005. Activation of protein kinase Cδ by proteolytic cleavage contributes to manganese-induced apoptosis in dopaminergic cells: protective role of Bcl2. Biochem. Pharmacol. 69, 133–146.

61. Knox, R., Jiang, X., 2015. Fyn in neurodevelopment and ischemic brain injury. Dev. Neurosci. 37, 311–320.

62. Ko, H.M., et al., 2018. Tyrosine kinase Fyn regulates iNOS expression in LPS-stimulated astrocytes via modulation of ERK phosphorylation. Biochem Biophys Res Commun. 495(1):1214-1220.

63. Kojima, N., et al., 1998. Higher seizure susceptibility and enhanced tyrosine phosphorylation of N-Methyl-D-Aspartate receptor subunit 2B in fyn transgenic mice. Learn. Mem. 5, 429–445.

64. Kwan, P., et al., 2011. Drug-Resistant Epilepsy. N. Engl. J. Med. 365, 919–926.

65. Leu, T.H., et al., 2006. Lipopolysaccharide-induced c-Src expression plays a role in nitric oxide and TNFalpha secretion in macrophages. Mol Immunol. 43, 308-16.

66. Liu, K.-J., et al., 2012. Saracatinib (AZD0530) is a potent modulator of ABCB1-mediated multidrug resistance in vitro and in vivo. Int. J. Cancer 132, 224–235.

67. Lobo, V., et al., 2010. Free radicals, antioxidants and functional food: Impact on human health. Pharmacogn Rev. 4, 118-126.

68. Long, L., et al., 2011. Selective loss of axonal sprouting of GABAergic interneurons in the sclerotic hippocampus induced by LiCl-pilocarpine. Int. J. Neurosci. 121, 69–85.

69. Loscher, W., 2002. Animal models of epilepsy for the development of antiepileptogenic and disease-modifying drugs. A comparison of the pharmacology of kindling and post-status epilepticus models of temporal lobe epilepsy. Epilepsy Res. 50, 105–123.

70. Lowell, C.A., et al., 1994. Functional overlap in the src gene family: inactivation of hck and fgr impairs natural immunity. Genes Dev. 8, 387–398.

71. Lu, Y.F., et al., 1999. Enhanced synaptic transmission and reduced threshold for LTP induction in fyn-transgenic mice. Eur. J. Neurosci. 11, 75–82.

72. Maiani, E., et al., 2011. DNA damage response: the emerging role of c-Abl as a regulatory switch? Biochem. Pharmacol. 82, 1269–1276.

73. Marx, M., et al., 2013. Differential vulnerability of interneurons in the epileptic hippocampus. Front. Cell. Neurosci. 7, 167.

74. Megahed, T., et al., 2015. Parvalbumin and neuropeptide Y expression hippocampal GABA-ergic inhibitory interneuron number declines in a model of Gulf War illness. Front. Cell. Neurosci. 8, 447.

75. Moussa, R.C., et al., 2001. Seizure activity results in increased tyrosine phosphorylation of the N-methyl-D-aspartate receptor in the hippocampus. Brain Res. Mol. Brain Res. 95, 36–47.

76. Nakazawa, T., et al., 2001. Characterization of Fyn-mediated tyrosine phosphorylation sites on GluRepsilon 2 (NR2B) subunit of the N-Methyl-D-aspartate Receptor. J. Biol. Chem. 276, 693–699.

77. Naylor, D.E., et al., 2013. Rapid surface accumulation of NMDA receptors increases glutamatergic excitation during status epilepticus. Neurobiol. Dis. 54, 225–238.

78. Nygaard, H.B., et al., 2014. Fyn kinase inhibition as a novel therapy for Alzheimer's disease. Alzheimers Res. Ther. 6, 8.

79. Nygaard, H.B., et al., 2015. A phase Ib multiple ascending dose study of the safety, tolerability, and central nervous system availability of AZD0530 (saracatinib) in Alzheimer's disease. Alzheimers Res. Ther. 7, 35.

80. Panicker, N., et al., 2015. Fyn kinase regulates microglial neuroinflammatory responses in cell culture and animal models of Parkinson's disease. J. Neurosci. 35, 10058–10077.

81. Parkhurst, C.N., et al., 2013. Microglia promote learning-dependent synapse formation through BDNF. Cell 155, 1596–1609.

82. Pitkanen, A., et al., 2007. Epileptogenesis in experimental models. Epilepsia 48 (Suppl. 2), 13–20.

83. Polikov, V.S., Tresco, P.A., Reichert, W.M. (2005). Response of brain tissue to chronically implanted neural electrodes. J Neurosci Methods. 148(1):1-18.

84. Puttachary, S., et al., 2015a. Seizure-induced oxidative stress in temporal lobe epilepsy. Biomed. Res. Int. 2015, 1–20.

85. Puttachary, S., et al., 2015b. Immediate epileptogenesis after kainate-induced status epilepticus in C57BL/6J mice: evidence from long term continuous video-EEG telemetry. PLoS One 10.

86. Puttachary, S., et al., 2016a. Immediate epileptogenesis: impact on brain in C57BL/6J mouse kainate model. Front. Biosci. 8, 390–411.

87. Puttachary, S., et al., 2016b. 1400W, a highly selective inducible nitric oxide synthase inhibitor is a potential disease modifier in the rat kainate model of temporal lobe epilepsy. Neurobiol. Dis. 93, 184–200.

88. Racine, R.J., 1972. Modification of seizure activity by electrical stimulation: II. Motor seizure. Electroencephalogr. Clin. Neurophysiol. 32, 281–294.

89. Rao, M.S., et al., 2006. Hippocampal neurodegeneration, spontaneous seizures, and mossy fiber sprouting in the F344 rat model of temporal lobe epilepsy. J. Neurosci. Res. 83, 1088–1105.

90. Rattka, M., et al., 2013. The intrahippocampal kainate model of temporal lobe epilepsy revisited: epileptogenesis, behavioral and cognitive alterations, pharmacological response, and hippoccampal damage in epileptic rats. Epilepsy Res. 103, 135–152.

91. Reddy, D., Kuruba, R., 2013. Experimental models of status epilepticus and neuronal injury for evaluation of therapeutic interventions. Int. J. Mol. Sci. 14, 18284–18318.

92. Rice, A.C., DeLorenzo, R.J., 1998. NMDA receptor activation during status epilepticus is required for the development of epilepsy. Brain Res. 782, 240–247.

93. Robel, S., et al., 2015. Reactive astrogliosis causes the development of spontaneous seizures. J. Neurosci. 35, 3330–3345.

94. Rogawaski, M.A., Loscher, W., 2004. The neurobiology of antiepileptic drugs. Nat. Rev. Neurosci. 5, 553–564.

95. Ryan, K., et al., 2014. Temporal and spatial increase of reactive nitrogen species in the kainate model of temporal lobe epilepsy. Neurobiol. Dis. 64, 8–15.

96. Sabilallah, M., et al., 2016. Evidence for status epilepticus and pro-inflammatory changes after intranasal kainic acid administration in mice. PLoS One 11.

97. Salatino, J.W., Ludwig, K.A., Kozai, T.D.Y., Purcell, E.K. 2017. Glial responses to implanted electrodes in the brain. Nat Biomed Eng. 1(11):862-877.

98. Salter, M.W., Kalia, L.V., 2004. Src kinases: a hub for NMDA receptor regulation. Nat. Rev. Neurosci. 5, 317–328.

99. Saminathan, H., et al., 2011. Environmental neurotoxic pesticide dieldrin activates a nonreceptor tyrosine kinase to promote pkcδ-mediated dopaminergic apoptosis in a dopaminergic neuronal cell model. Neurotoxicology 32, 567–577.

100. Sanna, P.P., et al., 2000. A role of Src kinase in spontaneous epileptiform activity in the CA3 region of the hippocampus. PNAS 97, 8653–8657.

101. Scharfman, H.E., Binder, D.K., 2013. Aquaporin-4 water channels and synaptic plasticity in the hippocampus. Neurochem. Int. 63, 702–711.

102. Schmidt, D., 2009. Drug treatment of epilepsy: options and limitations. Epilepsy Behav. 15, 56–65.

103. Schneider, C.A., et al., 2012. NIH image to imageJ: 25 years of image analysis. Nat. Methods 9, 671–675.

104. Seo, J., et al., 2014. Antisense methods to modulate pre-mRNA splicing. In: Methods in Molecular Biology Spliceosomal Pre-mRNA Splicing, pp. 271–283.

105. Sik, A., et al., 1997. Interneurons in the hippocampal dentate gyrus: an in vivo intracellular study. Eur. J. Neurosci. 9, 573–588.

106. Singh, R.J., 2002. Glutathione: A marker and antioxidant for aging. J Lab Clin Med. 140, 380-1.

107. Staley, K.J., Dudek, F.E., 2006. Interictal spikes and epileptogenesis. Epilepsy Curr. 6, 199-202.

108. Staley et al., 2005. Do interictal spikes drive epileptogenesis. Neuroscientist. 11, 272-6.

109. Steinhäuser, C., et al., 2016. Crucial role of astrocytes in temporal lobe epilepsy. Neuroscience 323, 157–169.

110. Stuart, L.M., et al., 2007. CD36 signals to the actin cytoskeleton and regulates microglial migration via a p130Cas complex. J. Biol. Chem. 282, 27392–27401.

111. Sun, C., et al., 2007. Selective loss of dentate hilar interneurons contributes to reduced synaptic inhibition of granule cells in an electrical stimulation-based animal model of temporal lobe epilepsy. J. Comp. Neurol. 500, 876–893.

112. Sundstrom, L.E., et al., 2001. Somatostatin- and neuropeptide Y-synthesizing neurons in the fascia dentate of humans with temporal lobe epilepsy. Brain J. Neurol. 124, 6888–6897.

113. Sutula, T.P., 2004. Mechanisms of epilepsy progression: current theories and perspectives from neuroplasticity in adulthood and development. Epilepsy Res. 60, 161–171.

114. Syslova, K., et al., 2014. Multimarker screening of oxidative stress in aging. Oxid Med Cell Longev. 2014:562860.

115. Szalay, G., et al., 2016. Microglia protect against brain injury and their selective elimination dysregulates neuronal network activity after stroke. Nat. Commun. 7, 11499.

116. Tamura, T., et al., 2001. Impairment in the expression and activity of Fyn during differentiation of naive CD4 T cells into the Th2 subset. J. Immunol. 167, 1962–1969.

117. Thomas, S.M., Brugge, J.S., 1997. Cellular functions regulated by Src family kinases. Annu. Rev. Cell Dev. Biol. 13, 513–609.

118. Todorovic, M.S., et al., 2012. Characterization of status epilepticus induced by two organophosphates in rats. Epilepsy Res. 101, 268–276.

119. Torres-Platas, S.G., et al., 2014. Morphometric characterization of microglial phenotypes in human cerebral cortex. J. Neuroinflammation 11, 12.

120. Tse, K., et al., 2014. Advantages of repeated low dose against single high dose of kainate in C57BL/6J mouse model of status epilepticus: behavioral and electroencephalographic studies. PLoS One 9.

121. Umpierre, A.D., et al., 2016. Repeated low-dose kainate administration in C57BL/6J mice produces temporal lobe epilepsy pathology but infrequent spontaneous seizures. Exp. Neurol. 279, 116–126.

122. Varvel, N.H., et al., 2015. Candidate drug targets for prevention or modification of epilepsy. Annu. Rev. Pharmacol. Toxicol. 55, 229–247.

123. Vezzani, A., et al., 2011. The role of inflammation in epilepsy. Nat. Rev. Neurol. 7, 31–40.

124. Vezzani, A., et al., 2013. The role of inflammation in Epileptogenesis. Neuropharmacology 69, 16–24.

125. Viviani, B., et al., 2003. Interleukin-1β Enhances NMDA Receptor-Mediated Intracellular Calcium Increase through Activation of the Src Family of Kinases. The Journal of Neuroscience. 23, 8692-8700.

126. Walker, D.G., Lue, L.F., 2015. Immune phenotypes of microglia in human neurodegenerative disease: challenges to detecting microglial polarization in human brains. Alzheimers Res. Ther. 7, 56.

127. Walker, L.E., et al., 2017. Molecular isoforms of high-mobility group box 1 are mechanistic biomarkers for epilepsy. J. Clin. Investig. 127, 2118–2132.

128. White, A., et al., 2010. EEG spike activity precedes epilepsy after kainate-induced status epilepticus. Epilepsia 51, 371–383.

129. Williams, P.A., et al., 2009. Development of spontaneous recurrent seizures after kainateinduced status epilepticus. J. Neurosci. 29, 2103–2112.

130. Xiao, M.-Y., et al., 2006. Metabotropic glutamate receptors in the trafficking of ionotropic glutamate and GABAA receptors at central synapses. Curr. Neuropharmacol. 4, 77–86.

131. Xing, L., et al., 2001. Genetic evidence for a role for Src family kinases in TNF family receptor signaling and cell survival. Genes Dev. 15, 241-253.

132. Yan, S.R., Novak, M.J., 1999. Src-family kinase-p53/ Lyn p56 plays an important role in TNF-alpha-stimulated production of O2- by human neutrophils adherent to fibrinogen. Inflammation. 23, 167-178.

133. Yang, J.C., et al., 2010. Effect of the specific Src family kinase inhibitor saracatinib on osteolytic lesions using the PC-3 bone model. Mol. Cancer Ther. 9, 1629–1637.

134. Zheng, F., et al., 1998. Tyrosine kinase potentiates NMDA receptor currents by reducing tonic zinc inhibition. Nat. Neurosci. 1, 185–191.

CHAPTER VI

GENERAL CONCLUSION AND FUTURE DIRECTIONS

This section describes an outline summary of the model characterization, inteventional drugs used in the experiments, summary of the results and relevant findings for each chapter and future directions in epilepsy research.

Kainate induced SE caused immediate epileptogenesis in C57BL/6J mice

In chapter 2, the results from C57BL/6J mice study on electrographic convulsive and non-convusive seizure characateristics in the kainate model of Temporal Lobe Epilepsy (TLE) are discussed. C57BL/6J mouse model as a KA model of epilepsy has been criticized for its high mortality rate, inconsistent seizure response, and importantly, resistance to KA-induced neurodegeneration. Therefore, we modified the model to achieve high seizure quality and consistency between animals with less mortality through repeated low dose (RLD) method of KA administration via intraperitoneal route for seizure induction. By means of this method, seizures can be titrated based on their severity, i.e., mild or severe. Seizure severity is the measure of the total time spent by an animal in convulsive status epilepticus (stage $\geq$3), during 2 hours of SE. To our knowledge, so far, there were no reports on the long-term continuous video-EEG studies performed in the mouse model of TLE. Herein, we performed 18 week continuous long-term EEG to study spontaneous convulsive (CS) and non-convulsive seizures (NCS) and epileptiform spike frequency in C57BL/6J mice model. The outcome of this study were: i) independent of the seizure severity, animals from both mild and severe groups became epileptic within the first week of post-SE and later showed spontaneous non-convulsive seizures throughout the 18 week period, ii) as predicted, animals in the severe group showed

higher number of CS compared to the mild group, and iii) the number of CS were maximum in the first 4-6 weeks in both groups, and the frequency reduced thereafter suggesting that this is an excellent regressive model of epilepsy with respect to CS. However, it is important to note that this model can also serve as a chronic model of NCS.

Numerous studies have demonstrated that episodes of NCS can increase glutamate, lactate, enolase, intracranial pressure and cerebral blood flow in the brain. Although considered as the mild form of seizures, NCS still can cause serious brain damage if they occur persistently over the long periods of time (Puttachary et al., 2015b and 2016b; Loscher et al., 2015; Wagenman et al., 2014). Moreover, recent unpublished data from our lab confirms that the first CS, which occurs after kainate-induced SE, preceeds NCS in 83% of the animals. The rest of the animals that did not show any CS also didn't show NCS (chapter 5, table 1 and 2). So far, only one study has demonstrated the role of NCS in promoting CS at a later stages of epileptogenesis. The study showed that of the 137 patients, 43% exhibited electrographic CS seizures and 23% showed NCS. Among the ones that showed NCS, 47% developed epilepsy (CS) at a later stage (Wagenman et al., 2014). Therefore, the significance of NCS in epilepsy research should not be overlooked and we were the first to provide this evidence in animal models from C57BL/6J and $Fyn^{+/+}$ mice studies (Puttachary et al., 2015b; Sharma et al., 2018). Our mouse model of C57BL/6J has several advantages over the other rodent models of epilepsy. This model can be useful for 1) testing the efficacy of novel investigational drug (NID) candidates to suppress CS in short term studies (four weeks), 2) testing the efficacy of NIDs against NCS in long-term studies, and 3) providing early window of opportunity to test/screen compounds thus reducing the cost and duration of the experiments.

The hallmarks of kainate-induced epileptogenesis: Immunohistochemical and behavioral analyses

Since we observed greater CS frequency during the first month of post-SE in both mild and severe models of TLE, in chapter 3, the consequences or cause of such occurrence of seizures on brain pathology is presented. We tested the hypothesis in different brain regions at various time-points using EEG, histological techniques and behaviour studies such as the Morris water maze to examine the effects of seizures on learning and memory. Due to high seizure frequency in the severe group, a significant increase in reactive astrogliosis and microgliosis were observed in the hippocampus, amygdala and entorhinal cortex at 7 d but were reduced by the 28th day of injury. Dysfunctional gliosis is detrimental and can cause serious injury to neurons resulting in inflammation and neurodegeneration (Eddleston and Mucke, 1993; Eng and Ghirnikar, 1994; Pekny and Pekna, 2016). Overtime, this can cause a significant neuronal loss in the brain, especially hippocampus, a condition known as hippocampal sclerosis (Swartz et al., 2006; Thom, 2014). Enhanced gliosis in the hippocampus was correlated with increased FJB positive cells in pyramidal cell layers of CA1 and CA3 and other regions of the brain in both mild and severe groups, compared to the controls. Furthermore, increased gliosis and neurodegeneration in these regions also corresponded with an increased spike frequency, a diagnostic electrographic marker for neuronal hyperexcitation, during the first week of post-SE suggesting that reactive gliosis might have caused abnormal neuronal hyperexcitation and neurodegeneration in these regions. An inflammation can be a cause or a consequence of seizures and cell death. Aberrant adult neurogenesis is also considered as one of the primary biomarker for chronic refractory TLE (Cho et al., 2015; Parent et al., 2005; Siebzuhnrubl and Blumcke, 2008). Numerous studies have described the role of

adult neurogenesis in regulating dentate granule cell hyperexcitation by forming abnormal synapses with the hilar interneurons modifying inhibitory drive of these neurons (Catavero et al., 2018; Ikrar et al., 2013; Jackson et al., 2012). Therefore, we investigated neurogenesis in the subgranular cell layer of dentate gyrus (DG) using doublecortin (DCX) immunostaining. Neurogenesis was higher at 7 d post-SE but reduced thereafter, in both mild and severe groups. Interestingly, DCX positive cells were also observed in the granular cell layer and hilus of DG. It has been shown that these neuroblasts migrate from subgranular zone into granular cell layer and synchronize to form cells of the granular layer (Murphy and Danzer, 2011; Scharfman et al., 2003). However, the purpose of their migration into the hilus is yet unknown and requires further investigation. Considering the impact of neuropathological changes in the brain due to seizure severity, we anticipated cognitive decline in these animals. So we tested discriminatory learning and memory using the Morris water maze. As expected, the animals that had severe injury spent more time in false platform zone compared to mild and control group during the probe trial. Also, these animals spent more time in the false platform zone during their training period. We knew that hippocampus plays a crucial role in regulating various types of memories such as spatial, declarative and procedural memory and in their consolidation (Burgess et al., 2002; Kumaran, 2008; Shrager et al., 2007). Numerous studies on human patients with TLE have reported serious problems in their memories and cognition due to hippocampal damage. Therefore, our results from the water maze experiment supports the notion that reactive gliosis, aberrant neurogenesis and neurodenegeration in the hippocampus due to CS may have affected discriminatory learning and memory in these animals during the four week study.

Several lines of evidence are now emerging acknowledging the role of NCS in brain pathology (Avdic et al., 2018; Nagayama et al., 2017; Reugg, 2017). However, the effect of

NCS induced brain pathology in long-term studies still remains to be determined. Therefore, our C57BL/6J mouse model is a robust model of NCS which can be used to investigate the impact of NCS such as neurodegeneration, gliosis, cerebral dysfunction and cognitive impairment, over the longer periods of time, on different brain regions such as hippocampus, cortical and subcortical structures.

Pharmacological inhibitor of iNOS, 1400W, reduced/prevented epileptogenesis

In chapter 4, disease modifying properties of iNOS inhibitor, 1400W, in the rat KA model of TLE is presented. 1400W is a highly selective iNOS inhibitor that inhibits iNOS by binding to L-arginine's guanidine moiety on iNOS functional group. 1400W's amidine moiety is a structural analogue of L-arginine's guanidine binding moiety therefore making it >5000 and >200 times more selective than eNOS and nNOS (Garvey et al., 1997). Although, the other iNOS inhibitors have high potency and specificity towards their target, they are not isoform selective and have off target side effects (Garvey et al., 1997; Laszlo et al., 1995). 1400W, however, did not have these limitations, is highly selective and tissue permeable iNOS inhibitor discovered so far (Alderton et al., 2001; Parmentier et al., 1999).

Many studies have demonstrated the role iNOS and nNOS in several neurodegenerative conditions such as Epilepsy, Parkinson's, Alzheimer's, Huntington's etc. Increased amounts of NO generated through iNOS and nNOS results in the production of peroxynitrites and reactive nitrogen dioxide free radicals. These highly reactive molecules target mitochondrial respiration either directly or through NMDA receptor mediated mechanisms leading to DNA damage, increased inflammation and nitrosylation of proteins thus causing cell death (Dawson, 1992; Puttachary et al., 2015a).

Epileptiform spiking patterns are used in the diagnosis and/or prediction of epilepsy. These discharges occur intermittently after SE and in between SRS. Persistant epileptiform activity for longer periods can lead to the development of SRS and cause gliosis and neurodegeneration or vice versa. To test this hypothesis in the rat chronic model of TLE, we performed IHC for GFAP and IBA1 to investigate gliosis. Severe SE caused reactive gliosis, increased neuroinflammation and neurodegeneration and also damage to BBB. BBB dysfunction facilitated the transport of serum albumin into the brain parenchyma which affected astrocytic proteins like glutamate transporters (GLT-1) and potassium channels (Kir4.1). 1400W treatment suppressed epileptiform discharges, reactive gliosis, neurodegeneration and serum albumin in neurons and astrocytes implying that 1400W preserved BBB integrity. We further investigated the expression of astrocytic proteins such as GLT-1 and Kir4.1. Enhanced serum albumin levels in astrocytes caused downregulation of Kir4.1 and GLT-1. Impaired potassium channels and glutamate transporters result in an increased potassium and glutamate in the extracellular space and cause hyperexcitability and nitrosylation of proteins (Steinhauser et al., 2016). Although Kir4.1 levels were recovered, GLT-1 levels were not fully restored after 1400W treatment.

The studies from human TLE patients have shown that seizures in early life can have long-term impact on the brain (Holmes, 2009; Jensen and Baram, 2011; Vingerhoets, 2006). Therefore, our hypothesis was that targeting iNOS, soon after the onset of SE, will protect the brain from SE-induced damage in the long-term. To test this, SE-induced animals, treated with 1400W or vehicle, were euthanized at six months after SE and investigated for potential biomarkers for epileptogenesis/epilepsy such as reactive microgliosis, astrogliosis, neurodegeneration and increased epileptiform spiking. Since mossy fiber sprouting is

considered as one of the important pathognomonic feature of established chronic epilepsy, we tested whether 1400W also modulate mossy fiber sprouting. We observed that 1400W post-treatment significantly decreased the number of CS, reduced reactive gliosis, neurodegeneration and mossy fiber sprouting. In summary, iNOS inhibition by 1400W suppressed gliosis, neurodegeneration, epileptiform activity and CS at 7d and 6m post-SE. It also reversed Kir4.1 levels in astrocytes and reduced 3-NT in neurons and microglia suggesting its neuroprotective role which is predominantly mediated by glial source of iNOS. Although a great degree of spontaneous CS frequency and neuroinflammatory markers were reduced after early 1400W treatment, the complete seizure freedom was still not achieved in some of the 1400W treated rats. Therefore, more advanced treatment strategies are required to achieve this goal. For instance, 1400W treatment alone or co-treatment with antiepileptogenic/antiepileptic drugs or with anti-inflammatory agents during acute and chronic conditions (after the establishment of disease) could prove to be an effective strategy to alter the course of the disease progression. The experimental outcome revealed anti-epileptogenic effects of 1400W, however, its anti-epileptic effects need to be tested by initiating 1400W treatment once the disease is established.

Fyn-PKCδ signaling enhanced seizure susceptibility and Fyn deletion or SFK/Fyn inhibition prevented disease onset and its progression

In chapter 5, disease modifying properties of Fyn modulation either through knocking out Fyn gene or using a pharmacological inhibitor of Src family kinase (SFK)/Fyn, Saracatinib, in mice and rat KA models of TLE is presented. For the first part of the project, we used $Fyn^{-/-}$ and $Fyn^{+/+}$ transgenic mice (C57BL/6J and Balb-c hybrid). Under normal physiological

conditions, Fyn is involved in regulating major central nervous system and non-central nervous system functions such as synaptic plasticity, myelination, cell proliferation and migration, synaptic density, cell differentiation, platelet function and T-cell signaling (Thomas and Brugge, 1997). Its role in hyperexcitability through PSD-95-NMDAR mediated mechanism in neurons in epilepsy, and its neuroinflammatory role via PKCδ-mediated mechanism in microglia in Parkinson's disease model are well known. Therefore, we investigated the role of Fyn in both neurons and glia in epileptogenesis in the $Fyn^{-/-}$ and $Fyn^{+/+}$ model of mice and Sprague Dawley rats. We quantified electrographic spontaneous NCS and CS and spike rate that includes all the epileptiform spikes including NCS and CS in these animals. In Fyn KO mice, we did not find any CS so we quantified NCS only. We observed that Fyn knockout reduced the number of NCS and spike frequency when compared to the wild type animals. We observed similar results for CS and spike rate in a four month long continuous study in saracatinib treated rats. We also investigated EEG signatures for the first CS in this model. Saracatinib treatment reduced the numer of NCS, epileptiform clusters and interictal spikes in these rats. Further, to investigate whether Fyn has any role in the maintenance of brain pathology, we did fractionation studies in both models (mice and rats) to understand whether it translocates to the nucleus or not. We observed increased Fyn translocation into the nucleus at all the time points especially at 24h post-SE in $Fyn^{+/+}$ mice and at 7 d and 4 month in kainate treated rats. Fyn's phosphorylation at tyrosine residue 416 is essential for its activation and translocation to the nucleus, we observed similar increase in phosphorylated Fyn (pSrc 416) levels at all the time-points. Since Fyn is also responsible for the activation of iNOS in astrocytes and macrophage, we further investigated the role of iNOS and 3-NT, a marker for protein nitrosylation. All these neuroinflammatory markers were downregulated in $Fyn^{-/-}$ group

and after saracatinib post-treatment. It has been reported that Fyn phosphorylates PKCδ and PKCδ phosphorylation and cleavage is essential for the production of reactive oxygen species, so we did similar fractionation studies, like Fyn, to investigate PKCδ nuclear translocation. PKCδ phosphorylation increases iNOS, and increased iNOS levels can activate Src family kinases and phosphorylate NMDA receptors causing calcium overload in the cell. This elevates the production of oxidative stress molecules (4-HNE, $gp91^{phox}$ and 3-NT) and cytochrome c enhancing cleaved caspase-3 levels resulting in cell death. $Fyn^{-/-}$ and saracatinib post-treatment reduced PKCδ nuclear translocation, oxidative and nitrosative stress, iNOS upregulation and caspase-3 and cleaved caspase-3 levels in the brain. Since, TNFα and IL-1β play a key role in regulating neuroinflammation, we further decided to examine mRNA gene expression (TNFα, IL-1β and iNOS) and protein levels (TNFα, IL-1β, IL-6, IL-12) of proinflammatory cytokines in the tissues and serum and also oxidant and anti-oxidant levels, using biochemical asays. All the proinflammatoy cytokines investigated in tissues and serum were downregulated in Fyn KO mice and in the saracatinib treated rats. The results from biochemical assays on serum further revealed that SFK/Fyn inhibition reduced oxidants such as nitrites and ROS and restored antioxidant glutathione levels suggesting neuroprotective role of saracatinib against oxidative damage. In summary, Fyn and PKCδ were upregulated in glial cells in the hippocampus and in neurons in most of the brain regions at both 7d and 4m post-SE. Proinflammatory cytokines and nitro-oxidative stressors were also upregulated to cause neurodegeneration, increased epileptiform spiking, and SRS. These changes were significantly reduced in $Fyn^{-/-}$ mice and saracatinib treated rats suggesting the role of Fyn in epileptogenesis. Further experiments on cell specific gene manipulation studies would reveal Fyn-PKCδ cell dependent neuroinflammatory response in epileptogenesis. Moreover, a combination/co-

treatment with another antiepileptic/neuroprotectant, e.g., carbamazepine/1400W in addition to saracatinib during acute and chronic conditions at different time intervals could prove to be an effective strategy to alter the course of the disease progression.

References

1. Alderton, W.K., Cooper, C.E., Knowles, R.G. (2001). Nitric oxide synthases: structure, function and inhibition. Biochemical Journal. 357(3):593–615.

2. Avdic, U., Ahl, M., Chugh, D., Ali, I., Chary, K., Sierra, A., Ekdahl, C.T. (2018). Nonconvulsive status epilepticus in rats leads to brain pathology. Epilepsia. 59, 945-958.

3. Burgess, N., Mahuire, E.A., O'Keefe, J. (2002). The human hippocampus and spatial and episodic memory. Neuron. 35(4):625-641.

4. Catavero, C., Bao, Hechen., Song, J. (2018). Neural mechnisms underlying GABAergic regulation of adult hippocampal neurogenesis. Cell Tissue Res. 371, 33-46.

5. Cho, K-O., Lybrand, Z.R., Ito, N., Brulet, R., Tafacory, F., Zhang, L., et al. (2015). Aberrant hippocampal neurogenesis contributes to epilepsy and associated cognitive decline. Nat Commun. 6:6606.

6. Dawson, T. M., Dawson, V. L., Snyder, S. H. (1992). A novel neuronal messenger molecule in brain: The free radical, nitric oxide. Annals of Neurology. 32(3):297-311.

7. Eddleston, L., Mucke, L. (1993). Molecular profile of reactive astrocytes–implications for their role in neurologic disease. Neuroscience. 54, 15-36.

8. Eng, L.F., Ghirnikar, R.S. (1994). GFAP and astrogliosis. Brain Pathol. 4, 229-237.

9. Garvey, E. P., Oplinger, J. A., Furfine, E. S., Kiff, R. J., Laszlo, F., Whittle, B. J., & Knowles, R. G. (1997). 1400W is a slow, tight binding, and highly selective inhibitor of inducible nitric-oxide synthase in vitro and in vivo. Journal of Biological Chemistry, 272, 4959–4963.

10. Holmes, G.L. (2009). The long-term effects of neonatal seizures. Cin Perinatol. 36(4):901-14.

11. Ikrar, T., Guo, N., He, K., Besnard, A., Levinson, S., Hill, A., Lee, H.K., Hen, R., Xu, X., Sahay, A. (2013). Adult neurogenesis modifies excitability of the dentate gyrus. Front Neural Circuits. 7:204.

12. Jackson, J., Chugh, D., Nilsson, P., Wood, J., Carlstrom, K., Lindvall, O., Ekdahl, C.T. (2012). Altered synaptic properties during integration of adult-born hippocampal neurons following a seizure insult. PLoS One. 7(4):e35557.

13. Jensen, F.E., Baram, T.Z. (2011). Developmental seizures induced by common early-life insults: short- and long-term effects on seizure susceptibility. Ment Retard Dev Disabil Res Rev. 6(4):253-257.

14. Kumaran, D. (2008). Short-term memory and the human hippocampus. Journal of Neuroscience. 28(15):3837-3838.

15. Laszlo, F., Evans, S.M., and Whittle, B.J. (1995). Aminoguanidine inhibits both constitutive and inducible nitric oxide synthase isoforms in rat intestinal microvasculature in vivo. Eur. J. Pharmacol. 272: 169–175.

16. Loscher, W., Hirsch, L. J., & Schmidt, D. (2015). The enigma of the latent period in the development of symptomatic acquired epilepsy — Traditional view versus new concepts. Epilepsy & Behavior. 52, 78-92.

17. Murphy, B. L., Danzer, S. C. (2011). Somatic translocation: A novel mechanism of granule cell dendritic dysmorphogenesis and dispersion. Journal of Neuroscience. 31, 2959–2964.

18. Nagayama, M., Yang, S., Geocadin, R., Kaplan, P.W., Hoshiyama, E., Shiromaru-Asugimoto, A., Kawamura, M. (2017). Novel clinical features of nonconvulsive status epilepticus. F1000Res. 6:1690.

19. Parent, J.M., Elliott, R.C., Pleasure, S.J., Barbaro, N.M., Lowenstein, D.H. (2006). Aberrant seizure-induced neurogenesis in experimental temporal lobe epilepsy. Ann Neurol. 59, 81-91.

20. Parmentier, S., Bohme, G. A., Lerouet, D., Damour, D., Stutzmann, J. M., Margaill, I., Plotkine, M. (1999). Selective inhibition of inducible nitric oxide synthase prevents ischaemic brain injury. British Journal of Pharmacology. 127, 546–552.

21. Pekny, M., Pekna, M. (2016). Reactive gliosis in the pathogenesis of CNS diseases. Biochemica et Biophysica Acta. 1862(3):483-491.

22. Puttachary, S., Sharma, S., Stark, S., Thippeswamy, T. (2015a). Seizure induced oxidative stress in temporal lobe epilepsy. BioMed Research International. 2015, 1–20.

23. Puttachary, S., Sharma, S., Thippeswamy, A., Thippeswamy, T. (2016b). Immediate epileptogenesis: Impact on brain in C57BL/6J mouse kainate model. Frontiers in Bioscience. 8, 390–411.

24. Puttachary, S., Sharma, S., Tse, K., Beamer, E., Sexton, A., Crutison, J., Thippeswamy, T. (2015b). Immediate epileptogenesis after kainateinduced status epilepticus in C57BL/6J mice: Evidence from long term continuous video-EEG telemetry. Plos One. 10, e0131705.

25. Reugg, S. (2017). Nonconvulsive status epilepticus in adults: Types, pathophysiology, epidemiology, etiology, and diagnosis. Neurology International Open. 1, E189-E203.

26. Scharfman, H.E., Sollas, A.E., Berger, R.E., Goodman, J.H., Pierce, J.P. (2003). Perforant path activation of ectopic granule cells that are born after pilocarpine-induced seizures. Neuroscience. 121(4):1017-29.

27. Sharma, S., Carlson, S., Puttachary, S., Sarkar, S., Showman, L., Putra, M., Kanthasamy, A.G., Thippeswamy, T. (2018). Role of the Fyn-PKCδ signaling in SE-induced neuroinflammation and epileptogenesis in experimental models of temporal lobe epilepsy. Neurobiology of Disease. 110:102-121.

28. Shrager, Y., Bayley, P.J., Bontempi, B., Hopkins, R.O., Squire, L.R. (2007). Spatial memory and the human hippocampus. Proc Natl Acad Sci. 104(8):2961-2966.

29. Siebzenhrubl, F.A., Blumcke, I. (2008). Neurogenesis in the human hippocampus and its relevance to temporal lobe epilepsies. Epilepsia. 49, 55-65.

30. Steinhauser, C., Grunnet, M., Carmignoto, G. (2016). Crucial role of astrocytes in temporal lobe epilepsy. Neuroscience. 323:157-69.

31. Swartz, B.E., Houser, C.R., Tomiyasu, U., Walsh, G.O., DeSalles, A., Rich, J.R., Delgado-Escueta, A. (2006). Hippocampal cell loss in posttraumatic human epilepsy. Epilepsia. 47(8):1373-82.

32. Thom, M. (2014). Review: Hippocampal sclerosis in epilepsy: a neuropathology review. Neuropathol Appl Neurobiol. 40(5):520-543.

33. Thomas, S. M., Brugge, J. S. (1997). Cellular Functions Regulated By Src Family Kinases. Annual Review of Cell and Developmental Biology. 13(1):513-609.

34. Vingerhoets, G. (2006). Cognitive effects of seizures. Seziure. 15(4):221-6.

35. Wagenman, K.L., Blake, T.P., Sanchez, S.M., et al. (2014). Electrographic status epilepticus and long-term outcome in critically ill children. Neurology. 82(5):396-404.

ACKNOWLEDGEMENTS

I would like to thank my principle investigator Dr. Thimmasettappa Thippeswamy for his continuous guidance, support and encouragement throughout my PhD. I would also like to thank him for giving me an opportunity to teach Anatomy to the graduate students which helped me to develop strong pedagogical skills. I admire him for his broad knowledge in the field of epilepsy research and most of all his professionalism and self-discipline attitude towards his work. Without his suggestions and guidance, it would have been impossible to come up with this Ph.D. thesis. I learnt a lot from him and I am sure the valuable experience I gained after working with him will surely benefit me in my future career.

I would also like to thank Dr. Chandrashekhar Charavaryamath for giving advice on how to succeed as a graduate student and on postdoctoral opportunities around the world and sharing some of his life experiences as a teacher and a researcher. I would like to thank my other committee members Dr. Mary W Greenlee for taking time out from her busy schedule and helping me dealing with my graduate school challenges, Dr. Wilson K Rumbeiha for his useful comments during committee meetings and Dr. Anumantha Kanthasamy for allowing me to use his lab space, equipments and antibodies for our work and for his advice during the meetings. I would also like to thank Dr. Kanthasamy for providing Fyn mice for our research projects.

I would like to extend my heartfelt gratitude to Dr. Nani Ghoshal, whose experience, continuous support, care, advice and sarcastic jokes helped me to deal with the difficult times I had while teaching Principles of Morphology I course to DVM students. I would also like to give credit to other instructors and Mr. Wolfgang Weber for helping me with the dissection and successfully teaching the course. Thanks to my postdoc mentor Dr. Sreekanth Puttachary, who initially helped me in settling down in Ames and taught me various lab skills. I would

also like to acknowledge the support of Laboratory Animal Resources for helping us with the animal work, all the Biomedical Science staff including Cathy Martens, William Robertson, Gary Zenitsky and all my colleagues, friends and everyone I came across while on this journey. I learned little, if not much, something from each one of them which will help me to become a better and a successful person in the future.

Finally, my deepest gratitude goes to my sister and parents, especially my mother, whose unconditional love, unwavering support, sacrifice and encouragement made me the person I am today. I would like to dedicate this thesis to my mother, without her support, I wouldn't have reached this far in life.